ORGANOMETALLIC CHEMISTRY OF SOME MANGANESE AND ZIRCONIUM COMPLEXES: A GREEN CHEMISTRY APPROACH

S S MANZINI

ORGANOMETALLIC CHEMISTRY OF SOME MANGANESE AND ZIRCONIUM COMPLEXES: A GREEN CHEMISTRY APPROACH

Sunnyboy Stanley Manzini

A thesis submitted to the Faculty of Science, University of the Witwatersrand, Johannesburg, in fulfillment of the requirements for the degree of Doctor of Philosophy
Johannesburg, 2005

DECLARATION

I declare that this thesis is my own, unaided work, performed under the supervision of Professor N. J. Coville and Dr W. Meyer. It is submitted for the Degree of Doctor of Philosophy in the University of Witwatersrand, Johannesburg, South Africa. It has not been submitted before for any degree or examination in any other University.

Sunnyboy Stanley Manzini
September 2005

ABSTRACT

The solventless reaction between $Mn(CO)_4(PPh_3)Br$ and PPh_3 as neat reagents using FTIRS was conducted and the activation enthalpy change of formation was found to be 143 ± 19 $kJmol^{-1}$ while the activation entropy change of formation was 104 ± 7 $Jmol^{-1}K^{-1}$. The same reaction was also carried out in chloroform and the activation enthalpy change of formation was found to be 146 ± 8 $kJmol^{-1}$ while the activation entropy change of formation was 114 ± 6 $Jmol^{-1}K^{-1}$. When the reaction was conducted in TCE solution, the activation enthalpy and entropy changes of formation were 137 ± 6 $kJmol^{-1}$ and 97 ± 5 $Jmol^{-1}K^{-1}$ respectively.

The solventless reaction of $Mn(CO)_4(PPh_3)Br$ with PPh_3 in KBr matrix using DRIFTS was also conducted and the activation enthalpy change of formation was found to be 169 ± 28 $kJ.mol^{-1}$ while the activation entropy change of formation was 204 ± 57 $J.mol^{-1}.K^{-1}$. The sample preparation method, the type of support and the particle size of the support material influenced the reaction rate. The soventless reaction $Mn(CO)_4LBr + L \rightarrow Mn(CO)_3L_2Br + CO$ [L= P(*p*-C_6H_4-R)$_3$, R = Ph, MeO, Cl, F] in KBr using DRIFTS was also studied. It was found that the electronic effects of the ligand already attached on the metal complex influenced the rate of the reaction.

An optical microscopy study of the reaction $Mn(CO)_4LBr + L' \rightarrow Mn(CO)_3LL'Br + CO$ [L= P(*p*-C_6H_4-R)$_3$, R = H, Ph, MeO] was undertaken in an attempt to reconcile the well-behaved reaction kinetics of the solventless reactions with solventless reactions by observing the microscopic behaviour of the reagents. The reactions were observed to go through a melt phase at temperatures much lower than the lowest melting point of the reagents, provided the reagents were in contact with each other. Isolated reagents neither reacted nor melted. The molten reagent thus served as a medium that allowed the diffusion of the reagents and products to ensure well-behaved kinetics. Investigation using ^{31}P NMR demonstrated that the dissociation of the attached phosphine ligands also

ACKNOWLEDGEMENTS

My immediate thanks go to God Jehovah for the life that I have, all-round support with day-to-day business activities particularly on bad days, protection (inclusive of unforeseen circumstances), help and encouragement (through his word) when I felt small and helpless, and needed constant guidance.

I am greatly indebted to the following people whose input and support made this thesis possible.

- Prof. N. J. Coville, My supervisor and mentor, for his luminosity. I would not have managed to produce this document without his timely interventions, particularly when nothing seemed to work. I am privileged to have had his expert guidance. I managed to see further than others by standing on the shoulders of a giant.
- SASOL, DoE NRF and The University of The Witwatersrand Scholarships for financial support
- Prof C. B. de Koning for encouragement and optimism.
- Prof M. Rollnick for her encouragement.
- Dr E.M. Mmutlane for his friendship and incessant nagging. Your support in many ways is appreciated.
- Mrs F. Nareetsile for friendship and support in the lab. Thanks a lot sister.
- My mother, S. N. Maswanganyi for everything. I would not have been where I am without her help and support and yes her prayers.
- Miss A. Budhai for being a good friend and her support.
- Mr R. Mampa for NMR work and friendship. Mrs S. Heiss also helped with NMR work.
- Dr M. Fernandes for X-ray crystallographic work.
- Dr M. Bala, Dr O. G. Adeyemi, Dr T. Molefetse, Mr T. Magadzu, Miss K. Khoabane for assistance in the lab.
- The entire CATOMCER group, Mr K. Mokoena, Mr. L. Sikwivhilu, Miss C. Mbileni, Miss S. Mohlala, Dr S. Ndou, Dr X Liu and Dr R. Mpfundzeni.

- My friends Mr S. Molele, Mr J. Maluleke, Mr I. Khosa, Mr C. P. Sibuyi and Mrs J. Nhlapo (thanks a lot sister particularly for your encouragements and prayers)
- Mr S. Gannon and Mr B. Fairbrother for glass blowing work.
- Mr B. Chassoulas for electronic work. I appreciative your assistance with the GC (assemble and calibration), heating jacket and autoclave constructions.
- Physics workshop for autoclave modifications.
- My wife, N. B. Sekgobela, for reasons too many to mention.

TABLE OF CONTENTS

DECLARATION……..ii

ABSTRACT.....iii

ACKNOWLEDGEMENTS…… v

TABLE OF CONTENTS……vii

LIST OF FIGURES xviii

LIST OF SCHEMES xxiv

LIST OF TABLES xxviii

LIST OF ABBREVIATIONS……xxxiii

CHAPTER 1: INTRODUCTION..... 1

CHAPTER 2: LITERATURE REVIEW..... 4

2.1. GREEN CHEMISTRY 4

2.2. EXAMPLES OF SOLVENTLESS REACTION 12

2.2.1. Organic reactions 12

2.2.1.1. Dimerisation reactions 13

2.2.1.2. Condensation reaction, solvent free Knoevenagel condensation..... 14

2.2.1.3. Thiozoles from α-tosyloxy ketones using microwave irradiation 16

2.2.1.4. Protection of sugars..... 17

2.2.2. Inorganic reactions..... 19

2.2.2.1. Main group compounds 19

2.2.2.2. *d*-Block compounds 19

2.2.2.2.1. Vanadium (V) phosphate synthesis 19

2.2.2.2.2. Solid-state synthesis of chromiun thiophosphate, $Cr_4(P_2S_6)_3$ 20

2.2.2.2.3. Solid-state synthesis of lithium metazirconate (Li_2ZrO_3) pellets .. 21

2.2.2.3. *f*-Block compounds 22

2.2.3. Organometallic compounds..... 23

2.2.3.2. Isomerisation reactions 25

2.2.3.2.1. Linkage isomerisation 25
2.2.3.2.2. Cis-trans isomerisations reactions 26
2.2.3.3. Migratory insertion reactions 29
2.2.3.4. Coupling reactions 35
2.2.3.5. Substitution reactions 37
2.2.3.5.1. Reaction of diag-(η^5-C_5H_5Me)$Re(CO)_2Br_2$ with excess NaI 37
2.2.3.5.2. Reaction between $RhX(PPh_3)_3$ and (η^5-C_5H_4Me)$W(CO)_3X$ in the solid-state 38
2.3. CONCLUSIONS 40
2.5. REFERENCES 41

CHAPTER 3: EXPERIMENTAL AND CHARACTERISATION PROCEDURES 50

3.1. INTRODUCTION 50
3.2. EXPERIMENTAL PROCEDURES 50
3.2.1. Work Bench Setup 50
3.2.2. Glove Box 51
3.2.3. Solvent Purification 51
3.2.4. Experimental techniques 51
3.3. CHARACTERISATION PROCEDURE 52
3.3.1. FTIRS 52
3.3.2. DRIFTS 52
3.3.3. NMR Spectroscopy 55
3.3.4. DSC (Differential Scanning Calorimetry) 55
3.3.5. Mass Spectrometry 56
3.3.6. Elemental Analysis 56
3.3.7. GC (Gas Chromatography) 57
3.3.8. XRD (X-Ray Diffraction) 58
3.4. REFERENCES 59

CHAPTER 4: SYNTHESIS OF MANGANESE CARBONYL COMPLEXES USING LITERATURE METHODS 60

4.1. INTRODUCTION 60

4.1.1. Historical perspective *60*
4.1.2. Synthesis and kinetics *62*
4.2. EXPERIMENTAL PROCEDURES 64
4.2.1. Synthesis of $Mn(CO)_5Br$[8] [1] *64*
4.2.2 Synthesis of $Mn_2(CO)_8Br_2$[10] [2] *65*
4.2.2.1 Dry heat; 138°C 66
4.2.2.2 Dry heat; 100°C 66
4.2.2.3. *n*-Octane; reflux 66
4.2.2.4. Petroleum ether; (110-120°C) 67
4.2.2.5. KBr; solid-state method (100°C) 67
4.2.3. Synthesis of $Mn(CO)_4(L)Br$ *68*
4.2.3.1 $Mn(CO)_4(PPh_3)Br$[9] [3] 68
4.2.4. Synthesis of $Mn(CO)_3L_2Br$ *69*
4.2.4.1. $Mn(CO)_3(PPh_3)_2Br$ [8] 69
4.3. RESULTS AND DISCUSSION 70
4.3.1. Synthesis of $Mn(CO)_5Br$ *70*
4.3.2 Synthesis of $Mn_2(CO)_8Br_2$ *71*
4.3.3 Synthesis of $Mn(CO)_4LBr$ *72*
4.3.4 Synthesis of $Mn(CO)_3L_2Br$ *73*
4.4. CONCLUSIONS 75
4.5. APPENDIX 78
4.6. REFERENCES 81

CHAPTER 5: THE USE OF FTIRS TO STUDY THE SOLVENTLESS REACTION OF MANGANESE CARBONYL COMPLEXES 83

5.1. INTRODUCTION 83
5.1.1. History and perspective *83*
5.1.2. FTIRS and manganese carbonyl complexes *84*
5.2. EXPERIMENTAL PROCEDURES 85
5.2.1. Kinetic study of the solventless reaction of $Mn(CO)_5Br$ and PPh_3 to form $Mn(CO)_4(L)Br$ using FTIRS *85*
5.2.1.1. Calibration curve for $Mn(CO)_5Br$ 86

5.2.1.2. Calibration curve for $Mn(CO)_4(PPh_3)Br$ 87
5.2.1.3. Calibration curve for $Mn(CO)_3(PPh_3)_2Br$ 88
5.2.1.4. Kinetic study of the solventless reaction of $Mn(CO)_5Br$ with PPh_3 (1:1 molar ratio) in chloroform as followed by FTIRS..... 89
5.2.1.5. Kinetic study of the solventless reaction of $Mn(CO)_5Br$ with PPh_3 (1:2 molar ratio) as followed by FTIRS 89
5.2.1.6. Kinetics of the solventless reaction of $Mn(CO)_5Br$ with PPh_3 (1:10 molar ratio) as followed by FTIRS..... 90
5.2.2. Kinetic study of the solventless reaction between $Mn(CO)_4(PPh_3)Br$ and PPh_3 90
5.3. RESULTS AND DISCUSSION 91
5.3.1. Reference IR spectra 91
5.3.2. Kinetics study of the formation of trans-$Mn(CO)_3(PPh_3)_2Br$ from $Mn(CO)_5Br$ 92
5.3.3. Reaction of $Mn_2(CO)_8Br_2$ and PPh_3 97
5.3.4. Kinetic study of the formation of trans-$Mn(CO)_3(PPh_3)_2Br$ from $Mn(CO)_4(PPh_3)Br$ 98
5.4. CONCLUSIONS..... 103
5.5. REFERENCES 104
CHAPTER 6: THE USE OF FTIRS TO STUDY THE TRANSFORMATION OF MANGANESE CARBONYL COMPLEXES IN SOLUTION..... 106
6.1. INTRODUCTION 106
6.2. EXPERIMENTAL PROCEDURES 107
6.2.1. Reaction of $Mn(CO)_4LBr$ with L to give $Mn(CO)_3L_2Br$ in TCE solution..... 108
6.2.1.1 Calibration curve for $Mn(CO)_5Br$ in TCE solution 108
6.2.1.2 Calibration curve for $Mn(CO)_4(PPh_3)Br$ in TCE solution..... 109
6.2.1.3 Calibration curve for $Mn(CO)_3(PPh_3)_2Br$ in TCE solution..... 110
6.2.1.4. FTIRS kinetic study of the reaction between $Mn(CO)_4(PPh_3)Br$ and PPh_3 in TCE solution 111

6.2.2. FTIRS kinetic study for the reaction between $Mn(CO)_4(PPh_3)Br$ and PPh_3 in chloroform *112*
6.3. RESULTS AND DISCUSSION 113
6.3.1. A kinetic study for the reaction of $Mn(CO)_4(PPh_3)Br$ with PPh_3 in chloroform *113*
6.3.2. A kinetic study for the reaction of $Mn(CO)_4(PPh_3)Br$ with PPh_3 in TCE *115*
6.3.3. Comparison of the solventless and solution kinetic parameters for the reaction between $Mn(CO)_4(PPh_3)Br$ with PPh_3 ..... *117*
6.4. CONCLUSIONS 118
6.5. REFERENCES 119

CHAPTER 7: THE SOLVENTLESS REACTION BETWEEN $Mn(CO)_4(L)BR$ AND L′ FOLLOWED BY ^{31}P NMR SPECTROSCOPY 120

7.1. INTRODUCTION 120
7.1.1. History and perspective *120*
7.1.2. ^{31}P NMR spectroscopy in organometallic chemistry *121*
7.1.3. Aims of this study *122*
7.2. EXPERIMENTAL PROCEDURES 122
7.2.1. The use of NMR spectroscopy to study the solventless reaction $Mn(CO)_4(L)Br$ with L' *122*
7.2.2. The solventless reaction between $Mn(CO)_4(PPh_3)Br$ and $P(p\text{-}MeOPh)_3$ (1:1.14) followed by ^{31}P NMR spectroscopy *123*
7.2.3. The solventless reaction between $Mn(CO)_4(PPh_3)Br$ and $P(p\text{-}MeO\text{-}C_6H_4)_3$ (1:3) followed by ^{31}P NMR spectroscopy *124*
7.2.4. The solventless reaction between $Mn(CO)_4(P(p\text{-}MeO\text{-}C_6H_4)_3)Br$ and PPh_3 (1:2) as followed by ^{31}P NMR spectroscopy *124*
7.3. RESULTS AND DISCUSSIONS 124
7.3.1. The solventless reaction between $Mn(CO)_4(PPh_3)Br$ and $P(p\text{-}MeO\text{-}C_6H_4)_3$ (1:1.4) followed by ^{31}P NMR spectroscopy at 60°C *124*

7.3.2. The solventless reaction between $Mn(CO)_4(PPh_3)Br$ and ..... $P(p\text{-}MeO\text{-}C_6H_4)_3$ (1:3) followed by ^{31}P NMR spectroscopy 129

7.3.3. The solventless reaction between $Mn(CO)_4(P(p\text{-}MeO\text{-}C_6H_4)_3)Br$ ..... with PPh_3 (1:2) as followed by ^{31}P NMR spectroscopy 130

7.4. CONCLUSIONS 134

7.5. REFERENCES 136

CHAPTER 8: THE USE OF DRIFTS TO STUDY THE SOLVENTLESS TRANSFORMATION OF MANGANESE COMPLEXES 138

8.1. INTRODUCTION 138

8.1.1. Historical perspective 138

8.1.2. DRIFTS in organometallic chemistry studies 139

8.1.3. Aim of the study 140

8.2. EXPERIMENTAL PROCEDURES 140

8.2.1. DRIFTS kinetic measurements: The solventless reaction between $Mn(CO)_4(PPh_3)Br$ and PPh_3 140

8.2.1.1. DRIFTS Spectra: $Mn(CO)_4(PPh_3)Br$ / KBr Standards 140

8.2.1.2. Reaction of $Mn(CO)_4(PPh_3)Br$ with variable amounts of PPh_3 141

8.2.1.3. Reaction of PPh_3 with varying amounts of $Mn(CO)_4(PPh_3)Br$ 142

8.2.2. Effects of sample preparation method on the solventless reaction of $Mn(CO)_4(PPh_3)Br$ with PPh_3 in KBr 143

8.2.2.1. Fine Power method 143

8.2.2.2. Solvent method 144

8.2.3. Effect of KBr particle size on the solventless reaction between $Mn(CO)_4(PPh_3)Br$ with PPh_3 at 60°C 144

8.2.4. The effect of supports on the solventless reaction between $Mn(CO)_4(PPh_3)Br$ with PPh_3 at 60°C 145

8.2.5. Variation of ligand: the solventless reaction of $Mn(CO)_4(L)Br$ ..... with L to give $Mn(CO)_3(L)_2Br$ [L = $P(p\text{-}MeO\text{-}C_6H_4)_3$, ... $P(pMe\text{-}C_6H_4)_3$, $P(p\text{-}F\text{-}C_6H_4)_3$, and $P(p\text{-}Cl\text{-}C_6H_4)_3$)] 146

8.3. RESULTS AND DISCUSSION 147

8.3.1. The effect of the amount of $Mn(CO)_4(PPh_3)Br$ on the reflectance spectra *147*
8.3.2. The effect of the amount of ligand on the solventless reaction of $Mn(CO)_4(PPh_3)Br$ with PPh_3 in KBr matrix at 60°C *148*
8.3.3. The effect of metal complex amount on the solventless reaction of $Mn(CO)_4(PPh_3)Br$ with PPh_3 in KBr matrix using DRIFTS *151*
8.3.4. The effects of sample preparation method on the solventless reaction of $Mn(CO)_4(PPh_3)Br$ with PPh_3 in KBr using DRIFTS *154*
8.3.4.1. Fine Power Method 154
8.3.4.2. Solvent Method 155
8.3.5. Effects of particle size of the KBr support on the rate of the solventless reaction of $Mn(CO)_4(PPh_3)Br$ with PPh_3 at 60 C using DRIFTS *156*
8.3.6. The effect of support on the solventless reaction of *158*
8.3.7. The use of DRIFTS for the kinetic studies of the solventless reaction of $Mn(CO)_4(L)Br$ with ligand, L (where L. ≠ PPh_3) *159*
8.4. CONCLUSIONS 163
8.5. REFERENCES 166

CHAPTER 9: OPTICAL MICROSCOPY EXPERIMENTS 168

9.1. INTRODUCTION 168
9.1.1. History and perspective *168*
9.1.2. Aims *169*
9.2. EXPERIMENTAL PROCEDURES 170
9.2.1. The reaction Device *170*
9.2.1.1. Heating plate cell design 170
9.2.1.2. Reaction Chamber Design and Operation 170
9.2.2. Optical microscopy study if the solventless reaction of thoroughly mixed powders of $Mn(CO)_4(PPh_3)Br$ and PPh3 (1:1 mol equiv) at 60°C *173*
9.2.3. Optical microscopy study of the solventless reaction between $Mn(CO)_4(PPh_3)Br$ and PPh_3 using crystalline reagents at 42°C *174*

9.2.4. Thermally induced solventless reaction between $Mn(CO)_4(PPh_3)Br$ and $P(p\text{-}Me\text{-}C_6H_4)_3$ using crystalline reagents *174*

9.3. RESULTS AND DISCUSSIONS 175

9.3.1. Optical microscopy study of the solventless reaction of thoroughly mixed powders of $Mn(CO)_4(PPh_3)Br$ and PPh_3 (1:1 mol equivalent) at 60°C *175*

9.3.2. Optical microscopy study of the solventless reaction of $Mn(CO)_4(PPh_3)Br$ and PPh_3 using crystalline reagents at 42°C *178*

9.4. CONCLUSIONS 187

9.5. REFERENCES 189

CHAPTER 10: CRYSTALLOGRAPHIC STUDIES OF MANGANESE CARBONYL COMPOUNDS 191

10.1. INTRODUCTION 191

10.1.1. History and perspective *191*

10.1.2. Aims of the study *193*

10.2. EXPERIMENTAL METHODS 193

10.3. RESULTS AND DISCUSSION 194

10.4. CONCLUSIONS 198

10.5. APPENDIX 199

10.6. REFERENCES 205

CHAPTER 11: SOLVENTLESS ZIRCONIUM CARBOXYLATE CHEMISTRY 207

11.1. INTRODUCTION 207

11.1.1. Historical perspective *207*

11.1.2. Aims of the study *211*

11.2. EXPERIMENTAL 211

11.2.1. Synthesis of sodium benzoates *211*

11.2.2. Synthesis of $(\eta^5\text{-}C_5H_5)_2ZrCl(RCOO)$, [R = C_6H_5 (14), $p\text{-}C_6H_4\text{-}NO_2$ (15), $p\text{-}C_6H_4\text{-}NH_2$ (16)] *212*

11.3. SINGLE CRYSTAL STUDIES 214

11.4. RESULTS AND DISCUSION 214
11.4.1. Synthesis of sodium benzoates 214
11.4.2. Synthesis of zirconium carboxylates 215
11.4.3. Single crystal analysis 216
11.5. CONCLUSIONS 224
11.6. REFERENCES 225

CHAPTER 12: ISOMERISATION OF OLEFINS: THE HYDROZIRCONATION REACTION 227

12.1. INTRODUCTION 227
12.1.1. Literature review 227
12.1.2. Aims of the study 234
12.2. EXPERIMENTAL PROCEDURES 234
12.2.1. Synthesis of substituted cyclopentadienes 234
12.2.2. Synthesis of substituted bis(cyclopentadienyl)zirconium 235
12.2.3. Synthesis of chlorobis(η^5-cyclopentadienyl)hydrido-zirconium(IV) complex 236
12.2.4. Synthesis of chlorobis(η^5-cyclopentadienyl)hexyl-zirconium(IV) Complex 237
12.2.5. Catalytic isomerisation of 1-hexene to internal hexene isomers 238
12.2.5.1. Isomerisation of 1-hexene using Na-Al_2O_3 238
12.2.5.2. Isomerisation of 1-hexene using KO^{t}Bu in DMSO 239
12.2.5.3. Isomerisation of 1-hexene using Rh(III) chloride trihydrate 239
12.2.6. Evaluation of (η^5-Cp)$_2$ZrClC$_6$H$_{13}$ as an isomerisation catalyst for 1-hexene 239
12.2.7. Catalytic isomerisation of internal to terminal hexene double bond 241
12.2.7.1. Isomerisation of internal hexene isomers to 1-hexene using (η^5-Cp)$_2$Zr(Cl)C$_6$H$_{13}$ 241
12.2.7.2. Isomerisation of internal hexene isomers to 1-hexene using substituted chlorobis(cyclopentadienyl)hexylzirconium(IV) complex 242

12.2.7.3. Reaction of Cp_2ZrCl_2 / PEt_3 / *n*-BuLi with hexenes 242
12.2.7.4. Reaction of Cp_2ZrCl_2 / PPh_3 / *n*-BuLi with hexenes..... 243
12.2.7.5. Reaction of Cp_2ZrCl_2 / *n*-BuLi with hexenes 243
12.2.7.6. Reaction of *n*-BuLi with hexenes 244
12.2.7.7. Reaction of Cp_2ZrCl_2 / NaH with hexenes 244
12.2.7.8. Reaction of Cp_2ZrH_2 with hexenes 245
12.2.7.9. Reaction of $(R\text{-}C_5H_4)_2ZrBu_2$ with hexenes 245
12.3. RESULTS AND DISCUSSION 246
12.3.1. Synthesis of substituted cyclopentadienes 246
12.3.2. Synthesis of substituted bis(cyclopentadienyl)zirconium (IV) halides 247
12.3.3. Synthesis of chlorobis(η^5-cyclopentadienyl)hydrido-zirconium(IV) complex 249
12.3.4. Synthesis of chlorobis(η5-cyclopentadienyl)hexyl-zirconium(IV) Complex 249
12.3.5. Catalytic isomerisation of 1-hexene to internal hexene isomers 250
12.3.5.1. Isomerisation of 1-hexene using $Na\text{-}Al_2O_3$..... 250
12.3.5.2. Isomerisation of 1-hexene using K^tOBu in DMF 252
12.3.5.3. Isomerisation of 1-hexene using Rh(III) chloride trihydrate 253
12.3.6. Evaluation of $(\eta^5\text{-}Cp)_2Zr(Cl)C_6H_{13}$ as an isomerisation catalyst for 1-hexene 254
12.3.7. Catalytic isomerisation of internal to terminal Hexene double bond..... 255
12.3.7.1. Isomerisation of internal hexene isomers to 1-hexene using $(\eta^5\text{-}Cp)_2Zr(Cl)C_6H_{13}$ 255
12.3.7.2. Isomerisation of internal hexene isomers to 1-hexene using substituted chlorobis(cyclopentadienyl)hexylzirconium(IV) complex..... 257
12.3.7.3. Reaction of Cp_2ZrCl_2 / PEt_3 / *n*-BuLi with hexenes 258
12.3.7.4. Reaction of Cp_2ZrCl_2 / PPh_3 / *n*-BuLi with hexenes..... 260
12.3.7.5. Reaction of Cp_2ZrCl_2 / *n*-BuLi with hexenes 262
12.2.7.6. Reaction of *n*-BuLi with hexenes 266

12.3.7.7. Reaction of Cp_2ZrCl_2 / NaH with hexenes 268
12.3.7.8. Reaction of Cp_2ZrH_2 with hexenes 269
12.3.7.9. Reaction of $(R\text{--}C_5H_4)_2ZrBu_2$ with hexenes 270
12.3.7.9.1. Reaction of $(Me\text{-}C_5H_4)_2ZrBu_2$ with hexenes 271
12.3.7.9.2. Reaction of $(^{i}Pr\text{-}C_5H_4)_2ZrBu_2$ with hexenes 272
12.3.7.9.3. Reaction of $(^{t}Bu\text{-}C_5H_4)_2ZrBu_2$ with hexenes 273
12.3.7.9.4. Reaction of $(SiMe_3\text{-}C_5H_4)_2ZrBu_2$ with hexenes 273
12.3.7.9.5. Reaction of $(Et\text{-}C_5H_4)_2ZrBu_2$ with hexenes 274
12.4. CONCLUSIONS 275
12.5. REFERENCES 277

CHAPTER 13: CONCLUSIONS AND FUTURE SUGGESTIONS 280

13.1. CONCLUSIONS 280
13.2. FUTURE SUGGESTIONS 284

LIST OF FIGURES

Figure 2.1. Detailed kinetic study of the solventless transformation of $(\eta^5\text{-}C_5H_5)M(CO)_3Me$, (M= Mo, W), using solid phosphines using DRIFTS when the sample was taken in KBr as a diluent…….33

Figure 5.1. Calibration curve for $Mn(CO)_5Br$ (chloroform, room temperature)……..86

Figure 5.2. Calibration curve for $Mn(CO)_4(PPh_3)Br$ obtained using FTIRS (chloroform, room temperature)……87

Figure 5.3. Calibration curve for $Mn(CO)_3(PPh_3)_2Br$ (chloroform, room temperature)……...88

Figure 5.4. Infrared spectra of $Mn(CO)_5Br$, $Mn(CO)_4(PPh_3)Br$ and $Mn(CO)_3(PPh_3)_2Br$……91

Figure 5.5. DSC profile of $Mn(CO)_5Br$ (heating rate:10° per minute) under Nitrogen…….92

Figure 5.6. DSC profile of PPh_3 (heating rate:10 per minute) under nitrogen……..…….93

Figure 5.7. DSC profile of the solventless reaction of $Mn(CO)_5Br$ with PPh_3 (1:1 mol equivalent, heating rate:10° per minute) under nitrogen…….94

Figure 5.8. Plot of composition versus time for the reaction of $Mn(CO)_5Br$ with PPh_3 (1:1 and 1:2 metal/ligand ratios) at 65°C under nitrogen using FTIRS…….……95

Figure 5.9. Plot of composition versus time for the reaction of $Mn(CO)_5Br$ with PPh_3 (1:5 and 1:10 metal/ligand ratios) at 65°C under nitrogen using FTIRS…….....96

Figure 5.10. DSC profile of the reaction of $(Mn_2(CO)_8Br_2)$ with PPh_3 (1:1 molar equivalent) at a heating rate of 10° per minute under nitrogen……..……97

Figure 5.11. Plot of composition versus time for the reaction of $Mn(CO)_4(PPh_3)Br$ with PPh_3 (1:1 and 1:2) at 65°C under nitrogen……..98

Figure 5.12. Plot of composition versus time for the reaction of $Mn(CO)_4(PPh_3)Br$ with PPh_3 (1:5 and 1:10) at 65°C under nitrogen……..……99

Figure 5.13. Plot of composition versus time for the solventless reaction of $Mn(CO)_4(PPh_3)Br$ with PPh_3 at 65°C and 74°C at various metal to ligand ratios as followed using FTIRS……100

Figure 5.14. Plot of ln[$Mn(CO)_4(PPh_3)Br$] with time for the solventless reaction of $Mn(CO)_4(PPh_3)Br$ with PPh_3 (1:10 mol equiv) at various temperatures followed by FTIRS in chloroform at the end of the reaction…….……...101

Figure 5.15. Plot of ln(% composition) versus $1/T$ for the reaction of $Mn(CO)_4(PPh_3)Br$ with PPh_3……...102

Figure 6.1. Calibration curve for $Mn(CO)_5Br$ in TCE using FTIRS at room temperature…….108

Figure 6.2. Calibration curve for $Mn(CO)_4(PPh_3)Br$ in TCE using FTIRS at room temperature…….109

Figure 6.3. Calibration curve for $Mn(CO)_3(PPh_3)_2Br$ in TCE using FTIRS at room temperature…….110

Figure 6.4. Arrhenius plot of the reaction of $Mn(CO)_4(PPh_3)Br$ with PPh_3 (1:17 mole equiv) in chloroform……..114

Figure 6.5. Arrhenius plot of the reaction of $Mn(CO)_4(PPh_3)Br$ with PPh_3 (1:17 mole equiv) in TCE……116

Figure 7.1. A ^{31}P NMR spectrum of a reaction between $Mn(CO)_4(PPh_3)Br$ and P(*p*-MeO-$C_6H_4)_3$ (1:1.4) taken after one minute of reaction at 60°C…….125

Figure 7.2. NMR spectra for the solventless reaction between $Mn(CO)_4(PPh_3)Br$ and P(*p*-MeO-$C_6H_4)_3$ (1:1.4) as followed by ^{31}P NMR spectroscopy at 60°C recorded after pre-determined periods……..127

Figure 7.3. ^{31}P NMR spectrum of a reaction between $Mn(CO)_4(PPh_3)Br$ and

P(p-MeO-C_6H_4)$_3$ (1:1.4) taken after 17 hours of reaction at 60°C. The expansion of the signals at 51 and 54 ppm is shown in the insert……128

Figure 7.4. ^{31}P NMR spectra generated from the solventless reaction of $Mn(CO)_4(P(p\text{-MeO-}C_6H_4)_3)Br$ with PPh_3 (1:2)……..……132

Figure 8.1. The solventless substitution of CO by solid phosphine……...……140

Figure 8.2. Plot of Kubelka-Munk units versus amount of $Mn(CO)_4(PPh_3)Br$ in KBr support using DRIFTS to check where deviation from linearity takes place due to the large amount of the metal complex used……...147

Figure 8.3. A plot of Kubelka-Munk units versus wavenumber for the solventless reaction between $Mn(CO)_4(PPh_3)Br$ and PPh_3 in KBr support to using DRIFTS……...……..149

Figure 8.4. Cartoon depicting the solventless reaction of $Mn(CO)_4(PPh_3)Br$:PPh_3 (1:1 mole ratio) in a KBr matrix……...150

Figure 8.5. Plot of ln(k) versus ln([$Mn(CO)_4(PPh_3)Br$]) for the reaction of $Mn(CO)_4(PPh_3)Br$ with PPh_3 while varying the amount of the metal complex and keeping the amount of PPh_3 constant……152

Figure 8.6. Plot of ln(k) versus ln([$Mn(CO)_4(PPh_3)Br$]) for the reaction of $Mn(CO)_4(PPh_3)Br$ with PPh_3 when varying the amounts of the metal complex and keeping the amount of PPh_3 constant…….……153

Figure 8.7. Cartoon depicting microscopic representation of the solventless reaction of $Mn(CO)_4(PPh_3)Br$ with PPh_3 (1:19 mol equiv) in KBr using the solvent method……..……..…….156

Figure 8.8. Cartoon showing the reaction of $Mn(CO)_4(PPh_3)Br$ with PPh_3 when fine KBr was used as a support……..157

Figure 8.9. Cartoon showing the reaction of $Mn(CO)_4(PPh_3)Br$ with PPh_3 when coarse KBr was used as a support……..157

Figure 8.10. The effect of phenyl substituents on the M-CO bond strengths of $Mn(CO)_4(L)Br$ (where L = para substituted arylphosphine)……..160

Figure 9.1. Heating plate design for the observation of solventless reactions……...…171
Figure 9.2. The reaction chamber……...172
Figure 9.3. Depiction of the reaction chamber placed under an optical microscope for the study of $Mn(CO)_4(PPh_3)Br$ to $Mn(CO)_3(PPh_3)_2Br$ under nitrogen……..……173
Figure 9.4. Pictures showing the solventless reaction of thoroughly mixed powders of $Mn(CO)_4(PPh_3)Br$ and PPh_3 (1:1 mol equivalent) at 60°C as seen through a an optical camera (resolution, 80× magnification)……..175
Figure 9.5. The relationship between microscopic visualisation and the extent of the solventless reaction of powdered $Mn(CO)_4(PPh_3)Br$ and PPh_3 (1:1 mol equivalent) at 60°C using optical microscopy and FTIRS……....177
Figure 9.6. Picture showing the arrangement of $Mn(CO)_4(PPh_3)Br$ and PPh_3 crystals under a microscope before thermal experimentation…….179
Figure 9.7. The reaction sequence of the thermal transformation of crystallised $Mn(CO)_4(PPh_3)Br$ with PPh_3 at 42°C observed using an optical microscope……...180
Figure 9.8. Pictures showing the positioning of crystals of $Mn(CO)_4(PPh_3)Br$ and PPh_3 before the reactions was initiated and at the end of thermal experimentation at 42°C as viewed under an optical microscope…….…..183
Figure 9.9. Pictures showing the reaction of $Mn(CO)_4(PPh_3)Br$ and PPh_3 at 42°C as viewed by an optical microscope after another ligand crytal was placed on the product-coated metal complex crystal…….184
Figure 9.10. The reaction of $Mn(CO)_4(PPh_3)Br$ with $P(p\text{-}Me\text{-}C_6H_4)_3$ at 70°C under an optical microscope……...186
Figure 10.1. ORTEP diagram of $Mn(CO)_4(PPh_3)Br$ [**3**] depicting two units making up the unit cell with 30% probability thermal ellipsoid……..195
Figure 10.2. ORTEP diagram of $Mn(CO)_4(PPh_3)Br$ [**3**] depicting one of two

units comprising the unit cell with 30% probability thermal ellipsoid……195
Figure 10.3. ORTEP diagram of $Mn(CO)_4(PPh_3)Br$ [**3**] depicting the other unit of the unit cell with 30% probability thermal ellipsoid……...196
Figure 10.4. ORTEP diagram of $Mn(CO)_3(PPh_3)_2Br$ [**8**] with 30% probability thermal ellipsoid……...198
Figure 11.1. Ionic sodium formate displaying the uncoordinated carboxylate Ligand……..208
Figure 11.2. Structure of lithium acetate displaying the monodentate bonding mode of the carboxylate ligand……208
Figure 11.3. The two types of bidentate bridging modes exhibited by inorganic compounds containing the carboxylate ligand…….209
Figure 11.4. The four types of bidentate bridging modes exhibited by inorganic compounds containing the carboxylate ligand…….209
Figure 11.5. Structure of sodium benzoate [R = C_6H_5 (**a**), p-C_6H_4-NO_2 (**b**), p-C_6H_4-NH_2 (**c**)] used for the synthesis of zirconium carboxylate complexes……211
Figure 11.6. Structure of $(\eta^5\text{-}C_5H_5)_2ZrCl(RCOO)$, R = C_6H_5, p-C_6H_4-NO_2, p-C_6H_4-NH_2……..212
Figure 11.7. ^1H NMR spectrum of $(\eta^5\text{-}C_5H_5)_2ZrCl(C_6H_5\text{-}COO)$……..……..213
Figure 11.8. An ORTEP diagram of $(\eta^5\text{-}C_5H_5)_2ZrCl(HCOO)$, **14**, showing one unit of 4 that makes up the unit cell…….217
Figure 11.9. An ORTEP diagram of $(\eta^5\text{-}C_5H_5)_2ZrCl(RCOO)$, R = NO_2, **15**, showing the positioning of two of 8 units that made up unit cell……218
Figure 11.10. An ORTEP diagram of $(\eta^5\text{-}C_5H_5)_2ZrCl(RCOO)$, R = NO_2, **15**, showing one of 8 units that made up unit cell……..219
Figure 11.11. An ORTEP diagram of $(\eta^5\text{-}C_5H_5)_2ZrCl(RCOO)$, R = NO_2, **15**, showing the other unit of 8 units that made up unit cell……..219
Figure 11.12. Structure of $(\eta^5\text{-}MeC_5H_4)ZrCl(\alpha\text{-}C_{10}H_7COO)$……..……..220
Figure 11.13. Structure of $(\eta^5\text{-}C_5H_5)_2ZrCl(FcCO(CH_2)_2CO_2)$……..……221

Figure 12.1. Schematic representation of an assembled autoclave used for the isomerisation of hexenes……..240

LIST OF SCHEMES

Scheme 2.1. Dimerisation of *N*-acyl- and *N*-acyloxy-3,5-methoxycarbonyl-4-phenyl-1,4-dihydropyridines to form a tetraasteranes in the solid state……..……...14

Scheme 2.2. Solventless Knoevenagel condensation of aromatic aldehydes with barbituric acids…….……..15

Scheme 2.3. Microwave assisted solid state formation of thiozoles…….…….17

Scheme 2.4. Solventless synthesis of N-benzyl-N-glycosylhydroxylamines from Sugars…….18

Scheme 2.5. The solventless ruthenium catalysed formation of terminal alkenyldeyde from terminal alkynes and allyl alcohol……..…24

Scheme 2.6. Linkage isomerism of nitrito to nitro of pentaammine nitritoCobalt(III) in the presence of heat……25

Scheme 2.7. Solventless isomerisation of *ttt*-$RuCl_2(RNC)_2(PPh_3)_2$ to *cct*-$RuCl_2(RNC)_2(PPh_3)_2$……..26

Scheme 2.8. Isomerisation of *diag*- and *lat*-$(\eta^5\text{-}C_5H_4R)Re(CO)(L)X_2$ (L = PPh_3, $POPh_3$, PCy_3, X = Cl, Br, I) in the absence of solvents…….27

Scheme 2.9. Combined Berry-tunstile isomerisation mechanism for $CpML_4$ complexes……..28

Scheme 2.10. Migratory insertion of carbon monoxide using Lewis acids in the absence of solvents……29

Scheme 2.11. Migratory insertion reactions using pohsphines, phosphites and $AsPh_3$……..31

Scheme 2.12. Proposed mechanism of the solventless transformation of $(\eta^5\text{-}C_5H_5)M(CO)_3Me$, (M= Mo, W), using solid phosphines……32

Scheme 2.13. Migratory insertion reaction when CO is used……...……...34

Scheme 2.14. Migratory insertion reaction when CO is used……...…...……35

Scheme 2.15. Solid state synthesis of mono- and disubstituted pyridine and

pyrimidine ferrocenyl derivatives……..36
Scheme 2.16. Solid state substitution of halogen ligands of rhenium complexes under thermal conditions……37
Scheme 2.17. Solid state substitution reaction of a tungsten complex using Wilkinson's catalyst under thermal conditions……..39
Scheme 4.1. The general reaction scheme for the reaction of $Mn(CO)_5X$ with monodentate tertiary phoshines, phosphites and arsines in solution……..…….62
Scheme 4.2. The proposed solution reaction mechanism for the substitution reaction of the metal complex, $Mn(CO)_5X$ with a ligand, L……..63
Scheme 4.3. The conversion of manganese decacarbonyl to manganese(I) pentacarbonyl bromide using oxidative cleavage with bromine in chloroform…….…….70
Scheme 4.4. The formation of $Mn_2(CO)_8Br_2$ from the treatment $Mn(CO)_5Br$ using different synthetic methods……..71
Scheme 4.5. Synthesis of *cis*-tetracarbonylmanganese(I) bromides from $Mn(CO)_5Br$……72
Scheme 4.6. Synthesis of *trans*-$Mn(CO)_3L_2Br$ from $Mn(CO)_5Br$…….……74
Figure 5.1. The solventless substitution of CO by substituted solid phosphine ligands, L, in manganese carbonyl complexes……...85
Scheme 5.2. The formation of *trans*-$Mn(CO)_3(PPh_3)_2Br$ from $Mn(CO)_5Br$ with PPh_3……92
Scheme 6.1. Formation of *cis*-$Mn(CO)_3LL'X$ from the substitution reaction between $Mn(CO)_4LX$ and L' in solution……..107
Scheme 7.1. Suggested reaction pathway for the formation of $Mn(CO)_4((p\text{-}MeOPh)_3)Br$ from the reaction of $Mn(CO)_4(PPh_3)Br$ with PPh_3P_3 (1:1.4) as followed by ^{31}P NMR spectroscopy……127
Scheme 7.2. Mechanism of the solventless reaction between $Mn(CO)_4(PPh_3)Br$ and PPh_3 as neat reagents as followed by ^{31}P NMR spectroscopy……..133
Scheme 9.1. The formation of the 5-coordianate intermediate by the partial

carbon monoxide dissociation from the metal complex in the presence of heat……...….181

Scheme 11.1. Synthesis of sodium carboxylates by the reaction of substituted benzoic acids with sodium metal lumps in ethanol……..215

Scheme 11.2. Synthesis of carboxylatochlorobis(cyclopentadienyl)zirconium(IV) complexes……216

Scheme 12.1. The conversion of an alkene to a metal alkyl using a metal hydride……..…230

Scheme 12.2. Formation of terminal alkylzirconium complexes via hydrozirconation of hexene isomers……230

Scheme 12.3. Proposed hydrozirconation isomerisation of *trans*-3-hexene to *trans*-2-hexene and eventually forming terminal hexylzirconium complex via olefin insertion and β-elimination reactions……231

Scheme 12.4. The recovery of terminal olefins using β-abstraction reagent from alkylzirconium complexes……...232

Scheme 12.5. Two pot displacement of α-olefins from the substituted alkylzirconium(IV) complexes using olefins of different chain lengths (R' and R")……..233

Scheme 12.6. The non-reactivity of propylene with the carbon-13 labelled chlorobis(cyclopentadienyl)propylzirconium(IV) complex in deuterated benzene……...233

Scheme 12.7. Synthesis of substituted cyclopentadienes……...……247

Scheme 12.8. Synthesis of dichlorobis(η^5-C_5H_4R)zirconium(IV) complexes using *n*-BuLi in THF……248

Scheme 12.9. Synthesis of chlorobis(η^5-cyclopentadienyl)hydridozirconium(IV) complex……249

Scheme 12.10. Synthesis of chlorobis(η^5-cyclopentadienyl)hexylzirconium(IV) complex……250

Scheme 12.11. Proposed pathway for the formation of trans-2-hexene from 1-hexene using Na-Al_2O_3 under reflux……251

Scheme 12.12. The reaction of zirconocene with *n*-BuLi and PEt_3 to generate

the pre-catalyst, (η^5-$C_5H_5)_2Zr(PEt_3)(C_4H_9)$ complex, required for olefin isomerisation……258

Scheme12.13. The reaction of zirconocene with *n*-BuLi and PPh_3 to generate the pre-catalyst, (η^5-$C_5H_5)_2Zr(PPh_3)(C_4H_9)$, required for olefin isomerisation…….……...261

Scheme 12.14. The formation of bis(η^5-cyclopentadienyl)dibutylzirconium(IV) complex as a pre-catalyst for the isomerisation of internal hexene isomers to 1-hexene in toluene……..……..262

Scheme 12.15. The attempted transformation of (η^5-$C_5H_5)_2ZrCl_2$ with NaH in toluene to generate a pre-catalyst for the isomerisation of internal hexene isomers to 1-hexene…….268

Scheme 12.16. The synthesis of bis(cyclopetadienyl)dihydridozirconium(IV) complex as a pre-catalyst for the isomerisation of internal hexene isomers to 1-hexene……..……...269

Scheme 12.17. The synthesis of substituted dibutylzirconocene complexex and their use as catalyst for the isomerisation of internal hexene isomers to hex-1-ene……..……..271

LIST OF TABLES

Table 2.1. Rate laws of solid state reactions…….10

Table 2.2. Reaction conditions and yields for the solventless Knoevenagel condensation of aromatic aldehydes with barbituric acids and comparative solution conditions……...…….15

Table 2.3. The solventless ruthenium catalysed formation of terminal alkenyldeyde from terminal alkynes and allyl alcohol using three methodologies……...…….24

Table 4.1. Carbonyl stretching frequencies of the complex, $Mn(CO)_5Br$, as found experimentally compared to the literature values……..……..70

Table 4.2. Data for the synthesis of $Mn_2(CO)_8Br_2$ from $Mn(CO)_5Br$……..…...71

Table 4.3. Synthesis of *cis*-tetracarbonylmanganese(I) bromides from $Mn(CO)_5Br$, and the respective melting points and carbonyl stretching frequencies in cm^{-1}……...…….73

Table 4.4. Characteristics of *trans*-$Mn(CO)_3L_2Br$ from $Mn(CO)_5Br$ as analysed using FTIRS……...74

Table 4.5. Characterisation o f $Mn(CO)_4(L)Br$ complexes….……...78

Table 4.6. Characterisation o f $Mn(CO)_4(L)_2Br$ complexes……..79

Table 6.1. The kinetic data for the reaction of $Mn(CO)_4(PPh_3)Br$ with PPh_3 (1:10 mole ratios) in TCE conducted at 70°C……..112

Table 6.2. Kinetic parameters of the reaction of $Mn(CO)_4(PPh_3)Br$ with PPh_3 (1:17 mole equiv) in chloroform……..114

Table 6.3. Kinetic parameters of the reaction of $Mn(CO)_4(PPh_3)Br$ with PPh_3 (1:17 mole ratio) in TCE…….....116

Table 6.4. Activation parameters for the reaction between $Mn(CO)_4(PPh_3)Br$ and PPh_3 to produce $Mn(CO)_3(PPh_3)_2Br$ as followed by FTIRS using both solvent and solventless methods……..……..117

Table 7.1. ^{31}P NMR of products and reagents involved in the solventless reaction of $Mn(CO)_4(PPh_3)Br$ with P(*p*-MeO-$C_6H_4)_3$ [$CDCl_3$; TMS reference]……...……..123

Table 7.2. The solventless reaction between $Mn(CO)_4(PPh_3)Br$ and $P(p\text{-}MeO\text{-}C_6H_4)_3$ (1:1.4) as followed by ^{31}P NMR spectroscopy at 60°C…….126

Table 7.3. The solventless reaction between $Mn(CO)_4(PPh_3)Br$ and $P(p\text{-}MeO\text{-}C_6H_4)_3$ (1:3) as followed by ^{31}P NMR spectroscopy……..…129

Table 7.4. The solventless reaction between $Mn(CO)_4(P(p\text{-}MeO\text{-}C_6H_4)_3)Br$ and PPh_3 (1:2) as followed by ^{31}P NMR……131

Table 8.1. Solventless reactions performed with $Mn(CO)_4(PPh_3)Br$ and varying amounts of PPh_3……...……...142

Table 8.2. Data showing the rate constants for the reaction of $Mn(CO)_4(PPh_3)Br$ with PPh_3 when varying the amount of the ligand (PPh_3) at 60°C…….…..149

Table 8.3. Data showing the rate constants for the reaction of $Mn(CO)_4(PPh_3)Br$ with PPh_3 when varying the amount of the metal complex while keeping the amount of the ligand (PPh_3) constant at different temperatures……..…..151

Table 8.4. Kinetic parameters of the solventless reaction of $Mn(CO)_4(PPh_3)Br$ with PPh_3 obtained using DRIFTS……..154

Table 8.5. Activation energy for the solventless reaction between $Mn(CO)_4(PPh_3)Br$ and PPh_3 (1:19mol ratio) in KBr support at various temperatures using DRIFTS, (fine, intermediate and coarse grained powder mixture samples)……..156

Table 8.6. The rate constants of the solventless reaction of $Mn(CO)_4(PPh_3)Br$ with PPh_3 (1:19mol ratio) in different support fine powders at 70°C using DRIFTS……..……158

Table 8.7. Activation parameters of the solventless reaction of manganese metal complexes with functionalised phosphines using DRIFTS……...161

Table 8.8. pKa values of tertiary phosphines used during the study…….…….....163

Table 10.1. Crystal data and structure refinement for **3**……..199

Table 10.2. Crystal data and structure refinement for **8**……..200

Table 10.3. Selected crystallographic structural data for **3** and **8**……...201

Table 10.4. Comparison of the crystal data for $C_{22}H_{15}BrMnO_4P$ and $C_{22}H_{15}ClMnO_4P$……...202

Table 10.5. Comparison of the crystal data for $C_{39}H_{30}BrMnO_3P_2$ and $C_{39}H_{24}BrCl_6MnO_3P_2.CHCl_3$……203

Table 11.1. Selected crystallographic structural data for **14** and **15**……...216

Table 11.2. Crystal data and structure refinement for **14**……222

Table 11.3. Crystal data and structure refinement for **15**……223

Table 12.1. The analysis of the dichlorobis(η^5-substitutedcyclopentadienyl)-zirconium(IV) complexes obtained using *n*-BuLi in THF……...248

Table 12.2. Hexene isomers obtained when 1-hexene was stirred with Na-Al_2O_3 for 16 hours at room temperature, as analysed using a GC….251

Table 12.3. Hexene isomers obtained when 1-hexene was stirred with KO^{t}Bu in DMSO at various conditions……252

Table 12.4. Hexene isomers obtained when 1-hexene was stirred with Rh(III) chloride trihydrate as a catalyst for 24 under reflux, as seen using a GC……253

Table 12.5. Thermodynamic isomer ratios of straight chain hexene isomers at 55° and 110°C as generated by ASPEN……..253

Table 12.6. Isomerisation of 1-hexene to internal hexene isomers using chlorobis(η^5-cyclopentadienyl)hexylzirconium(IV) complex in toluene at various temperatures and pressures……...……..254

Table 12.7. Isomerisation of *trans*-2-hexene to 1-hexene using chlorobis(cyclopentadienyl)hexylzirconium(IV) complex as analysed using GC……...255

Table 12.8. Isomerisation of internal hexene isomers to 1-hexene using chlorohexylbis(cyclopentadienyl)zirconium(IV) complex……..256

Table 12.9. Isomerisation of internal hexene isomers cocktail using substituted zirconium metallocenes in toluene at 150°C and 50 bar for 24 h……..257

Table 12.10. Isomerisation of internal hexene cocktail to 1-hexene in toluene using $(\eta^5\text{-}C_5H_5)_2Zr(PEt_3)(C_4H_9)$ as a catalyst at various temperatures……259

Table 12.11. Isomerisation of internal hexene cocktail to 1-hexene in toluene using $(\eta^5\text{-}C_5H_5)_2Zr(PEt_3)(C_4H_9)$ as a catalyst at -78°C……...260

Table 12.12. Isomerisation of internal hexene cocktail to 1-hexene in toluene using $(\eta^5\text{-}C_5H_5)_2Zr(PPh_3)(C_4H_9)$ as a catalyst at 78°C……261

Table 12.13. Isomerisation of internal hexene cocktail (4.0mmol, 0.5cm^3) using Cp_2ZrCl_2 and 1.4M *n*-BuLi in toluene…….……..263

Table 12.14. Isomerisation of internal hexene cocktail (16.0mmol, 2.0cm^3) using Cp_2ZrCl_2 and 1.4 M *n*-BuLi in toluene……..264

Table 12.15. Isomerisation of internal hexene isomers (0.5 cm^3) using Cp_2ZrCl_2 (102 mg) and 1.4 M *n*-BuLi in the presence of dispersed sodium in alumina (Na-Al_2O_3) for the generation of the active catalyst in toluene……265

Table 12.16. Isomerisation of internal hexene isomers (0.5 cm^3) using Cp_2ZrCl_2 (104 mg) and 1.4 M *n*-BuLi in the presence of dispersed sodium in sodium chloride (Na-NaCl) for the generation of the active catalyst in toluene……..265

Table 12.17. Isomerisation of internal hexene isomers using Cp_2ZrCl_2 (105 mg, 359 μmol) and *n*-BuLi (0.7 mmol, 0.5 cm^3) in the presence of dispersed sodium in lithium chloride (Na-LiCl) at –78°C for the generation of the active catalyst in THF……..……266

Table 12.18. Isomerisation of internal hexene isomers using 1.4 M *n*-BuLi (0.5 cm^3) at -78°C in toluene (no zirconocene dichloride utilised)…….267

Table 12.19. Isomerisation of *cis*-2- hexene (4.0 mmol, 0.5 cm^3) using Cp_2ZrCl_2 and *n*-BuLi at –78°C for the generation of the active catalyst in toluene……..……..267

Table 12.20. Isomerisation of internal hexene isomers (1.0 cm^3) using Cp_2ZrCl_2 (101 mg) and NaH (27.6 mg, 2 mol equiv) in toluene at various temperatures……268

Table 12.21. Isomerisation of internal hexene isomers (0.5 cm^3) using Cp_2ZrH_2 generated *in situ* from Cp_2ZrCl_2 and $LiAlH_4$ in toluene at various experimental conditions……...……...269

Table 12.22. Isomerisation of internal olefins isomers using Cp_2ZrH_2 generated *in situ* from Cp_2ZrCl_2 and $LiAlH_4$ at elevated temperatures and pressures……..……270

Table 12.23. The use of $(Me\text{-}C_5H_4)_2ZrBu_2$ generated *in situ* from *n*-BuLi and $(Me\text{-}C_5H_4)_2ZrCl_2$ for the isomerisation of internal hexenes in toluene……..272

Table 12.24. The use of $(^{i}Pr\text{-}C_5H_4)_2ZrBu_2$ generated *in situ* from *n*-BuLi and $(^{i}Pr\text{-}C_5H_4)_2ZrCl_2$ for the isomerisation of internal hexenes in toluene…….……272

Table 12.25. The use of $(^{t}Bu\text{-}C_5H_4)_2ZrBu_2$ generated *in situ* from *n*-BuLi and $(^{t}Bu\text{-}C_5H_4)_2ZrCl_2$ for the isomerisation of internal hexenes in toluene……..……273

Table 12.26. The use of $(SiMe_3\text{-}C_5H_4)_2ZrBu_2$ generated *in situ* from *n*-BuLi and $(SiMe_3\text{-}C_5H_4)_2ZrCl_2$ for the isomerisation of internal hexenes in toluene…….……274

Table 12.27. The use of $(Et\text{-}C_5H_4)_2ZrBu_2$ generated *in situ* from *n*-BuLi and $(Et\text{-}C_5H_4)_2ZrCl_2$ for the isomerisation of internal hexenes in toluene……..274

Table 12.28. Isomerisation of internal hexene isomers using $(Et\text{-}C_5H_4)_2ZrBu_2$ as a catalyst in toluene at -78°C……...275

LIST OF ABBREVIATIONS

AFM	Atomic force spectroscopy
CCl_4	Carbon tetrachloride
$CDCl_3$	Deuterated chloroform
$CHCl_3$	Chloroform
Cp_2ZrCl_2	Dichlorobis(η^5-cyclopentadienyl)Zirconium(IV) complex
CSD	Cambridge structural database
DCM	Dichloromethane
DMSO	Dimethyl sulfoxide
DRIFTS	Diffuse Reflectance infrared Fourier transform spectroscopy
DSC	Differential scanning calorimeter
ESR	Electron spin resonance
EtOH	Ethanol
FID	Flame ionisation detector
FTIRS	Fourier transform infrared spectroscopy
GC	Gas chromatography
HDPE	High-density polyethylene
IR	Infrared
KBr	Potassium bromide
KO^tBu	Potassium tertiary butoxide
LLDPE	Linear low-density polyethylene
MeOH	Methanol
n-BuLi	Butyl lithium
NMR	Nuclear magnetic resonance
PPh_3	Triphenylphosphine
ppm	Parts per million
PTC	Programmable temperature controller

SHOP	Shell higher olefin processes
TCD	Thermal conductivity detector
TCE	1,1,2,2-Tetrachloroethane
THF	Tetrahydrofuran
TLC	Thin layer chromatography
XRD	X-ray diffraction
ΔH	Enthalpy change
ΔS	Entropy change

CHAPTER 1: INTRODUCTION

Environmental pollution due to hazardous chemicals has reached alarming proportions. Greenhouse gas emissions have also reached a point that threatens the existence of many species including humans. These problems have forced the chemistry industry to look at sustainable chemistry. To this end, finding alternative reaction pathways that minimise chemical waste and possibly eliminate auxiliary reagents like solvents, is among the key development areas. The design and use of catalysts and agents that maximise atom economy are also major development areas.

Solventless reactions potentially eliminate the need to use solvents and should be used whenever possible. The aim of the study was to investigate solventless reactions of manganese carbonyl complexes. These organometallic compounds are relatively air stable making analysis easy. Another objective was to investigate an atom economical reaction, the isomerisation of internal hexene isomers to hex-1-ene using substituted *bis*(cyclopentadienyl)zirconium dichloride metallocenes as pre-catalysts. As such the thesis is broadly made-up of two sections; (i) solventless reactions of manganese carbonyl complexes and (ii) olefin catalysis using substituted *bis*(cyclopentadienyl)zirconium dichloride metallocenes.

This thesis begins with Chapter two, a literature survey of solventless reactions in organic, inorganic and organometallic chemistry. The chapter begins by stating the principles of green chemistry. Solid-state and melt reactions are then defined before the thesis focuses on published information related to these solventless reaction topics.

Chapter three deals with the general experimental procedures used during the investigations carried out in the thesis. The experimental techniques used during the investigation are also briefly explained.

Chapter four details the synthesis of a range of manganese carbonyl complexes. Most of the methods used were the well-established solution protocols. Analysis of the products was done to ensure that they were the envisaged compounds.

Chapter five mainly deals with the use of FTIRS to investigate the solventless reaction of $Mn(CO)_4(PPh_3)Br$ with PPh_3 (as neat reagents) to form $Mn(CO)_3(PPh_3)_2Br$. The reaction temperature chosen was lower than the melting points of both the metal complex and ligand. Kinetic parameters for the reaction were obtained.

To compare the kinetic parameters obtained, it was necessary to compare the data with literature values for the same reaction. Chapter six deals with the reaction between $Mn(CO)_4(PPh_3)Br$ and PPh_3 using $CHCl_3$ and TCE as solvents.

The use of ^{31}P NMR spectroscopy to study the products of the solventless reaction of $Mn(CO)_4LBr$ with L' is detailed in chapter seven. The investigation helped to deduce some missing links related to the mechanism of the reaction. Indeed this section revealed a reaction pathway that was not reported in the solution protocols in the literature.

Chapter eight deals with the use of DRIFTS to study the reaction between $Mn(CO)_4LBr$ with L [L = P(*p*-C_6H_4-R)$_3$, R = H, F, Cl, Br, Me, MeO] using both fine powder and solvent methods. The effect of the matrix on the rate of the reaction was also investigated.

The well-behaved kinetic data obtained for the solventless reaction between $Mn(CO)_4LBr$ with L were unexpected and initially difficult to explain. There was a need to use another technique that would shed some light as to how the reaction took place. Chapter nine details an optical microscopy study between $Mn(CO)_4LBr$ with L or L'. The results of the investigation using optical miscroscopy convincingly confirmed the mechanism proposed in chapter seven.

Chapter ten deals with the X-ray crystallographic data for $Mn(CO)_4(PPh_3)Br$ and $Mn(CO)_3(PPh_3)_2Br$ complexes. The data generated were used to compare the complex with related reported structures listed in the literature.

The reaction, η^5-$C_5H_5)_2ZrCl_2$ + Na^+RCOO^-, R = C_6H_5, p-C_6H_4-NO_2, p-C_6H_4-NH_2 → (η^5-$C_5H_5)_2ZrCl(RCOO)$ + NaCl, is detailed in Chapter 11. A single crystal XRD study of (η^5-$C_5H_5)_2ZrCl(RCOO)$, R = C_6H_5, p-C_6H_4-NO_2 is also included.

Chapter twelve details investigations made to isomerise internal hexenes to hex-1-ene using substituted *bis*(cyclopentadienyl)zirconium dichloride metallocenes as pre-catalysts.

The thesis concludes with Chapter thirteen that summarises the conclusions of the study.

The structure of the thesis is such that reaction schemes, figures and tables are part of the body of the thesis but detailed information or tables are listed at the end of each chapter as appendixes. List of figures, schemes and tables is found in the preliminary section of the thesis.

CHAPTER 2: LITERATURE REVIEW

2.1. GREEN CHEMISTRY

It has been suggested that the turn of the 21st century has witnessed a paradigm shift away from traditional chemistry research[1]. The shift has been brought about by the rapid environmental pollution that the globe has been subjected to since the beginning of the industrial revolution[2,3]. The consequence of the pollution has been unprecedented plant and animal extinction that has worsened in the past decades[4]. Water pollution has resulted in the depletion of both fresh water and ocean fish stock, thus leaving less of these resources for human consumption[5]. Emission of greenhouse gases potentially can also result in massive extinction of plant and animal lives due to global warming[6].

As early as the 1990s, a new concept was introduced in the chemistry language known as green (sustainable) chemistry[7,8,9]. Green and sustainable chemistry is largely concerned with the development of processes and technologies that result in more efficient chemical reactions that generate less waste and less environmental emissions. Thus, instead of limiting risk by controlling our exposure to hazardous chemicals, green chemistry attempts to reduce and preferentially eliminate hazards[10].

There are twelve principles of green chemistry that have been set down by Anastas and Warner[11].

1. Prevention

   It is better to prevent waste than to treat or clean it up after it has been created.
2. Atom Economy

   Synthetic methods should be designed to maximise the incorporation of all materials used in the process into the final product
3. Less Hazardous Chemical Synthesis

Whenever practicable, synthetic methods should be designed to use and generate substances that possess little or no toxicity to people and the environment.

4. Designing Safer Chemicals

   Chemical products should be designed to effect their desired function while minimising their toxicity.

5. Safer Solvents and Auxiliaries

   The use of auxiliary substances (e.g. solvents or separation agents) should be made unnecessary whenever possible and innocuous when used.

6. Design for Energy Efficiency

   Energy requirements of chemical processes should be recognised for their environmental and economic impacts and should be minimised. If possible, synthetic methods should be conducted at ambient temperature and pressure.

7. Use of Renewable Feedstock

   A raw material or feedstock should be renewable rather than depleting whenever technically and economically practicable.

8. Reduce Derivatives

   Unnecessary derivatisation (use of blocking groups, protection/de-protection and temporary modification of physical/chemical process) should be minimised or avoided, if possible, because such steps require additional reagents and can generate waste.

9. Catalysis

   Catalytic reagents (as selective as possible) are superior to stoichiometric reagents.

10. Design for Degradation

    Chemical products should be designed so that at the end of their function they break down into innocuous degradation products and do not persist in the environment.

11. Real-time Analysis for Pollution Prevention

Analytical methodologies need to be further developed to allow for real-time, in process monitoring and control prior to the formation of hazardous substances.

12. Inherently Safer Chemistry for Accident Prevention
    Substances and the form of a substance in a chemical process should be chosen to minimise the potential for chemical accidents, including releases, explosions and fires.

Chemistry, being defined as a central science, is one of the keys to finding ways to drive green and sustainable development[12]. It is an integrated study in the chemical, biological, physical and engineering fields. Even the newer field of study, materials science, that includes nano materials[13,14,15] and hard materials[16] can be approached using green chemistry principles.

As this thesis is centred on green chemistry in particular an exploration of synthetic routes that (i) require no solvents or (ii) may be catalytic, examples of some green chemistry approaches to synthesis are given below. The survey is not intended to be comprehensive but rather to include some of the novel approaches or findings possible using the philosophy of green chemistry.

While much of thesis relates to issues of synthesis using solvent free conditions, another issue dealt with in this thesis is atom economy. In particular the latter part of the thesis will deal with issues of converting an available internal olefin into a terminal olefin via green chemistry approach. The section deals with a recycling of chemicals rather than methodologies for making them. To that effect attempts to use catalysts to achieve this will be described.

The work presented herein thus provides examples in some of the disciplines in which researchers have applied themselves to finding innovative ways to produce useful products in a sustainable way. Particular focus shall be placed on examples from

organometallic chemistry, organic chemistry, and inorganic chemistry. In particular, the survey below deals with reactions that take place in the absence of solvents.

Two reaction types of solventless reaction can be envisaged, (i) solid-state and (ii) melt reactions.

(i). Solid-state Reactions

The study of reactions involving the synthesis and inter-conversion of solids is an important aspect of solid-state chemistry[17]. The study of solid-state reactions aids in our understanding of the influence of structure and imperfections on the chemical reactivity of solid materials. Hence, the identification of factors that govern solid-state reactions is of critical importance in understanding this reaction type[18].

Solid-state reactions differ from those that take place in fluid media in two important respects. Firstly, solid-state reactions depend to a large extent on the arrangement of the chemical constituents in a crystal in contrast to reactions in gaseous and liquid media that depend on the reactivity and concentrations of chemical reagents. The separation distances and the orientations of reactants in the solid(s) determine the product(s). Secondly, the reactants are fixed in position for reactions in the solid-state such that reactivities are governed by the crystal structures and crystal defects of the constituents rather than their chemical reactivity. This means that the reactants crystal lattices control both the kinetic features of the reaction and the nature of products formed.

In general then, most solid-state reactions can be regarded as topochemically controlled reactions[19]. Topochemically controlled reactions are those where the reactivity is controlled by the crystal structure rather than by the chemical constituents of the crystal(s). It should be understood that the topochemical control of a reaction product is analogous to kinetic control of reactions in solution. This means that the product formed is a ‘kinetic’ rather than a ‘thermodynamic’ product, dictated by the reaction pathway made possible by the crystal lattice. Taking the above points into consideration, it is safe

to conclude that solid-state reactions are controlled by crystal chemistry. Solid-state reactions can also be referred to as topotactic reactions even when the atomic arrangement in the reactant crystal(s) remain(s) largely unaffected during the course of the reaction, provided that the crystal changes dimension in one or more directions.

Solid-state reactions are heterogeneous processes with clear boundaries between reactant and product phases. The initiation stage of a solid-state reaction is called a nucleation stage, signalling the formation of a new product made visible by a formation of a boundary line between reactants and products. Nucleation of reactant crystals usually begins at the surface of a crystal. In the case of a single crystal reaction, nucleation begins where the resulting product would not be enveloped by the reactants. The reaction continues at the boundary between reactant and product in a process called a growth stage, resulting in the reduction of reactant(s) phase and an increase in the product(s) phase.

The method of compound preparation (prehistory) and handling influences both surface area and the number and types of crystal defects in a crystal. The rate of a solid-state reaction can thus depend on how the sample was prepared. This introduces a variable in measuring the kinetics of such reactions. It also means that the same sample, prepared by two different methods, may result in two different reaction rates in the solid-state, a situation not found in the fluid media. Thus, solid-state kinetic data should be treated with great circumspection and significant meaning and interpretation should be avoided until other complementary data can substantiate the process proposed by the kinetic data.

Furthermore, the rate of nuclei growth is influenced by the geometry of the sample. This means that crystal morphologies play a critical role in the rate. Thus knowledge of crystal structures as well as their morphologies must be known with great certainty if their kinetics is to be fully deduced.

Solid-state reactions are generally of two types[20]:

1. Reactions between neat reactants
2. Reactions between supported reagents on solid mineral supports in dry media after impregnation e.g. onto compounds of silica, alumina or clays

Solid-state reactions between neat reactants can be sub-classified into the following categories[21];

(a) solid $\rightarrow$ products, as in decomposition and polymerisation reactions brought about by thermal or photochemical activation.
(b) solid + gas $\rightarrow$ products, as in oxidation and insertion reactions
(c) solid + solid $\rightarrow$ products, as in the formation of inorganic complex oxides from simpler components and composite materials
(d) solid + liquid $\rightarrow$ products, as in intercalation
(e) reactions of solid surfaces.

Solid-state reactions may involve one or more of the following elementary (rate determining) steps[21]:

(i) adsorption (and desorption) of gaseous species on the solid surface
(ii) chemical reaction on an atomic scale
(iii) nucleation of a new phase
(iv) transport phenomena through solids

In addition, external factors such as temperature, ambient atmosphere, pressure, and irradiation affect the reactivity of substances in the solid-state[21]. 'Internal' factors like particle size, gas atmosphere and foreign additives affect the rate of solid-state reactions. In heterogeneous catalysis, an increase in reactivity is accompanied by a decrease in particle size. Gas atmosphere can have significant effects on reactivity, demonstrated by the fact that the formation of a spinel like $ZnFe_2O_4$ is favoured in the presence of air rather than a nitrogen atmosphere. Doping with foreign additives has been found to affect reaction rates as shown by the reaction between ZnO and $CuSO_4$ (see below) that is favoured by doping ZnO with Li_2O[21].

$$ZnO + CuSO_4 \rightarrow ZnSO_4 + CuO$$

Reactions in the solid-state are described by rate laws that are different from those in the fluid media. The concentration term found in solution kinetics has no meaning in heterogeneous system and particularly in the solid-state. Consequently, rate laws of solid-state reactions are described in terms of the fraction of reaction, α. The symbol, α, denotes the quantity of reacted material divided by the original quantity of the sample. **Table 2.1** below shows the most common reaction rate laws in the solid-state. The rate laws and their application to solid-state reactions are described in detail elsewhere[22,23,24,25,26]. The method of varying the initial concentrations of reactants in order to establish rate laws, which are of great importance in solution studies, is not possible in solid-state reactions. The choice of the rate law that fits the data is therefore difficult to establish.

Table 2.1. Rate laws of solid-state reactions[27]

Description	Integrated form of rate law
Diffusion control, one dimension	$\alpha^2 = (k/x^2)t$
Diffusion control, two dimensions	$(1-\alpha)\ln(1-\alpha) + \alpha = (k/r^2)t$
Diffusion control, three dimensions	$(1-2\alpha/3) - (1-\alpha)^{2/3} = (k/r^2)t$
Phase boundary control, two dimensions	$(1-\alpha)^{1/2} = 1-kt$
Phase boundary control, three dimensions	$(1-\alpha)^{1/3} = = 1-kt$
First order (random nucleation)	$\ln(1-\alpha) = -kt$
Nucleation and growth, two dimensions	$\ln(1-\alpha) = -kt^2$
Nucleation and growth, three dimensions	$\ln(1-\alpha) = -kt^3$

Mechanisms for solid-state reactions of coordination compounds have often been formulated based on comparison of activation parameters for a series of compounds.

However, there are problems associated with kinetic parameter interpretation in the solid-state because of the problems related to finding the correct kinetic descriptions.

If kinetic parameters and rate laws derived from solid-state reaction are to have meaning, then other experiments must be conducted to support the rate law. It is through such studies that other features of the reaction emerges that either support or refute a proposed mechanism. An expansion on the meaning of mechanism in inorganic chemistry is given in **Section 2.4**.

(ii). Melt Reactions

Diffusion is an important physical phenomenon that is essential for the propagation of a reaction. The reacting entities must be brought into close contact for a reaction to take place and the product formed removed so that further reaction can take place. Reactions taking place in the gaseous and liquid states have the advantage in that the diffusion rates are higher. Sometimes reactions in the absence of solvents take place in the melt and this permits migration of reagents and products. Liquid phases formed by heating a solid substance or a mixture of substances above their melting points in the absence of a solvent is usually called a melt[28]. For example, when potassium nitrate is heated beyond 350°C, the liquid formed is called a melt. There is rudimentary information about the topic. There are examples of molten materials (salts and metals) that are used as solvents for reactions at high temperatures or crystallizations commonly referred to as fluxes[29]. For example, crystals of yttrium iron garnet, $Y_3Fe_5O_{12}$, can be produced by dissolving a sample of the garnet in a molten mixture of PbO and PbF_2, followed by cooling[30,31]. An example of a melt used as a solvent is that of liquid tin (mp 232°C) used in the reaction of ruthenium and phosphorus to produce RuP_2[32].

2.2. EXAMPLES OF SOLVENTLESS REACTION

No attempt has been made to differentiate between melt and solid-state reactions in this section. Indeed it was only during the time period that this thesis was underway that these differences became significant. Many early studies in which solventless reactions were assumed to occur via a solid-state reaction have since been shown to occur in the melt[33,34]. This issue will be dealt with explicitly in later chapters.

2.2.1. Organic reactions

Many organic compounds can be prepared in the solid form and the majority can be crystallised under ambient conditions. Consequently, reactions of organic solids with other solids, gases or liquids are possible. Organic reactions in the solid-state have been reported regularly since before the turn of the 20th century[35].

Although solid-state chemistry has been frequently regarded as a speciality field with few industrial applications, the importance of the behaviour unique to crystalline organic solids has been long appreciated. Polymerisation in the solid-state is an example that has also been thoroughly studied[36].

The rates of solid-state reactions like decomposition reactions are also important in the pharmaceutical industry. Manufactured drugs for example should survive long storage times without undergoing chemical change[37]. Unless this is achieved the desired medicinal effect of a drug would disappear with time. Indeed in the extreme, the decomposed material may be a poison rather than a remedy or a cure!

It is possible for two different crystalline forms of the same material (called polymorphs) to have different physical (and even chemical) properties. For example, chloramphenicol palmitate exists in two different crystalline forms with differing antibiotic activity[38]. The

need to obtain the potent crystalline form of the product thus becomes an important economic consideration in synthesis.

Examples of solventless organic reactions are given below. Some examples involve compounds that have known biological activities that have been applied (or show potential) in the treatment of human ailments. Some examples are uniquely produced by solventless transformations. In most of the cases described the solventless transformation reaction was found to be superior to solution protocols.

2.2.1.1. Dimerisation reactions

There are few examples of functionalised tetraasteranes in the literature (see structure in **Scheme 2.1**)[39]. Tetraasteranes are all centrosymmetric compounds with uniform substituents. Their synthesis in solution is not easy and gives yields of < 10%[40]. Tetraasteranes are closely related to other carbocycles like cubanes that have observed pharmacological effects[41]. Phenylsubstituted cubanes and bishomocubanes have been found to exhibit anticancer activity[42]. Carboxylated cubanes have been found to be active anti-HIV agents[43]. Thus a synthetic route that would generate these compounds in good yields is desired.

A solventless reaction showing the formation of tetraasteranes is shown in **Scheme 2.1** below. The starting material was irradiated neat using Ultra-Vitalux lamps under dihydropyridine chromophore excitation at λmax = 308 over a period of 3-4 weeks and gave the desired cage dimers (89-91% yield). The photo stable *syn*-dimers were exclusively produced. The solid-state synthesis is advantageous in that (i) higher yields of the desired product was produced and (ii) the method was selective.

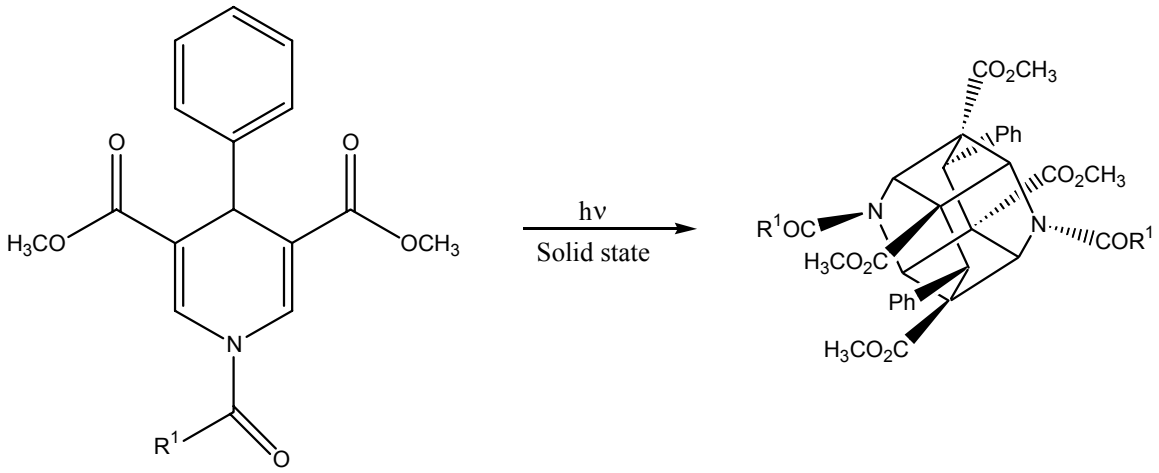

Scheme 2.1. Dimerisation of *N*-acyl- and *N*-acyloxy-3,5-methoxycarbonyl-4-phenyl-1,4-dihydropyridines to form a tetraasteranes in the solid-state

2.2.1.2. Condensation reaction, solvent free Knoevenagel condensation

Knoevenagel condensation reactions of aldehydes with active methylene compounds provide a route to olefins[44]. The reactions are usually base catalysed[45,46], Lewis acid catalysed[47], or surfactant catalysed[48] but current solvent methodologies create wastes. Numerous synthetic routes require the use of noxious phosphorylating agents such as phosphorus oxychloride ($POCl_3$)[49,50], impotence-inducing bases like piperidine[51] and cancer-suspect solvents like DMF[52] when the transformations are conducted in solution. Other methods recently employed to synthesise these compounds utilise solid supports promoted by infrared[53] or microwave[54,55,56] irradiation. These techniques although much more efficient, require solvents to extract products from the support at the end of the reaction. Other researchers have looked at the synthesis of products via catalyst-free Knoevenagel reactions in water[57,58,59], a method that works well except that the reaction does not give quantitative yields.

Asolventless transformation protocol is shown in **Scheme 2.2**. The method entails ball-milling equimolar amounts of solid aldehyde and a solid barbituric acid at room temperature for an hour. The solid powders were then dried at 80°C in a vacuum to

quantitatively yield the desired product. Comparative solution experimental conditions and yields are shown in **Table 2.2**.

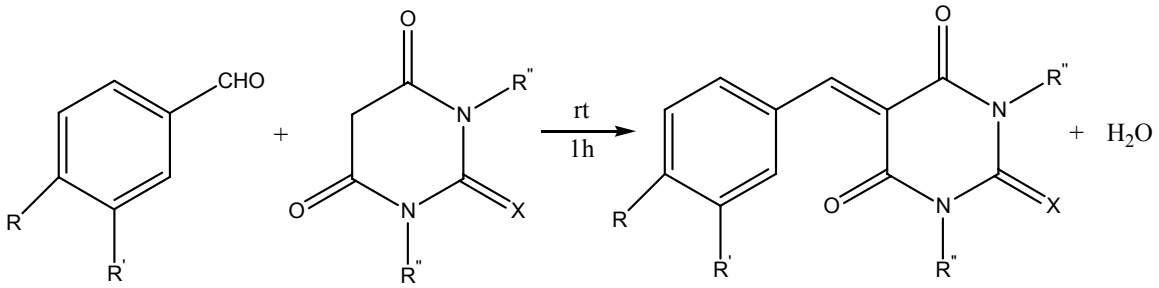

(a) R = NMe_2, R'= H, R"= Et, X = S

(b) R = OH R'= H, R"= Me, X = O

(c) R = OH, R'= H, R"= H, X = O

(d) R = OH, R'= OMe, R"= H, X = O

Scheme 2.2. Solventless Knoevenagel condensation of aromatic aldehydes with barbituric acids

Table 2.2. Reaction conditions and yields for the solventless Knoevenagel condensation of aromatic aldehydes with barbituric acids and comparative solution conditions

Solventless reaction			Solvent conditions	
Product	Yield/%	Reaction conditions	Comparative solution conditions	Yield/%
(a)	100	1h, rt	EtOH, 20°C[60]	87
(b)	100	1h, rt	H_2O or EtOH (aq), steam bath[61]	80-90
(c)	100	1h, rt to 50°C	MeOH, rt, 12h[62]	95
(d)	100	1h, 50°C	EtOH	Not reported

The yields under solventless conditions were quantitative and required less time compared to solution studies. The synthetic method employed had the added advantage in that the reaction could be carried out on 2000 g scale using a 2 litre horizontal ball-mill and gave identical results to that found using smaller amounts of reagents.

It is apparent from the results (**Table 2.2**) that the solventless methodology is superior to the solution methods in terms of yields and time. In addition, the solventless transformation is waste-free as it avoids the use of auxiliary reagents.

2.2.1.3. Thiozoles from α-tosyloxy ketones using microwave irradiation

1,3-Thiozoles[63] and 3-aryl-5,6-dihydroimidazol[2,1-*b*][1,3]thiozoles[64] are important classes of heterocyclic compounds that are known to posses important biological properties[65]. They exhibit cyclooxygenase inhibitory activity such that they are used as thromboembolic agents. They also form integral structural components of vitamin B_1 and coenzyme carboxylase[66]. The related bridgehead heterocyclic compounds, 3-aryl-5,6-dihydroimidazo[2,1-*b*][1,3]thiozoles exhibits a broad spectrum of anthelmintic and fungicidal activity[67]. Solution chemistry synthesis of these compounds generally uses lachrymatory starting materials and hazardous reagents, which requires long reaction times under harsh conditions.

The solventless method employed involved mixing thioamides with α-tosyloxyketones in the presence of acidic montmorillonite K-10 clay followed by brief (2-5 min) exposure of the reaction mixture to microwave irradiation (**Scheme 2.3**). The products were obtained in good yields (88-96%)

Scheme 2.3 below shows the formation of thiozoles in the absence of solvents.

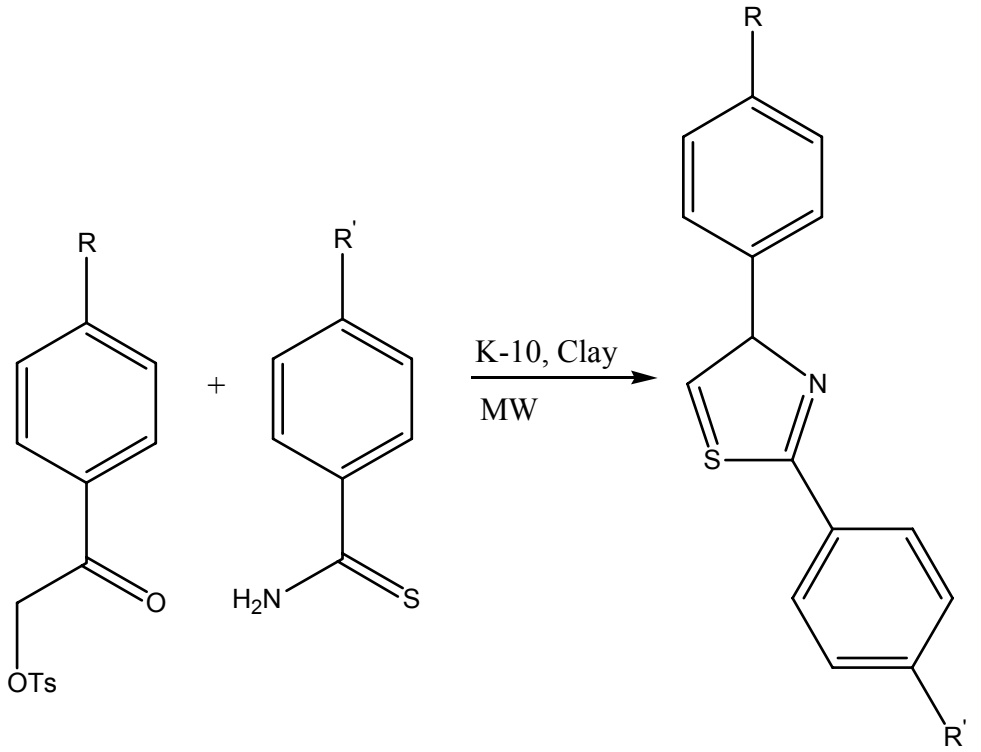

Scheme 2.3. Microwave assisted solid-state formation of thiozoles

The method offers advantages over solution work in that it eliminates solvent, takes less time (minutes rather than hours[68]) and also eliminates the need to use mineral acids to activate the reaction.

2.2.1.4. Protection of sugars

Polyhydroxylated pyrrolines and piperidines (iminosugars) are known for their biological properties as glycosidase and glycosyltransferase inhibitors[69]. They act on glycosidic linkages of oligosaccharides and glycopeptides by stabilising an intermediate oxonium ion, thus facilitating the lyses and modification of the anomeric centre[70]. Gylcosidases are involved in a wide range of important biological processes, such as intestinal digestion, post-translational processing of glycoproteins and lysosomal catabolism of glycoconjugates. Glycosidase inhibitors have potential application in the treatment of viral infections[71], cancer[72], diabetes and other metabolic disorders[73].

The solventless protection of sugars is shown in **Scheme 2.4** below. The protection was carried out by heating the sugars with *N*-benzylhydroxylamine (1.5 mole equiv) in the absence of solvents for 30 minutes at 110°C followed by crystallisation. The solventless protection protocol was successful in that 75-80% yield of the desired product was obtained (after crystallisation). The yields were comparable to the solution methodology yields that utilise complex reaction conditions involving high boiling solvents or Lewis acids and used much longer reaction times[74].

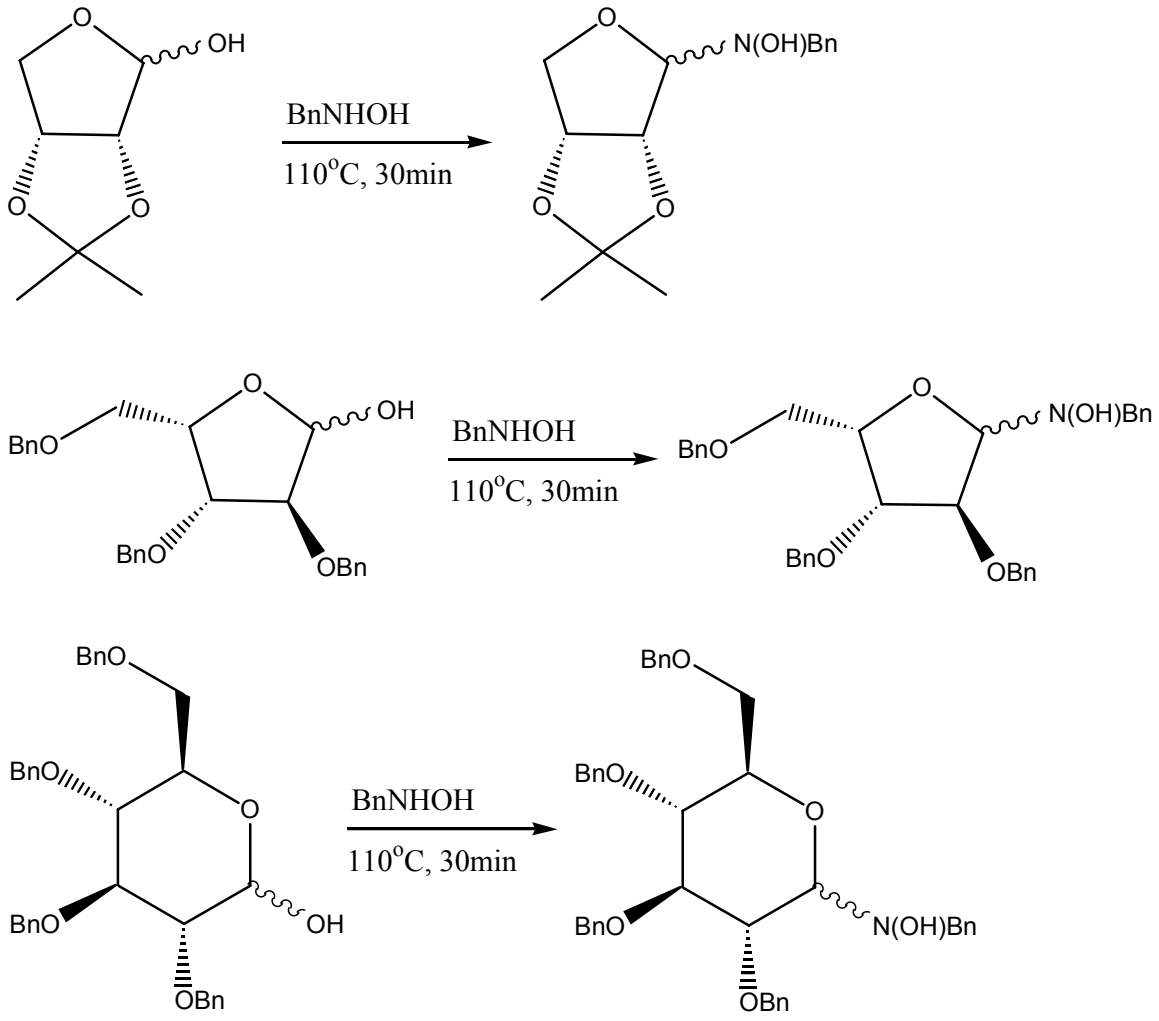

Scheme 2.4. Solventless synthesis of N-benzyl-N-glycosylhydroxylamines from sugars

2.2.2. Inorganic reactions

2.2.2.1. Main group compounds

The need to produce chemicals that are environmentally friendly is a priority in today's society. Waste water, discharged by companies that process ores and concentrates of non-ferrous metals, can be polluted with heavy metal ions such as cadmium (Cd^{2+}), lead (Pb^{2+}), copper (Cu^{2+}), nickel (Ni^{2+}) and zinc (Zn^{2+})[75]. These transition metals need to be removed from the polluted water system. An adsorbent, $Ca_2Al_2SiO_7$, was found to be effective in removing the metals ions, particularly Ni^{2+} [76].

Gehlenite ($Ca_2Al_2SiO_7$) commonly called calcium aluminium silicate was synthesised in the solid-state by treating a mixture of kaolinite ($Al_2(OH)_4(Si_2O_5)$), calcite ($CaCO_3$) and aluminium hydroxide ($Al(OH)_3$) by mechanochemical treatment (ball milling) for 24 hours at room temperature followed by heating 600-900°C for 24 hours. Gehlenite crystallised at temperatures lower than 850°C. The compound is solely compound of main group elements (Ca, Al, Si and O).

2.2.2.2. *d*-Block compounds

2.2.2.2.1. Vanadium (V) phosphate synthesis

Vanadium phosphates are one of the most studied heterogeneous catalysts[77,78,79,80]. They are used commercially for the oxidation of *n*-butane to maleic anhydride[81]. Experimental studies have shown that vanadium phosphates are also effective catalysts for propane[82] and pentane[83] partial oxidation.

Virtually all the preparation methods used to make vanadium phosphates use a vanadium compound like V_2O_5, a phosphorus compound like H_3PO_4, and a reducing agent/solvent such as C_6H_5OH. The drive towards environmentally friendly chemical transformation

resulted in a method to synthesise vanadium phosphates in the absence of solvents according to the following balanced equation[84].

$$V_2O_5 + 2H_3PO_4 \rightarrow 2VOPO_4 + 3H_2O$$

The solventless synthesis method was conducted by heating V_2O_5 (5.0 g) and H_3PO_4 (41.0 g) in an autoclave at 150°C for 16 h. At the completion of the reaction the resultant yellow solid was slurried with acetone, recovered by filtration, washed with acetone and dried in air (110°C, 16 h). The product was analysed by X-ray diffraction, Raman spectroscopy and ^{31}P NMR spectroscopy and identified as the desired product, anhydrous $VOPO_4$. The method does utilise a solvent to extract the product but it solvents were not used during the reactant transformation.

2.2.2.2.2. Solid-state synthesis of chromiun thiophosphate, $Cr_4(P_2S_6)_3$

Considerable interest has been focused on the first-row transition metal hexathiodiphosphate, $M_2P_2S_6$ (M = Mn, Fe, Co, Ni, Zn) which has semi-conducting two-dimensional phases and presents many novel properties such as two-dimensional magnetic behaviour, strong anisotropy of conductivity and large density waves[85]. These lamellar compounds may undergo intercalation-deintercalation reactions involving host-guest redox processes and the relevant intercalated materials may have many new properties. For example, intercalated layered materials, $Mn_{1.72}P_2S_6(DAMS)_{0.56}$ exhibit both large optical nonlinearity and magnetic ordering, lithium-intercalated $Ni_2P_2S_6$ showed the potential to function as a cathode in lithium batteries[86].

Recently, the syntheses of $M_2P_2S_6$ with elements preceding manganese have been made. These elements lead to greater stability of the resulting complex[87,88]. The balanced equation for the reaction is shown below[89] when using chromium as the metal centre.

$$4CrCl_3.6H_2O + 3Na_4P_2S_6.6H_2O \rightarrow Cr_4(P_2S_6)_3 + 12NaCl + 42H_2O$$

The synthesis procedure is achieved by mixing $CrCl_3.H_2O$ (green crystals) and $Na_4P_2S_6.6H_2O$ (white powder) in a 4:3 molar ratio followed by grinding in an agate mortar to produce a homogeneous solid mixture. The colour of the mixture immediately changed from green and white to dark brown signalling the formation of a new product and the reaction was complete after one hour of continuous grinding and produced an amorphous solid. The amorphous material was annealed at 400°C or 500°C for 24 hours. The crystalline product was then characterised by X-ray diffraction and Raman spectroscopy.

2.2.2.2.3. Solid-state synthesis of lithium metazirconate (Li_2ZrO_3) pellets

Lithium ceramics are of interest because of their technological applications. They have been used as electronic devices[90], breeder materials for nuclear fusion reactors [91,92,93], as cathodes for rechargeable lithium batteries[94,95], in low thermal expansion glass-ceramics[96] and in ceramic hobs[97].

Lithium aluminate ($LiAlO_2$), lithium silicates (like Li_2SiO_3, $Li_2Si_2O_5$ and Li_4SiO_4) and lithium zirconates (like Li_2ZrO_3 and $Li_6Zr_2O_7$) are candidate materials in nuclear research as tritium (^3T) breeding materials[98]. Such materials enable the reaction shown below to be exploited[99].

$$^6Li + n_t \rightarrow {}^3T + {}^4He$$

Lithium metazirconate (Li_2ZrO_3) has been proposed as a good candidate breeding material because of its high potential to produce tritium[100] and it exhibits good irradiation characteristics.

The solid-state synthesis of low density (60-70% theoretical density) lithium metazirconate (Li_2ZrO_3) from lithium carbonate (Li_2CO_3) and ZrO_2 powder[101] according to the following equation, has been reported.

$$Li_2CO_3(s) + ZrO_2(s) \rightarrow Li_2ZrO_3(s) + CO_2(g)$$

The method was an improvement on earlier methods in that better yields were obtained. The product was also produced in pellet form making it possible for analysis using X-ray diffraction and electron microscopy (both scanning and transmission).

2.2.2.3. *f*-Block compounds

Little is known about ternary oxotellurates (VI) of lanthanides[102]. The first rare-earth oxotellurates (VI) were prepared by reacting equimolar amounts of rare-earth sesquioxide (M_2O_3) and orthotelluric acid (H_6TeO_6) at elevated temperatures (>1000°C)[103]. In order to obtain structural information on these compounds, a solid-state reaction to form these compounds was undertaken and the reaction was shown to take place at lower reaction temperatures (800°C). The reaction equation is shown below.

$$Gd_2O_3 + TeO_3 \rightarrow Gd_2TeO_6$$

A typical solid-state reaction was conducted by mixing equimolar amounts of Gd_2O_3 and TeO_3 in a silica tube. The vacuum-sealed tube was then heated to 800°C and kept at the set temperature for 10 days. The furnace was then cooled back to room temperature. The tube was then broken open to expose colourless pillar like single crystals analysed by X-ray structure to be Gd_2TeO_6. The results demonstrated that inorganic salts of f-block elements could also undergo solid-state transformation reactions.

2.2.3. Organometallic compounds

As this thesis details studies of the solventless reaction of organometallic complexes, this section will include a more detailed survey than described in **Sections 2.2.1 – 2.2.2**. Again no attempt has been made to be comprehensive but the objective is to give a sense of what has been achieved to date.

2.2.3.1. Use of organometallic compounds in organic synthesis

Ruthenium-catalysed coupling of allyl alcohols with alkynes

Ruthenium vinylidenes that result from the activation of terminal alkynes are key intermediates in the catalytic synthesis of alkenylcarbamates[104], enynes[105] and butatrienes[106] by alkyne dimerisation or α,β-unsaturated ketones by coupling of alkynes with allyic alcohols. Recently three synthetic methods were reported and the data compared to determine the method that yielded the desired product efficiently, selectively and was most environmentally friendly. Below is described the experimental procedure for the three methods employed. The general reaction scheme for the transformation is shown in **Scheme 2.5**.

1. Reactions in allyl alcohol
Alkyne (2.5 mmol) was added to a mixture of ruthenium complex (0.125 mmol) and allyl alcohol (5 cm^3). The mixture was then stirred and heated at 90°C for 4 h (**Scheme 2.5**). The results are summarised in **Table 2.3**.

2. Reactions in water
Degassed water (4 cm^3) was added to a mixture of ruthenium complex (0.125 mmol), allyl alcohol (7.5-15 mmol) and alkyne (2.5 mmol). The heterogeneous mixture was stirred and heated at 90°C for 1-4 h (**Scheme 2.5**). The results are summarised in **Table 2.3**.

3. Solventless reaction

The ruthenium complex $(C_5Me_5)RuCl(cod)$ (0.125 mmol) was dissolved in allyl alcohol (7.5 mmol) under argon and the alkyne (2.5 mmol) was added to the mixture. For most alkynes, the reaction was completed in 10-15 minutes (**Scheme 2.5**). The results are summarised in **Table 2.3**.

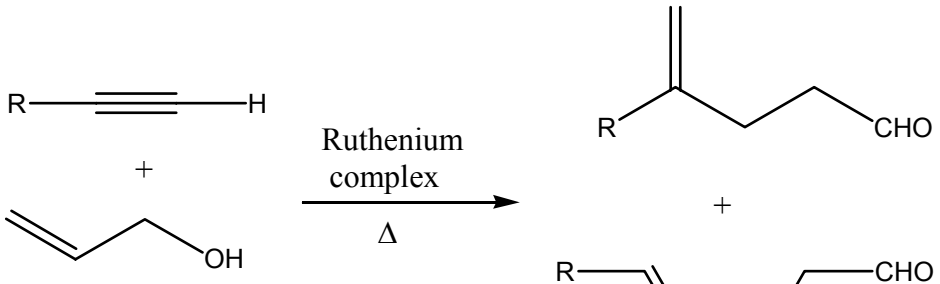

(a) R = Ph

(b) R = C_6H_{13}

(c) R = $(CH_2)_2OH$

(d) = Bu^t

Scheme 2.5. The solventless ruthenium catalysed formation of terminal alkenyldeyde from terminal alkynes and allyl alcohol

Table 2.3. The solventless ruthenium catalysed formation of terminal alkenyldeyde from terminal alkynes and allyl alcohol using three methodologies

	Reactions in allyl alcohol		Reactions in water		Solventless reaction	
Alkyne	Selectivity	Yield/%	Selectivity	Yield/%	Selectivity	Yield/ %
(a)	75/25	70	75/25	85	75/25	85
(b)	-	-	80/20	80	80/20	83
(c)	-	-	58/42	70	58/42	75
(d)	-	-	100/0	50	100/0	60

The superiority of the solventless transformation was also shown by the higher yield. The duration of the experiment was about 15 min for the reaction taking place in the absence

of solvent whereas it took hours when the reaction was conducted in solution. The selectivity of the reaction was the same using the three methods.

2.2.3.2. Isomerisation reactions

2.2.3.2.1. Linkage isomerisation

Linkage isomerisation entails a formation of two isomers that differ due to the way in which an ambidentate ligand binds to a metal. Linkage isomerisation has been found to occur with ligands such as NO_2^- and SCN^-. Jorgensen first noted Nitrito to nitro isomerisation of ligands bound to a metal in 1893 (see **Scheme 2.6**).

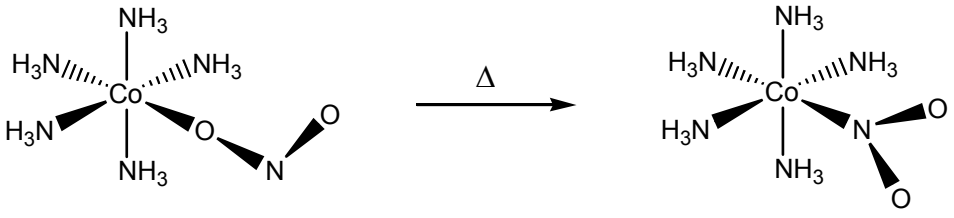

Nitrito Complex Nitro Complex

Scheme 2.6. Linkage isomerism of nitrito to nitro of pentaammine nitritoCobalt(III) in the presence of heat

The red nitrito compound (shown above) is unstable and isomerises to the more stable nitro compound even under ambient conditions (**Scheme 2.6**). The reaction can occur in the solid-state[107] and indeed most nitrito compounds that isomerise in solution also isomerise in the solid-state. Single crystal crystallographic studies of the above isomerisation reactions have been performed as the crystal does not disintegrate or fragment during the reaction. For example, the crystal structures of the nitrito and nitro compounds of *trans*-$[Co(en)_2(NCS)(ONO)]X$, ($X = I^-$, Cl^-, ClO_4^-)[108] are essentially identical, and analysis of the data indicated that the isomerisation occured intramolecularly by rotation of the NO_2^- group[109].

2.2.3.2.2. Cis-trans isomerisations reactions

Isomerisation of a range of organometallic reactions in the solid-state has been conducted for many years[110] with isomerisation of pseudo 7 coordinate complexes of the type $CpML_4$ (M = Re, Mo, W, L a range of ligands) providing one example[111,112,113] (see below).

(a) Isomerisation of *ttt*-$RuCl_2(RNC)_2(PPh_3)_2$ to *cct*-$RuCl_2(RNC)_2(PPh_3)_2$

The reaction was carried out by placing *ttt*-$RuCl_2(RNC)_2(PPh_3)_2$ (10 mg) in an NMR tube and the contents were then subjected to thermal experimentation at a constant temperature (range 160-180°C) as outlined in **Scheme 2.7**. The reaction went smoothly as shown by high yields of products (all yields in excess of 85%)[114].

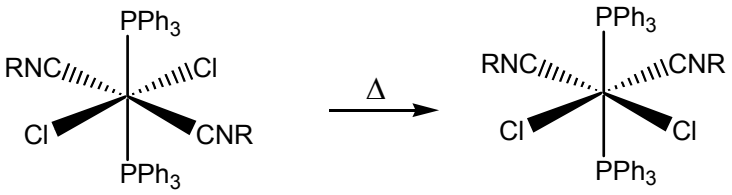

R = Xylyl, MeClPh, ^{t}Bu, Benzyl, ^{i}Propyl

Scheme 2.7. Solventless isomerisation of *ttt*-$RuCl_2(RNC)_2(PPh_3)_2$ to *cct*-$RuCl_2(RNC)_2(PPh_3)_2$

The experiment also yielded kinetic data. The reaction was found to be first order, unimolecular and unidirectional. Kinetic parameters like rate constants and activation energies were recorded for some of the complexes. For example, for the R = ^{t}Bu complex, the rate constants were $0.0044 \pm 6.2 \times 10^{-4}$, $0.0025 \pm 3.2 \times 10^{-4}$, $8.58 \pm 4.3 \times 10^{-4}$ at 185, 180 and 175°C respectively. The activation energy of the reaction was found to be 210 $kJmol^{-1}$.

A mechanism for the reaction was also proposed. This entails exchange of one pair of ligands (Cl, RCN) to bring about isomerisation (see the structure below)[115]. The

movement of the larger ligand, PPh_3, in the solid-state was ruled out although the flexing of this ligand in assisting the process was deemed necessary. The isomerisation of the reaction was thus thought of as a direct Cl/RNC exchange via ligand rotation of 180° around an axis through Ru[116], with the high energy process consistent with the large activation energy barrier.

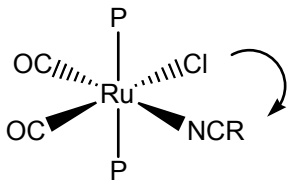

(b) Isomerisation of *diag*- and *lat*-(η^5-C_5H_4R)Re(CO)(L)X_2

Half-sandwich rhenium complexes have been known for decades [117,118,119,120,121,122,123,124]. The piano stool rhenium complexes have been prepared and the solution isomerisation behaviour has been thoroughly studied[125,126,127,128,129]. Only in the last few years have solid-state isomerisation reactions of the system been recorded[130] (**Scheme 2.8**).

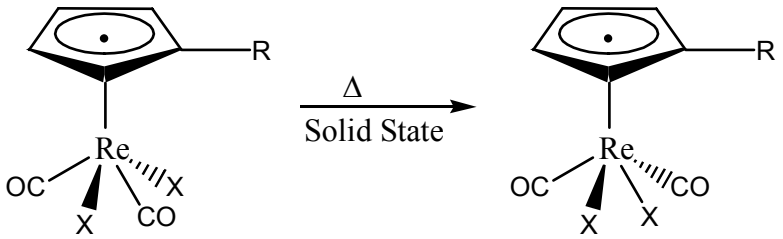

X = Cl, Br, I R = Me, ^{t}Bu, $SiMe_3$, H

Diag Lat

Scheme 2.8. Isomerisation of *diag*- and *lat*-(η^5-C_5H_4R)Re(CO)(L)X_2 (L = PPh_3, $POPh_3$, PCy_3, X = Cl, Br, I) in the absence of solvents

Solid *diag*-(η^5-C_5H_4R)Re(CO)(L)X_2 (L = PPh_3, $POPh_3$, PCy_3, X = Cl, Br, I) was heated under nitrogen in an oil bath at temperatures of 10-15°C below the melting point of the complex[131] for a period less than 6 hours to give the new isomer in yields of 70-92%.

The isomerisation process was found to be unidirectional, i.e., from *diag*-(η^5-C_5H_4R)Re(CO)(L)X_2 to *lat*-(η^5-C_5H_4R)Re(CO)(L)X_2. The *lateral* isomer remained unchanged when subjected to the same experimental conditions. For X = Br, the isomerisation reaction was influenced by the cyclopentadienyl ring substituents (R).

Initially the mechanism of the reaction was tentatively proposed to be similar to that of the mechanism determined in solution studies[132,133]. It involved an associative process that combined a Berry and a turnstile isomerisation mechanism, as shown below (**Scheme 2.9**). The Berry mechanism was the model used by Faller and Anderson to evaluate the cis-trans isomerisation of (η^5-C_5H_5)$MoWL_3X$ complexes in solution[134]. However, later studies by Bogadi and co-workers revealed that the isomerisation involved a trivial two-atom/ligand exchange and not a three- or four- ligand turnstile or Berry-rotation pathway[135].

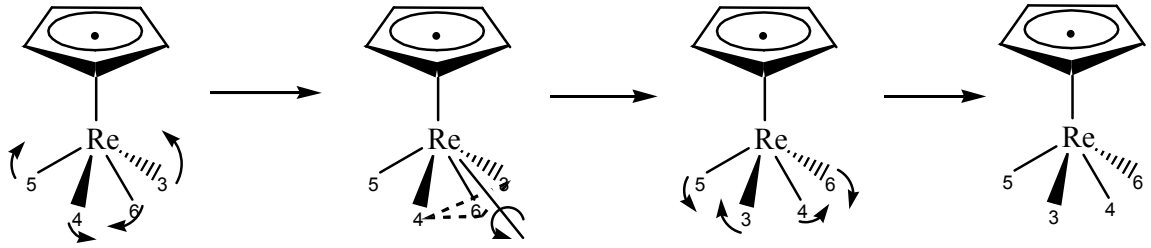

Scheme 2.9. Combined Berry-tunstile isomerisation mechanism for $CpML_4$ complexes

2.2.3.3. Migratory insertion reactions

The reaction of $Mn(CO)_5Me$ with $AlBr_3$ in the solid-state to give $Mn(CO)_5(COMeAlBr_2)$has been conducted successfully, although extensive decomposition accompanied the transformation[136]. The reaction represents an early migratory insertion reaction that was conducted in the solid-state. The initial interest in this kind of reaction was to find better ways to activate metal-coordinated carbon monoxide[137,138,139140,141]. The scheme below (**Scheme 2.10**) shows two possible products obtained when equimolar amounts of the complex and a Lewis acid were mixed together under a carbon monoxide atmosphere.

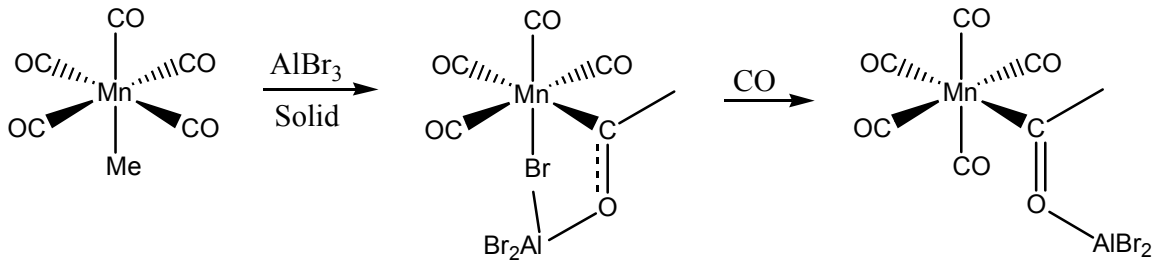

Scheme 2.10. Migratory insertion of carbon monoxide using Lewis acids in the absence of solvents

The reaction was so facile that after some few minutes, it had gone to 89% completion. In fact acyl formation seemed to have taken place as soon as the two reagents were placed in contact with each other. The Lewis acid was proposed to play three functions; it increased the rate of alkyl migration, stabilised the acyl group and provided an electron-rich atom, which acted as a ligand to fill the vacant coordination site left by the creation of the acyl group[142].

Later on other researchers looked at the interaction of metal complexes with nucleophilic reagents. One such reaction that has been an extensively studied is the reaction of $(\eta^5\text{-}C_5H_5)M(CO)_3Me$, (M= Mo, W), and $(\eta^5\text{-}C_5H_5)Fe(CO)_2Me$ with nucleophilic ligands[143].

Most of the early work focused on the mechanism of the reaction between (η^5-C_5H_5)M(CO)$_3$Me, (M= Mo, W), (η^5-C_5H_5)Fe(CO)$_2$Me with nucleophilic ligands[144,145,146,147,148,149,150,151,152]. These reactions were conducted in solution but there are early reports of reaction of these complexes with ligands in the absence of solvents[153,154,155,156].

Coville e*t al* undertook such investigation in a quest to see whether such transformation could be achieved in the condensed phase. They reported a CO insertion/methyl migration reaction of (η^5-C_5H_5)M(CO)$_3$Me, (M= Mo, W), and (η^5-C_5H_5)Fe(CO)$_2$Me with phosphines, phosphites and $AsPh_3$, in the absence of solvents[157] (**Scheme 2.11**).

Most of the reactions performed above were reactions that took place in the melt (below the melting point of most ligands). The yields of the reaction depended on the ligand used but were generally high (above 60% conversion). The experiments also yielded kinetic data. The conversion of (η^5-C_5H_5)Mo(CO)$_3$Me to (η^5-C_5H_5)Mo(CO)$_2$(L)Me in the presence of the ligand was dependent on the ligand. The rate of reaction decreased in the order PEt_3 > $P(OPh)_3$ > PPh_3 ≈ P(*p*-$C_6H_4OMe)_3$ ≈ $P(OEt)_3$ > PCy_3 > $AsPh_3$. The trend obtained here was in agreement with solution studies. Only the *trans* isomer was isolated in all the transformations (**Scheme 2.11**).

There was also an attempt to elucidate the activation energies of the reactions. The difficulty of trying to obtain such data in the condensed phase was stated and mention was made of the reaction having two activation energies, one for the reaction and the other for diffusion control. For example, the reaction between (η^5-C_5H_5)Mo(CO)$_3$Me with PPh_3 had the values; *Ea* (reaction) < 75 kJmol^{-1} and *Ea* (diffusion) > 120 kJmol^{-1}. A mechanism for the reaction was not reported.

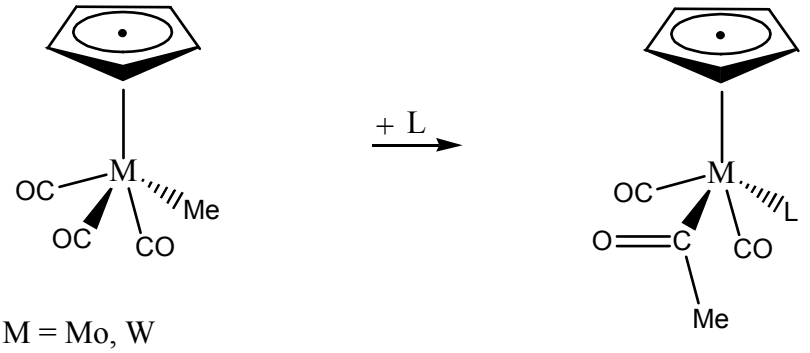

M = Mo, W

L = PPh_3, P(*p*-$C_6H_4OMe)_3$, PCy_3, PEt_3, $AsPH_3$, $POPh_3$, $P(OEt)_3$

Scheme 2.11. Migratory insertion reactions using pohsphines, phosphites and $AsPh_3$

A sequel to this work was then undertaken, which proposed a mechanism for the reaction[158]. This work focused on the solventless transformation of (η^5-C_5H_5)$M(CO)_3Me$, (M= Mo, W), using solid phosphines at temperatures below the melting points of the reactants and products (**Scheme 2.12**). The techniques that were used to elucidate the mechanism were DRIFTS, NMR, DSC, IR and elemental analysis. The key technique used to elucidate the mechanism was optical microscopy, which revealed that although the experiment was conducted at temperatures much lower than the melting points of the reagents, the reaction went through the melt phase.

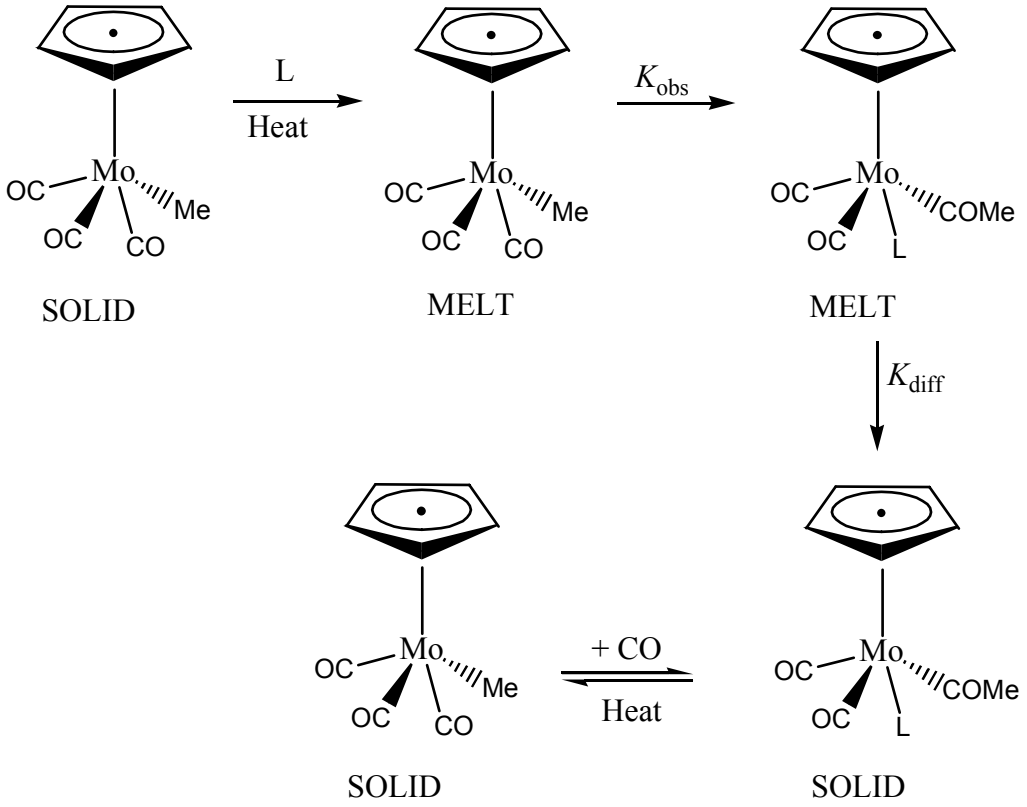

M = Mo, W

L = Phosphines

Scheme 2.12. Proposed mechanism of the solventless transformation of (η^5-C_5H_5)$M(CO)_3Me$, (M= Mo, W), using solid phosphines

A detailed kinetic study was also conducted using DRIFTS when the sample was taken in KBr as a diluent. A picture depicting the findings is shown below (**Figure 2.1**).

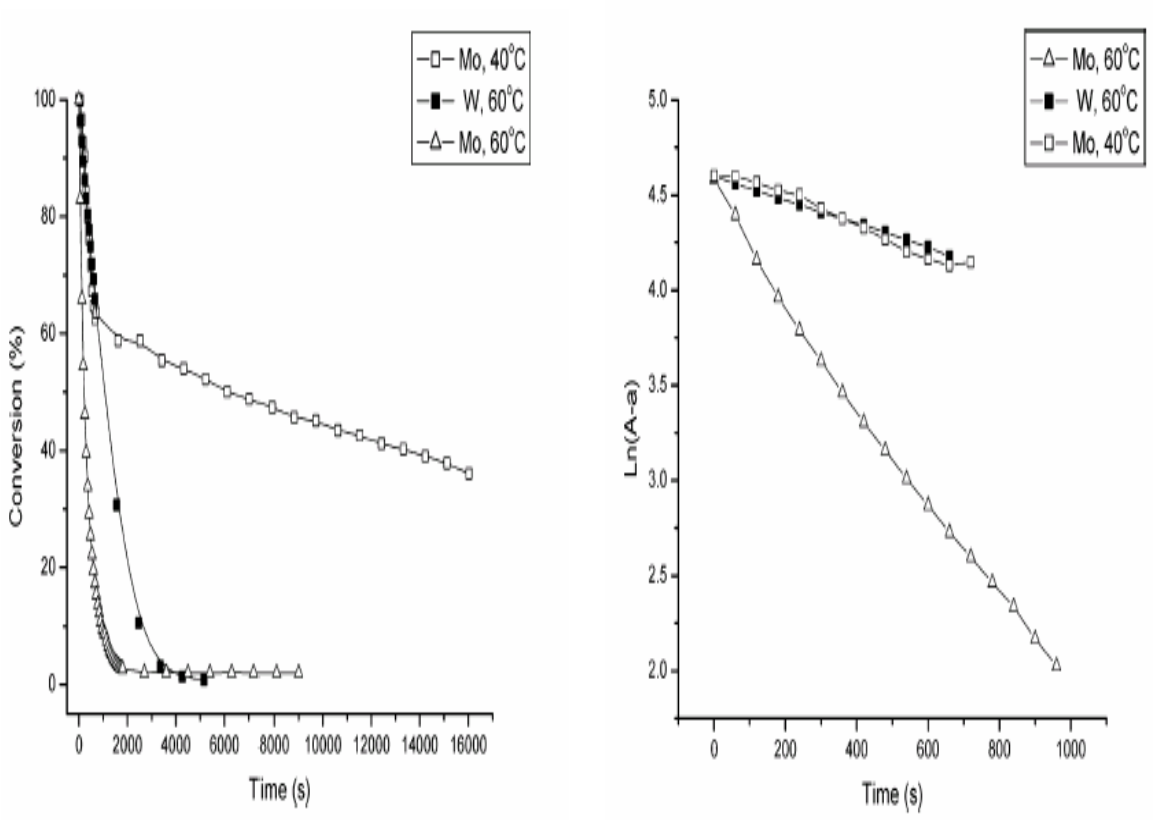

Figure 2.1. Detailed kinetic study of the solventless transformation of (η^5-C_5H_5)M(CO)$_3$Me, (M= Mo, W), using solid phosphines using DRIFTS when the sample was taken in KBr as a diluent[159]

The assumption was made that the first part of the reaction occurred via a first order rate law (**Figure 2.1a**) and the expansion of that time interval is shown in **Figure 2.1b**. In the first part, there is smooth conversion of the starting material with time as would be expected of first order kinetics. The reaction between (η^5-C_5H_5)Mo(CO)$_3$Me and PPh_3 (1:1 ratio) gave a rate constant of 4.34×10^{-5} s^{-1} comparable with early studies reported to be 1.81×10^{-5} s^{-1} at 40 C[159]. The finding ruled out the effect of the diluent, KBr, on the rate of reaction and studies using other diluents like NaCl also resulted in rate constants of the same order.

The second part of the reaction was dominated by a deceleration in the rate ($k = 3.37 \times 10^{-5}$ s^{-1}) signifying the diffusion effects due to mass transfer problems associated with condensed matter. The justification for this was that the product started to solidify and in

the process started to block reagents from reacting any further. The evidence for such crystallisation of the product was captured by camera when the optical studies were monitored by optical microscopy.

A report of the soventless reaction of (η^5-C_5H_5)$Mo(CO)_3Me$ with CO has also appeared (**Scheme 2.13**). The complex was loaded into a sample vial and placed a steel autoclave and subjected to thermal experimentation under CO gas (10 bar).

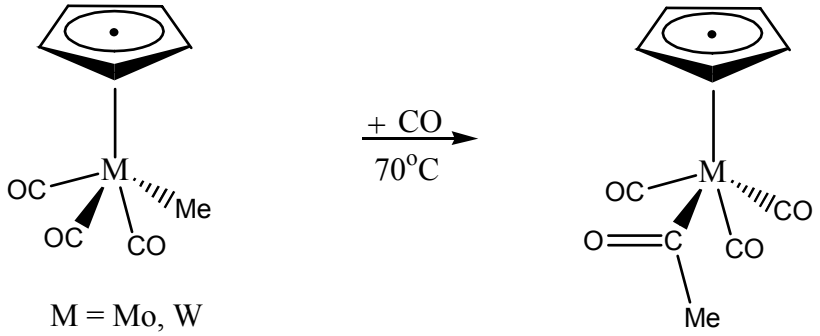

Scheme 2.13. Migratory insertion reaction when CO is used

The reaction proceeded in quantitative yield under mild thermal conditions. The results were in contrast to a report that the transformation in solution is difficult (when M = W) [160]. No kinetic data were reported for the transformation. No mention of the mechanism of the reaction was made.

The authors also reported the migratory insertion reaction for iron complexes conducted in the absence of solvents (**Scheme 2.14**). The solution work for the conversion is well documented. The investigation demonstrated that the reaction between (η^5-C_5H_5)$Fe(CO)_2Me$ and PPh_3 was much slower than for the corresponding reaction of ((η^5-C_5H_5)$Mo(CO)_3Me$) with PPh_3. The CO insertion reaction was conducted in an autoclave and the reaction was also found to be slower than for the molybdenum reaction.

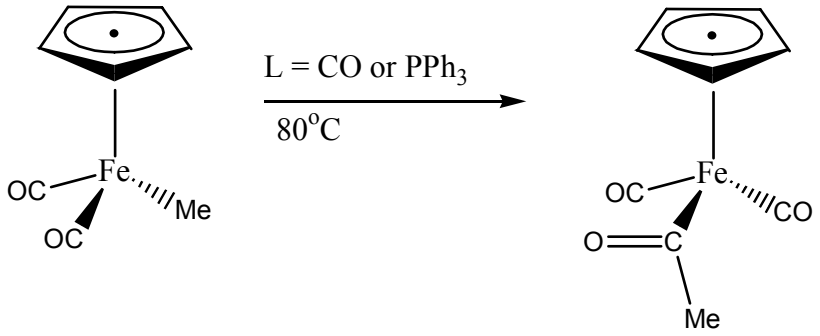

Scheme 2.14. Migratory insertion reaction when CO is used

2.2.3.4. Coupling reactions

A coupling reaction involves the joining together of two or more reagents to form a product, usually in the presence of a catalyst[161]. The method has found extensive use in organic chemistry synthesis[162]. Coupling reactions have also been conducted in the absence of solvents although with the aid of mechanical grinding. Mechanically induced solid-state reactions have been carried out successfully in the solid-state mainly in the areas of inorganic[163,164] and organic[165,166] chemistry. There have also been reports of the exploitation of this method to synthesise coordination polymers[167] and supermolecules[168] from transition metals and ligands, organic-organometallic hydrogen bonded network compounds[169] and encapsulated inorganic cations in supramolecular organometallic cages. All these examples above show that the mechanochemical reactions offers an alternative route for the preparation of molecular materials[170].

The reaction shown in **Scheme 2.15** below shows the use of this method to transform ferrocene-1,1'-diboronic acid using KF/alumina as a solid-phase support in the absence of solvents[171]. The yields were low (30-57%) but the method demonstrated that solventless coupling reactions of organometallic compounds could also be conducted.

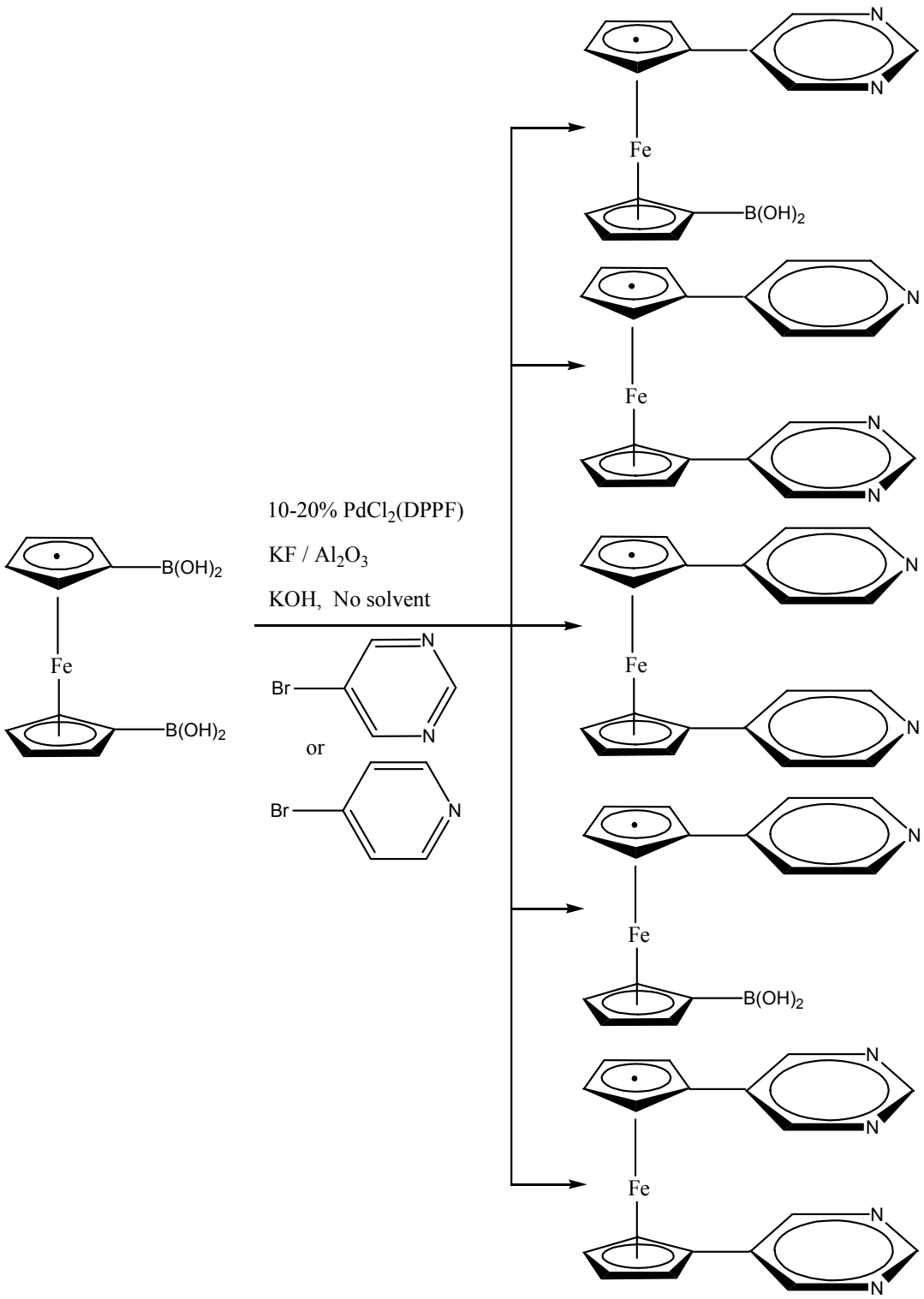

Scheme 2.15. Solid-state synthesis of mono- and disubstituted pyridine and pyrimidine ferrocenyl derivatives

2.2.3.5. Substitution reactions

2.2.3.5.1. Reaction of diag-(η^5-C_5H_5Me)$Re(CO)_2Br_2$ with excess NaI

The rhenium complex / sodium iodide solid mixture was heated at 100-125°C for 18 h. Separation of the product from the salt using column chromatography yielded the desired product in quantitative yield (**Scheme 2.16**).

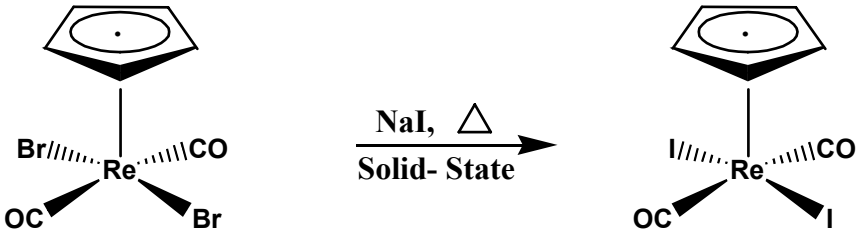

Diagonal (trans) **Diagonal (trans)**

Scheme 2.16. Solid-state substitution of halogen ligands of rhenium complexes under thermal conditions

The kinetics and the mechanism of the reaction were not pursued but a speculative suggestion as to how the reaction took place was hinted at. A mention was made that during a related process (isomerisation reaction of the same complex) all the metal-ligand bonds were weakened. In the presence of an appropriate ligand like sodium iodide, substitution could thus take place. The reaction is unidirectional as the formation of the dibromo complex from the iodo complex did not occur.

A similar transformation of *diag*-(η^5-C_5H_5Me)$Re(CO)[P(OPh)_3]Br_2$ with NaI also resulted in the formation of an unexpected product, *diag*-(η^5-C_5H_5Me)$Re(CO)_2I_2$, as a sole product in 50% yield after purification by column chromatography. The methodology offered a convenient method for the preparation of cyclopentadienyl dicarbonyldiiodide rhenium complex from the dibromine complexes.

The formation of *diag*-(η^5-C_5H_5Me)$Re(CO)_2I_2$ as a sole product during the reaction of *diag*-(η^5-C_5H_5Me)$Re(CO)[P(OPh)_3]Br_2$ with NaI indicated that both Re-Br and Re-$P(OPh)_3$ bonds were broken in the solid-state. It also demonstrated that a neutral ligand could be substituted by another neutral ligand (phosphite by CO) in the solid-state.

2.2.3.5.2. Reaction between $RhX(PPh_3)_3$ and (η^5-C_5H_4Me)$W(CO)_3X$ in the solid-state

Reactions between two organometallic complexes in the solid-state have been rarely published[172]. Coville and Eke[173] investigated the feasibility of the following transformation:

$$RhCl(PPh_3)_3 + M(CO)_n \rightarrow RhCl(CO)(PPh_3)_2 + M(CO)_{n-1}(PPh_3)$$

The basis for the choice of this reaction for study was because Wilkinson's catalyst was known to decarboxylate both organic[174,175] and organometallic carbonyl complexes[176] in the solution phase. Another study also demonstrated that the Wilkinson's catalyst reacted with CO in the solid-state to produce the stable $RhCl(CO)(PPh_3)_2$ complex in good yield[177].

The reaction between $RhX(PPh_3)_3$ and (η^5-C_5H_4Me)$W(CO)_3X$ in the solid-state was also studied (**Scheme 2.17**). The tungsten reagent was chosen due to its stability[178], the ability of the CO group to be displaced easily and that the solid-state isomerisation reactions of the complex had been undertaken successfully[179,180]. Grinding together equimolar amounts of reagents carried out the transformation.

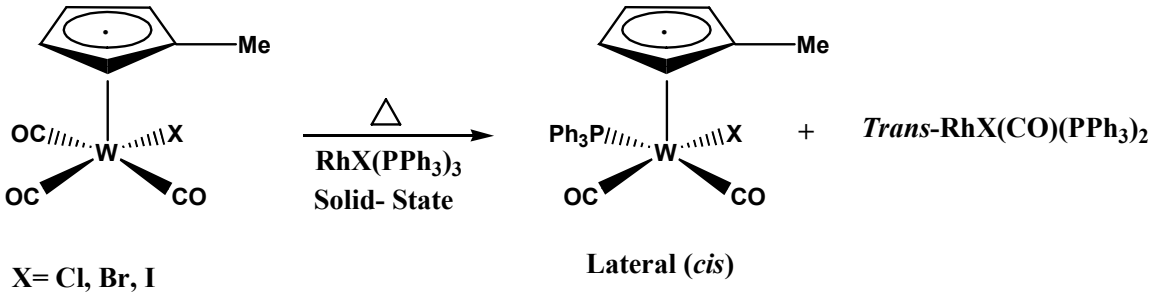

Scheme 2.17. Solid-state substitution reaction of a tungsten complex using Wilkinson's catalyst under thermal conditions

The reaction seemingly went to completion with the consumption of all the starting materials. The yields of the various manipulations were not mentioned. The fact that all starting materials were consumed is rather puzzling for two solid materials that were ground and reacted in equimolar amounts. Mass transfer problems associated with condensed matter could have prevented the completion of the reaction.

Another explanation for the completion of the reaction would be the intervention of a melt state, which would allow for the diffusion of reagents and products. The free PPh_3 ligand that was displaced has a melting point of 78°C, and this could provide a "flux" for the reaction.

The surprising result of the study was that the grinding process did not yield new products considering that the reaction was conducted at a low temperature, 75°C. The grinding process should have resulted in heat gain in the system, which could have resulted in new products being formed.

Two possible mechanisms consistent with data were proposed. Firstly, the Wilkinson's catalyst is known to contain a weakly coordinated *trans* PPh_3 ligand[181], such that a highly reactive unsaturated entity, $RhX(PPh_3)_2$, is formed at the reaction temperature. The reagent, in the presence of $(\eta^5\text{-}C_5H_4Me)W(CO)_3X$, would then interact with the bound

CO ligand to yield the exchange product. Secondly, the reaction could proceed via a penta-coordinated intermediate, $RhCl(CO)(PPh_3)_3$, as proposed in a related solid-state reaction[173].

2.3. CONCLUSIONS

- The survey reveals generality of solventless approach
- The methodology has been used in organic, inorganic and organometallic studies to produce novel products.
- Detailed methods, particularly in organometallic chemistry, were described.
- It was found, in most cases, that the reaction goes through the melt.
- Analytical techniques such as FTIRS and DRIFTS are invaluable in studying solventless reactions, particularly when kinetic and mechanistic investigations are undertaken.

2.5. REFERENCES

1. J. Thornton, *Pure Appl. Chem.,* 2001, **73**, 1231.
2. C. Walker, *Environmental Pollutions by Chemicals*, Hutchinson Educ, London, 1971.
3. B. N. Roy, A. Kumar and A. Sankaran, *J. Indian Chem. Soc.,* 2000, **77**, 459.
4. V. Antoniou, H. Tsoukali and N. Zantopoulos, *Proceeding of the 7th International Conference on Environmental Science and Technology*, Ermoupolis, Greece, 2001.
5. T. Bagarinao and I. Lantin-Olaguer, *Hydrobiologia*, 1998, **382**, 137.
6. D. Spurgeon, *Nature,* 2000, **407**, 121.
7. F. Martins da Silva, P. S. Bergo de Lacerda and J. J. Jones Jr, *Quim. Nova,* 2005, **28**, 103.
8. M. Misono, *J. Indian Eng. Chem.,* 2004, **10**, 1126.
9. J. F. Jenck, F. Agterberg and M. J. Droescher, *Green Chem.*, 2004, **6**, 544.
10. K. G. Steinhäuser, S. Richter, P. Greiner, J. Penning and M. Angrick, *Environ. Sci. Pollut. Res*., 2004, **11**, 284.
11. P. T. Anastas and J. C. Warner, *Green Chemistry: Theory and Practice*, Oxford University Press, Oxford, 1998.
12. J. Fiksel, *Environ. Sci. Technol.*, 2003, **37**, 5330.
13. F. Rohmund, L. K. L. Falk and E. E. B. Campbell, *Chem. Phys. Lett*., 2000, **328**, 269.
14. S S.B. Sinnott, R. Andrews, D. Qian, A.M. Rao, Z. Mao, E.C. Dickey and F. Derbyshire, *Chem. Phys. Lett*., 1999, **315**, 25.
15. R. Andrews, D. Jacques, A. M. Rao, F. Derbyshire, D. Qian, X. Fan, E. C. Dickey and J. Chen, *Chem. Phys. Lett*., 1999, **303**, 467.
16. K. Kondoh, *Mater. Integration*, 2001, **14**, 19.
17. . Haber, A. Sosnowska and J. Ziolkowski, *J. Solid-state Chem.*, 1976, **16**, 83.
18. J. O. Williams, *Sci. Prog.*, 1977, **64**, 247.
19. J. P. Glusker, M. Lewis and M. Rossi, *Crystal Structure Analysis for Chemists*

and Biologists, VCH publishers, New York, 1994.

20. A. Loupy, *Top. Curr. Chem.,* 1999, **206**, 155.
21. D. Young, *Decomposition of Solids*, Pergamon, London, 1966
22. W. E. Garner, *Chemistry of the Solid-state,* Butterworths, London, 1955.
23. P. D. Garn, *CRC Crit. Rev. Anal. Chem*., 1972, **3**, 65.
24. W. L. Ng, *Aust. J. Chem*., 1975, **28**, 1169.
25. C. J. Keattch and D. Dollimore, *An Introduction to Thermogravimetry*, 2nd Ed, Heyden, New York, 1975.
26. P. O'Brien, *Polyhedron*, 1983, **2**, 233.
27. C. H. Bamford and C. H. F. Tipper, *Comprehensive Chemical Kinetics*, Elsevier, New York, 1980, Vol 22.
28. J. Nyvlt, *Solid-Liquid Phase Equilibrium*, Elsevier Scientific Publishing Company, New York, 1977.
29. A. B. Ellis, M. J. Geselbracht, B. J. Johnson, G. C. Lisensky and W. R. Robinson, *Teaching General Chemistry: A Materials Science Companion*, American Chemical Society, Washington, DC, 1993.
30. N. J. Nielsen, *J. Appl. Phys.*, 1960, **31**, S51
31. K. Fischer and E. Sinn, *Cryst. Res. Technol.*, 1986, **21**, 711.
32. E. D. Jones, *Phys. Rev.,* 1967, **158**, 295.
33. G. Rothenberg, A. P. Downie, C. L. Raston and J. L. Scott, *J. Am. Chem. Soc*., 2001, **123**, 8701.
34. G. W. V. Cave, C. L. Raston and J. L. Scott, *J. Chem. Soc. ,Chem. Com*., 2001, 2159.
35. A. Werner and J. Subak, *Ber*., 1896, **29,** 1153.
36. H. Morawetz, In *Physics and Chemistry of the Organic Solid-state*, D. Fox, M.M. Labes, A. Weissberger, eds., Interscience Publishers, New York, 1963, Vol I.
37. I. C. Paul and D. Y. Curtin, *Acc. Chem. Res.*, 1973, **6**, 217.
38. J. Haleblian and W. McCrone, *J. Pharm. Sci.,* 1969, **58**, 911.
39. H. G. Fritz, H. M. Hutmacher, H. Musso, G. Algren, B. Akermark and R. Karlsson, *Chem. Ber*., 1976, **109**, 3781.

40. K. Mohri, A. Kanie, Y. Horigushi and K. Isobe, *Heterocycles*, 1999, **51**, 2377.
41. T. Hasegawa, N. Tomohiro, T. Kakita, H. Toyoda, H. Toya and I. Deda, *Chem. Pharm. Bull*., 1993, **41**, 1760.
42. P. E. Eaton, *Angew. Chem, Int. Ed.,* 1992, **31**, 1421.
43. S. T. Bormann, *Chem. Eng. News*, 1994, **28**, 34.
44. G. Kaupp, M. R. Naimi-Jamal and J. Schmeyers, *Tetrahedron*, 2003, **59**, 3753.
45. B. M. Choudary, M. K. Lakshmi, B. Kavita, Ch. R. Venkat and F. Figueras, *Tetrahedron*, 2000, **56**, 9357.
46. T. Sugino and K. Tanaka, *Chem. Lett*, 2001, 110.
47. R. H. Khan, R. K. Mathur, and A. C. Ghosh, *Synth. Commun.*, 1996, **1996**, 26, 683.
48. D. S. Bose and A. V. Narsaiah, *J. Chem. Res*, 2001, 36.
49. C. P. Phadke, S. L. Kelkar and M. S. Wadia, *Synth. Commun.*, 1984, **14**, 407.
50. A. K. Awasthi and R. S. Tewari, *Synthesis*, 1986, 1061.
51. L. Bonsignore, F. Cottiglia, S. M. Lavagna, G. Loy and D. Secci, *Heterocycl.*, 1999, **50**, 469.
52. V. Armstrong, O. Soto, J. A. Valderrama and R. Tapia, *Synth. Commun*, 1988, **8**, 717.
53. E. Obrador, M. Castro, J. Tamariz, G. Zepeda, R. Miranda and F. Delgado, *Synth. Commun.*, 1998, **28**, 4649.
54. S. Balalaie and N. Nemati, *Synth Commun*., 2000, **30**, 869.
55. G. Sabitha, B. V. S. Reddy, R. S. Satheesh and J. S. Yadav, *Chem. Lett.*, 1998, 773.
56. A. Loupy, S. Song, S. Sohn, Y. Lee and T. Known, *J. Chem. Soc., Perkin Trans.* 1, 2001, 1220.
57. R. Maggi, F. Bigi, S. Carloni and A. Mazzoc, *Green Chem.*, 2001, 173.
58. F. Bigi, M. L. Conforti, R. Maggi, A. Piccinno and G. Sartori, *Green Chem*., 2000, 173.
59. F. Bigi, S. Carloni, L. Ferrari, R. Maggi, A. Mazzacani and G. Sartori, *Tetrahedron Lett*., 2001, **42**, 5203.

60. J. Adamson, B. J. Coe, H. L. Grassam, J. C. Jeffrey, S. J. Coles and M. B. Hursthouse, *J. Chem. Soc, Perkin Trans 2*, 1999, **17**, 2483.
61. S. Akabori, *Chem. Ber.,* 1933, **66**, 139.
62. B. S. Jursic, *Heterocycl. Chem.,* 2001, **38**, 655.
63. B. S. Kulkarni, B. S. Fernandez, M. R. Patel, R. A. Bellare and C. A. Deliwala, *J. Pharm. Sci*., 1969, **58,** 852.
64. A. Mustafa, *Chem. Heterocycl. Comp.,* 1974, **29,** 1**.**
65. R. S. Varma, D. Kumar and P. J. Liesen, *J. Chem. Soc., Perkin Trans.* 1, 1998, 4093.
66. M. K. Rout and H. K. Pujari, *J. Am. Chem. Soc.,* 1953, **75**, 4057.
67. A. H. M. Raeymaekers, F. T. N. Allewijin, J. Vandenberk, P. J. A. Demon, T. T. T. Van Offenwent and P. A. J. Jansen, *J. Med. Chem*., 1966, **9**, 545.
68. L. C. King and R. J. Hlavacek, *J. Am. Chem.,* 1950, **72**, 3722.
69. P. Sears and C.–H. Wong, *Angew. Chem, Int. Ed.*, 1999, **38**, 2300.
70. M. L. Sinnot, *Chem. Rev*, 1990, **90**, 1171.
71. H. Hausler, P. Kawakami, E. Mlaker, W. B. Severn, T. M. Wrodnigg and A. E. Stutz, *Carbohydr. Chem.,* 2000, **19**, 423.
72. Y. Nishimura, T. Satoh, H. Adachi, S. Kondo, T. Takeuchi, M. azetaka, H. Fukuyasu and Y. Lizuka, *J. Med. Chem*, 1997, **40**, 2626.
73. P. B. Anzeveno, L. J. Creemer, J. K. Daniel, C.–H. King and P. S. Liu, *J. Org. Chem*., 1989, **54**, 2539.
74. A. Dondoni, D. Perrone and M. Rinaldi, *J. Org. Chem.*,1998, **63**, 9252.
75. M. Panayotova and B. Velikov, *J. Environ. Sci. Health,* Part A, 2002, **2**, 139.
76. K. Okada, N. Watanabe and V. K. Jha, Y. Kameshima, A. Yasumori, *J. Mater. Chem.,* 2003, **13**, 550.
77. G. Centi, F. Trifiro, G. Busca, J. Ebner and J. Gleaves, *Faraday Discuss.,* 1989, **87**, 499.
78. G. Centi, *Catal. Today*, 1994, 16.
79. E. Bordes, *Catal. Today*, 1987, **1**, 499.
80. G. J. Hutchings, *Appl. Catal.*, A, 1992, **72**, 1.

81. R. M. Contractor, H. S. Horowitz, G. M. Sisler and E. Bordes, *Catal. Today,* 1997, **106**, 51.
82. G. Centi, T. Tosarelli and F. Trifiro, *J. Catal.*, 1993, **42**, 70.
83. F. Trifiro, *Catal. Today*, 1993, **16**, 91.
84. J. K. Bartley, C. J. Kiely, R. P. K. Wells and G. J. Hutchings, *Catal. Lett.*, 2001, **72**, 99.
85. P. G. Lacroix, R. Clement and K. Nakatani, *Sci.*, 1994, **263**, 658.
86. R. Brec, *Solid-state Ionics*, 1986, **22**, 3.
87. R. Diel and C. D. Carpentier, *Acta Crystallogr., Sect B: Struct. Sci.*, 1977, **33**, 1399.
88. P. Toffoli, P. Khodadad and N. Rodier, *Acta Crystallogr., Sect B: Struct. Sci.,* 1977, **33**, 285.
89. Z. Huang, J. Zhao, J. Mi, S. Moa and L. Zheng, *J. Solid State Chem.*, 1999, **144**, 391.
90. C. A. Vincent, *Solid State Ionics*, 2000, **134**, 159.
91. H. Pfeiffer, P. Bosch and S. Bulbulian, *J. Nucl. Mater.,* 1998, **257**, 309.
92. C. E. Johnson, *J. Nucl. Mater.,* 1999, **270**, 212.
93. L. Montanaro, A. Negro and J. P. Lecompte, *J. Mater. Sci.,* 1995, **30**, 4335.
94. M. Broussely, F. Perton, P. Biensan, J. M. Bodet, J. Labat, A. Lecerf, C. Delmas, A. Rougier and J. P. Peres, *J. Power Sources,* 1995, **54**, 109.
95. V. Subramanian, C. L. Chen, H. H. Chou and G. T. K. Fey, *J. Mater. Chem.,* 2001, **11**, 3348.
96. C. –H. Lu and L. Wei-Cheng, *J. Mater. Chem*, 2000, **10**, 1403.
97. X. Yang, W. Tang, H. Kanoh and K. Ooi, *J. Mater. Chem*., 1999, **9**, 2683.
98. H. Kudo, K. Okuno and S. O'hira, *J. Nucl. Mater.,* 1988, **155-157**, 524.
99. M. Nagai, M. Hibino, T. Nishino and K. Noda, *J. Mater. Sci. Lett*., 1993, **12**, 107.
100. Y. Kawamura and M. Nishikawa, *J. Nucl. Mater*., 1995, **218**, 57.
101. H. Pfeiffer and K. M. Knowles, *J. Europ. Ceram.. Soc.,* 2004, **24**, 2433.
102. S. F. Meier and T. Schleid, *J. Solid-state Chem.*, 2003, **171**, 408.
103. S. Nathansohn, *J. Inorg. Nucl. Chem.,* 1968, **30**, 741.

104. R. Mahe, P. H. Dixneuf and S. Lecolier, *Tetrahedron Lett*., 1986, **27**, 6333-6336.
105. C. Bianchini, M. Peruzzini, F. Zanobi, P. Frediani and A. Albinati, *J. Am. Chem. Soc*., 1991, **113**, 5453.
106. Y. Wakatsuli, H. Yamazaki, N. Kumegawa and T. Satoh, *J. Am. Chem. Soc*., 1991, **113**, 9604.
107. I. R. Beattie and D. P. N. Satchell, *J. Chem. Soc., Faraday Trans*., 1956, **52**, 1590.
108. I. Grenthe and E. Nordin, *Inorg. Chem.*, 1979, **18**, 1869
109. I. Grenthe and E. Nordin, *Inorg. Chem.*, 1979, **18**, 1109
110. R. H. Herber and Y. Goscinny, *Inorg. Chem*., 1968, **7**, 1293.
111. N. J. Coville and D. C. Levendis, *Eur. J. Inorg. Chem.*, 2002, 3067.
112. K. Katsuki, Y. Ooyama, M. Okamoto and Y. Yamamoto, *Inorg. Chim. Acta*, 1994, **217,** 181.
113. D. W. Krassowski, K. Reimer, H. E. LeMay and J. H. Nelson, *Inorg. Chem.*, 1988, **27**, 4307.
114. F. M. Nareetsile, O. P. M. Horwood, D. G. Billing, D. C. Levendis and N. J. Coville, *J. Organomet. Chem*., 2003, **682**, 2.
115. C. Soubra, Y. Oishi, T. A. Albright and H. Fujimoto, *Inorg. Chem.*, 2001, **40**, 620.
116. A. A. Ismail, F. Sauriol and I. S. Butler, *Inorg. Chem.*, 1989, **28**, 1007.
117. M. L. H. Green and G. H. Wilkinson, *J. Chem. Soc*., 1958, 4314.
118. C. P. Casey, M. A. Andrews, D. R. McAlister and J. E. Rinz, *J. Am.Chem. Soc.,* 1980, **102**, 1927.
119. K. I. Goldberg and R. G. Bergman, *J. Am. Chem. Soc.,* 1989, **111**, 1285.
120. W. Tam, G. Y. Lin, W. K. Wong, W. A. Kiel, V. K. Wong and J. A. Gladysz, *J. Am.Chem. Soc*., 1982, **104**, 141.
121. A. H. Klahn and D. Sutton, *Organometallics,* 1985, **4**, 198.
122. Y. X. He, R. J. Batchelor, F. W. B. Einstein, L. K. Peterson and D. Sutton, *J. Organomet. Chem.,* 1997, **531**, 27.
123. M. D. Cavanaugh, S. M. Tetrick, C. J. Masi and A. R. Cutler, *J. Organomet. Chem*., 1997, **538**, 41.
124. W. H. Bosch, U. Englert, B. Pfister, R. Stauber and A. Salzer, *J. Organomet.*

Chem., 1996, **506**, 273.

125. F. W. B. Einstein, A. H. Klahn-Oliva, D. Sutton and K. G. Tyers, *Organometallics*, 1986, **5**, 53.
126. G. K. Yang and R. G. Bergman, *Organometallics*, 1985, **4**, 129.
127. D. F. Dong, J. K. Hoyano and W. A. G. Graham, *Can. J. Chem.,* 1981, **59**, 1455.
128. C. M. Nunn, A. H. Cowley, S. W. Lee and M. G. Richmond, *Inorg. Chem*., 1990, **29**, 2105.
129. A. H. Klahn, C. Manzur, A. Toro and M. Moore, *J. Organomet. Chem*, 1996, **516**, 51.
130. L. Cheng and N. J. Coville, *Organometallics*, 1996, **15**, 867.
131. L. Cheng and N. J. *Coville, J. Organomet. Chem*., 1998, **556**, 111.
132. R. H. Hill and B. J. Palmer, *Organometallics,* 1989, **8**, 1651.
133. W. Xia, R. S. Hill, A. H. Klahn, C. Leiva and G. E. Buono-Core, *Polyhedron*, 1996, **15**, 3093.
134. J. W. Faller and A. S. Anderson, *J. Am. Chem. Soc*., 1970, **92**, 5852.
135. R. S. Bogadi, D. C. Levendis and N. J. Coville, *J. Am. Chem. Soc*., 2002, **124**, 1104.
136. S. B. Butts, E. M. Holt, S. H. Strauss, N. W. Alcock, R. E. Stimson and D. F. Shriver, *J. Am. Chem. Soc.,* 1979, **101**, 5864.
137. J. Tsuji, *Organic Synthesis by Means of Transition Metal Complexes*, Springer-Verlag, Berlin, 1975.
138. A. Wojcicki, *Adv. Organomet. Chem.,* 1973, **11**, 67.
139. F. Calderazzo, *Angew. Chem. Int. Ed.,* 1977, **16**, 299.
140. R. L. Pruett, *Adv. Organomet. Chem.,* 1979, **17**, 1.
141. D. Forster, *Adv. Organomet. Chem.,* 1979, **17**, 255.
142. S. B. Butts, S. H. Strauss, E. M. Holt, R. E. Stimson, N. W. Alcock and D. F. Shriver, *J. Am. Chem. Soc.,* 1980, **102**, 5093.
143. T. S. Piper and G. Wilkinson, *J. Inorg. Nucl. Chem*., 1956, **3**, 104.
144. I. S. Butler, F. Basolo and R. G. Pearson, *Inorg. Chem*., 1967, **6**, 2074.
145. J. D. Cotton, G. T. Crisp and V. A. Daly, *Inorg. Chim. Acta*, 1981, **47**, 165.

146. K. W. Barnett, D. L. Beach, S. P. Gaydos and T. G. Pollmann, *J. Organomet. Chem*., 1974, **69**, 121.
147. K. W. Barnett and P. M. Treichel, *Inor. Chem*., 1967, **6**, 294.
148. M. J. Wax and R. G. Bergman, *J. Am. Chem. Soc.,* 1981, **103**, 7028.
149. M. P. Craig and M. Green, *J. Am. Chem. Soc.,* 1969, 157.
150. M. R. Churchill and M. P. Fennessey, *Inorg. Chem*., 1968, **7**, 953.
151. J. D. Cotton, M. M. Kroes, R. D. Markwell and E. A. Miles, *J. Organomet. Chem.,* 1990, **288**, 133.
152. P. J. Craig and M. Green, *J. Chem. Soc.*, 1968, 1978.
153. J. A. McCleverty and G. Wilkinson, *J. Chem. Soc.,* 1963, 4096.
154. R. D. Closson, T. H. Coffield and J. Kozikowski, *Int. Conf. Coord. Chem., Soc. Spec. Pub*., 1959, **13**, 126.
155. G. Capron-Cotigny and R. C R. Poiblanc, *Acad. Sci. Paris, Ser. C*, 1966, **266**, 285.
156. K. W. Barnett and D. W. Slocum, *J. Organomet. Chem*., 1972, **44**, 1.
157. O. G. Adeyemi and N. J. Coville, *Organometallics*, 2003, **22**, 2284.
158. M. D. Bala, A. Budhai and N. J. Coville, *Organometallics*, 2004, **23**, 2048.
159. G. Kaupp, J. Schmeyers and J. Boy, *Chemosphere*, 2001, **43,** 243.
160. R. B. King, A. D. King, M. Z. Iqbal and C. C. Frazier, *J. Am. Chem. Soc.,* 1978, **100**, 1787.
161. S. Thorand and N. Krause, *J. Org. Chem.*, 1998, **63**, 8551.
162. K. Sonogashira, Y. Tohda and N. Hagihara, *Tetrahedron Lett.,* 1975, 4467.
163. V. Boldyrev and K. Tkacova, *J. Mater. Synth. Process,* 2000, **8**, 121.
164. J. F. Fernandez-Bertran, *Pure Appl. Chem.,* 1999, **71(4)**, 581.
165. J. F. Fernandez-Bertran, J. C. Alvarez and E. Reguera, *Solid State Ionics, 1998, **106,*** 129.
166. V. R. Pedireddi, W. Jones, A. P. Chorlton, R. Docherty, *J. Chem. Soc., Chem. Commun.*, 1996, 987.
167. D. Braga, F. Grepioni, L. Maini, M. Polito and L. Mirolo, *Chem. Eur*., 2003, **9**, 4362.

168. D. Braga, F. Grepioni and L. Maini, *Chem. Commun.*, 1999, 937.
169. D. Braga and F. Grepioni, *Chem. Soc. Rev*, 1999, **29**, 229.
170. P. J. Nichols, C. L. Raston and J. W. Steed, *Chem. Commun.,* 2001, 1062.
171. D. Braga, D. D'Addario and M. Polito, *Organometallics*, 2004, **23**, 2810.
172. A. K. Galwey, *Pure Appl. Chem.,* 1995, **67**, 1809.
173. U. B. Eke and N. J. Coville, *Inorg. Chem. Commun.*, 2000, **3**, 368.
174. J. A. Osborn, F. H. Jardine, J. F. Young and G. Wilkinson, *J. Chem. Soc.*, 1966, 1711.
175. D. Evans, J. A. Osborn and G. Wilkinson, *Inorg. Synth.*, 1968, **11**, 99.
176. M. O. Albers and N. J. Coville, *Coord. Chem. Rev*, 1984, **53**, 227.
177. F. Porta, S. Tollari and C. Bainchi, *Inorg. Chim. Act*, 1996, **249**, 79.
178. E. W. Abel, F. G. A. Stone and G. Wilkinson, *Comprehensive Organometallic Chemistry II*, Pergamon, New York, 1995.
179. A. C. Filippou, J. G. Winter, M. Fiest, G. Kociok-Kohn and I. Hinz, *Polyhedron*, 1998, **17**, 1103.
180. L. Cheng, Doctoral Thesis, University of the Witwatersrand, Johannesburg, 1998.
181. C. A. Tolman, P. Z. Meakin, D. L. Lindner and P. J. Jesson, *J. Am. Chem. Soc*., 1974, **96**, 2762.

CHAPTER 3. EXPERIMENTAL AND CHARACTERISATION PROCEDURES

3.1. INTRODUCTION

Experimental and characterisation procedures are described for all the transformations performed in this study. The chapters that follow will not repeat information on the procedures mentioned here.

3.2. EXPERIMENTAL PROCEDURES

3.2.1. Work Bench Setup

All reactions were performed using a dual manifold line with nitrogen and vacuum lines connected by 2-way ground glass taps. The vacuum line was connected to a solvent trap that was in turn connected to a vacuum pump that enabled a maximum pressure of 0.1 mm of Hg when fully opened. Nitrogen (99.999%) was passed through a tube (3.2 × 30 cm) containing molecular sieves (4 Å) and dry blue copper sulphate (2-6 cm grain size) indicator. The flow rate of the gas passing through was monitored using a paraffin oil bubbler that was connected to the nitrogen line. This also acted as a guard against accidental atmospheric air intrusion to the reaction line though a back suction force when the system was evacuated. The molecular sieves used were periodically regenerated by heating at 200°C under vacuum, cooled back to room temperature and purged with ultra dry nitrogen gas. The copper sulphate granules were regenerated by heating at 250°C overnight or until they turned blue again.

3.2.2. Glove Box

Some of the transformations were deemed extremely air sensitive such that the experiment was carried out in a glove box. The glove box is a standard instrument armed with three openings for attachments of neoprene gloves, two isolable chambers to introduce and remove samples from the chamber, a exhaust valve leading to an oil trap to guard against pressure increments, a dew point indicator to indicate humidity levels inside the chamber, a diaphragm pump to circulate inert gas and an air purifier armed with two reactors, one containing copper to trap oxygen as copper oxide and the other containing molecular sieves to trap water. The chamber was connected to an argon cylinder that introduced the inert gas continuously. The procedure of introducing and removing samples through the isolable chambers were adhered to at all times to avoid accidental introduction of atmospheric air into the chamber.

3.2.3. Solvent Purification

Solvents used for the reactions were dried and deoxygenated before use. The procedure followed was to pre-dry the solvents using 4 Å molecular sieves for 24 h in the reagent bottle (5% m/v of molecular sieves were used). The pre-dried solvents were then dried by distilling the solvent from an appropriate drying medium under nitrogen flow. The solvents were distilled as required immediately before use for a particular experiment.

3.2.4. Experimental techniques

All reactions and manipulations were performed using standard inert atmosphere techniques using the manifold described. Most of the glassware used were standard Schlenk tubes with 2.5 mm glass taps and standard glass vessels (round-bottom flasks, reaction tubes, funnels, sintered glass filters) bought from Sigma-Aldrich. The transfer of reagents was accomplished using either syringes or cannulae.

3.3. CHARACTERISATION PROCEDURE

3.3.1. FTIRS

Infrared spectra were recorded on a Bruker Vector FTIR spectrometer. The sample to be analysed was dissolved in a small amount of a solvent (usually dichloromethane) and the reflectance of the samples in the infrared region recorded using the solvent as a blank. Sometimes it was necessary to analyse the compound as a solid material. In this case a small amount of sample (5 mg) was thoroughly mixed with KBr (200 mg) and the mixture ground to a fine powder before being pressed to form a thin transparent sheet using an aluminium alloy press. The product was a small transparent disk of material to be analysed that was held in place by a ready-made paper container that docked to the groove side for analysis in the IR spectrometer. A spectrum of the sample was then recorded after obtaining a background spectrum.

3.3.2. DRIFTS

This technique was the main technique used during the project. Its use is explained in detail below. Diffuse reflectance infrared Fourier transform spectroscopy (DRIFTS) is a useful technique for measuring the amount of solid material in a matrix of choice. The technique is useful for following reactions that takes place in the solid-state. DRIFTS offers the following advantages:

1. It is a sufficiently sensitive technique that requires minute amounts of sample for detection (100 μg of material can be detected).
2. It is a relatively fast method of analysis. Preparation of samples, recording of FTIR-spectra and data analysis can be carried out in a short time.

The technique has been used for the analysis of a variety of powdered materials, these include:

1. Inorganic materials; coals[1], cement[2], kaolin clay[3], silicon nitride[4], calcium carbonate[5] and superconductor precursor powders[6].
2. Organic materials; carbohydrates[7] and caffeine[8].

The data can be recorded in three ways:

1. Transmittance. The transmittance data is generated automatically from the following formula:

$$Transmittance\ file = \frac{Sample\ file}{Background\ file} \times 100$$

The ratio operation is useful in spectroscopic applications where the sample and background (also known as the reference) spectra are collected and stored separately (such as in a FTIR instrument). The Y-axis units are arbitrary so that the program can calculate the ratio succinctly.

Transmittance analysis can also generate a transmission spectrum from an absorbance spectrum using the formula below. The data is automatically converted from absorbance to percent transmittance. The data used is stored and there is no need to run the background spectrum for this operation.

$$\%\ Transmittance = 10^{(2-\text{Absorbance})}$$

2. Absorbance. Absorbance can produce an absorbance spectrum using the formula shown below. Here again the ratio operation in spectroscopic applications involve the sample and background spectra being collected and stored separately. As before, the Y-axis must have arbitrary units.

$$Absorbance\ \ file = -\log \frac{Sample\ \ file}{Bachground\ \ file}$$

Absorbance can also generate an absorbance spectrum from a transmittance spectrum using the formula below. The data is automatically converted from percent transmittance to absorbance. A background spectrum is not required for this operation.

$$Absorbance = log \frac{100}{\%\ Transmittance}$$

3. Kubelka-Munk. A Kubelka-Munk spectrum is created from the following formula:

$$Kubelka - Munk\ \ file = \left[\frac{\left[1 - \left[\frac{Sample\ \ file}{Background\ \ file} \right] \right]^2}{\left[2 \times \left[\frac{Sample\ \ file}{Background\ \ file} \right] \right]} \right]$$

The ratio application is useful in spectroscopic applications where the sample and background spectra are collected and stored separately. The Y-axis must have arbitrary units for the operation to work properly.

Kubelka-Munk can also convert a transmittance or absorbance spectrum into a Kubelka-Munk spectrum using the following formula:

$$Kubelka - Munk = \frac{\left[1 - Transmittance \right]^2}{\left[2 \times Transmittance \right]}$$

The conversion from absorbance data, requires a two-step process. First, the absorbance data are converted to transmission data as described above, and secondly, the

transmission data is then converted to Kubelka-Munk spectrum using the formula above. However, a background spectrum is not required for the operation.

Our experience in the laboratory of use of a Bruker FT-IR instrument available for analysis was the difficulty of converting Kubelka-Munk data to absorbance or transmittance data. There was no automatic conversion from the former to the latter (sometimes transmittance data better represented the experimental data). The conversion of transmittance/absorbance data to Kubelka-Munk data was achieved with ease. Thus the strategy adopted in all the experiments was to record the data as transmittance files, which were then converted to the other two forms when the need arose.

3.3.3. NMR Spectroscopy

NMR spectra were recorded using either a Bruker AC200 MHz (^{1}H = 200.13MHz, ^{13}C = 50.32MHz, ^{31}P = 200.13MHz) connected to an Aspect 3000 data processing unit or a Bruker DRX 400MHz (^{1}H = 400.13MHz, ^{13}C = 100.61MHz, ^{31}P = 400.13MHz) connected to a Silicon Graphics Indy workstation. Most spectra were recorded in Chloroform-*d* (99.8 atom %D, containing 0.03% v/v TMS). Spectra were then referenced to trimethylsilane, on the δ-scale. When dealing with manganese complexes, the solvent was used directly from the bottle without further purification. When zirconium complexes were analysed the solvent was dried and deoxygenated using the appropriate method before use. This involved drying the solvent in calcium hydride for at least three days followed by transfer to a clean dry dark-coated container, containing zinc wire, using a metal cannula. The solvent was then deoxygenated by 5 freeze-pump-thaw cycles. It was then purged with dried argon and kept in a dark bottle, in the dark, at all times.

3.3.4. DSC (Differential Scanning Calorimetry)

The melting points and other useful endotherms and exotherms were determined using a Du Pont 910 differential scanning calorimeter (DSC). Approximately 3 mg of sample was weighed into an aluminium weighing pan of known weight and heated at 10°C/min (sometimes there was a need to use a slower heating rate e.g. 1°C/min) from 30°C to 300°C under nitrogen gas. The sample was then cooled back to room temperature before the next sample was analysed.

3.3.5. Mass Spectrometry

Mass spectrometry was carried out using a VG70 SEQ mass-spectrometer utilising a MSS II/32 Windows Data System. Samples were introduced using a solid probe and ionisation accomplished by electron impact (70eV, 200μA).

3.3.6. Elemental Analysis

Element analyses were performed by the Agricultural Research Council, CSIR, Pretoria. The analysis was conducted using a Carlo Erba Na 1500 C/N/S Analyser armed with 2 furnaces, one containing the combustion quartz tube reactor and the other containing the reduction quartz reactor. The two furnaces were separated by a space to allow the installation of two traps, including a water vapour trap. The instrument also had an oven containing a gas chromatographic separation column to separate N_2, CO_2, H_2O vapour and SO_2, a thermal conductivity detector (TCD). Helium was used as a carrier gas (reference for TCD) and for purging the sample before analysis. When configured for C and H analysis, the combustion reactor was packed with a chrome oxide catalyst above a layer of silvered cobalt oxide, while the reduction reactor contained copper (at 450°C) to consume excess oxygen gas. The instrument was modified to determine H, by removing the water in the water vapour trap and by heating the sample (heating was required to prevent a long retention time of the water (H) peak, which made integration difficult, due to the broad peak).

All samples were analysed in duplicate, using 1-6 mg for each analysis. The sample and tin container were ignited at high temperature (1020°C) in oxygen, with the sample temperature rising to over 1500°C for a fraction of a second on ignition of the tin container. The GC oven temperature was set at 80°C for the entire analysis period. Benzoic acid (specified > 99.9% pure, BDH AR) was used as calibration standard, while potassium hydrogen phthalate (specified > 99.9% pure, Merck GR) was used to check the accuracy of the calibration. Linear regression calibrations were used for the H analysis, while the C analysis was computed using a non-linear regression calibration including 14 standard runs, covering a range from 0.3 mg to 1mg C.

3.3.7. GC (Gas Chromatography)

GC analysis was carried out using GC machine containing a ZB5 column (30 m × 0.32mm × 0.5 μm). The carrier gas was argon (UHP) at a flow rate of 1.4 cm^3 per min. Hydrogen and compressed air gases were supplied at a pressure of 0.5 bars. The oven temperature was kept at 30°C while the injection and the FID temperatures were set at 200°C and 250°C respectively. The FID was attached to a recorder.

The liquid sample to be analysed (0.5 μl) was injected into the column using a micro syringe. The sample was then resolved according to its affinity for the stationary phase (absorbent) as it moved along the coiled column. The resolved components of the sample were eventually ionised just before it reached the FID. The detected ionisation signals were subsequently recorded, using a coupled recorder, as a series of peaks with different retention times. Pure hex-1-ene, *trans*-hex-2-ene, *cis*-hex-2-ene, *trans*-hex-3-ene, *cis*-hex-3-ene, hexane, pentane, 1-pentene, butane, 1-butene and 2-butene were run as standards prior to the investigation to check their respective retention times.

3.3.8. XRD (X-Ray Diffraction)

Determination of the unit cell parameters, crystal orientation and data collection were performed on the SMART system[9]. The programme SHELXTLplus (Ver 5.1) was used for the structure solution, refinement and publication preparation[10]. Molecular graphics were prepared using ORTEP-3 for Windows[11].

Crystallographic comparison data from similar compounds (manganese and zirconium complexes) were obtained from the Cambridge Structural Database (CSD)[12,13,14]. The structures were solved by direct methods using Fourier techniques and refined by full matrix least squares method based on F^2.

3.4. REFERENCES

1. I. M. Hamadesh, S. A. Yeboah, K. A. Trumbull and P. R. Griffiths, *Appl. Spectrosc*., 1984, **38**, 486.
2. T. L. Hughes, C. M. Methven, T. G. J. Jones, S. E. Pelham, P. Fletcher and C. Hall, *Adv. Cem. Bas. Mater.,* 1995**, 2**, 91.
3. T. J. Porro and S. C. Pattacini, *Appl. Spectrosc*., 1990, **44**, 1170.
4. A. Tsuge, Y. Uwamino, T. Ishizuka and K. Suzuki, *Appl. Spectrosc*., 1991, **45**, 1377.
5. D. M. Hembree and H. R. Smyrl, *Appl. Spectrosc*., 1989, **43**, 267.
6. J. Bak and B. Kindle, *Appl. Spectrosc*., 1997, **51**, 1730.
7. J. M. Olinger and P. Griffiths, *Appl. Spectrosc*., 1993, **47**, 687.
8. S. Agyare, S. Wang and P. R. Griffiths, *Appl. Spectrosc*., 1984, **38**, 259.
9. Bruker Analytical X-ray Instruments Inc., *SMART Reference Manual*, 1997, Madison, Wisconsin, USA.
10. Bruker Analytical X-ray Instruments Inc., *SHELXTLplus (Windows NT version)-Structure Determination Package*, Ver5.1, 1988, Madison, Wisconsin, USA.
11. L. J. Farrugia, *J. Appl. Cryst.,* 1997, **30**, 565.
12. F. H. Allen, J. E. Davies, J. J Galoy, O. Johnson, O. Kennard, C. F. Macrae, E. M. Mitchell, J. M. Smith and D. G. Watson, *J. Chem. Inf. Comput. Sci*, 1991, **31**, 187.
13. The Cambridge Data Centre, *The Cambridge Structural Database,* Ver5.17, Cambridge, 1999.
14. F. H. Allen and O. Kennard, *Chem. Des. Autom. News*, 1993, **8**, 31.

CHAPTER 4: SYNTHESIS OF MANGANESE CARBONYL COMPLEXES USING LITERATURE METHODS

4.1. INTRODUCTION

4.1.1. Historical perspective

A study of the organometallic chemistry of manganese started in earnest about the middle of the 20th century. Fischer and co-workers reported the preparation of manganocene [bis(cyclopentadienyl)manganese][1] from manganese(II) iodide in 1954. During the same time period $Mn_2(CO)_{10}$ that was first synthesised in 1949 by the carbonylation of a mixture of MnI_2 and a Grignard reagent[2], was fully characterized by Brimm *et al*[3]. These two complexes have served as starting materials for a variety of other useful manganese reagents.

For example, the treatment of manganocene with CO under pressure resulted in the formation of $Mn(CO)_3(\eta^5\text{-}C_5H_5)$ by Wilkinson's research group[4]. The antiknock agent for petrol, $Mn(CO)_3(\eta^5\text{-}C_5H_5Me)$, was also prepared for the first time in 1954. The economical importance of these manganese complexes sparked a sustained research interest in these metal compounds.

Reactions involving dimanganese decacarbonyl include its reduction using sodium amalgam to form $Na[Mn(CO)_5]$[5] that was used to make $MnMe(CO)_5$ [6], the first reported complex containing a genuine Mn-C σ-bond. $MnMe(CO)_5$ was further investigated and found to undergo insertion reactions of a CO molecule under pressure[7]. The reaction of dimanganese decacarbonyl with halogens results in the cleavage of the Mn-Mn bond to form $Mn(CO)_5X$ (X = Cl, Br, I)[8].

Manganese pentacarbonyl iodide [$Mn(CO)_5I$] was the first halomanganese carbonyl to be characterised. It was synthesised during the carbonylation of MnI_2. The yield was rather low (<10%) and the oxidative cleavage of $Mn_2(CO)_{10}$ by I_2 provides better yields. Once the complexes $Mn(CO)_5X$ (X = Cl, Br, I) were synthesised with relative ease, their chemistry was investigated. It was found that heating $Mn(CO)_5X$ in an inert solvent at 120°C afforded the dinuclear species $Mn_2(CO)_8X_2$[9].

Substitution reactions involving $Mn(CO)_5X$ by neutral ligands to liberate CO and produce $Mn(CO)_{5-n}L_nX$ (n = 1-4) have been widely studied. The reactions were conducted under thermal conditions or by using UV photolysis in non-polar solvents like benzene, toluene and xylene. Mono- and di-substituted products were easily achieved with most ligands but tri- and tetra-substitution of CO ligands were rarely encountered. The steric features of the ligands governed the restriction. The resulting complexes were found to be stable and were used as precursors for the synthesis of other manganese compounds.

The synthesise of $Mn(CO)_4LX$ complexes from $Mn(CO)_5X$ was driven by the quest to study migratory insertion reactions of the manganese complexes. When problems arose in the synthesis of $Mn(CO)_4LX$ from $Mn(CO)_5X$ due to the formation of di-substituted complexes, [$Mn(CO)_3L_2X$], an alternate route using $Mn_2(CO)_8X_2$ was discovered and has been the favoured synthetic route since then. When using $Mn_2(CO)_8X_2$ it was discovered that the rate of cleavage of the halide bridged dimeric species was rapid resulting in the reaction being more favourable than found for the preparation of the mono-substituted complexes[10].

Disubstituted complexes, $Mn(CO)_3(L)_2X$, are easily prepared from $Mn(CO)_5X$ using excess ligand under moderate conditions[11,12]. The reaction always resulted in the formation of the *fac* isomer as a kinetic product. If the ligand was bulky like PPh_3, rearrangement to the *mer* (*trans*) isomer occurred to minimise steric strain even when mild conditions were employed[13]. The isomerisation reaction[14] was easily followed using FTIRS and the kinetics of the reaction indicated a dissociative mechanism[12].

Manganese complexes containing carbonyl groups have been characterised by their carbonyl stretching frequencies, υ(CO), which give precise molecular structures as well as ligand electronic contributions. The method was also employed to study the reaction rates of manganese complexes. NMR spectroscopy was also used as an analytical tool for structural elucidation, molecular dynamics and reaction rate studies. Other techniques like mass spectrometry[15], XRD[16], ESR[17] and DSC[18] have been rarely used during investigations related to manganese(I) chemistry.

4.1.2. Synthesis and kinetics

The latter part of the 20th century has witnessed the synthesis of many manganese carbonyl complexes[19]. As a result many reactions have been performed on these complexes, chief of which is the substitution reaction. For example, detailed studies on the substitution reactions of $Mn(CO)_5X$ (X = Cl, Br, I) compounds with a variety of monodentate tertiary phosphine[20], phosphite[21] and arsine[22] ligands have been reported. The general reaction scheme for these reactions is shown in **Scheme 4.1**.

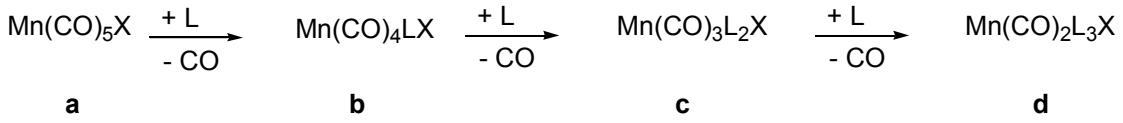

Scheme 4.1. The general reaction scheme for the reaction of $Mn(CO)_5X$ with monodentate tertiary phoshines, phosphites and arsines in solution

The monosubstituted complexes **b** were found to exhibit a *cis*-geometry for all complexes synthesised. The disubstituted complexes **c** were found to first form a *fac*-isomer that then isomerised with time, particularly in the presence of excess ligand, to the more stable *trans* isomer[23]. If the ligand was bulky, like triphenylphosphine, the reaction failed to progress beyond complex **c**, but with smaller ligands, like $P(OMe)_3$, the reaction progressed further to produce complex **d** [24].

Kinetic studies on CO substitution reactions of $Mn(CO)_5X$ (**a**) have been reported[25]. A

kinetic scheme for the substitution of CO on $Mn(CO)_5X$ by L (in solution) is shown in **Scheme 4.2**[26, 27]). The studies indicated that the rate of substitution was independent of the concentration and the nature of the ligand, L, and was first order in metal carbonyl complex, **a**.

The accepted mechanism, deduced from the studies, involved the rate determining CO dissociation from the 18-electron complex **a**, to form a 16-electron intermediate, followed by rapid entry of the incoming ligand such that the substitution reaction consisted of two steps (**Scheme 4.2**). The first step, CO dissociation from the complex, was much slower than the addition step of the ligand to reform the more stable 18-electron complex.

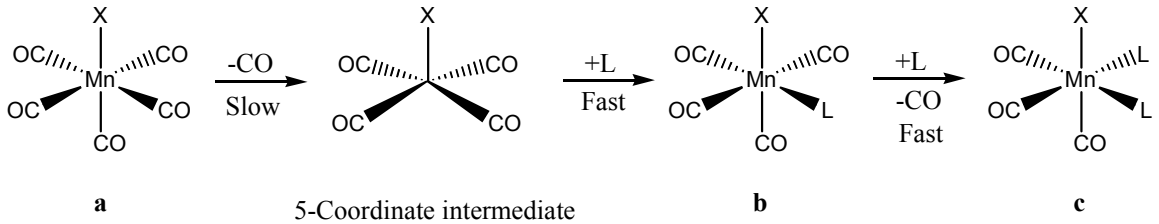

a 5-Coordinate intermediate **b** **c**

Scheme 4.2. The proposed solution reaction mechanism for the substitution reaction of the metal complex, $Mn(CO)_5X$ with a ligand, L

The solution kinetics of the conversion of complex **b** to **c** (**Scheme 4.1**) using a variety of ligands has also been studied. For all the manganese compounds that have been investigated, the rate was found to be independent of the concentration and the nature of the incoming ligand. The kinetic product of the reaction of **b** with L to give **c** was the *cis* isomer, which then rearranged to the thermodynamically stable *trans* isomer. When CO is *trans* to Br, the CO bond is strengthened relative to the case where CO is *trans* to another CO ligand. Consequently CO removal will occur in the equatorial plane. The kinetic product is then expected to be the *cis* isomer (**Scheme 4.1**). The thermodynamically stable isomer is the *trans* isomer. The preference here relates to steric factors. Two bulky ligands should be as far away from each other as possible and this will lead to *trans* isomer formation. The rate of the *cis* to *trans* isomerisation reaction of **c** has also been studied. Again a dissociative process (similar to the one shown in **Scheme 4.2**) was postulated as the path taken during the isomerisation[28].

While numerous studies of the reaction discussed above have been performed in solution, no studies have been performed in the absence of solvents.

Below is described an investigation into a study of the solvetless substitution reactions of $Mn(CO)_5Br$ and $Mn(CO)_4LBr$ by a range of phoshine ligands. It was also necessary to perform a range of reactions in the solution phase to permit comparison with the solventless data.

The ligands chosen for the study were $P(C_6H_4R)_3$ ligands with R a *para* substituted group. These ligands chosen had melting points greater than the reaction temperatures used. By using *para* substituted derivatives, the steric effect of the ligand was kept constant while the electronic effect was varied. All the ligands considered here had the same Tolman cone angle ($\theta = 145°$)[29,30,31]. Although the treatment of steric effects of ligands using the said method is semi-quantitative as it assesses the extent to which various ligands crowd each other by approximating the volume occupied by the ligand by a cone with an angle determined from a space-filling model, it has been the approach of choice used in the literature. This chapter deals with the synthesis of the metal complexes involved in the kinetic investigations described in later chapters.

4.2. EXPERIMENTAL PROCEDURES

4.2.1. Synthesis of $Mn(CO)_5Br$[8] [1]

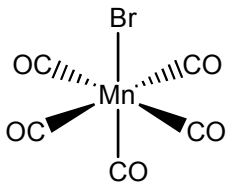

1

Yellow crystals of $Mn_2(CO)_{10}$ (2.00 g, 5.13 mmol) were taken up in dry CCl_4 (25 cm^3). The solution was then degassed for 5 min. Br_2 (0.35 cm^3, 1.06 g, 6.67 mmol, 1.30 mol equiv) in CCl_4 (15 cm^3) was also degassed for 5 min. The latter was added drop wise to the manganese carbonyl solution over a period of about 15 min. The extent of the reaction was monitored by TLC and found to be complete after about 45 min of reaction. During this time there was a gradual deposition of yellowish orange crystals as the reaction progressed.

Once the reaction was complete, the solvent was removed *in vacuo* to leave behind a yellow residue that was washed copiously with water (30 cm^3) to remove hydrophilic salts. The suspension was then filtered by suction. The filtrate was again washed with water (10 cm^3) and methanol (10 cm^3) respectively. The filtrate was then sucked dry in air and allowed to dry overnight in a desiccator. Yellowish orange crystals of pentacarbonyl manganese(I) bromide [**1**] (2.55 g, 90% yield) were characterised by IR spectroscopy: ν (CO) ($CHCl_3$), cm^{-1} (2138, 2064, 2017). The melting point was found to be 101-102°C.

4.2.2 Synthesis of $Mn_2(CO)_8Br_2$[10] [2]

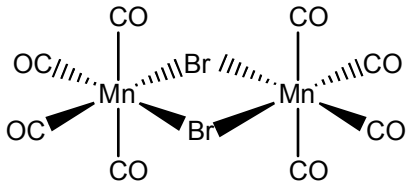

2

The dimer [**2**] was made using the following methods.

4.2.2.1 Dry heat; 138°C

$Mn(CO)_5Br$ (100 mg, 0.363 mmol) was heated at 138°C inside a reaction tube, under nitrogen gas, for an hour to give $Mn_2(CO)_8Br_2$. The sample progressively turned from yellow to orange and then to dark-brown. At the end of the reaction IR analysis showed the presence of the required product was as envisaged, (carbonyl stretching frequencies in chloroform solutions) ν(CO) ($CHCl_3$), cm^{-1}: 2056, 2023, 1994, 1954. Purification of the product by column chromatography yielded the pure product [**2**] (5 mg, 6.0% yield) that melted at 146°C.

4.2.2.2 Dry heat; 100°C

$Mn(CO)_5Br$ (100 mg, 0.363 mmol) was heated at 100°C inside a reaction tube, under nitrogen gas, for an hour. The sample progressively turned from yellow to orange and then to dark-brown. IR analysis ν (CO) ($CHCl_3$), cm^{-1} (2056, 2025, 1987, 1956) confirmed the product. Purification of the product by column chromatography resulted in separation of the pure product (14 g, 16% yield) and the melting point was found to be 146-147°C.

4.2.2.3. *n*-Octane; reflux

$Mn(CO)_5Br$ (500 mg, 1.82 mmol) was taken up in dry *n*-octane (15 cm^3) in a 50 cm^3 round bottom flask. The resulting mixture was heated at reflux (125°C) for an hour under a nitrogen flow. The mixture was allowed to cool back to room temperature. The light brown crystals that deposited at the bottom of the flask were then filtered off using a glass sinter. The crystals were then allowed to dry under vacuum suction for two h and then in a dessicator overnight to obtain pure crystals of the desired product [**2**] (11 mg, 12% yield). The melting point of the product was found to be 146°C.

4.2.2.4. Petroleum ether; (110-120°C)

$Mn(CO)_5Br$ (502 mg, 1.83 mmol) was taken up in dry petroleum ether mixture (40 cm^3) in a 100 cm^3 round bottom flask and heated for 2 h at 120°C. The reaction mixture was cooled back to room temperature, but the solution remained homogeneous. The solvent was then removed under reduced pressure to leave behind light brown crystals. IR analysis revealed a mixture of compounds composed mostly of the starting material. No attempt was made to separate the mixture.

4.2.2.5. KBr; solid-state method (100°C)

$Mn(CO)_5Br$ (100 mg, 0.363 mmol) was mixed with dry KBr (400 mg) and the mixture ground using a mortar and pestle to obtain a homogeneous mixture. The ground mixture was then heated at 100°C, inside a reaction tube, under nitrogen gas, for an hour. The sample progressively turned from yellow to orange. The mixture was then taken up in hexane (20 cm^3) and the KBr removed by filtration. The filtrate was then concentrated using high vacuum suction to give a brown amorphous powder (74 mg, 82% yield). At the end of the reaction the, IR analysis showed that the desired product was obtained with melting point of 145-146°C.

4.2.3. Synthesis of $Mn(CO)_4(L)Br$

4.2.3.1 $Mn(CO)_4(PPh_3)Br$[9] [3]

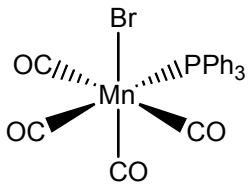

3

$Mn(CO)_5Br$ (1.00 g, 3.64 mmol) and PPh_3 (954 mg, 3.64 mmol, 1.0 mol equiv) were dissolved in dry $CHCl_3$ (50 cm^3) resulting in the formation of a yellow homogeneous solution. The solution was then allowed to stir at room temperature under nitrogen for 36 h during which time the substituted product formed. The solvent was then removed under reduced pressure to leave behind a yellow residue that was then dissolved in hot dry hexane (40 cm^3). The hot solution was filtered and the supernatant cooled to 0°C overnight in a freezer. Orange needle shaped crystals formed, which were then collected by filtration using a glass sinter to leave behind tetracarbonyltriphenyl-phosphinemanganese(I) bromide $[Mn(CO)_4(PPh_3)Br]$ [**3**] (1.82 g, 91% yield). IR analysis, ν (CO) ($CHCl_3$), cm^{-1} (2101, 2020, 2009, 1965). The melting point of the product was found to be 131°C. Anal. Calcd for $C_{22}H_{15}BrMnO_4P$: C, 51.90; H, 2.97. Found: C, 51.94; H, 3.06. HR-MS (*m / z*): Calcd for $C_{22}H_{15}BrMnO_4P$ (M^+): 507.9272. Found (EI), 507.8321.

The other compounds (**4-7**) were made the same way. The characterisation of these compounds are summarised in **Table 4.3**.

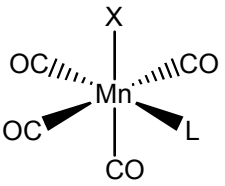

L = P(*p*-MeO-C_6H_4)$_3$ (**4**), P(*p*-Me-C_6H_4)$_3$ (**5**),
P(*p*-F-C_6H_4)$_3$ (**6**), P(*p*-Cl-C_6H_4)$_3$ (**7**)

4.2.4. Synthesis of $Mn(CO)_3L_2Br$

4.2.4.1. $Mn(CO)_3(PPh_3)_2Br$[32] [8]

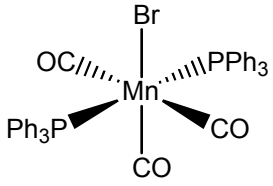

8

$Mn(CO)_5Br$ (100 mg, 0.364 mmol) and PPh_3 (479 mg, 1.82 mmol, 5.0 mol equiv) solids were dissolved in DCM (5 cm^3) resulting in the formation of a yellow homogeneous solution. The solvent was removed flushing with nitrogen gas. The yellowish orange residue was allowed to dry further in a desiccator overnight. The dry mixture was then heated at 110°C for an hour in a reaction tube under a nitrogen blanket. During the heating process, there was a gradual fading of the yellowish orange colour to a striking yellow colour, signalling the formation of a new product. The excess ligand was removed by washing the solid material with diethyl ether (3 x 5 cm^3). The yellow residue was then taken up in chloroform (2 cm^3) and mixed with hexane (6 cm^3). The solution was cooled to -30 C for 24 h to yield pale-yellow rectangular crystals, which were filtered off as the desired product, [**8**] (198 mg, 66% yield). IR analysis, ν (CO) ($CHCl_3$), cm^{-1} (2038, 1950, 1916). The compound melted at 180-182°C. Anal. Calcd for $C_{39}H_{30}BrMnO_3P_2$: C, 63.01; H, 4.07. Found: C, 62.62; H, 3.85. HR-MS (*m / z*): Calcd for $C_{39}H_{30}BrMnO_3P_2$ (M^+): 742.0234. Found $C_{39}H_{30}MnO_3P_2^+$ (M^+), 657.8136.

The other compounds were prepared similarly. The other complexes (**9-12**) were made the same way. A summary of the characterisation data for these complexes is found in **Table 4.4**.

4.3. RESULTS AND DISCUSSION

4.3.1. Synthesis of $Mn(CO)_5Br$

The method of synthesis chosen to prepare $Mn(CO)_5Br$ was the literature method[33] initially described by Wilkinson and co-workers is in **Scheme 4.3**. In our study a yield of 90% based on $Mn_2(CO)_{10}$ was obtained; higher than the reported method of 73% by the original authors. There are two possible reasons for the improvement. The first reason stems from the fact that we were able to follow the reaction using TLC such that the reaction was terminated immediately the starting material had disappeared. This would have avoided over-oxidation by Br_2. The s reason would be the use of an efficient filtration method used in the study rather than the sublimation methodology employed by the earlier researchers. IR data obtained agreed with the literature data (**Table 4.1)**.

$$Mn_2(CO)_{10} \xrightarrow[\text{rt, 45min}]{Br_2,\ CCl_4} Mn(CO)_5Br$$

Scheme 4.3. The conversion of manganese decacarbonyl to manganese(I) pentacarbonyl bromide using oxidative cleavage with bromine in chloroform

Table 4.1. Carbonyl stretching frequencies of the complex, $Mn(CO)_5Br$, as found experimentally compared to the literature values

Literature	2137	2064	2016
Experimental	2138	2064	2017

4.3.2 Synthesis of $Mn_2(CO)_8Br_2$

The literature method employed to synthesise the dimer involved thermal decomposition of manganese pentacarbonyl chlorides, bromides and iodides in an inert solvent at 120°C (light petroleum ether). Reported yields were on average 40% due to extensive decomposition. We started our synthesis using the method as described in the literature. **Scheme 4.4** shows the envisaged structure of the dimer formed from $Mn(CO)_5Br$. The methods used to make the dimer are shown in **Table 4.2**.

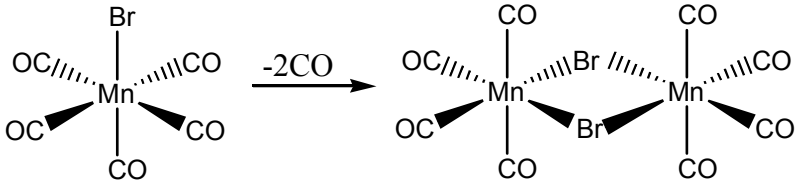

Scheme 4.4. The formation of $Mn_2(CO)_8Br_2$ from the treatment $Mn(CO)_5Br$ using different synthetic methods

Table 4.2. Data for the synthesis of $Mn_2(CO)_8Br_2$ from $Mn(CO)_5Br$

Method	Yield / %	Mp / °C	CO stretching frequencies/cm^{-1}			
Dry heat, @ 138°C	6	146	2056	2023	1994	1954
Dry heat, @ 100°C	16	146-147	2056	2025	1987	1956
n-Octane reflux,	12	146	2056	2023	1993	1954
KBr support @ 100°C	82	145-146	2059	2026	1988	1955
Literature values[34], Petroleum ether reflux	53	-	2056	2023	1982	1954

a Solventless reactions gave a mixture consisting of 30% of the required product.

The yields of the dimer when using all methods but KBr were low (6-16%). Even the reaction using light petroleum reflux (yield 53%) gave only a mixture of products in our case (**Table 4.2**). The solid-state method of heating a solid solution of $Mn(CO)_5Br$ and KBr at 100°C yielded 82% of the dimer. This method resulted in the generation of a high

yield of the product because of the lower temperature conditions used, that would have prevented decomposition. The reaction was also monitored by the colour change from yellow to orange signalling the formation of the desired product; terminating the reaction immediately, again minimised the chance of decomposition. No attempt was made to optimise the solventless reaction. What is clear is that the proximity of reagents at the temperature used (100°C) permits formation of product, possibly followed by the precipitation of the product, thus removing the product from the reaction. In solution dilution means a slower reaction.

4.3.3 Synthesis of $Mn(CO)_4LBr$

The method adopted for the synthesis of these complexes entailed the treatment of equimolar amounts of the pentacarbonylmanganes(I) bromide with phosphines in chloroform for periods exceeding 24 h at room temperature (**Scheme 4.5**)[35]. All products obtained from the transformation had a *cis* arrangement. The details of the synthesised complexes are tabulated in **Table 4.3**.

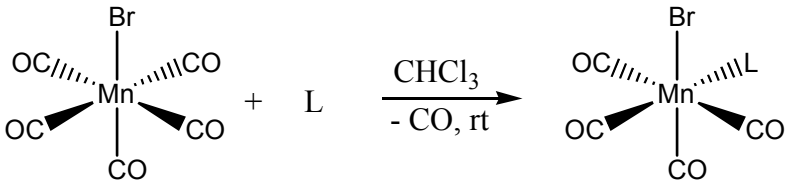

Scheme 4.5. Synthesis of *cis*-tetracarbonylmanganese(I) bromide from $Mn(CO)_5Br$

Table 4.3. Synthesis of *cis*-tetracarbonylmanganese(I) bromides from $Mn(CO)_5Br$, and the respective melting points and carbonyl stretching frequencies in cm^{-1}

Complex	Yield /%	Mp / °C	ν_{CO}	ν_{CO}	ν_{CO}	ν_{CO}
$Mn(CO)_4(PPh_3)Br$[b] (**3**)	91	188	2091(s) (2101)	2021(sh)	2009(s) (2012)	1961(s) (1965)
$Mn(CO)_4(P(p\text{-}MeO\text{-}C_6H_4))_3Br$(**4**)	70	138-140	2090(s)	2020(sh)	2006(s)	1952(s)
$Mn(CO)_4(P(p\text{-}Me\text{-}C_6H_4))_3Br$ (**5**)	66	192-195	2091(s)	2018(sh)	2007(s)	1961(s)
$Mn(CO)_4(P(p\text{-}F\text{-}C_6H_4))_3Br$ (**6**)	55	112-113	2093(s)	2026(sh)	2009(s)	1064(s)
$Mn(CO)_4(P(p\text{-}Cl\text{-}C_6H_4))_3Br$ (**7**)	51	172-173	2092(s)	2026(sh)	2008(s)	1964(s)

b Values in parentheses are literature values as chloroform solutions

The methodology employed usually led to good yields of the crude products (~100%). Purification by recrystallisation resulted in lower yields. The complexes were obtained in moderate to good yields (51%-91%) using the method adopted after recrytallisation..

4.3.4 Synthesis of $Mn(CO)_3L_2Br$

The general scheme for the synthesis of $Mn(CO)_4L_2Br$ is shown in **Scheme 4.6** below. The synthetic method involved the reaction of $Mn(CO)_5Br$ with an excess of ligand[36]. The details of the synthesised complexes are highlighted in **Table 4.4**.

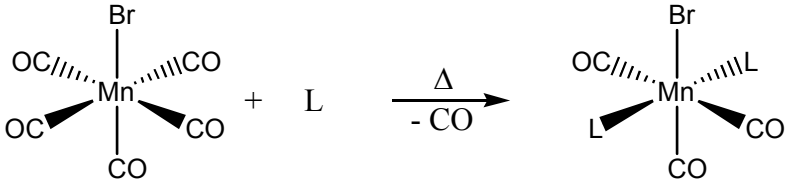

Scheme 4.6. Synthesis of *trans*-$Mn(CO)_3L_2Br$ from $Mn(CO)_5Br$

Table 4.4. Characteristics of *trans*-$Mn(CO)_3L_2Br$ from $Mn(CO)_5Br$ as analysed using FTIRS

Complex	Yield[c]	Mp/ °C	ν_{CO}	ν_{CO}	ν_{CO}
$Mn(CO)_3(PPh_3)_2Br$[d] (**8**)	66	180-182	2038 (2046)	1950 (1955)	1916 (1916)
$Mn(CO)_3(P(p\text{-}MeO\text{-}C_6H_4)_3)_2Br$ (**9**)	46	98-99	2034	1947	1912
$Mn(CO)_3(P(p\text{-}Me\text{-}C_6H_4)_3)_2Br$ (**10**)	65	132-133	2032	1948	1905
$Mn(CO)_3(P(p\text{-}F\text{-}C_6H_4)_3)_2Br$ (**11**)	42	176-178	2025	1947	1900
$Mn(CO)_3(P(p\text{-}Cl\text{-}C_6H_4)_3)_2Br$ (**12**)	19	95-97	2028	1951	1905

c After crystallasation

d Values in parentheses are literature values as chloroform solutions

The transformation was accompanied by the evolution of carbon monoxide gas as a co-product, signalling that the substitution reaction was in progress. The metal complexes obtained had a *trans* geometry from the moment they were detected using IR spectroscopy. As would be expected, the remaining carbonyls had infrared excitations at lower frequencies than would have been the case for the tetracarbonyls.

4.4. CONCLUSIONS

$Mn(CO)_5Br$ was synthesised, from $Mn_2(CO)_{10}$ using oxidative cleavage with bromine in carbon tetrachloride, in 90% yield. The dimer, $Mn_2(CO)_8Br_2$, was synthesised in 82% yield by heating a solid mixture of $Mn(CO)_5Br$ and KBr at 100°C. $Mn(CO)_4LBr$ complexes were synthesised by the reaction of $Mn(CO)_5Br$ and the appropriate phosphine ligand as chloroform solutions (51-91% yield after crystallisation). $Mn(CO)_3L_2Br$ complexes were made by heating $Mn(CO)_5Br$ in the presence of the appropriate solid ligand in excess, in the absence of solvents, at 100°C in reasonable yields (19-66%). All the complexes were characterised by FTIRS and their melting points were determined.

4.5. APPENDIX

Table 4.5. Characterisation o f $Mn(CO)_4(L)Br$ complexes

L	Code	Yield	ν_{CO}	Mp	CHN (calc)	CHN (found)	*m / z* (M^+)	EI
PPh_3	**3**	91%	2101 2020 2009 1965	188°C	$C_{22}H_{15}BrMnO_4P$ C, 51.90 H, 2.97	C, 51.94 H, 3.06	507.9272	507.8321
P(*p*-MeO-C_6H_4)$_3$	**4**	70%	2091 2020 2006 1952	138-140°C	$C_{25}H_{21}BrMnO_7P$ C, 49.08 H, 3.53	C, 50.11 H, 3.65	597.9589	597.7825
P(*p*-Me-C_6H_4)$_3$	**5**	66%	2091 2018	192-195°C	$C_{25}H_{21}BrMnO_4P$ C, 54.47	C, 55.16	549.9741	549.9736

			2008		H, 3.84	4.01		
			1961					
P(*p*-F-C_6H_4)$_3$	**6**	55%	2093,	112-113°C	$C_{22}H_{12}BrF_3MnO_4P$			
			2026		C, 46.92	C, 46.61	561.8989	561.7864
			2009		H, 2.15	H, 2.13		
			1964					
P(*p*-Cl-C_6H_4)$_3$	**7**	51%	2092	172-173°C	$C_{22}H_{12}BrCl_3MnO_4P$			
			2026		C, 43.14	C, 43.94	609.8103	611.6175
			2006		H, 1.97	H, 2.15		
			1964					

Table 4.6. Characterisation o f $Mn(CO)_4(L)_2Br$ complexes

L	Code	Yield	ν_{CO}	Mp	CHN (calc)	CHN (found)	*m / z* (M^+)	EI
PPh_3	**8**	66%	2038	180-182°C	$C_{39}H_{30}BrMnO_3P_2$			

		1950		C, 63.01	C, 62.62	742.0234	742.6172
		1916		H, 4.07	H, 3.85		
P(*p*-MeO-C_6H_4)$_3$	**9**	70% 2091	98-99°C	$C_{45}H_{42}BrMnO_9P_2$			
		1937		C, 58.52	C, 60.12	922.0868	921.8936
		1912		H, 4.58	H, 4.89		
P(*p*-Me-C_6H_4)$_3$	**10**	65% 2036	132-133°C	$C_{45}H_{42}BrMnO_3P_2$			
		1936		C, 65.31	C, 66.90	826.1173	827.2057
		1910		H, 5.12	5.73		
P(*p*-F-C_6H_4)$_3$	**11**	42% 2039,	176-178°C	$C_{39}H_{24}BrF_6MnO_3P_2$			
		1942		C, 55.02	C, 56.16	849.9669	849.8793
		1917		2.84	H, 3.04		
P(*p*-Cl-C_6H_4)$_3$	**12**	19% 2039	95-97°C	$C_{39}H_{24}BrC_{l6}MnO_3P_2$			
		1944		C, 49.30	C, 50.86	947.7866	865.7091
		1916		H, 2.55	H, 2.94		

4.6. REFERENCES

1. E. O. Fischer and R. Jira, *Z. Naturforsch*., *Teil B*, 1954, **9**, 618.
2. D. T. Hurd, G. W. Sentell Jr and F. J. Norton, *J. Am. Chem. Soc.,* 1949, **71**, 1899.
3. E. O. Brimm, M. A. Lynch Jr and W. J. Sesny, *J. Am. Chem. Soc.,* 1954, **76**, 3831.
4. G. Wilkinson, F. A. Cotton and J. M. Birmingham, *J. Org. Chem.,* 1956, **2**, 95.
5. W. F. Edgell, A. T. Watts, J. Lyford, W. M. Risen Jr, *J. Am. Chem. Soc.,* 1966, **88**, 1815.
6. R. D. Closson, J. Kozikowski and T. H. Coffield, *J. Org. Chem.,* 1957, **22**, 478.
7. A. Wojcicki, *Adv. Organomet. Chem.,*1973, **11**, 87.
8. E. W. Abel and G. Wilkinson, *J. Chem. Soc*., 1959, 1501.
9. E. W. Abel and I. S. Butler, *J. Chem. Soc., Faraday Trans.*, 1967, **63**, 45.
10. F. Zingales and U. Sartorelli, *Inorg. Chem.,* 1967, **6**, 1243.
11. R. J. Angelici, F. Basolo and A. J. Poe, *J. Am. Chem. Soc.,* 1963, **85**, 2215.
12. R. H. Reimann and E. Singleton, *J. Chem. Soc., Dalton Trans.,* 1973, 841.
13. G. J. Kruger, R. O. Heckroodt, R. H. Reimann and E. Singleton, *J. Organomet. Chem*., 1975, **87**, 323.
14. L. F. Wuyts, G. P. Van der Kelen, *Inorg. Chim. Acta,* 1977, **23**, 19.
15. H. Sakiyama, H. Okawa and R. Isobe, *J. Chem. Soc., Chem. Commun.,* 1993, **10**, 882.
16. H. D. Simpson and H. Steinfink, *J. Am. Chem. Soc*., 1969, **91**, 6229.
17. L. Lynds, J. E. Crawford, R. M. Lynden-Bell and S. I. Chan, *J. Chem. Phys,* 1972, **57**, 5216.
18. E. L. Simmons and W. W. Wendlandt, *Thermochim. Acta*, 1971, **2**, 217.
19. N. Shaikh, A. Panja, S. Goswami, P. Banerjee, P. Vojticek, Y. Zhang, G. Su and S. Gao, *Inorg. Chem*., 2004, **43**, 849.
20. A.G. Osborne and M. H. B. Stiddard, *J. Chem. Soc*., 1964, 634.
21. F. Zingales, M. Graziani, F. Faraone and U. Belluco, *Inorg. Chim. Acta*,

1967,**1**, 172.

22. L. F. Wuyts and G. P. Van der Kelen, *Inorg. Chim. Acta*, 1977, **23**, 19.
23. F. Basolo and R. G. Pearson, *Mechanisms of Inorganic Reactions; A Study of Metal Complexes in Solution ,2nd edition*, 1968, 526.
24. P. M. Treichel and J. J. Benedict, *J. Organomet. Chem*., 1969, **17**, P37.
25. A. Wojcicki and F. Basolo, *J. Am. Chem. Soc*.,1961, **83**, 525.
26. R. J. Angelici, F. Basolo and A. J. Poe, *J. Am. Chem. Soc*., 1963, **85**, 2215.
27. R. J. Angelici, *Inorg. Chem*., 1964, **3**, 1099.
28. F. Zingales, M. Graziani, F. Faraone and U. Belluco, *Inorg. Chim. Acta*, 1967, **1**, 172.
29. C. A. Tolman, *Chem. Rev*., 1975, **77**, 313.
30. L. Stahl and R. D. Ernst, *J. Am. Chem. Soc.*, 1987, **109**, 5673.
31. D. White and N. J. Coville, *Adv. Organomet. Chem*.,
32. R. J. Angelici, *Inorg. Chem.*, 1964, **3**, 1099.
33. E. W. Abel and G. Wilkinson, *J. Am. Chem. Soc*., 1959, 1501.
34. F. Zingales and U. Sartorelli, *Inorg. Chem*., 1967, **6**, 1243.
35. A. G. Osborne and M. H. B. Stiddard, *J. Chem. Soc*., 1964, 634.
36. R. J. Angelici and F. Basolo, *J. Am. Chem. Soc*., 1962, **84**, 2495.

CHAPTER 5: THE USE OF FTIRS TO STUDY THE SOLVENTLESS REACTION OF MANGANESE CARBONYL COMPLEXES

5.1. INTRODUCTION

5.1.1. History and perspective

Infrared spectroscopy is the study of the interaction of infrared radiation (heat) with matter[1]. A plot of measured infrared radiation intensity versus wavenumber is known as an infrared spectrum[2]. When infrared radiation interacts with matter it can be absorbed, causing chemical bonds (holding the matter together) to vibrate. Structural fragments that make the matter, known as functional groups, absorb infrared radiation at the same wavenumber[3]. The position and intensity of absorption bands of a substance are specific to that substance[4]. The result is a correlation between the wavenumber at which a molecule absorbs infrared radiation and its structure. Thus the structure of an unknown molecule could be identified using an infrared spectrum.

In addition to chemical structures, infrared spectra can provide quantitative information based on Beer's Law[5] that relates concentration to absorbance and has the following form:

$$A = \varepsilon l c$$

Where A = absorbance, ε = absorptivity, l = pathlength and c = concentration

An instrument used to obtain an infrared spectrum is called an infrared spectrometer and the most widely used today is the Fourier Transform Infrared (FTIR) spectrometer[6]. Most

FTIR spectrometers record IR spectra in the range 4000 to 400cm^{-1}, a radiation range know as the infrared range[7].

The development of FTIR spectroscopy stems from experiments performed by Albert Abraham Michelson[8] who developed an optical device called an interferometer in 1880[9]. The instrument was used to accurately measure wavelengths of light. Due to laborious and time-consuming calculations required to convert an interferogram into a spectrum, the development of the technique for practical analysis had to wait until the advent of computers. In 1965, Cooley and co-workers invented the Cooley-Tukey Algorithm or Fast Fourier Transform (FFT) that quickly performed Fourier transforms on a computer[10]. This led to the first commercially available FTIRS being manufactured in the late 1960s[11]. Jones details a comprehensive historical survey of the development of infrared technology in his book[12].

The use of FTIRS in chemical analysis dates back to the early 20th century. For instance Zaidel and co-workers reported the use of the technique to analyse rare earth elements[13]. Vibrational spectra of organometallic compounds were also first recorded in the 1950s[14,15]. In this thesis the IR technique has been used to monitor the reactions of manganese carbonyl complex reactions performed in the absence of solvents.

5.1.2. FTIRS and manganese carbonyl complexes

IR spectroscopy was used to analyse the reaction $Mn(CO)_4(L)Br + L \rightarrow Mn(CO)_3(L)_2Br + CO$ (**Scheme 5.1**) since (i) minute quantities of reagents for the solventless reaction could be used and (ii) both products and reactants had distinct (non-overlapping) carbonyl stretching frequency peaks that could be used for quantification purposes. The specific complexes investigated, with L = PPh_3, i.e. $Mn(CO)_5Br$, $Mn(CO)_4(PPh_3)Br$ and $Mn(CO)_3(PPh_3)_2Br$ have well defined IR spectra[16].

The envisaged transformation involves the replacement of CO by phosphines in the absence of solvents. Substitution reactions are influenced by steric[17] and electronic[18] factors of the incoming ligand. The study aimed at investigating the electronic effects of a series of ligands in the substitution reaction. *Para*-substituted solid phosphine ligands [$P(C_6H_4$-R), R = H, MeO, Me, F, Cl] were chosen as they all have the same Tolman cone angle[19] (145°). This choice, in theory should ensure that there are no steric effects that would impact on the relative reaction rates.

The solution substitution reactions of manganese carbonyl complexes have been extensively studied[20,21]. For all the manganese compounds that have been investigated, the rate was found to be independent of the concentration and the nature of the incoming ligand. We wished to check whether the same phenomenon would be observed in the absence of solvents.

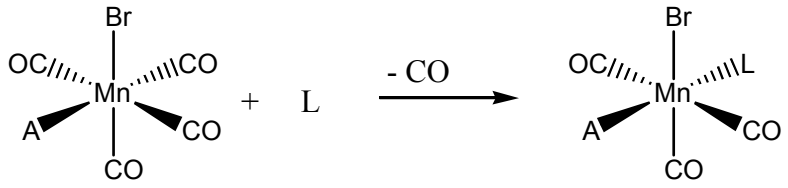

A = CO or phosphine ligand

Scheme 5.1. The solventless substitution of CO by substituted solid phosphine ligands, L, in manganese carbonyl complexes

5.2. EXPERIMENTAL PROCEDURES

5.2.1. Kinetic study of the solventless reaction of $Mn(CO)_5Br$ and PPh_3 to form $Mn(CO)_4(L)Br$ using FTIRS

5.2.1.1. Calibration curve for $Mn(CO)_5Br$

$Mn(CO)_5Br$ (2 mg) was added to a 10 cm^3 volumetric flask and the complex was dissolved in chloroform (6 cm^3). Dilutions of the solution were then made (3/4, 1/2, 1/5, 1/10, 1/20 and 1/50). The absorbance of each sample was measured using FTIRS (υ_{CO} = 2138 cm^{-1}), utilising chloroform as a blank to obtain a calibration curve (**Figure 5.1**).

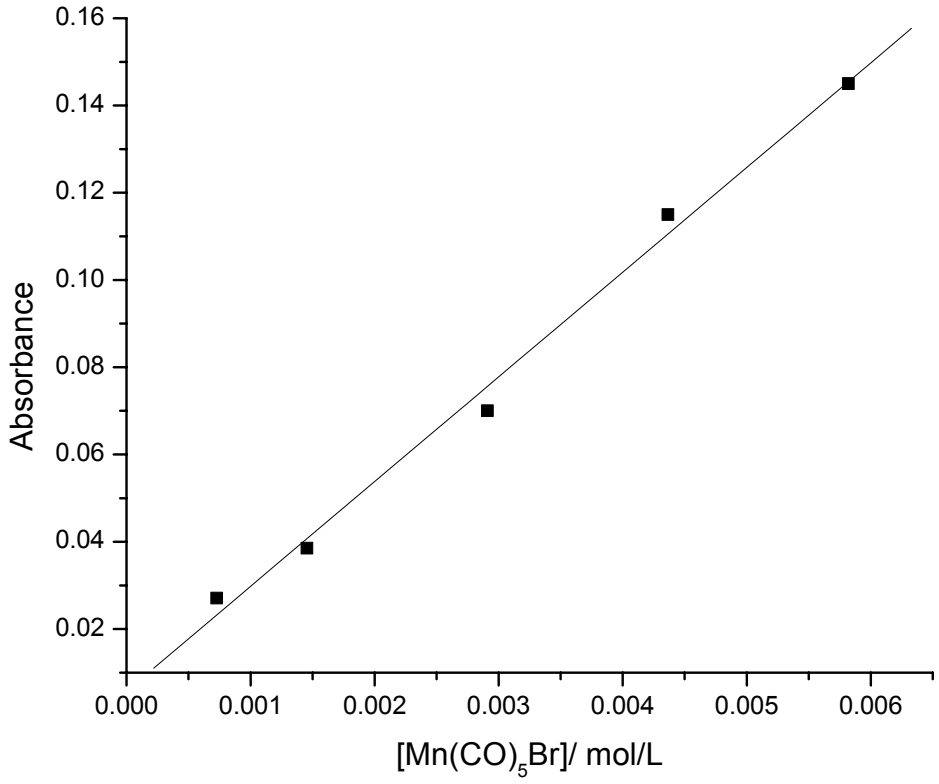

Figure 5.1. Calibration curve for $Mn(CO)_5Br$ (chloroform, room temperature)

5.2.1.2. Calibration curve for $Mn(CO)_4(PPh_3)Br$

$Mn(CO)_4(PPh_3)Br$ (3.2 mg) was placed in a 5 cm^3 round bottom flask and dissolved in enough chloroform (3 cm^3). Dilutions of the solution (1/2, 1/5, 1/10, 1/20 and 1/50) were made and the absorbance measured using FTIRS (ν_{CO} 2091 cm^{-1} as a reference peak) to obtain a calibration curve (**Figure 5.2**).

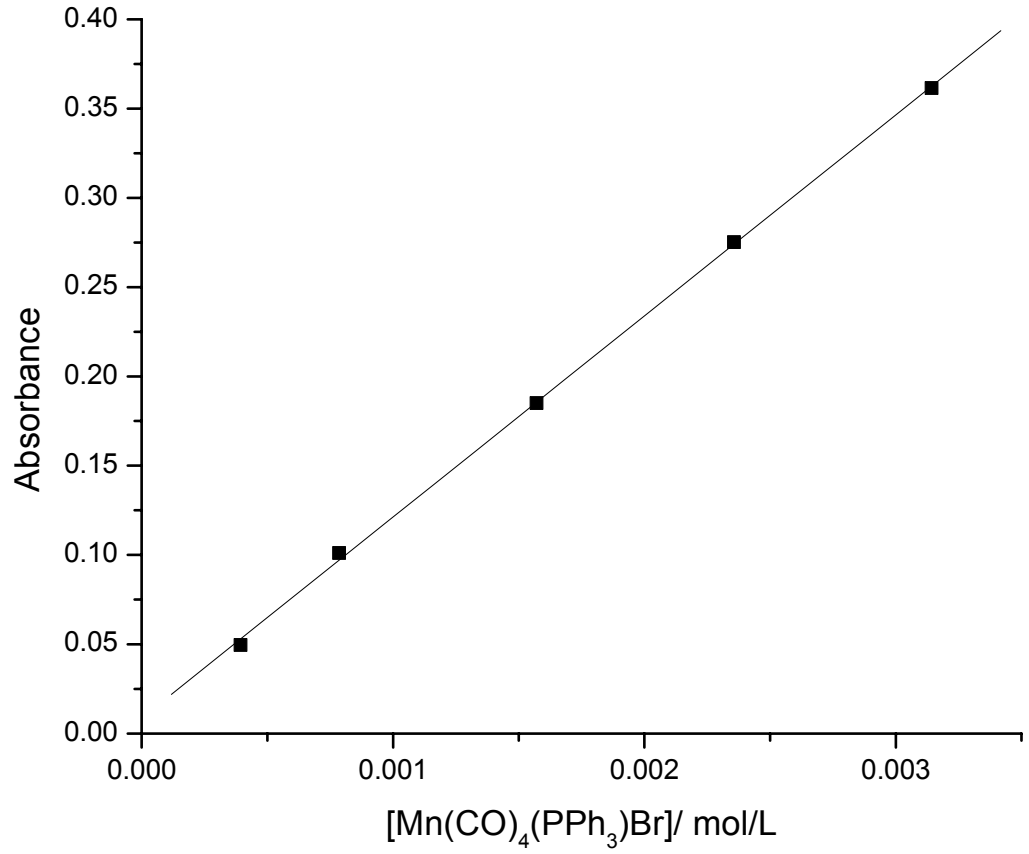

Figure 5.2. Calibration curve for $Mn(CO)_4(PPh_3)Br$ obtained using FTIRS (chloroform, room temperature)

5.2.1.3. Calibration curve for $Mn(CO)_3(PPh_3)_2Br$

$Mn(CO)_3(PPh_3)_2Br$ (2.0 mg) was placed in a 5 cm^3 round bottom flask and dissolved in chloroform (3 cm^3). Dilution of the solution (1/2, 1/5, 1/10, 1/20 and 1/50) was made and the absorbance measured using FTIRS to give a calibration curve using the ν_{CO} 1916 cm^{-1} as a reference peak (**Figure 5.3**).

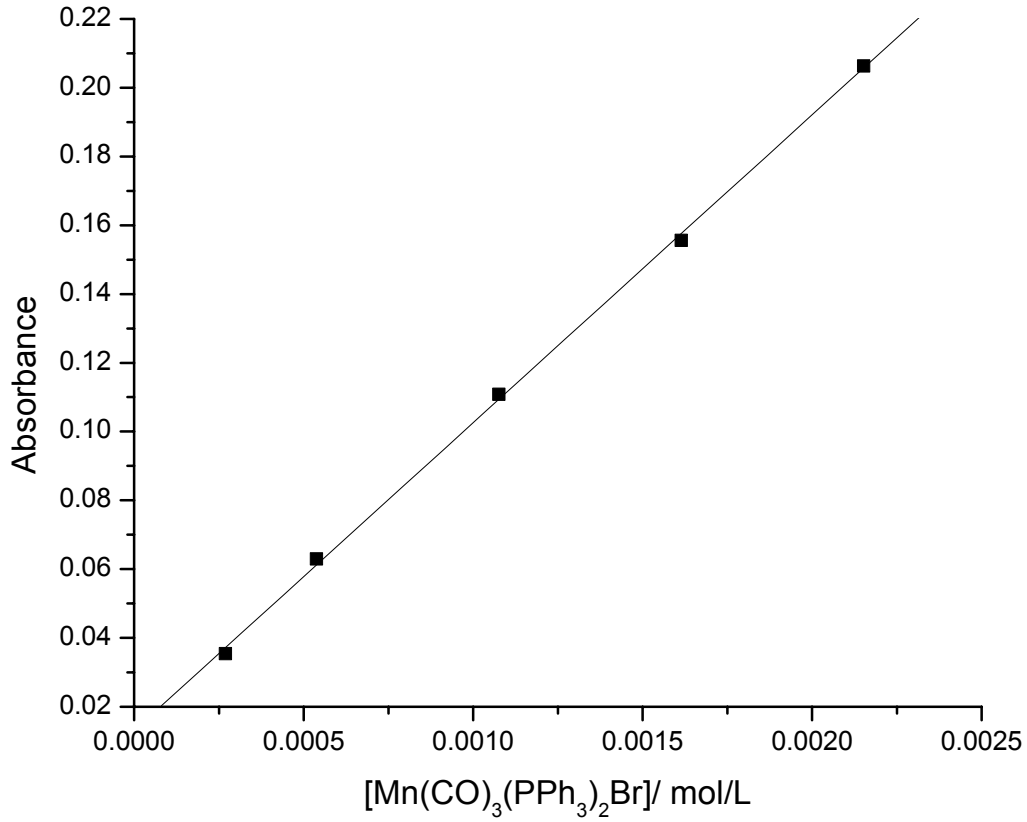

Figure 5.3. Calibration curve for $Mn(CO)_3(PPh_3)_2Br$ (chloroform, room temperature)

5.2.1.4. Kinetic study of the solventless reaction of $Mn(CO)_5Br$ with PPh_3 (1:1 molar ratio) in chloroform as followed by FTIRS.

$Mn(CO)_5Br$ (100 mg, 0.364 mmol) and PPh_3 (95.4 mg, 0.364 mmol, 1.0 mol equiv) were dissolved in dry dichloromethane (2 cm^3), inside a 5 cm^3 reaction tube. The solvent was quickly removed by flushing with dry nitrogen gas to leave behind a thoroughly mixed solid material. The sample was then allowed to stand overnight inside a desiccator to ensure complete removal of the solvent. The dried sample was then partitioned into 6 smaller samples, each containing ~4 mg of the compound. One sample was left in the desiccator as a reference sample, and the other five samples were each placed in 5 cm^3 reaction tube and heated in an oil bath pre-set at 65°C under nitrogen. Sample tubes were removed periodically from the oil bath and cooled with liquid nitrogen. Each sample was then dissolved in chloroform (~3 cm^3) and transferred into a 5 cm^3 volumetric flask. Care was taken to ensure that the entire sample was transferred from the reaction tube to the volumetric flask by rinsing the reaction flask with chloroform, and the rinses were added to the volumetric flask. The volume of chloroform in the volumetric flask was then adjusted to the meniscus using more of the solvent. The solutions contained varying amounts of reactant, $Mn(CO)_4(PPh_3)Br$ and $Mn(CO)_3(PPh_3)_2Br$. These complexes were readily detected by their IR spectra. The absorbance values were used to evaluate the amounts of the three components in each reaction solution.

5.2.1.5 Kinetic study of the solventless reaction of $Mn(CO)_5Br$ with PPh_3 (1:2 molar ratio) as followed by FTIRS

$Mn(CO)_5Br$ (50 mg, 0.182 mmol) and PPh_3 (95.4 mg, 0.364 mmol, 2.0 mol equiv) were dissolved in dry dichloromethane (5 cm^3), inside a 5 cm^3 reaction tube and the solvent quickly removed by flushing with nitrogen to leave behind a solid mixture. A similar procedure as described above (**Section 5.2.1.4**) was used to conduct the experiment.

5.2.1.6. Kinetics of the solventless reaction of $Mn(CO)_5Br$ with PPh_3 (1:10 molar ratio) as followed by FTIRS

$Mn(CO)_5Br$ (20 mg, 0.0728 mmol) and PPh_3 (191 mg, 0.728 mmol, 10.0 mol equiv) were dissolved in dry dichloromethane (5 cm^3), inside a 5 cm^3 reaction tube. The removal of the solvent by flushing with nitrogen afforded a yellow powder that was reacted as described above.

5.2.2. Kinetic study of the solventless reaction between $Mn(CO)_4(PPh_3)Br$ and PPh_3

The generation of calibration curves for $Mn(CO)_4(PPh_3)Br$ and $Mn(CO)_3(PPh_3)_2Br$ in chloroform were described in **Sections 5.2.1.2** and **5.2.1.3**. The extent of the reaction of $Mn(CO)_4(PPh_3)Br$ with PPh_3 in the absence of solvents was performed.

$Mn(CO)_4(PPh_3)Br$ was mixed with varying amounts of PPh_3, ranging from one to ten mole equivalents. The data for the 1:2 mol equivalent reaction is shown below. $Mn(CO)_4PPh_3Br$ (50 mg, 0.098 mmol) and PPh_3 (2.0 mg, 25 mg, 2 mol equiv) were placed in a 5 cm^3 reaction tube and dissolved in dry dichloromethane (2 cm^3) to yield a yellow solution. The solvent was quickly removed by flushing with nitrogen gas to produce a homogenous solid that was left to stand in a desiccator overnight. The sample was then partitioned into several smaller samples (4 mg) and placed in 5 cm^3 reaction tubes. One sample was left unreacted in the desiccator and it served as the reference sample before the reaction was initiated. Five samples were then placed in an oil bath pre-set at a particular temperature (50°C, 60°C or 70°C). Samples were removed from the oil bath after pre-determined times and immediately cooled by immersing in liquid nitrogen to stop the reaction. The samples were then allowed to warm back to room temperature and each sample dissolved in chloroform (~2 cm^3) and transferred to 5 cm^3 volumetric flasks. The reaction tube was thoroughly rinsed with small portions of chloroform to ensure complete transfer of the reaction mixture to the volumetric flask.

The absorbance of the solution was then measured using FTIRS utilizing chloroform as a blank. The amount of starting material and product were deduced using the disappearance of the peak at 2093 cm^{-1} and appearance of the product peak at 1916 cm^{-1}. The above procedure was used to monitor samples with different metal:complex ratios.

5.3. RESULTS AND DISCUSSION

5.3.1. Reference IR spectra

The IR spectra for the three carbonyl manganese(I) bromide complexes (υ_{CO} regions) are shown below. They were obtained by dissolving 2 mg samples of each compound in chloroform (5 cm^3) and the absorbance measured using FTIRS, with dry chloroform as background. It is apparent from **Figure 5.4** that if the conversion of $Mn(CO)_5Br$ with PPh_3 were to be followed, there are distinct carbonyl carbon stretching frequencies of the three complexes that are unique for each complex. These frequencies (2138, 2091 and 1916 cm^{-1}) are associated with each of the three materials.

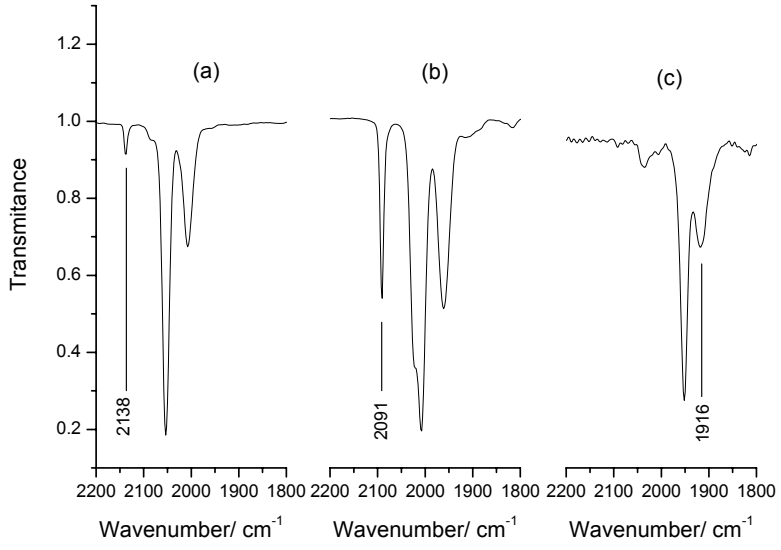

Figure 5.4. Infrared spectra of $Mn(CO)_5Br$, $Mn(CO)_4(PPh_3)Br$ and $Mn(CO)_3(PPh_3)_2Br$

5.3.2. Kinetics study of the formation of *trans*-$Mn(CO)_3(PPh_3)_2Br$ from $Mn(CO)_5Br$

Scheme 5.2 shows the envisaged pathway of the solventless reaction of $Mn(CO)_5Br$ with PPh_3 to yield *trans*-$Mn(CO)_3(PPh_3)_2Br$.

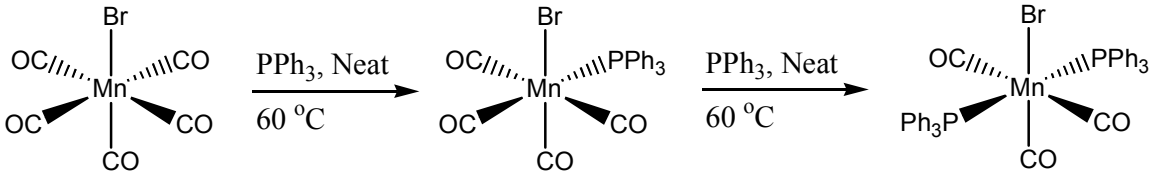

Scheme 5.2. The formation of *trans*-$Mn(CO)_3(PPh_3)_2Br$ from $Mn(CO)_5Br$ with PPh_3

A DSC profile of $Mn(CO)_5Br$ is shown in **Figure 5.5**. The plot shows that $Mn(CO)_5Br$ melted and decomposed at 120°C as indicated by the broad endotherm at the said temperature. The experimentally determined melting point of the compound was found to be 101-102°C. Presumably the difference in heating rates by the different methodologies is responsible for the difference in melting points.

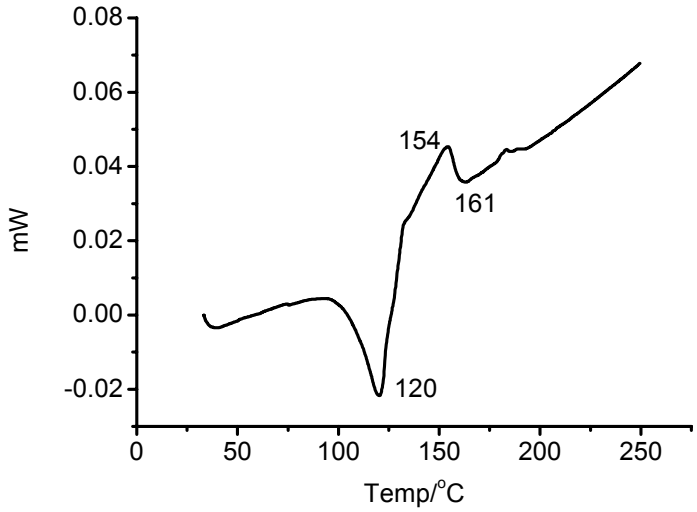

Figure 5.5. DSC profile of $Mn(CO)_5Br$ (heating rate:10° per minute) under nitrogen

The DSC profile of triphenylphosphine is shown in **Figure 5.6** (run under nitrogen gas). It is apparent from the plot that the reagent melts at 78°C where the prominent endotherm appeared. The exotherm at 125°C probably corresponds to decomposition or an oxidation reaction. The colour of the material changed from white to dark brown and the material in the DSC experiment coated the aluminium container.

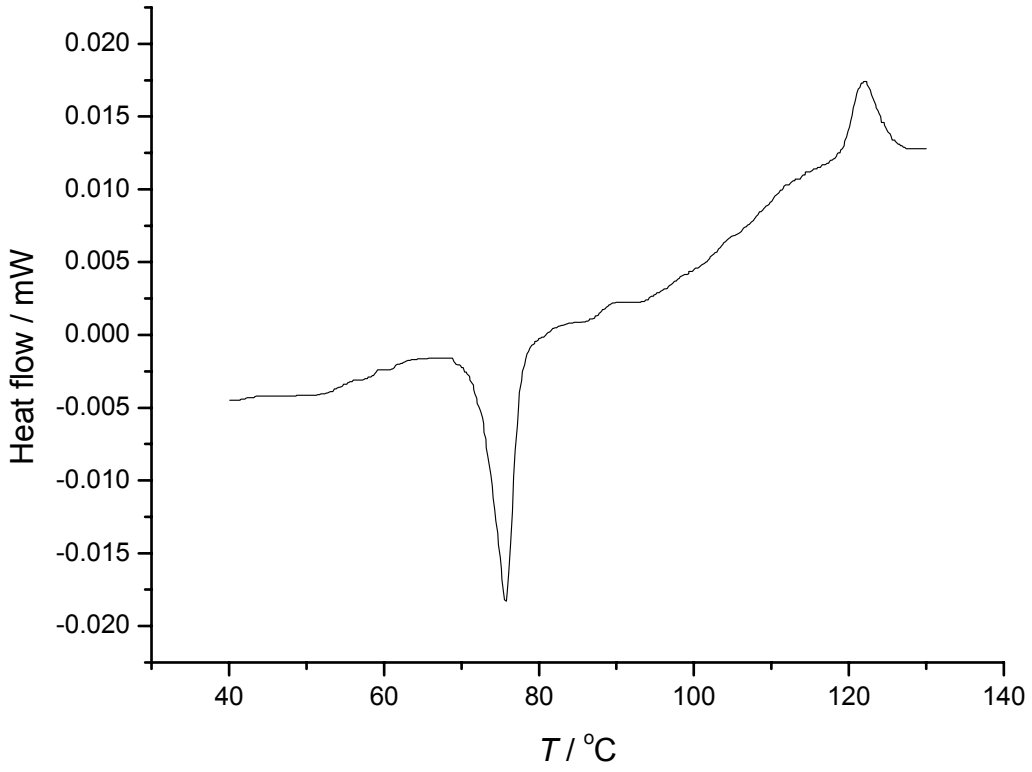

Figure 5.6. DSC profile of PPh_3 (heating rate:10 per minute) under nitrogen

The DSC profile of the mixture of $Mn(CO)_5Br$ with PPh_3 (1:1 mol equivalent, under nitrogen) is shown in **Figure 5.7**. The DSC reveals the presence of PPh_3 (exotherm at 78°C) and $Mn(CO)_5Br$ (exotherm at 101°C). The endothermic peak at 142°C suggests possible formation of product ($Mn(CO)_4(PPh_3)Br$). The peak at 188°C suggests another endothermic reaction or a phase change.

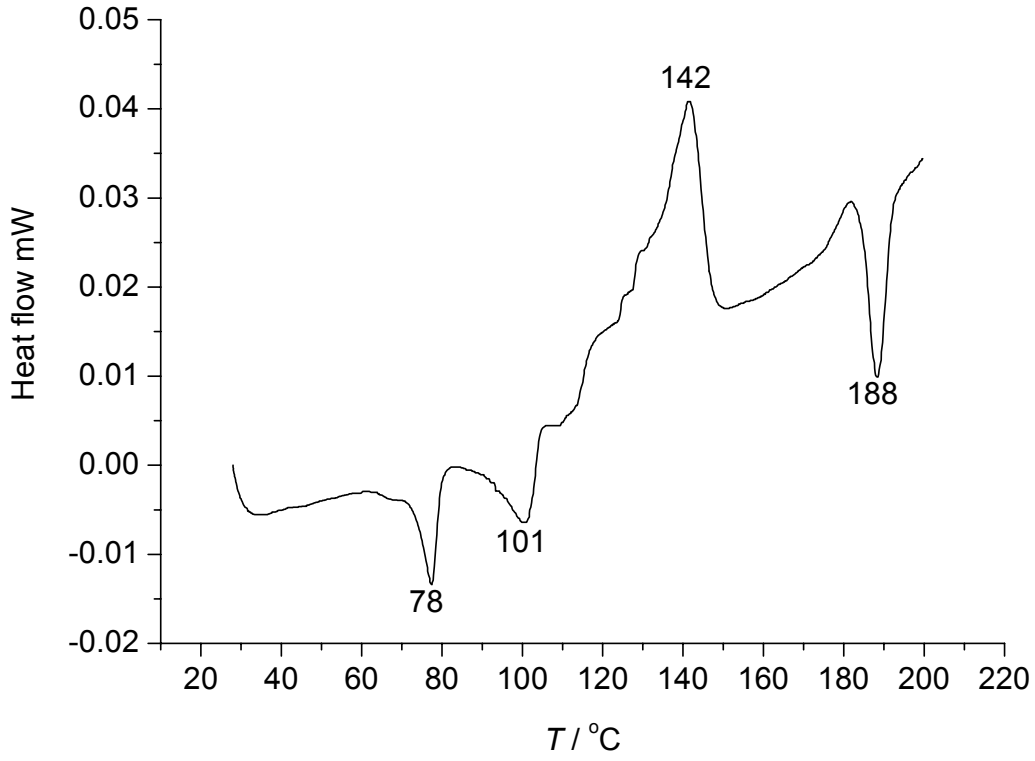

Figure 5.7. DSC profile of the solventless reaction of $Mn(CO)_5Br$ with PPh_3 (1:1 mol equivalent, heating rate:10° per minute) under nitrogen

From the above DSC data it was decided to carry out the solventless reactions at $T \leq 70°C$. This would correspond to a reaction that would occur below the temperature of the melting point of the solid reagents. A reaction was then performed at 65°C (**Figure 5.8**). The reaction was monitored by FTIRS and the amounts of reactants and products plotted as a function of reaction time.

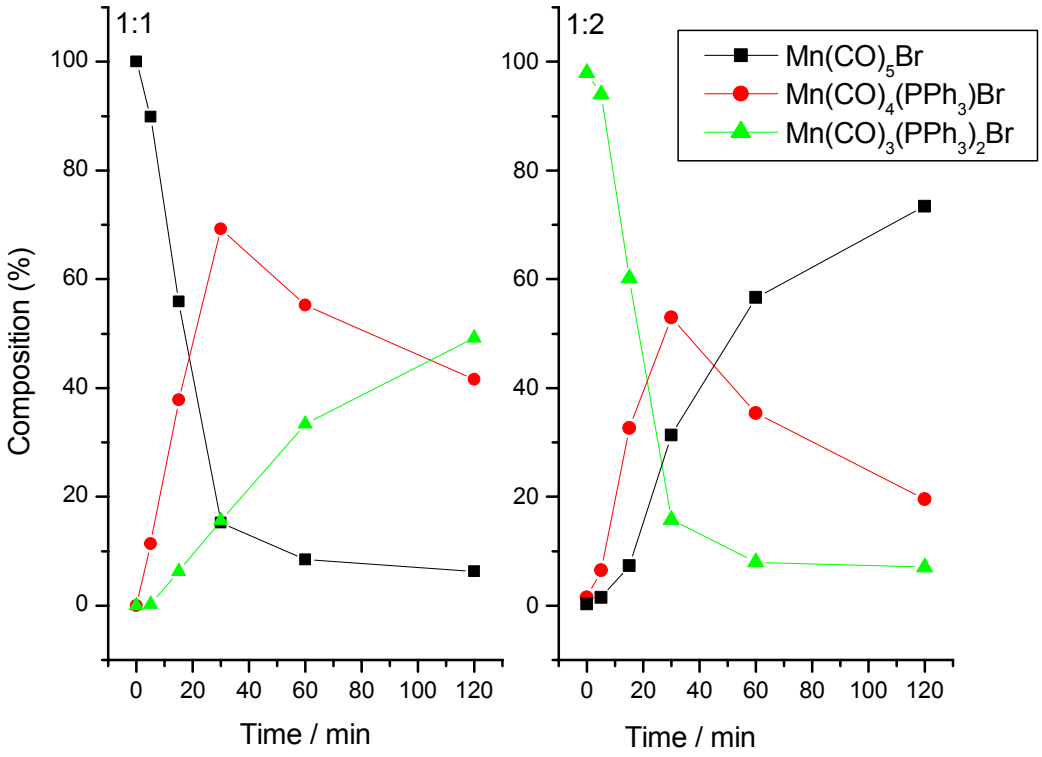

Figure 5.8. Plot of composition versus time for the reaction of $Mn(CO)_5Br$ with PPh_3 (1:1 and 1:2 metal/ligand ratios) at 65°C under nitrogen using FTIRS

The plot showed that the rate of formation of $Mn(CO)_4(PPh_3)Br$ from $Mn(CO)_5Br$ was of the same order as that of the formation of $Mn(CO)_3(PPh_3)_2Br$ from $Mn(CO)_4(PPh_3)Br$ at 65°C. Formation of $Mn(CO)_3(PPh_3)_2Br$ occurred before all the $Mn(CO)_4(PPh_3)Br$ had been formed.

Reactions were also conducted at ligand-to-metal ratios of 1:5 and 1:10 as shown in **Figure 5.9**. The results obtained followed the expected trends. The reaction temperature was lowered in an attempt to enhance the formation of $Mn(CO)_4(PPh_3)Br$. However, little reaction occurred at temperatures lower than 50°C and no reaction was observed at 35°C for periods exceeding 10 days. Data revealed that the solventless procedure did not lead to the selective formation of $Mn(CO)_4(PPh_3)Br$.

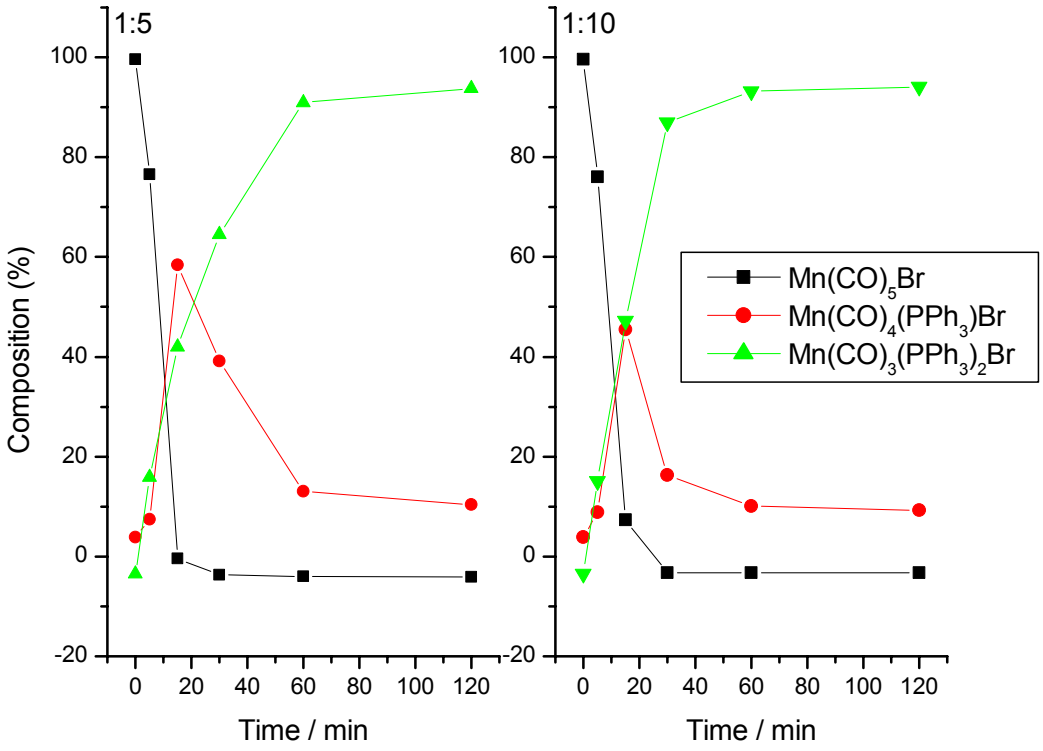

Figure 5.9. Plot of composition versus time for the reaction of $Mn(CO)_5Br$ with PPh_3 (1:5 and 1:10 metal/ligand ratios) at 65°C under nitrogen using FTIRS

5.3.3. Reaction of $Mn_2(CO)_8Br_2$ and PPh_3

The DSC profile obtained when equimolar amounts of $Mn_2(CO)_8Br_2$ and PPh_3 were mixed together and heated at constant rate under nitrogen is shown below (**Figure 5.10**).

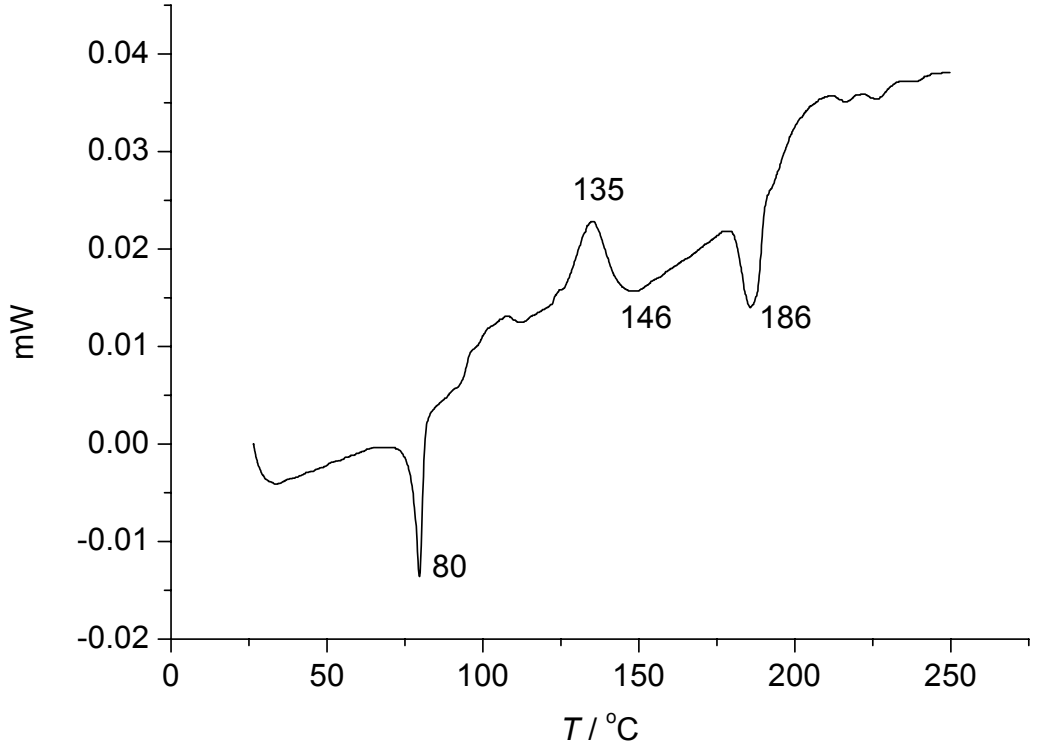

Figure 5.10. DSC profile of the reaction of ($Mn_2(CO)_8Br_2$) with PPh_3 (1:1 molar equivalent) at a heating rate of 10° per minute under nitrogen

The DSC profile was similar to that observed when $Mn(CO)_5Br$ and PPh_3 were reacted together (compare **Figure 5.7**). The endotherm at 80°C is associated with the melting point of PPh_3. The other endotherm at 186°C is due to the formation of a new product and the exotherm at 135°C represents the temperature at which transformation to new product(s) was prominent. The small endotherm at 146°C corresponds to the melting point of the dimer, $Mn_2(CO)_8Br_2$ (observed at 145°C-146°C). These results suggested

that selective formation of the product, $Mn(CO)_4(PPh_3)Br$, using the dimer, $Mn_2(CO)_8Br_2$, was not possible under the reaction conditions employed.

5.3.4. Kinetic study of the formation of *trans*-$Mn(CO)_3(PPh_3)_2Br$ from $Mn(CO)_4(PPh_3)Br$

A solventless reaction between $Mn(CO)_4(PPh_3)Br$ and PPh_3 (1:1 mole ratio) was performed. The reaction failed to go to completion even after 50 hours (**Figure 5.11**). When $Mn(CO)_5(PPh_3)Br$ was reacted with 2 mol equivalent of the ligand, about 90% of product was detected at the end of 50 hours (**Figure 5.11**. When 5 or 10 mol equivalent of the ligand was used, the reaction went to completion (**Figure 5.12**).

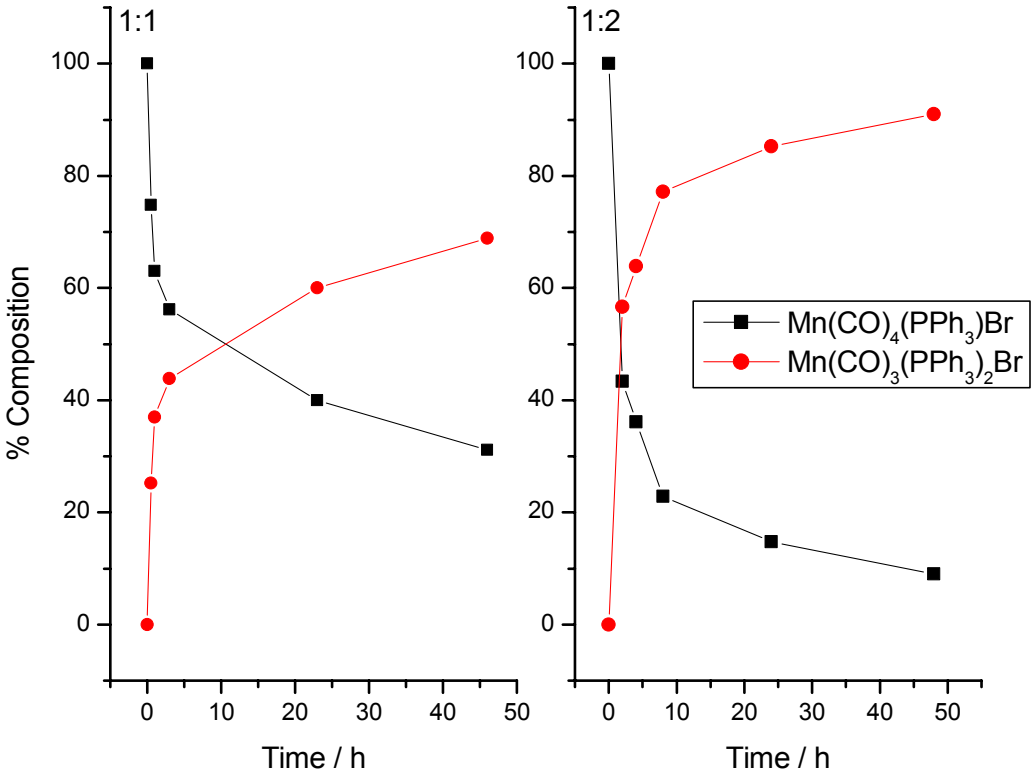

Figure 5.11. Plot of composition versus time for the reaction of $Mn(CO)_4(PPh_3)Br$ with PPh_3 (1:1 and 1:2) at 65°C under nitrogen

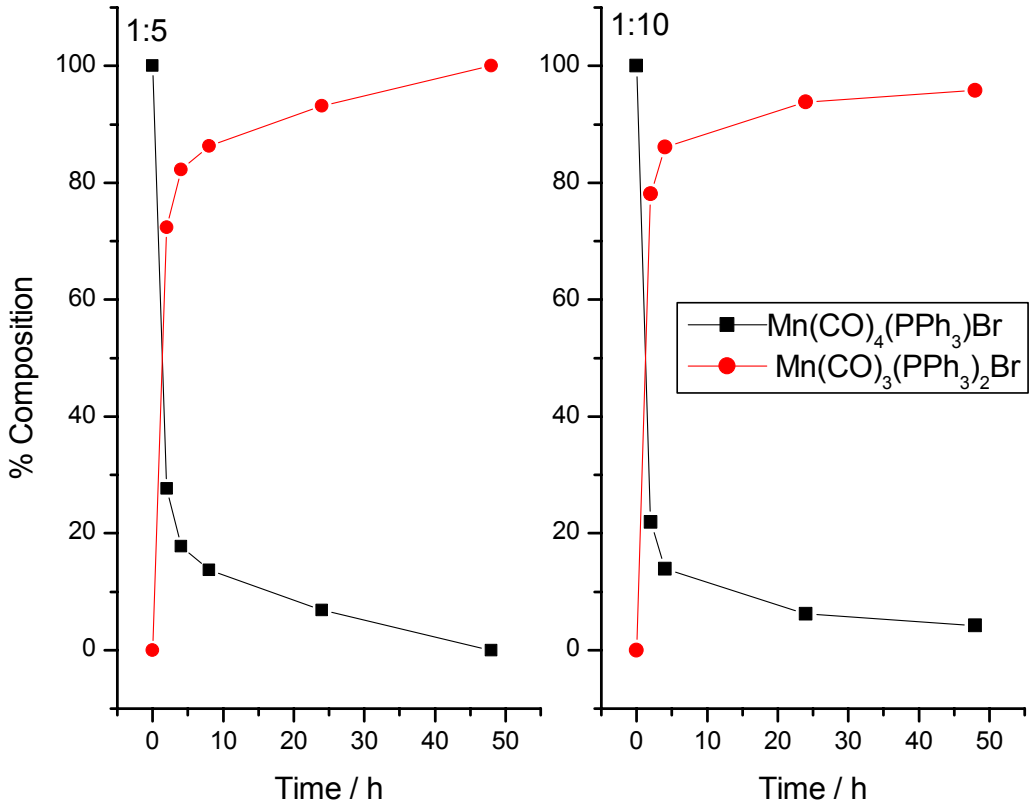

Figure 5.12. Plot of composition versus time for the reaction of $Mn(CO)_4(PPh_3)Br$ with PPh_3 (1:5 and 1:10) at 65°C under nitrogen

The above data have been re-plotted in **Figure 5.13** to show the rate of disappearance of $Mn(CO)_4(PPh_3)Br$ as a function of reaction time at 65°C. A similar set of data was obtained at 74°C and the data was also plotted in **Figure 5.13**.

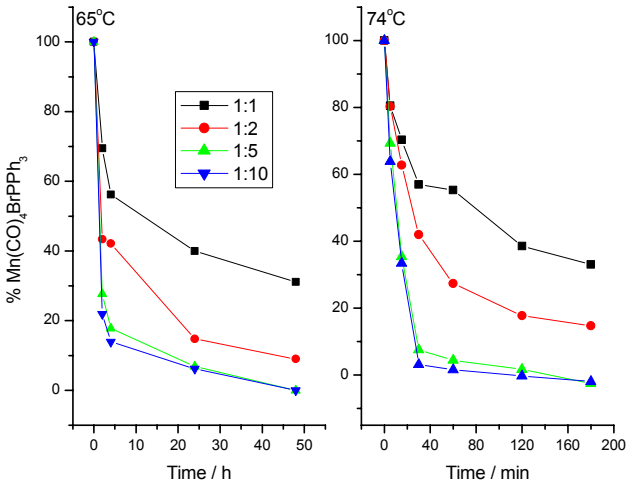

Figure 5.13. Plot of composition versus time for the solventless reaction of $Mn(CO)_4(PPh_3)Br$ with PPh_3 at 65°C and 74°C at various metal-to-ligand ratios as followed using FTIRS

If it is **assumed** that the reaction is a first order reaction, the rate constant can be determined. A plot of ln(% composition) of the starting material, $Mn(CO)_4(PPh_3)Br$, against reaction time at both 65°C and 74°C indeed gave straight line graphs suggesting the assumption was reasonable. The rate constant for the reaction was also determined at 53°C. A similar set of data (not shown) was obtained for a 1:5 metal/PPh_3 ratio. These were also plotted to generate rate constants as shown for the data of 1:10 metal/PPh_3 ratio (**Figure 5.14**).

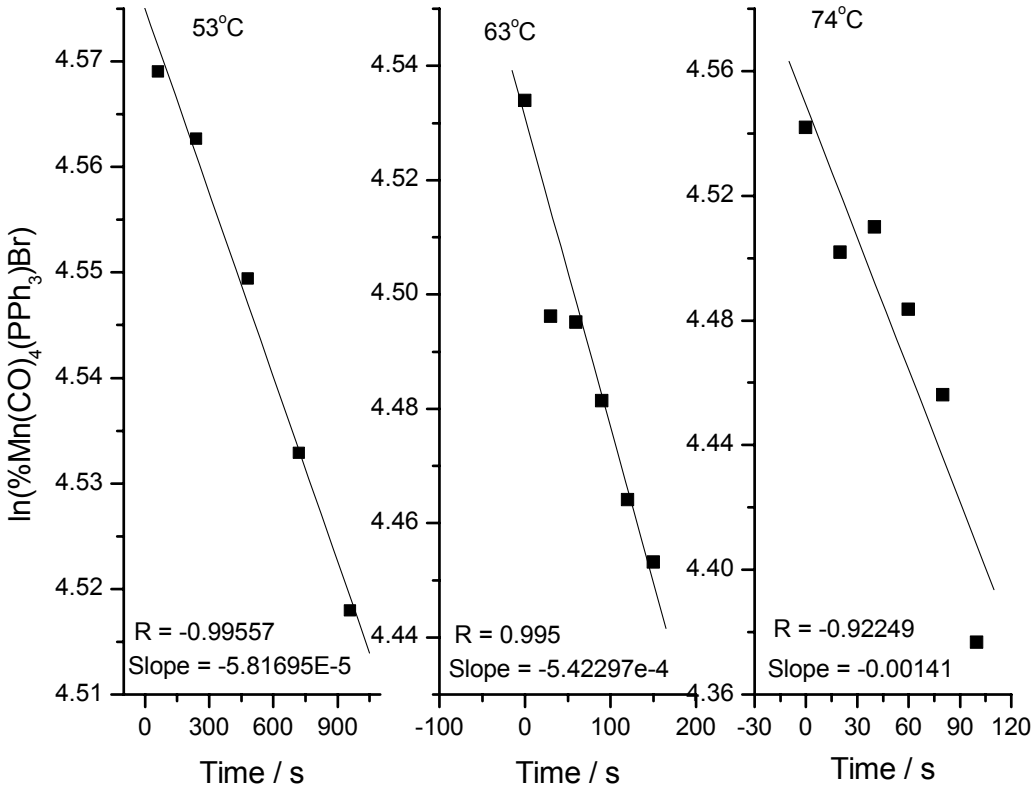

Figure 5.14. Plot of ln[$Mn(CO)_4(PPh_3)Br$] with time for the solventless reaction of $Mn(CO)_4(PPh_3)Br$ with PPh_3 (1:10 mol equiv) at various temperatures followed by FTIRS in chloroform at the end of the reaction

The activation energy, Ea, of the reaction was determined from a plot of ln(k) versus 1/T. From the plot (**Figure 5.15**), the activation energy of the reaction was found to be 143 ± 19 $kJmol^{-1}$ and 144 ±19 $kJmol^{-}1$ at the 1:5 and 1:10 metal-to-ligand ratios respectively.

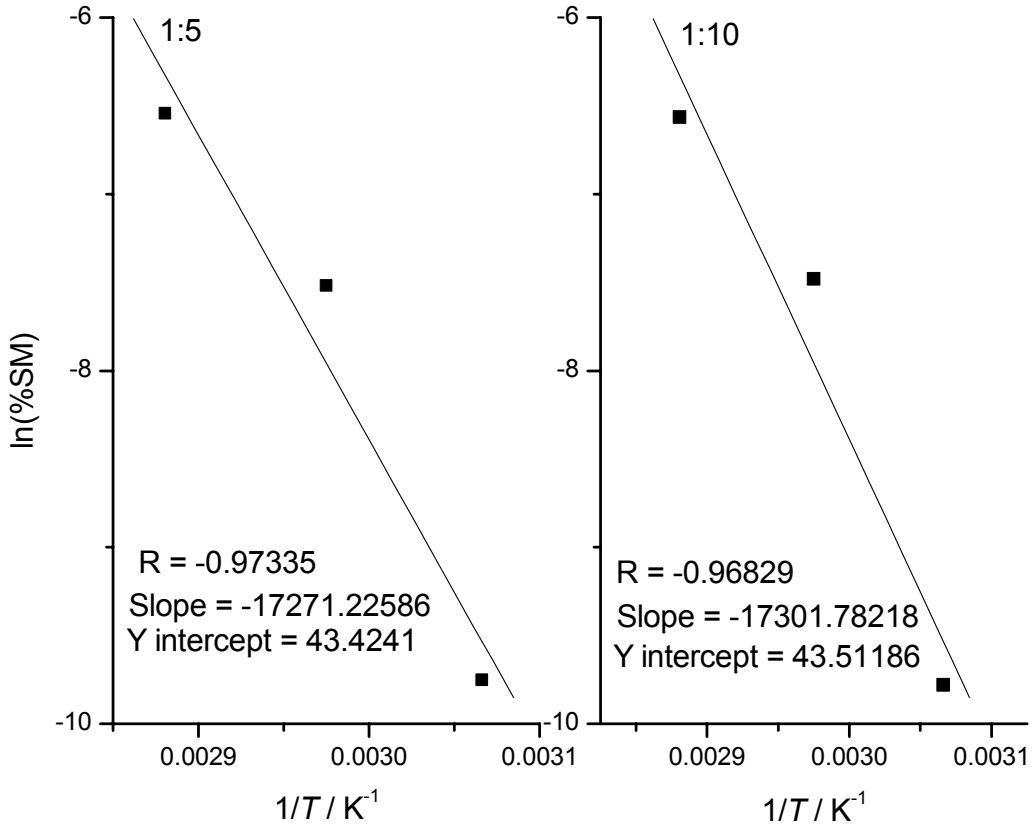

Figure 5.15. Plot of ln(% composition) versus $1/T$ for the reaction of $Mn(CO)_4(PPh_3)Br$ with PPh_3

The entropy of activation was determined from the plot of $\ln(k/T)$ versus $(1/T)$ and found to be large and positive (104 ± 7 $Jmol^{-1}K^{-1}$), suggestive of a dissociation mechanism.

5.4. CONCLUSIONS

The solventless synthesis of $Mn(CO)_4(PPh_3)Br$ from the reaction of $Mn(CO)_5Br$ with PPh_3 was not found to be selective. As soon as $Mn(CO)_4(PPh_3)Br$ formed, it reacted further with the available ligand to yield $Mn(CO)_3(PPh_3)_2Br$ even at a 1:1 metal/ligand mole ratio. The kinetic study revealed that the formation of $Mn(CO)_4(PPh_3)Br$ from $Mn(CO)_5Br$ occurred at the same rate as the formation of $Mn(CO)_3(PPh_3)_2Br$ from $Mn(CO)_4(PPh_3)Br$. The reaction failed to take place at temperatures lower than 35°C.

The solventless reaction between $Mn(CO)_4(PPh_3)Br$ and PPh_3 was successfully followed by FTIRS and the kinetic parameters were elucidated. The activation energy of the reaction was found to be 143 ± 19 $kJmol^{-1}$. The entropy of activation was found to be 104 ± 7 $Jmol^{-1}K^{-1}$. The reaction most likely went through a dissociative mechanism as is found in solution studies (see next chapter).

5.5. REFERENCES

1. J. McMurry, *Organic Chemistry*, Thomson Learning-Brooks/Cole, Belmont, 2004.
2. B. H. Stuart, *Infrared Spectroscopy: Fundamentals and Applications*, John Wiley and Sons, Chichester, England, 2004.
3. B. C. Smith, *Fourier Transform Infrared Spectroscopy*, CRC Press, New York, 2000.
4. H. Gunzler and H. Gremlich, *IR Spectroscopy: An Introduction*, Wiley-VCH Verlag, Weinheim, 2002.
5. B. C. Smith, *Infrared Spectral Intepretation: A Systematic Approach*, CRC Press, Boca Raton, 1999.
6. A. Cristy, Y. Ozaki and V. G. Gregoriou, *Modern Fourier Transform Infrared Spectroscopy,* Elsevier, Amsterdam, 2001.
7. W. Heschel, *Philos. Trans.,* 1800, **MDCCC**, 284.
8. D. M. Livingston, *The Master of Light: A Biography of Albert Abraham Michelson,* The University Press of Chicago, Chicago, 1973.
9. A. Michelson, *Phil. Mag.,* 1891, **31**, 338.
10. J. W. Cooley and J. W. Tukey, *Math. Comput.,* 1965, **19**, 297.
11. P. R. Griffiths, R. Curbelo, C. T. Foskett and S. T. Dunn, *Anal. Instr. (Inst. Society of America),* 1970, **8**, II-4.
12. R. N. Jones, *Analytical Applications of Vibrational Spectroscopy - A Historical Review*, John Wiley and Sons, Chichester, 1985.
13. A. N. Zaidel and Y. I. Larionov, *Uspekhi Fizicheskikh Nauk*, 1939, **21**, 211.
14. E. R. Lippincott and R. D. Nelson, *J. Chem. Phys.*, 1953, **21**, 1307.
15. G. Wilkinson, P. L. Pauson, J. M. Birmingham and F. A. Cotton, *J. Am. Chem. Soc.,* 1953, **75**, 1011.
16. G. Pacchioni and P. S. Bagus, *Inorg. Chem.,* 1992, **31**, 4391.
17. R. J. Angelici and F. Basolo, *J. Am. Chem. Soc*., 1962, **84**, 2495.
18 F. Basolo, *Inorg. Chim. Acta*, 1981, **50**, 65.

19. C. A. Tolman, *Chem. Rev*., 1977**, 77**, 313.

20. R. J. Angelici and F. Basolo, *Inorg. Chem*., 1963, **2**, 728.

21. S. J. A. Pope and G. Reid, *J. Chem. Soc.,* 1999, 1615.

CHAPTER 6: THE USE OF FTIRS TO STUDY THE TRANSFORMATION OF MANGANESE CARBONYL COMPLEXES IN SOLUTION

6.1. INTRODUCTION

Substitution of carbonyl groups on $Mn(CO)_4LBr$ by neutral ligands, L, in solution has been studied[1, 2,3,4]. For all the manganese compounds that have been investigated, the rate of the substitution reaction was found to be independent of the concentration and the nature of the incoming ligand. The kinetic product of the reaction was the *cis* isomer, *cis*-$Mn(CO)_3L_2Br$, that was isolated and characterised. This isomer then rearranged to the thermodynamically stable *trans* isomer. A literature review failed to reveal previous solution kinetic data for the formation of $Mn(CO)_3(PPh_3)_2Br$ from $Mn(CO)_5Br$ or $Mn(CO)_4(PPh_3)Br$ in chloroform or TCE. However Atwood and Brown conducted an extensive kinetic study of $Mn(CO)_5Br$ and $Mn(CO)_4(PPh_3)Br$ in hexane using other substituting ligands other than PPh_3[5,6,7].

A review by Angelici detailed the kinetic findings[8] of their studies of substitution reactions of metal carbonyls and is summarised below. The majority of metal carbonyl complexes are non-ionic substances that are soluble in a variety of organic solvents. Kinetic studies of these complexes have been exclusively conducted in non-aqueous solvents. One of the reactions investigated in detail was the substitution reaction of metal carbonyl complexes such that a carbonyl (CO) ligand was substituted by another ligand. The ligands involved in the substitution process were usually neutral ligands that did not interact strongly with solvents. Thus the rate and activation parameters of the reactions were found to be slightly dependent on the nature of the solvent. The nature of the reactants was solely responsible for the kinetic results. The specifics for the reaction of $Mn(CO)_4LX$ (X =Cl, Br, I) + L' → $Mn(CO)_3L$ L'X + CO is shown in **Scheme 6.1**. The reaction was found to go through an S_N1 mechanism. When L' is a phosphine or a

phosphite, the rate of the substitution reaction is not that different to that of $Mn(CO)_5X$. The rate of the reaction was also found to be dependent on X (the order being I < Br < Cl). The *cis* isomer isomerised to the more stable *trans* isomer when the reaction was allowed to proceed for longer periods or the reaction temperature was elevated.

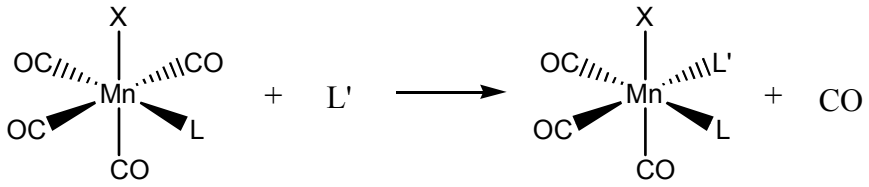

Scheme 6.1. Formation of *cis*-$Mn(CO)_3LL'X$ from the substitution reaction between $Mn(CO)_4LX$ and L' in solution

The study described in Chapter 6 is aimed at generating kinetic parameters for the reaction $Mn(CO)_4LBr + L \rightarrow Mn(CO)_3L_2Br + CO$, in solution, so that comparison with the solventless reaction could be done. Here the ligand used for the substitution reaction was identical to the ligand already attached to the metal complex. Two different solvents, TCE (1,1,2,2-tetrachloroethane) and chloroform, were used in the study. $Mn(CO)_3(PPh_3)_2Br$ was found to be partially soluble in hexane and the solvent was excluded for kinetic investigations.

6.2. EXPERIMENTAL PROCEDURES

Calibration curves were constructed for the three compounds that were involved with the reaction *viz.* ($Mn(CO)_5Br$, $Mn(CO)_4(PPh_3)Br$ and $Mn(CO)_3(PPh_3)_2Br$. The non-overlapping peak positions for the three compounds used in the analysis are shown in **Figure 5.1** (chloroform). Similar peak positions were obtained when TCE was used as a solvent.

6.2.1. Reaction of $Mn(CO)_4LBr$ with L to give $Mn(CO)_3L_2Br$ in TCE solution

6.2.1.1 Calibration curve for $Mn(CO)_5Br$ in TCE solution

$Mn(CO)_5Br$ (2.0 mg, 0.0073 mmol)) was dissolved in 1,1,2,2-tetrachloroethane, TCE, (~3 cm^3) in a 5 cm^3 volumetric flask and TCE added to fill the volumetric flask to the appropriate level. The solution was thoroughly shaken to produce a homogeneous mixture. The solution was used to make more dilute solutions (2 ×, 5 ×, 10 ×, 20 ×, 50 × and 100 × dilutions) from the original solution. The absorbance of each solution was measured using FTIRS and the data are shown in **Figure 6.1**.

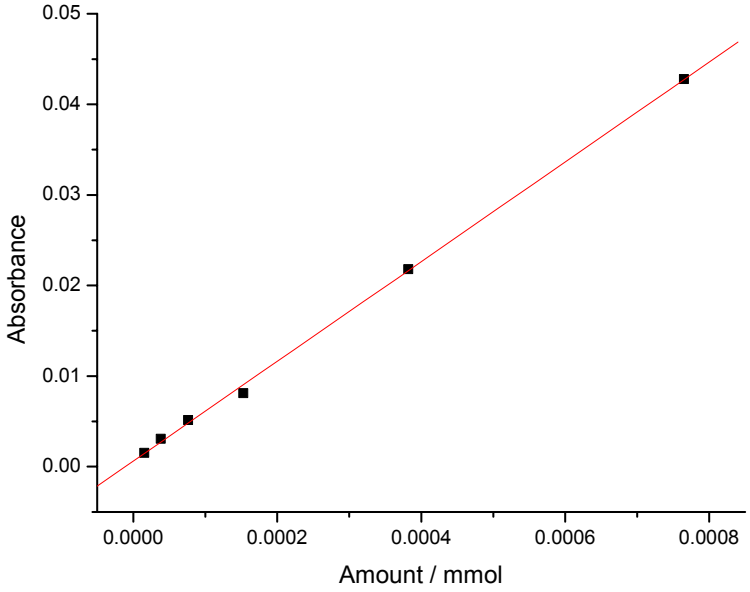

Figure 6.1. Calibration curve for $Mn(CO)_5Br$ in TCE using FTIRS at room temperature

6.2.1.2 Calibration curve for $Mn(CO)_4(PPh_3)Br$ in TCE solution

$Mn(CO)_4(PPh_3)Br$ (3.5 mg, 0.0069 mmol) was placed in a 5 cm^3 volumetric flask and dissolved in TCE (2 cm^3). The same procedure as described above was used to yield a plot as shown in **Figure 6.2**.

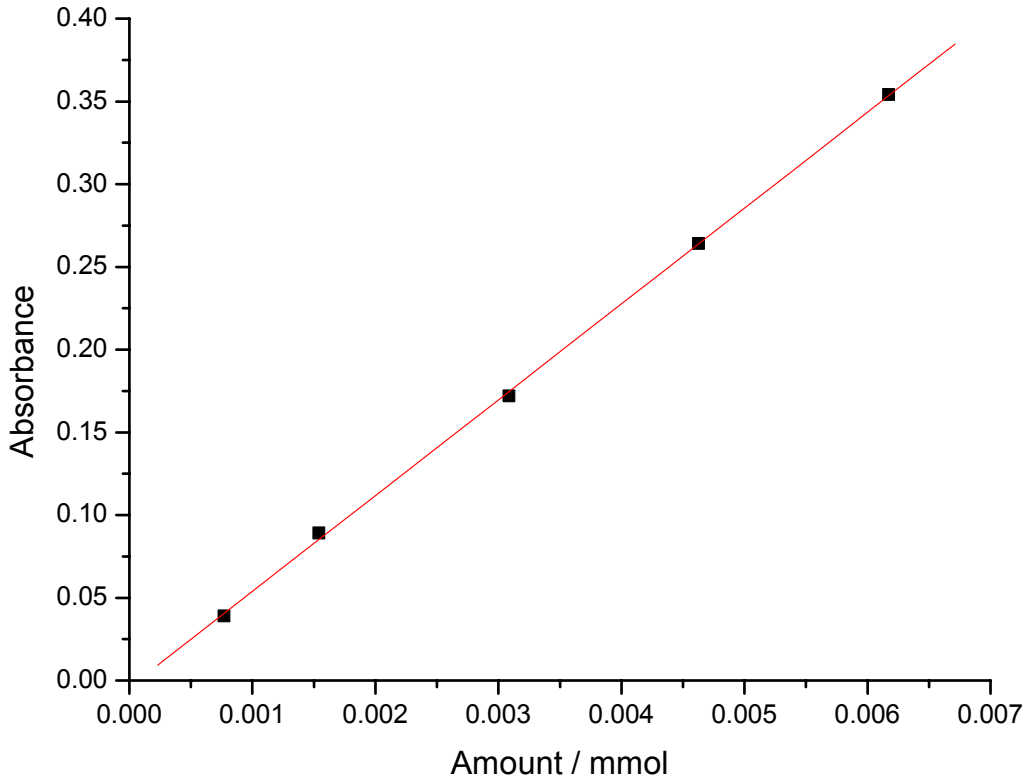

Figure 6.2. Calibration curve for $Mn(CO)_4(PPh_3)Br$ in TCE using FTIRS at room temperature

6.2.1.3 Calibration curve for $Mn(CO)_3(PPh_3)_2Br$ in TCE solution

$Mn(CO)_3(PPh_3)_2Br$ (5.0 mg, 0.0067 mmol) was placed in a 5 cm^3 volumetric flask and dissolved in dry TCE (3 cm^3). The same procedure as described above was used to yield a plot as shown in **Figure 6.3**.

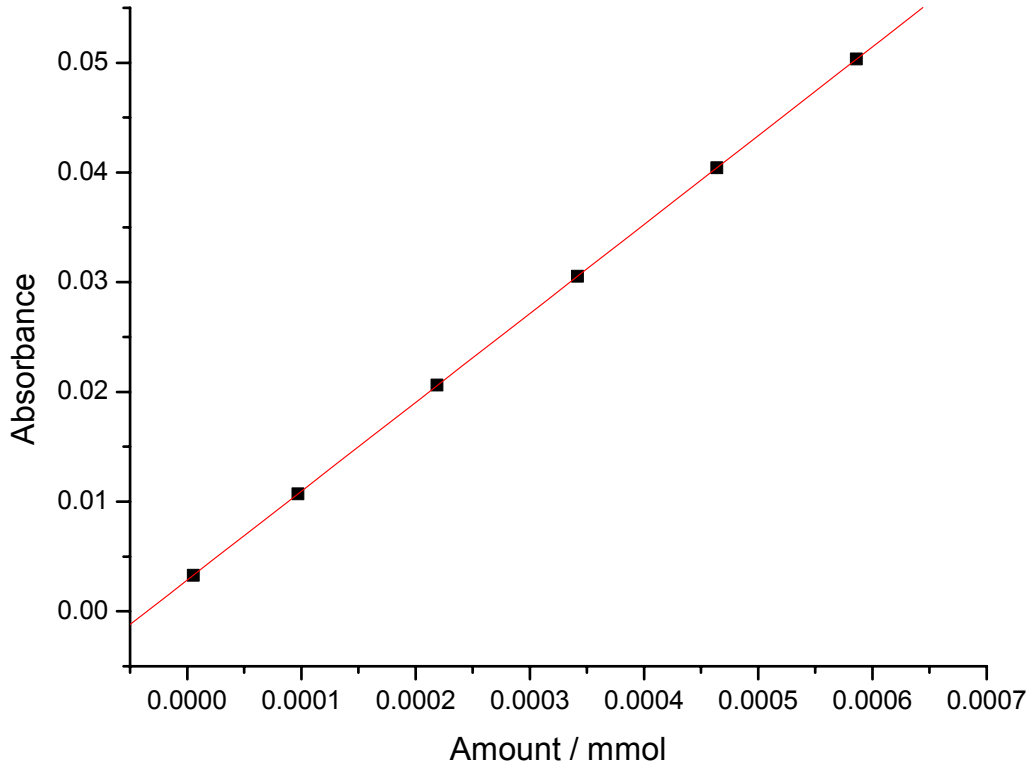

Figure 6.3. Calibration curve for $Mn(CO)_3(PPh_3)_2Br$ in TCE using FTIRS at room temperature

6.2.1.4. FTIRS kinetic study of the reaction between $Mn(CO)_4(PPh_3)Br$ and PPh_3 in TCE solution

Pre-dried 1,1,2,2-tetrachloroethane (TCE) was distilled under nitrogen immediately before use as a solvent. $Mn(CO)_4(PPh_3)Br$ (50 mg, 0.098 mmol) was placed in a 250 cm^3 Schlenk flask equipped with a stirrer bar and dissolved in 30 cm^3 of TCE. The resulting yellow solution was then degassed for 5 min under a nitrogen flow with constant stirring. PPh_3 (450 mg, 1.7 mmol) was dissolved in 100 cm^3 of TCE contained in a 250 cm^3 round bottom flask. The colourless solution was also degassed for 5 min under an inert atmosphere. The reaction vessels containing the two solutions were placed in an oil bath set at the temperature of choice (50°C, 60°C and 70°C) for 10 min. The ligand solution was quickly transferred to the metal complex solution under a nitrogen counter flow while stirring. A small reaction sample (less than 1 cm^3) was quickly withdrawn using a glass Pasture pipette, placed in a small sample vial that was placed in an ice bath (to stop the reaction) for two minutes, and its absorbance quickly measured using FTIRS with a TCE solution as background. This reaction sample gave an initial absorbance value, I_o. Reaction samples were periodically withdrawn from the reaction mixture and their respective time of withdrawal noted. The reaction flask was kept at the set temperature under a nitrogen atmosphere for the entire experimentation period.

By following the disappearance of the starting material peak at 2094 cm^{-1} with time, it was possible to determine the rate constant for the reaction. **Table 6.1** shows the results obtained for the reaction of $Mn(CO)_4(PPh_3)Br$ with PPh_3 (1:10 mole ratios) in TCE conducted at 70°C.

Table 6.1. The kinetic data for the reaction of $Mn(CO)_4(PPh_3)Br$ with PPh_3 (1:10 mole ratios) in TCE conducted at 70°C

Time/h	Time/s	Absorbance at 2094	% $Mn(CO)_4(PPh_3)Br$ Remaining at time t	ln(%$Mn(CO)_4(PPh_3)Br$)
0	0	0.0689	100	4.61
1	300	0.0629	91.3	4.51
2	600	0.0610	88.6	4.48
3	900	0.0560	81.3	4.40
4	1200	0.0516	74.9	4.32
5	1500	0.0475	68.9	4.23
6	1800	0.0434	63.0	4.14
7	2100	0.0390	56.6	4.04
8	2400	0.0359	52.1	3.95
9	2700	0.0318	46.12	3.83

6.2.2. FTIRS kinetic study for the reaction between $Mn(CO)_4(PPh_3)Br$ and PPh_3 in chloroform

Calibration curves of $Mn(CO)_5Br$, $Mn(CO)_4(PPh_3)Br$ and $Mn(CO)_3(PPh_3)_2Br$ were recorded in $CHCl_3$. The procedure for the construction of the curves for each compound was outlined in **Chapter 5**.

Pre-dried chloroform ($CHCl_3$) was freshly distilled under a nitrogen blanket immediately before use as a solvent. $Mn(CO)_4(PPh_3)Br$ (100 mg, 0.196 mmol) was placed in a 500 cm^3 long neck Schlenk flask (at least 10 cm neck length) equipped with a stirrer bar and dissolved in $CHCl_3$ (100 cm^3). The resulting yellow solution was then degassed for 5 min with constant stirring under a nitrogen flow. PPh_3 (900 mg, 3.4 mmol) was taken up in 150 cm^3 of TCE contained in a 250 cm^3 round bottom flask. The colourless solution was also degassed for 5 min under an inert atmosphere. The reaction vessels containing the two solutions were then placed in an oil bath, set at the temperature of choice (40°C,

50°C and 55°C) for 30 min. The ligand solution was quickly transferred to the metal complex solution under a nitrogen counter flow while stirring. A small reaction sample (less than 1 cm^3) was quickly withdrawn using a Pasture pipette, placed in a small sample vial that was then placed in an ice bath (to stop the reaction) for two minutes. The IR spectrum was then measured using FTIRS with $CHCl_3$ solution as background. The reaction sample measurement described above represents the initial absorbance value. Reaction samples were periodically withdrawn from the reaction mixture and their respective time of withdrawal noted in the kinetic study. The reaction flask was kept at the set temperature under a nitrogen atmosphere for the entire experiment.

6.3. RESULTS AND DISCUSSION

6.3.1. A kinetic study for the reaction of $Mn(CO)_4(PPh_3)Br$ with PPh_3 in chloroform

Table 6.2 shows the rate constants at different temperatures for the reaction between $Mn(CO)_4(PPh_3)Br$ and PPh_3 in chloroform, assuming a first order rate law. The Arrhenius [ln(k) versus 1/T] plot is shown in **Figure 6.4** and was used to determine the enthalpy change of activation. Using the Eyring [ln(k/T) versus 1/T] plot the entropy of activation was also determined.

Table 6.2. Kinetic parameters of the reaction of $Mn(CO)_4(PPh_3)Br$ with PPh_3 (1:17 mole equiv) in chloroform

T/°C	*T*/K	$1/T$ / K^{-1}	*k*	ln(*k*)	ln(*k*/*T*)	$\Delta H^{\ddagger}$/ $kJmol^{-1}$	$\Delta S^{\ddagger}$ / $Jmol^{-1}K^{-1}$
40	328	0.00304	3.69E-05	-10.2	-16.0	146 ± 8	114 ± 6
50	323	0.00309	1.37E-05	-11.2	-16.9		
55	313	0.00319	2.63E-06	-12.8	-18.6		

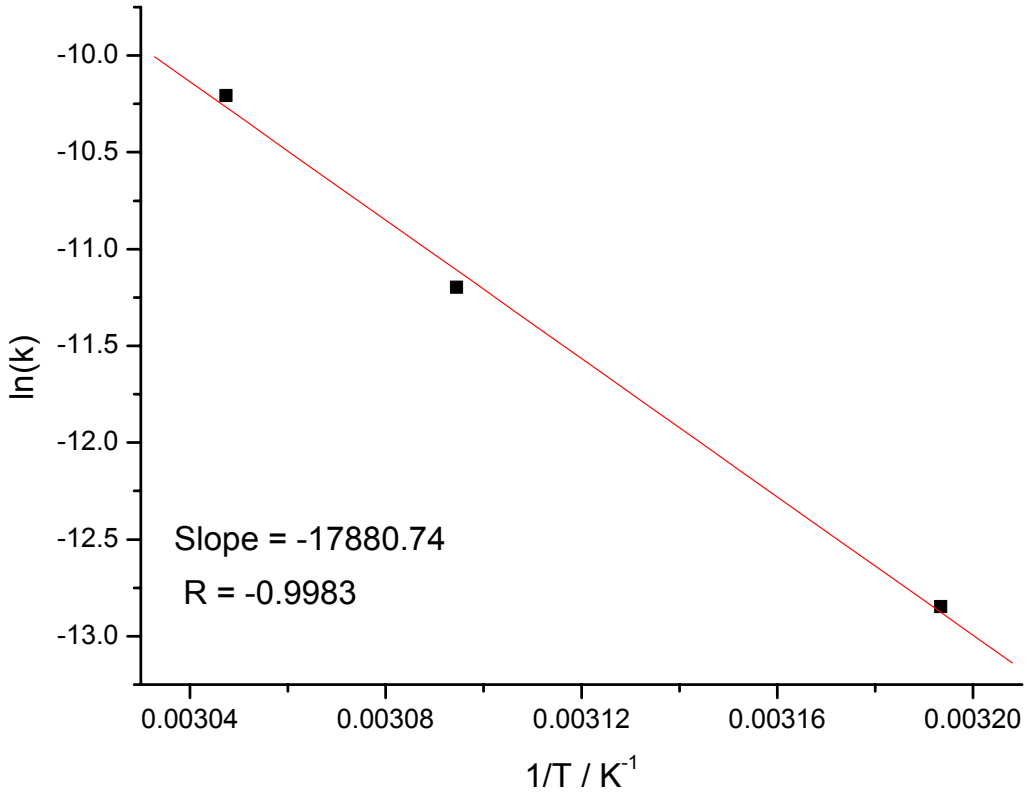

Figure 6.4. Arrhenius plot of the reaction of $Mn(CO)_4(PPh_3)Br$ with PPh_3 (1:17 mole equiv) in chloroform

The activation enthalpy for the formation of $Mn(CO)_3(PPh_3)_2Br$ from the reaction of $Mn(CO)_4(PPh_3)Br$ and PPh_3 (1:17 mol equiv) in chloroform solution was found to be 146

± 8 kJmol^{-1}. The entropy of activation was large and positive (114 ± 6 Jmol^{-1}K^{-1}) suggestive of a reaction that goes through a dissociative type of mechanism.

The activation parameters of the dissociation of CO from $Mn(CO)_5Br$ have been reported to be E_a = 125 ± 2 kJmol^{-1} and $\Delta S^{\ddagger}$ = 79 ± 2 Jmol^{-1}K^{-1} in chloroform[4]. The activation parameters of the formation of $Mn(CO)_4(AsPh_3)Br$ were found to be 125 ± 3 kJmol^{-1} and $\Delta S^{\ddagger}$ = 74 ± 2 Jmol^{-1}K^{-1} in chloroform[9].

The experimentally determined values are thus comparable to the literature values. The similarity of the data suggests that the nature of L in $Mn(CO)_4LBr$ (L = CO, $AsPh_3$, PPh_3) does not impact significantly on the rate of dissociation of CO, presumably in a *cis* position relative to the L group. This also explains the difficulty experienced in isolating the $Mn(CO)_4(PPh_3)Br$ when $Mn(CO)_5Br$ and PPh_3 were reacted together in the absence of solvents.

6.3.2. A kinetic study for the reaction of $Mn(CO)_4(PPh_3)Br$ with PPh_3 in TCE

The rate constants for the reaction between $Mn(CO)_4(PPh_3)Br$ and PPh_3 in TCE are shown in **Table 6.3**. The rate constants were obtained by assuming first order kinetics. The Arrhenius plot [ln(k) versus (1/T)] for the reaction is shown in **Figure 6.5**. From the Arrhenius plot the enthalpy change of activation was determined. Similarly, the entropy change of activation was obtained from the Eyring plot [ln(k/T) versus (1/T)].

Table 6.3. Kinetic parameters of the reaction of $Mn(CO)_4(PPh_3)Br$ with PPh_3 (1:17 mole ratio) in TCE

T/ C	*T*/K	$1/T$ / K^{-1}	*k*	ln(*k*)	ln(*k*/*T*)	$\Delta H^{\ddagger}$/ kJ.mol^{-1}	$\Delta S^{\ddagger}$ / Jmol^{-1}K^{-1}
50	323	0.00309	4.94E-05	-9.92	-15.7	137	97
60	333	0.00300	0.000197	-8.53	-14.3		
70	343	0.00291	0.001036	-6.87	-12.7		

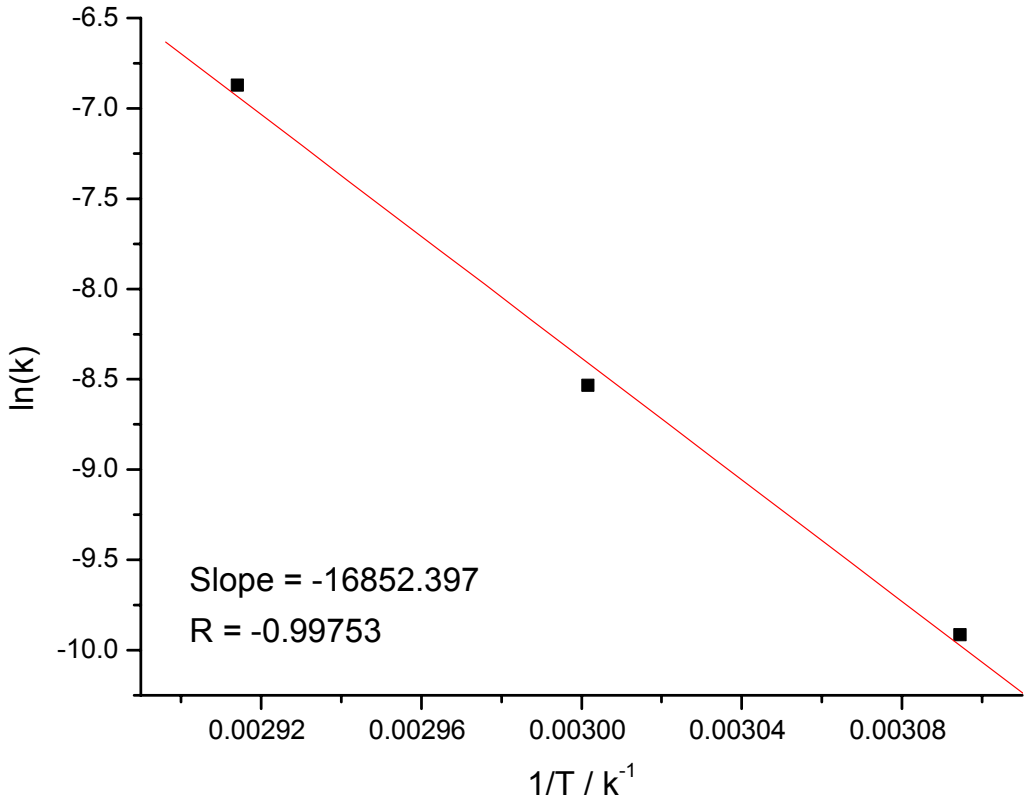

Figure 6.5. Arrhenius plot of the reaction of $Mn(CO)_4(PPh_3)Br$ with PPh_3 (1:17 mole equiv) in TCE

The activation enthalpy of formation of $Mn(CO)_3(PPh_3)_2Br$ from TCE solutions of $Mn(CO)_4(PPh_3)Br$ and PPh_3 (1:17 mol equiv) was found to be 137 ± 6 kJmol^{-1}. The

entropy of activation was also large and positive (97 ± 5 $Jmol^{-1}K^{-1}$) suggestive again of a reaction that goes through a dissociative type of mechanism.

The activation parameters of the reaction between $Mn(CO)_4(PPh_3)Br$ and PPh_3 in both chloroform and TCE are similar. The similarity in the activation energy suggested that minimal solvents effects are detected. The results agree with literature findings that solvents effects in metal carbonyl substitution reactions are very small[10].

6.3.3. Comparison of the solventless and solution kinetic parameters for the reaction between $Mn(CO)_4(PPh_3)Br$ with PPh_3

The kinetic data for the formation of $Mn(CO)_3(PPh_3)_2Br$ from the substitution reaction between $Mn(CO)_4(PPh_3)Br$ and PPh_3 was conducted successfully using both solution and solventless methodologies. The results are summarised in **Table 6.4**. The activation energy for the reaction was the same in the three systems investigated. Similarly, the entropy of activation was the same in the three systems. The conclusion made from the studies is that the mechanism of the reaction must be the same in both solventless and solution systems.

Table 6.4. Activation parameters for the reaction between $Mn(CO)_4(PPh_3)Br$ and PPh_3 to produce $Mn(CO)_3(PPh_3)_2Br$ as followed by FTIRS using both solvent and solventless methods

Activation parameter	Solventless reaction	Chloroform solution	TCE solution
E_a / $kJmol^{-1}$	143 ± 19	146 ± 8	137 ± 6
$\Delta S^{\ddagger}$ / $Jmol^{-1}K^{-1}$	104 ± 7	114 ± 6	97 ± 5

The results were however puzzling. The solution reactions occurred in a fluid media that would have facilitated the diffusion of reactants and products. The manifestation of easy diffusion was well-behaved kinetics as was observed when chloroform or TCE solutions were used. However, the kinetic data for the solventless reactions were also well

behaved. Here, mass transfer problems were expected to inhibit contact between reacting molecules leading to diffusion controlled reaction kinetics.

6.4. CONCLUSIONS

The reaction of $Mn(CO)_4(PPh_3)Br$ and PPh_3 in TCE and chloroform solutions was successfully conducted and the reaction kinetics studied. The activation energy change was found to be 146 ± 8 $kJmol^{-1}$ and 137 ± 6 $kJmol^{-1}$ in TCE and chloroform respectively. The entropy change of activation was found to be 114 ± 6 $Jmol^{-1}K^{-1}$ and 97 ± 5 $Jmol^{-1}K^{-1}$ in TCE and chloroform respectively. The similarity in the activation energy suggested that there were minimal solvent effects. The findings are understandable because a neutral complex, $Mn(CO)_4(PPh_3)Br$, dissociates a neutral ligand (CO) leading to a neutral intermediate, $[Mn(CO)_3(PPh_3)Br]$ so that solvation changes are minimal during the course of the reaction[11]. The activation parameters were found to be the same in both solution and solventless transformations leading to the conclusion that the mechanism of the reaction was the same in both systems. The activation parameters supported a dissociative reaction mechanism.

6.5. REFERENCES

1. R. J. Angelici, F. Basolo and A. J. Poe, *J. Am. Chem. Soc*., 1963, **85**, 2215.
2. R. J. Angelici, *Inorg. Chem*., 1964, **3**, 1099.
3. S. J. A. Pope and G. Reid, *J. Chem. Soc.,* 1999, 1615.
4. R. J. Angelici and F. Basolo, *J. Am. Chem. Soc*., 1962, **84**, 2495.
5. J. D. Atwood and T. L. Brown, *J. Am. Chem. Soc*., 1975, **97**, 3380.
6. J. D. Atwood and T. L. Brown, *J. Am. Chem. Soc*., 1976, **98**, 3160.
7. J. D. Atwood and T. L. Brown, *J. Am. Chem. Soc*., 1976, **98**, 3155.
8. R. J. Angelici, *Organomet. Chem. Rev*., 1968, **3**, 173.
9. R. J. Angelici and F. Basolo, *Inorg. Chem.,* 1963, **2**, 728.
10. R. J. Angelici and F. Basolo, *J. Am. Chem. Soc*., 1962, **84**, 2495.
11. J. D. Atwood, *Inorganic and Organic Reaction Mechanisms* 2nd Ed, Wiley-VCH, New York, 1997, p 103.

CHAPTER 7: THE SOLVENTLESS REACTION BETWEEN $Mn(CO)_4(L)Br$ AND L′ FOLLOWED BY ^{31}P NMR SPECTROSCOPY

7.1. INTRODUCTION

7.1.1. History and perspective

Spectroscopy may be defined as the interaction between matter and electromagnetic radiation[1]. Energy is either absorbed or emitted by matter according to the Bohr frequency condition, $\Delta E = h\upsilon$. ΔE is the energy difference between the initial and final states of the matter, h is Planck's constant and υ is the frequency of the radiation[2]. Spectroscopy has become recognized as an important tool for investigating molecular structure and molecular processes.

Nuclear magnetic resonance (NMR) is that branch of spectroscopy that involves the magnetic energy of nuclei when they are placed in a magnetic field[3]. The interaction of the nuclear magnetic moment of a nucleus with an external magnetic field, B_0, leads to a nuclear energy level diagram. Through a high frequency transmitter, the absorption of energy between energy levels can be detected, amplified and recorded as a spectral line called a resonance signal. In that way a spectrum can be generated for a compound containing atoms whose nuclei have a non-zero magnetic moments. Among these nuclei are ^{1}H, ^{13}C, ^{15}N, ^{19}F and ^{31}P isotopes.

The first NMR signals were independently observed by two groups of physicists-Purcell, Torrey and Pound[4] at Harvard University and Block, Hansen and Packard[5] at Stanford University in 1945. Useful chemical application of the technique became possible after the discovery of the chemical shift effect in 1949[6,7]. Since that time, the development of

NMR technique has been rapid leading to the production of the first commercial high-resolution proton NMR spectrometer in 1953[8].

All forms of spectroscopy give spectra that are described in terms of frequency, intensity and shape of spectral lines[9]. These observable properties depend on molecular parameters of the system. For NMR the parameters are shielding constants and coupling constants of nuclei, and the life times of the energy levels[10].

^{31}P NMR spectroscopy has been in use since the mid 1950s. A book about the technique was first published by Crutchfield, Dugan, Letcher, Mark and Van Wazer[11] in 1967 and since then the volume of ^{31}P NMR data continues to grow. The development of Fourier transform (FT) NMR spectroscopy has led to the development of sensitive instruments that produce accurate data[12].

^{31}P chemical shifts have been observed over a range exceeding 1000 ppm but many classes of phosphorus compounds give signals with a small chemical shift range. The relationship between structure and phosphorus chemical shift is sufficiently established to permit detailed structural inferences. For organophosphorus compounds ^{1}H and ^{13}C NMR data are often linked directly to the ^{31}P information[13]. The multiplicity of phosphorus signals due to coupling to neighbouring protons is also useful for determining the nature of groups bound to the phosphorus atoms[14].

7.1.2. ^{31}P NMR spectroscopy in organometallic chemistry

^{31}P NMR spectroscopy has been extensively used in organometallic chemistry. Examples of the use of the technique include studies involving $Mo(CO)_5L$, $Mo(CO)_4L_2$ and $Mo(CO)_3L_3$ (L = phosphorus bonded ligand)[15,16,17], structural problems in ruthenium chemistry[18,19], examination of the hydroformalation catalyst, $Co_2(CO)_8/PPh_3$[20], and the study of transition metal complexes containing nickel, palladium, rhenium, copper, mercury etc.

7.1.3. Aims of this study

The aim of this investigation was to study the solventless reaction of $Mn(CO)_4(L)Br$ with a range of ligands, L′ to give $Mn(CO)_4(L)(L')Br$. The sensitivity of ^{31}P NMR spectroscopy was used to detect the different metal-P containing complexes and free ligands used – following dissolution of the solid manganese sample in appropriate solvents.

7.2. EXPERIMENTAL PROCEDURES

7.2.1. The use of NMR spectroscopy to study the solventless reaction $Mn(CO)_4(L)Br$ with L′

The reaction of $Mn(CO)_4(PPh_3)Br$ with P(*p*-MeO-$C_6H_4)_3$,was initially chosen for study. Four possible products are expected from the reaction: *trans*-$Mn(CO)_3(PPh_3)_2Br$, *trans* $Mn(CO)_3(P(p\text{-MeO-}C_6H_4)_3)_2Br$, *trans*-$Mn(CO)_3(PPh_3)(P(p\text{-MeO-}C_6H_4)_3)Br$ and $Mn(CO)_4(P(p\text{-MeO-}C_6H_4)_3)Br$. The ^{31}P chemical shifts of all the compounds except *trans*-$Mn(CO)_3(PPh_3)(P(p\text{-MeO-}C_6H_4)_3)Br$, were independently determined (**Table 7.1**). The ^{31}P chemical shifts of two ligands involved, P(*p*-MeO-$C_6H_4)_3$ and PPh_3 were also recorded (**Table 7.1**).

Table 7.1. ^{31}P NMR of products and reagents involved in the solventless reaction of $Mn(CO)_4(PPh_3)Br$ with P(*p*-MeO-$C_6H_4)_3$ [$CDCl_3$; TMS reference]

Compound	^{31}P NMR ($CDCl_3$) /ppm
PPh_3	-4.7
(*p*-MeO-$C_6H_4)_3P$	-9.5
$Mn(CO)_4(PPh_3)Br$	41.0
$Mn(CO)_3(PPh_3)_2Br$	54.6
$Mn(CO)_4$(P(*p*-MeO-$C_6H_4)_3$)Br	36.7
$Mn(CO)_3$(P(*p*-MeO-$C_6H_4)_3)_2Br$	50.2

7.2.2. The solventless reaction between $Mn(CO)_4(PPh_3)Br$ and P(*p*-MeOPh)$_3$ (1:1.14) followed by ^{31}P NMR spectroscopy

$Mn(CO)_4(PPh_3)Br$ (200 mg, 390 μmol) was mixed with P(*p*-MeO-$C_6H_4)_3$ (200 mg, 567 μmol) in a sample vial. Finely ground reagents (50-90 μm particle size) were used to maximise their surface area. The resulting mixture was then divided and placed into nine separate NMR tubes (40 mg samples). The NMR tubes were purged with nitrogen gas before sealing with a rubber seal. Eight of the samples were simultaneously placed in an oil bath pre-set at 60°C. One sample was placed in a dessicator for later analysis. Samples were withdrawn periodically at pre-determined time periods and the NMR tube immediately placed in an ice bath to stop the reaction that might otherwise continue at room temperature. Each sample was immediately taken up in enough $CDCl_3$ to dissolve the solid materials contained in the NMR tube. ^{31}P NMR spectra of the samples were then recorded and the relative composition of the sample determined.

7.2.3. The solventless reaction between $Mn(CO)_4(PPh_3)Br$ and P(*p*-MeO-$C_6H_4)_3$ (1:3) followed by ^{31}P NMR spectroscopy

$Mn(CO)_4(PPh_3)Br$ (200 mg, 390 μmol) was mixed with P(*p*-MeO-$C_6H_4)_3$ (400 mg, 1.13 mmol) in a sample vial. The same experimental procedure as described above was used to carry out the experiment.

7.2.4. The solventless reaction between $Mn(CO)_4(P(p\text{-}MeO\text{-}C_6H_4)_3)Br$ and PPh_3 (1:2) as followed by ^{31}P NMR spectroscopy

Finely ground powders of $Mn(CO)_4(P(p\text{-}MeO\text{-}C_6H_4)_3P)Br$ (200 mg, 0.334 mmol) and PPh_3 (200 mg, 0.762 mmol) were mixed together using a spatula in a vial. Further experimentation was conducted the same way as described above.

7.3. RESULTS AND DISCUSSIONS

7.3.1. The solventless reaction between $Mn(CO)_4(PPh_3)Br$ and P(*p*-MeO-$C_6H_4)_3$ (1:1.4) followed by ^{31}P NMR spectroscopy at 60°C

The reaction was conducted by firstly preparing a well mixed solid material [($Mn(CO)_4(PPh_3)Br$ and P(*p*-MeO-$C_6H_4)_3$ 1:1, w/w] using solvents. The solid material was then partitioned into 8 samples, each sample containing enough metal complex to be detected by NMR spectroscopy. At reaction temperatures greater than 115°C, the reaction formed a melt. The samples were then subjected to thermal experimentation at pre-set temperatures lower than 100°C. Samples were periodically withdrawn at pre-determined times. **Figure 7.1** shows an NMR spectrum of a reaction between $Mn(CO)_4(PPh_3)Br$ and P(*p*-MeO-$C_6H_4)_3$ (1:1 w/w) taken after a minute of reaction at 60°C.

The spectrum shows signals due to starting materials, $Mn(CO)_4(PPh_3)Br$ (41 ppm) and the ligand P(*p*-MeO-$C_6H_4)_3$ (-9 ppm). It also shows signals at 36 ppm (due to $Mn(CO)_4$(P(*p*-MeO-$C_6H_4)_3$)Br) and -4 ppm (due to PPh_3) indicating that a reaction has already taken place during that time period. Integration shows equal amount of products formed, $Mn(CO)_4$(P(*p*-MeO-$C_6H_4)_3$)Br), and PPh_3.

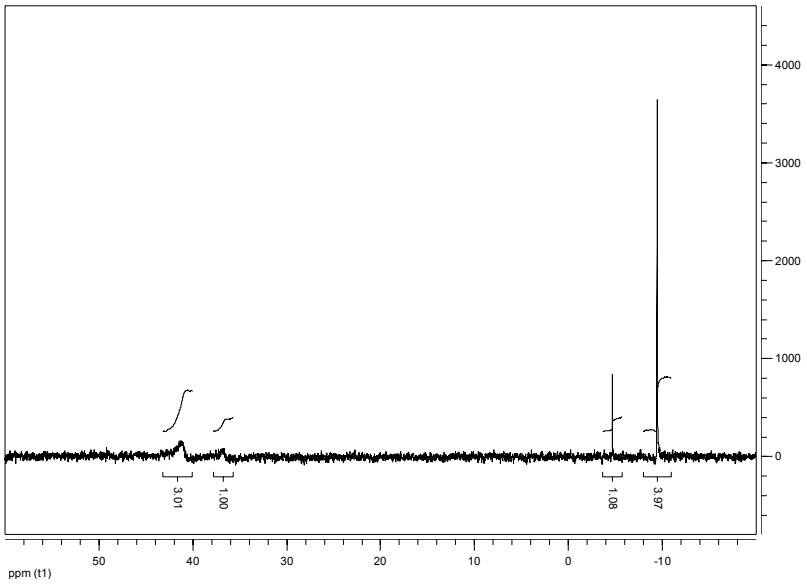

Figure 7.1. A ^{31}P NMR spectrum of a reaction between $Mn(CO)_4(PPh_3)Br$ and P(*p*-MeO-$C_6H_4)_3$ (1:1.4) taken after one minute of reaction at 60°C

^{31}P NMR spectra were also recorded after different time intervals to check the extent of the reaction. The results of the experiments are summarised in **Table 7.2**. The amount of each compound is given as a percentage of the total phosphorus content. **Figure 7.2** shows the reaction sequence captured as ^{31}P NMR spectra recorded at different time intervals. The integration values of each phosphorus signal are also included. These integral values were used to construct **Table 7.2**.

Table 7.2. The solventless reaction between $Mn(CO)_4(PPh_3)Br$ and P(*p*-MeO-$C_6H_4)_3$ (1:1.4) as followed by ^{31}P NMR spectroscopy at 60°C

Time (min)	1	2	5	10	15	60	180	1020
Compound[a] (↓) (experiment number (→)	1	2	3	4	5	6	7	8
PPh_3	11.1	19.1	23.6	22.0	20.9	21.8	18.6	9.1
(*p*-MeOPh)$_3$P	44.5	37.8	30.9	27.1	24.5	12.9	10.8	3.4
$Mn(CO)_4(PPh_3)Br$	33.3	26.3	21.8	21.7	14.8	7.5	5.7	0.1
$Mn(CO)_3(PPh_3)_2Br$	0	0	0	1.5	7.2	11.9	16.5	24.7
$Mn(CO)_4$(P(*p*-MeO-$C_6H_4)_3$)Br	11.1	16.8	23.7	20.5	17.1	18.4	14.3	1.2
$Mn(CO)_3$(P(*p*-MeO-$C_6H_4)_3)_2$Br	0	0	0	5.7	10.4	19.2	23.4	40.1
$Mn(CO)_3$(P(*p*-MeO-$C_6H_4)_3$) (PPh_3)Br	0	0	0	1.5	5.1	8.3	10.7	21.4

a. The values given are as percentages of the total phosphorus content per given experiment.

The fact that immediately after a minute of reaction between $Mn(CO)_4(PPh_3)Br$ and P(*p*-MeO-$C_6H_4)_3$ at 60°C (**Table 7.2** and **Figure 7.1**), $Mn(CO)_4$(P(*p*-MeO-$C_6H_4)_3$)Br was formed also suggests that P(*p*-MeO-$C_6H_4)_3$ is a better Lewis base than PPh_3. Additionally, it means that the dissociation of the PPh_3 ligand from $Mn(CO)_4(PPh_3)Br$ to form a five coordinate intermediate $Mn(CO)_4Br$ is faster than the dissociation of CO ligand to form the intermediate $Mn(CO)_3(PPh_3)Br$. If this was not the case $Mn(CO)_3(PPh_3)_2Br$ should have been formed in theearly stage of the reaction. **Scheme 7.**1 shows the dissociation of the PPh_3 ligand from $Mn(CO)_4(PPh_3)Br$ to yield a five-coordinate intermediate that was trapped by the P(*p*-MeO-$C_6H_4)_3$ ligand to yield $Mn(CO)_4$(P(*p*-MeO-$C_6H_4)_3$)Br.

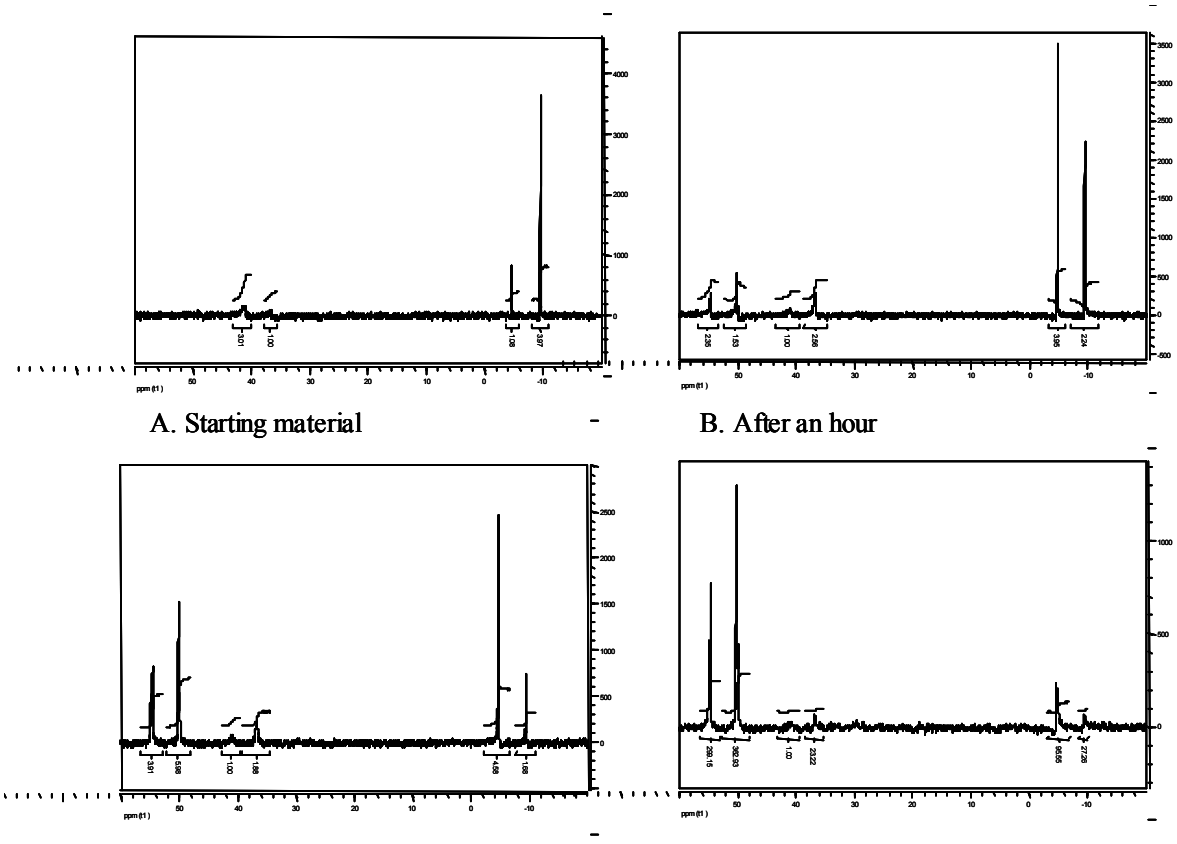

Figure 7.2. NMR spectra for the solventless reaction between $Mn(CO)_4(PPh_3)Br$ and P(*p*-MeO-$C_6H_4)_3$ (1:1.4) as followed by ^{31}P NMR spectroscopy at 60°C recorded after pre-determined time periods

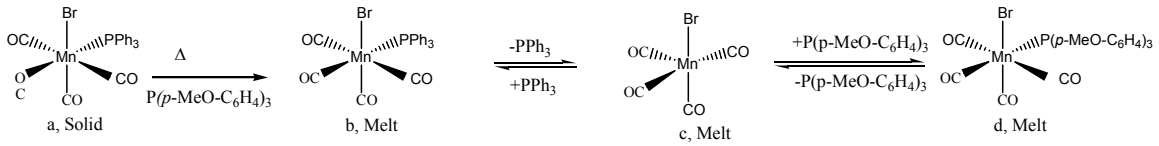

Scheme 7.1. Suggested reaction pathway for the formation of $Mn(CO)_4((p\text{-MeO-}C_6H_4)_3)Br$ from the reaction of $Mn(CO)_4(PPh_3)Br$ with PPh_3P_3 (1:1.4) as followed by ^{31}P NMR spectroscopy

The tricarbonyl complex, $Mn(CO)_3(P(p\text{-MeO-}C_6H_4)_3)_2Br$, was preferentially formed over $Mn(CO)_3(PPh_3)_2Br$ (formed after 10 minutes of reaction while the latter was formed after an hour. The availability of free ligand [more P(*p*-MeO-$C_6H_4)_3$ than PPh_3] dictated the results obtained as there was greater chance of the more abundant P(*p*-MeO-$C_6H_4)_3$

ligand trapping the intermediate to reform a stable six coordinate product. The above-mentioned statement is supported by the fact that at the end of the reaction (17 hours), there was more $Mn(CO)_3(P(p\text{-}MeO\text{-}C_6H_4)_3)_2Br$ (40.6%) that formed than $Mn(CO)_3(PPh_3)_2Br$ (24.7%). Both tetracarbonyl complexes [$Mn(CO)_4(PPh_3)Br$ and $Mn(CO)_4(P(p\text{-}MeO\text{-}C_6H_4)_3)Br$] had been consumed when the reaction was terminated after 17 hours.

The mixed ligand complex, $Mn(CO)_3(P(p\text{-}MeO\text{-}C_6H_4)_3)(PPh_3)Br$, was detected by NMR spectroscopy (**Figure7.3**). Its peaks overlapped with those of $Mn(CO)_3(P(p\text{-}MeO\text{-}C_6H_4)_3)_2Br$ and $Mn(CO)_3(PPh_3)_2Br$. The expansion of the signals at 51 ppm and 54 ppm of the ^{31}P NMR spectrum revealed the two peaks that grew together as the reaction continued.

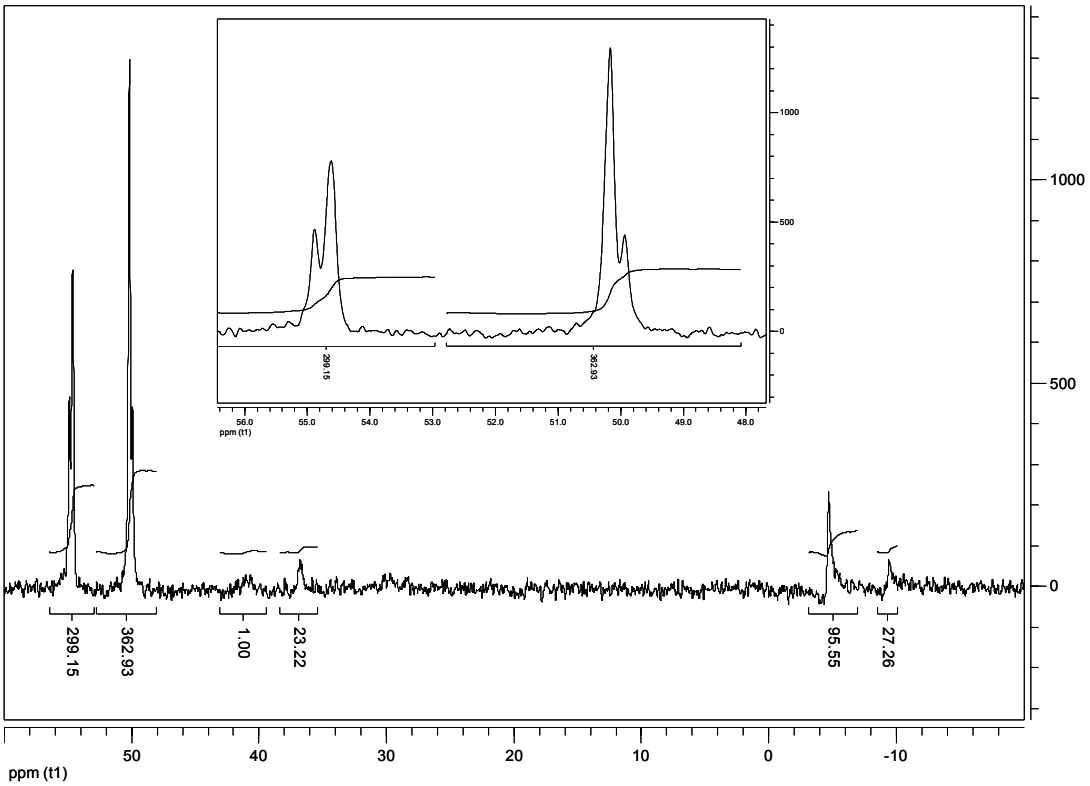

Figure 7.3. ^{31}P NMR spectrum of a reaction between $Mn(CO)_4(PPh_3)Br$ and $P(p\text{-}MeO\text{-}C_6H_4)_3$ (1:1.4) taken after 17 hours of reaction at 60°C The expansion of the signals at 51 and 54 ppm is shown in the insert

By comparing the intensity peaks from at the specific chemical shift the percentage composition of the complexes were determined (**Table 7.2**). $Mn(CO)_3(P(p\text{-}MeO\text{-}C_6H_4)_3)(PPh_3)Br$ emerged after 10 minutes of reaction and at the end of the reaction, 21.4% of the total phosphorus content was due to the complex.

7.3.2. The solventless reaction between $Mn(CO)_4(PPh_3)Br$ and $P(p\text{-}MeO\text{-}C_6H_4)_3$ (1:3) followed by ^{31}P NMR spectroscopy

The facile nature of the reaction was shown by the rapid formation of $Mn(CO)_4(P(p\text{-}MeO\text{-}C_6H_4)_3)Br$ (**Table 7.3**). Trace amount (2%) of the tricarbonyl complex, $Mn(CO)_3(PPh_3)_2Br$, emerged after 10 min while $Mn(CO)_4(PPh_3)Br$ started to decrease substantially. The other tricarbonyl complexes, $Mn(CO)_3(P(p\text{-}MeO\text{-}C_6H_4)_3)(PPh_3)Br$ also started to form after 10 minutes.

Table 7.3. The solventless reaction between $Mn(CO)_4(PPh_3)Br$ and $P(p\text{-}MeO\text{-}C_6H_4)_3$ (1:3) as followed by ^{31}P NMR spectroscopy

Time (min)	1	2	5	10	15	60	120	960
Compound[a] (↓)(experiment number(→)	1	2	3	4	5	6	7	8
PPh_3	14.1	15.8	16.4	19.1	21.0	13.0	10.5	6.5
$P(p\text{-}MeO\text{-}C_6H_4)_3$	60.9	59.2	58.6	52.3	46.0	46.4	44.6	26.1
$Mn(CO)_4(PPh_3)Br$	11.9	10.1	9.8	4.7	0	0	0	0
$Mn(CO)_3(PPh_3)_2Br$	0	0	0	2	3.4	9.3	11.0	17.4
$Mn(CO)_4(P(p\text{-}MeO\text{-}C_6H_4)_3)Br$	13.1	14.9	15.2	16.7	17.0	9.3	5.3	0
$Mn(CO)_3(P(p\text{-}MeO\text{-}C_6H_4)_3)_2Br$	0	0	0	3.8	9.7	15.8	19.5	35.3
$Mn(CO)_3(P(p\text{-}MeO\text{-}C_6H_4)_3)(PPh_3)Br$	0	0	0	1.4	2.9	6.2	9.1	14.7

a. The values given are as percentages of the total phosphorus content per given experiment.

At the end of 16 hours of experimentation, only $Mn(CO)_3(P(p\text{-}MeO\text{-}C_6H_4)_3P)_2Br$ (35.3%), $Mn(CO)_3(P(p\text{-}MeO\text{-}C_6H_4)_3)(PPh_3)Br$ (14.7%) and $Mn(CO)_3(PPh_3)_2Br$ (17.4%) were present together with small amounts of the ligands.

The results obtained suggested that the reaction followed the same trend to the one conducted using equal amounts of starting materials. The percentage composition of $Mn(CO)_3(P(p\text{-}MeO\text{-}C_6H_4)_3)_2Br$ (35.3%) was more than double that of $Mn(CO)_3(PPh_3)_2Br$ (17.4%). This finding was expected because the more abundant $P(p\text{-}MeO\text{-}C_6H_4)_3$ ligand would have lead to the formation of a higher percentage of the corresponding tricabonyl manganese bromide complex.

7.3.3. The solventless reaction between $Mn(CO)_4(P(p\text{-}MeO\text{-}C_6H_4)_3)Br$ with PPh_3 (1:2) as followed by ^{31}P NMR spectroscopy

The reaction was also facile as there was product formation, $Mn(CO)_3(P(p\text{-}MeO\text{-}C_6H_4)_3)_2Br$ (4.1%), after just a minute of experimentation (**Table 7.4**). **Table 7.4** also shows that $Mn(CO)_4(PPh_3)Br$ (4.5%) formed as early as two min after the start of the reaction. This point alone suggest that $P(p\text{-}MeO\text{-}C_6H_4)_3$ is a better Lewis base than PPh_3, a finding deduced in **Sections 7.3.1-7.3.2**. After 15 min of thermal experimentation, $Mn(CO)_3(PPh_3)_2Br$ (2.6%) and $Mn(CO)_3(P(p\text{-}MeO\text{-}C_6H_4)_3)(PPh_3)Br$ (1.6%) started to emerge as well.

Table 7.4. The solventless reaction between $Mn(CO)_4(P(p\text{-}MeO\text{-}C_6H_4)_3)Br$ and PPh_3 (1:2) as followed by ^{31}P NMR

Time (min)	1	2	5	15	30	60	120	960
Compound[a] (↓)(experiment number(→)	1	2	3	4	5	6	7	8
PPh_3	57.2	53.3	52.0	44.2	42.0	39.5	33.3	20.5
$P(p\text{-}MeOPh)_3$	7.8	11.5	12.6	15.0	15.6	19.8	19.6	10.8
$Mn(CO)_4(PPh_3)Br$	0	4.5	5.5	8.5	9.5	9.0	6.4	0
$Mn(CO)_3(PPh_3)_2Br$	0	0	0	2.6	4.9	7.4	14.0	30.7
$Mn(CO)_4(P(p\text{-}MeO\text{-}C_6H_4)_3P)Br$	30.9	26.3	25.1	20.5	18.7	13.2	6.4	0
$Mn(CO)_3(P(p\text{-}MeO\text{-}C_6H_4)_3)_2Br$	4.1	4.4	4.8	6.6	6.4	7.7	12.7	24.4
$Mn(CO)_3(P(p\text{-}MeO\text{-}C_6H_4)_3)(PPh_3)Br$	0	0	0	2.6	2.9	3.4	7.6	13.6

a. The values given are as percentages of the total phosphorus content per given experiment.

The reaction progress is captured by ^{31}P NMR spectra recorded at different time intervals as shown in **Figure 7.4**. The figure shows that the amounts of the three tricarbonyl complexes increased with time while that of $Mn(CO)_4(P(p\text{-}MeO\text{-}C_6H_4)_3)Br$ decreased with time until it disappeared after 16 h. $Mn(CO)_3(P(p\text{-}MeO\text{-}C_6H_4)_3)_2Br$ (24.4%), $Mn(CO)_3(P(p\text{-}MeO\text{-}C_6H_4)_3)(PPh_3)Br$ (13.6%) and $Mn(CO)_3(PPh_3)_2Br$ (30.7%) were the only metal complexes left after 16 hours of reaction. However there were still unreacted ligands the end of 16 h.

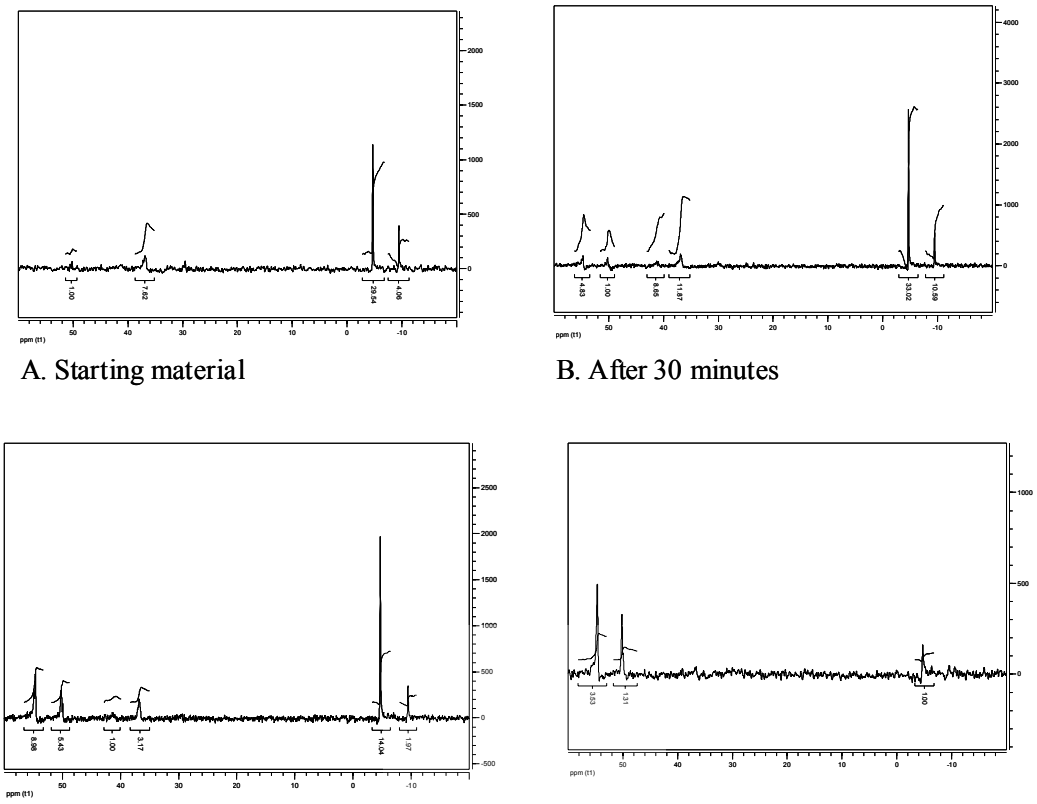

Figure 7.4. ^{31}P NMR spectra generated from the solventless reaction of $Mn(CO)_4(P(p\text{-}MeO\text{-}C_6H_4)_3)Br$ with PPh_3 (1:2)

From the above experiments an overall mechanism for the reactions discussed can be proposed. This is shown in **Scheme 7.2**. The reaction occurs in the melt and the various products produced in the overall reaction are displayed.

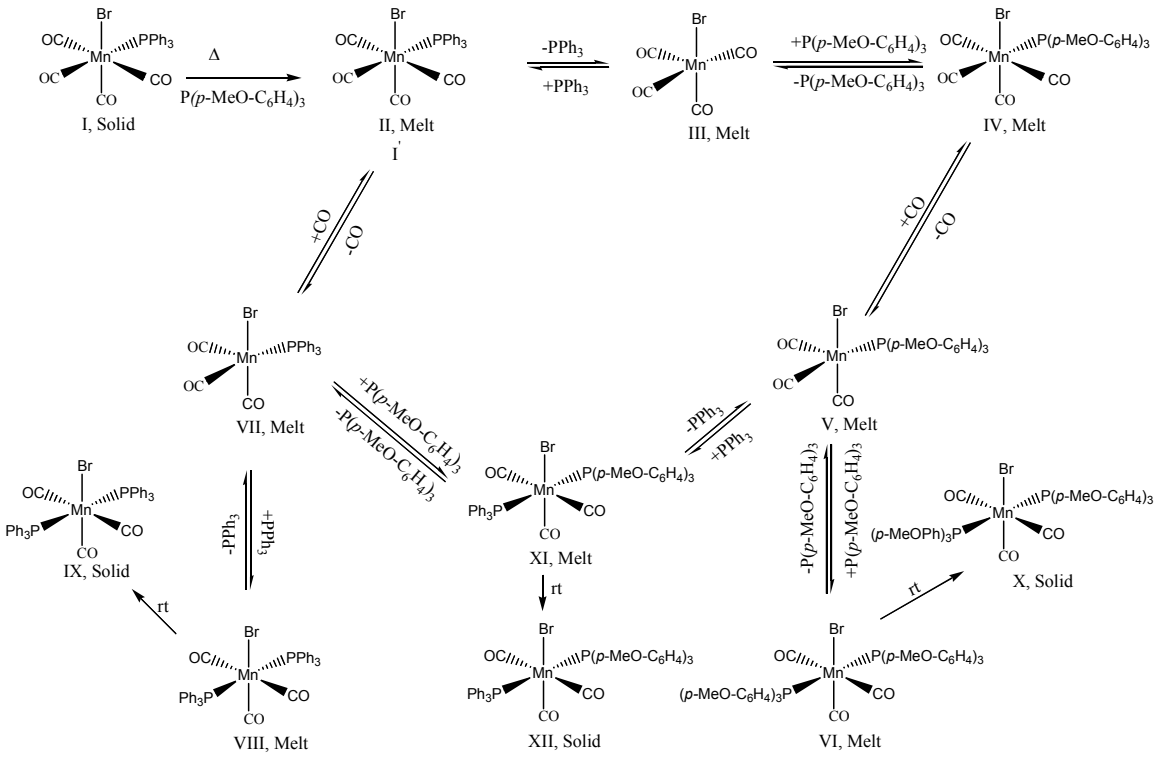

Scheme 7.2. Mechanism of the solventless reaction between $Mn(CO)_4(PPh_3)Br$ and P(*p*-MeO-$C_6H_4)_3$ as neat reagents as followed by ^{31}P NMR spectroscopy

The reaction was initiated by the mixing of solid $Mn(CO)_4(PPh_3)Br$ (**I**) with solid P(*p*-MeO-$C_6H_4)_3$ at 60°C that resulted in the generation of a melt. This was followed by the dissociation of PPh_3 leading to the formation of a five coordinate intermediate $Mn(CO)_4Br$ (**III**) that would have reacted with the available ligand, P(*p*-MeO-$C_6H_4)_3$, in the melt, to form $Mn(CO)_4$(P(*p*-MeO-$C_6H_4)_3$)Br (**IV**). This reaction appears to be more rapid than the dissociation of CO from $Mn(CO)_4(PPh_3)Br$ (**II**) to form the intermediate $Mn(CO)_3(PPh_3)Br$ (**VII**) (**Tables 7.2** and **7.3**).. $Mn(CO)_3(PPh_3)Br$ (**VII**) was either trapped by the ligand, P(*p*-MeO-$C_6H_4)_3$, resulting in the formation of the mixed ligand complex, $Mn(CO)_3$(P(*p*-MeO-$C_6H_4)_3$)(PPh_3)Br (**XI**), or it could react with the less abundant PPh_3 ligand to form $Mn(CO)_3(PPh_3)_2Br$ (**VIII**). $Mn(CO)_4$(P(*p*-MeO-$C_6H_4)_3$)Br (**IV**) could also lose CO to yield $Mn(CO)_3$(P(*p*-MeO-$C_6H_4)_3$)Br (**V**) as an intermediate. **V** had two reaction pathways; (i) it could react with the more abundant P(*p*-MeOPh)$_3$ to yield $Mn(CO)_3$(P(*p*-MeO-$C_6H_4)_3)_2Br$ (**X**) or it could react with PPh_3 to produce

$Mn(CO)_3(P(p\text{-}MeO\text{-}C_6H_4)_3)(PPh_3)Br$ (**XI**). All the above reactions are proposed to take place in the melt. As the same products are also found when $Mn(CO)_4(P(p\text{-}MeO\text{-}C_6H_4)_3)Br$ reacted with PPh_3 a similar mechanism is expected for the reverse reaction.

There has not been a detailed solution study in which a phosphine ligand displaces another phosphine ligand rather than CO from $Mn(CO)_4LX$ (L= phosphine, X = a halogen). This reaction is observable following the solventless methodology.

7.4. CONCLUSIONS

There are several conclusions that can be made from the study. The formation of the 5-coordinate intermediate from $Mn(CO)_4(PPh_3)Br$ via the detachment of the phosphine ligand was formed at a faster rate than the dissociation of the carbonyl ligand under the experimental conditions (**Table 7.2**). This was highlighted by the formation of $Mn(CO)_4(P(p\text{-}MeO\text{-}C_6H_4)_3)Br$ in the early stages of the reaction. The rate of formation of $Mn(CO)_3(P(p\text{-}MeO\text{-}C_6H_4)_3)_2Br$ was also faster than the rate of formation of $Mn(CO)_3(PPh_3)_2Br$. Both tricarbonyl complexes are thermodynamically favoured. The reaction rates of $Mn(CO)_4(MeO\text{-}C_6H_4)_3)Br/PPh_3$ and $Mn(CO)_4(PPh_3)Br/P(p\text{-}MeO\text{-}C_6H_4)_3$ and suggest that $P(p\text{-}MeO\text{-}C_6H_4)_3$ is a better Lewis base than PPh_3, as already discussed (**Table 7.2**).

What is apparent from the study was the definite trend in the final composition of the tricarbonyl complexes at the end of the experiment. The composition was determined by the amount of free ligand in the reaction mixture (**Tables 7.2 – 7.4**). It can be seen from the data that reaction of $Mn(CO)_4(P(p\text{-}MeO\text{-}C_6H_4)_3)Br$ with PPh_3 (1:2) resulted in formation of $Mn(CO)_3(P(p\text{-}MeO\text{-}C_6H_4)_3)_2Br$: $Mn(CO)_3(PPh_3)_2Br$ of ~1:2 (check the percentage composition in **Table 7.1**). When $Mn(CO)_4(PPh_3)Br$ reacted with $(P(p\text{-}MeO\text{-}C_6H_4)_3)$ (1:1.4) the final tricarbonyl complex ratio taken from their percentage composition, $Mn(CO)_3(P(p\text{-}MeO\text{-}C_6H_4)_3P)_2Br$: $Mn(CO)_3(PPh_3)_2Br$ was 1:1.3 (**Table 7.4**). The same reaction when conducted at 1:2.8mol equivalent, the $Mn(CO)_3(P(p\text{-}MeO\text{-}$

$C_6H_4)_3P)_2Br$: $Mn(CO)_3(PPh_3)_2Br$ ratio at the end was 1:2.4 showing the same trend (**Table 7.3**). The amount of the free ligand at the beginning of the reaction determines the tricarbonyl complex ratio after prolonged reaction time. The two tricarbonyl metal complexes have different rates of formation and their respective interconversion must be reversible as shown in **Scheme 7.2**. The mixed ligand, $Mn(CO)_3(P(p\text{-}MeO\text{-}C_6H_4)_3)(PPh_3)Br$, was produced in conjunction with the other two tricarbonyl complexes. The displacement of the phosphine ligand at a faster rate than CO displacement appears to be specific to the solventless reaction.

7.5. REFERENCES

1. R. S. Macomber, *A Complete Introduction to Modern NMR Spectroscopy*, John Wiley and Sons, New York, 1998.
2. H. Günther, *NMR Spectroscopy:Basic Principles, Concepts, and Applications in Chemistry*, 2nd Ed, John Wiley and Sons, Chichester, 1995.
3. J. K. M. Saunders and B. K. Hunter, *Modern NMR Spectroscopy: A Guide for Chemists*, Oxford University Press, Oxford, 1987.
4. E. M. Purcell, H. C. Torrey and R. V. Pound, *Phys. Rev*., 1946, **69**, 37.
5. F. Bloch, W. W. Hansen and M. E. Packard, *Phys. Rev*., 1946, **69**, 127.
6. W. G. Proctor and F. C. Yu, *Phys. Rev*., 1950, **77**, 717.
7. W. C. Dickinson, *Phys. Rev*., 1950, **77**, 736.
8. R. J. Abraham, J. Fisher and P. Loftus, *Introduction to NMR Spectroscopy*, John Wiley and Sons, New York, 1988.
9. M. Oki, *Applications of Dynamic NMR Spectroscopy to Organic Chemistry*, VCH, New York, 1985.
10. R. K. Harris, *Nuclear Magnetic Resonance Spectroscopy*, *A Physicochemical View*, John Wiley and Sons, New York, 1986.
11. M. M. Crutchfield, C. H. Dungan, J. H. Letcher, V. Mark and J. R. Van Wazer, *Topics in Phosphorous Chemistry*, Vol. 5, Wiley-Interscience, New York, 1967.
12. L. Ernst and D. N. Lincoln, *Magn. Reson.,* 1974, **16**, 190.
13. D. G. Gorenstein, *Phosphorous-31 NMR principles and Application*, Academic Press, New York, 1984.
14. D. G. Gorenstein, R. Rowell and J. Findlay, *J. Am. Chem. Soc.,* 1980, **102**, 5077.
15. A. F. Masters, R. T. C. Brownlee, M. J. O'Connor, A. G. Wedd and J. D. Cotton, *J. Organomet. Chem*., 1980, **195**, C17.
16. S. Dysart, I. Georgii and B. E. Mann, *J. Organomet. Chem.,* 1981, **213**, C10.
17. G. M. Gray and R. J. Gray, *Organometallics*, 1983, **2**, 1026.
18. T. D. Tilley, R. H. Grubbs and J. E. Bercaw, *Organometallics*, 1984, **3**, 274.
19. C. W. Jung, J. D. Fellmann and P. E. Garrou, *Organometallics*, 1983, **2**, 1042.

20. H. Werner and J. Gotzig, *Organometallics*, 1983, **2**, 547.

CHAPTER 8: THE USE OF DRIFTS TO STUDY THE SOLVENTLESS TRANSFORMATION OF MANGANESE COMPLEXES

8.1. INTRODUCTION

8.1.1. Historical perspective

In the literature, diffuse reflectance is also known as Kubelka-Munk reflection in honour of the two scientists that developed the theory of radiation transport in scattering media[1]. The technique was made possible by the advent of FTIR spectroscopy[2]. Diffuse reflectance is mostly used for studying powders and solids that have a rough surface[3]. Reflectance sampling techniques differs from the transmission technique in that the infrared beam is bounced off the sample rather than being passed through it[4]. Two fractions of radiation can be distiquished: one fraction is reflected from uneven areas of the rough surface. The other fraction penetrates the sample and is partially absorbed to be eventually scattered in the interior and return to the surface. The optical properties of a sample are then defined by its absorption and scattering coefficients in the Kubelka-Munk equation shown below

$$f(R_\infty = (1 - R_\infty)^2 / 2R_\infty = K / S$$

R_∞ is the degree of reflection on the sample surface at infinite thickness,
K is the absorption modulus and S the scattering modulus.

DRIFTS spectra are dependent on various sample preparation parameters as well as on geometric optical effects of the spectral measurement such that spectra of the same sample differ depending on the accessories used[5]. Parameters that are important in spectral acquisition include sample preparation method[6], particle size[7,8], packing

density[9,10] and reaction mixture homogeneity[11]. It is critical that the above parameters are kept constant in investigations to obtain experimental reproducible results.

The use of DRIFTS negates the need to press pellets such that sample preparation is faster[12]. Also DRIFTS can be used on a wide variety of samples other than KBr pellets. The application of DRIFTS is widespread in the chemical industry. It has been used for the analysis of catalysts[13], mechanistic studies[14], and characterisation of samples[15,16]. The technique has also found use in forensic science[17,18]. Quantitative analysis using DRIFTS has also been used for some time[19,20].

8.1.2. DRIFTS in organometallic chemistry studies

Diffuse Reflectance Infrared spectroscopy (DRIFTS) is an analytical tool that has been used in this thesis to investigate solventless reactions[21]. Like FTIRS, it was used to detect reagents and products at very low concentrations[22]. The advantages that it has over FTIRS are that (i) it requires less sample per given reaction[23], (ii) the same sample can be used for a full experiment and many data points are generated per reaction so that it offers more accurate results and less experimental errors, (iii) there is no need to construct calibration curves, (iv) it takes less time to conduct an experiment and (v) the ability to work at a wide range of temperatures.

There are only a few other organometallic chemistry publications that have reported the use of the technique in the literature[24]. Examples include the study of the formation of chromogenic calyx[4]arene derivatives[25], a DRIFTS and NIR Raman investigations of supported and unsupported allyl-lanthanide complexes[26] and the reaction of molybdenum hexacarbonyl and benzene under thermal activation[27].

8.1.3. Aim of the study

The aim of the study was to follow the solventless reaction between manganese carbonyl complexes and phosphines using DRIFTS and to establish the kinetic parameters for the reaction. **Figure 8.1** outlines the reaction investigated.

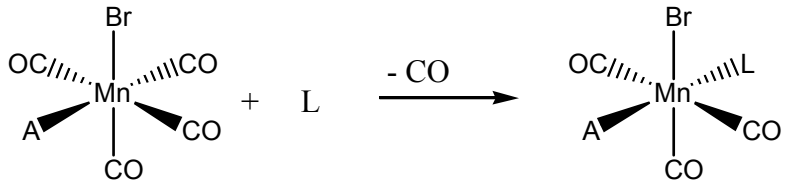

A = CO or phosphine ligand

Figure 8.1. The solventless substitution of CO by solid phosphine

To evaluate the technique, (i) the sample preparation method and (ii) the type of solid matrix used to disperse the reagents were also investigated.

8.2. EXPERIMENTAL PROCEDURES

8.2.1. DRIFTS kinetic measurements: The solventless reaction between $Mn(CO)_4(PPh_3)Br$ and PPh_3

8.2.1.1. DRIFTS Spectra: $Mn(CO)_4(PPh_3)Br$ / KBr Standards

$Mn(CO)_4(PPh_3)Br$ (160 mg, 0.31 mmol) was mixed with KBr (804 mg) powder to yield a solid mixture composed of 16% (w/w) of $Mn(CO)_4(PPh_3)Br$/KBr. The resulting mixture was thoroughly ground to give a fine homogenous powder (50-70 μm particle size) and stored in a vial (sample 1). $Mn(CO)_4(PPh_3)Br$/KBr (500 mg of 16% (w/w) was then

mixed with an equal amount of finely ground KBr (50-70 μm particle size) and labelled accordingly (sample 2). The resulting sample (500 mg) was in turn mixed with an equal mass of finely ground KBr (500 mg) to prepare sample 3. The mixing process was repeated until the υ_{CO} of $Mn(CO)_4(PPh_3)Br$ in Kubelka-Munk units could no longer be detected using DRIFTS. The background material used before loading each sample in the DRIFTS reaction cell was a finely ground KBr powder (50-70 μm particle size). The reflectance of each sample at 50°C, 60°C and 70°C was measured using DRIFTS.

8.2.1.2. Reaction of $Mn(CO)_4(PPh_3)Br$ with variable amounts of PPh_3

$Mn(CO)_4(PPh_3)Br$ (10 mg, 0.02 mmol) was mixed with KBr (990 mg) powder to give 1% (w/w) of $Mn(CO)_4(PPh_3)Br$/KBr. The solid mixture was thoroughly ground to generate a fine homogenous powder (50-70 μm particle size). A sample of PPh_3 (5 mg, 0.02 mmol) was also crushed and mixed with KBr (fine powder, 995 mg) so that a 0.5% (w/w) PPh_3/KBr sample was made. The ligand/KBr mixture was also ground thoroughly to obtain an evenly distributed fine solid mixture (40-60 μm particle size). The 0.5% (w/w) PPh_3/KBr mixture was mixed with an equal mass of finely ground KBr ((50-70μm particle size) to yield a 0.25% (w/w) PPh_3/KBr mixture. This mixture was used as background material for the DRIFTS measurements. Equal amounts of the 1% (w/w) $Mn(CO)_4(PPh_3)Br$/KBr and 0.5% (w/w) PPh_3/KBr were thoroughly mixed in a sample vial using a spatula, to yield a 1:1 (mol/mol) of $Mn(CO)_4(PPh_3)Br/PPh_3$ mixture contained in a 0.25% (w/w) PPh_3/KBr mixture.

A background DRITFS spectrum was then recorded. The powder was then removed and replaced with 1:1 (mol/mol) of $Mn(CO)_4(PPh_3)Br/PPh_3$ in 0.25% (w/w) PPh_3/KBr. The reflectance spectrum of the sample was then measured at room temperature and periodically at 50°C, 60°C, and 70°C (in separate experiments). The reflectance spectra were recorded at pre-set time intervals using a standard computer program.

Other samples with different metal complex to ligand ratios were prepared in the same way. **Table 8.1** shows the different Mn/PPh_3 ratios used. The background material for each experiment was prepared by mixing equal amounts of the PPh_3/KBr mixture with an equal mass of finely ground KBr.

Table 8.1. Solventless reactions performed with $Mn(CO)_4(PPh_3)Br$ and varying amounts of PPh_3

Mn/mg (mmol)	KBr/mg	Mn:KBr (mg/mg)	PPh_3/mg (mmol)	KBr/mg	PPh_3/KBr (mg/mg)	Mn/PPh_3 (mmol/mmol)
10 (0.02)	990	1%	5 (0.02)	995	0.5%	1:1
10 (0.02)	990	1%	10 (0.04)	990	1%	1:2
10 (0.02)	990	1%	25 (0.1)	975	2.5%	1:5
10 (0.02)	990	1%	50 (0.2)	950	5%	1:10
10 (0.02)	990	1%	100 (0.4)	900	10%	1:20

DRIFTS data were recorded on all the mixtures. All the experiments were done in duplicate and the average of the two experiments was used for subsequent data treatment.

8.2.1.3. Reaction of PPh_3 with varying amounts of $Mn(CO)_4(PPh_3)Br$

PPh_3 (8 mg, 0.031 mmol) was crushed and mixed with KBr (fine powder, 995 mg) to produce a 0.8% (w/w) PPh_3/KBr sample. The mixture was then ground using a mortar and pestle to give an evenly distributed fine solid mixture with particle sizes between 40-60 μm. $Mn(CO)_4(PPh_3)Br$ (16 mg, 0.031 mmol) was mixed with KBr (984 mg) powder to yield a solid mixture composed of 1.6% (w/w) $Mn(CO)_4(PPh_3)Br$/KBr. The resulting mixture was thoroughly ground to give a fine homogenous powder (50-70 μm particle size). $Mn(CO)_4(PPh_3)Br$/KBr (500 mg. 1.6% w/w) was then mixed with equal amounts of finely ground KBr (50-70 μm particle size) and labelled accordingly (sample 2). 500 mg of the resulting sample was in turn mixed with fine KBr (500 mg) to prepare sample 3.

The process was repeated to generate ten samples. Each sample was thoroughly mixed with an equal mass of the 0.8% (w/w) PPh_3/KBr using a spatula in a sample vial. The DRIFTS spectrum was measured on each sample immediately after an appropriate background material (made by mixing equal masses of PPh_3/KBr with fine KBr powder) was measured. The rate constant of each reaction was then determined at three different temperatures (50°C, 60°C and 70°C), assuming first order kinetics.

8.2.2. Effects of sample preparation method on the solventless reaction of $Mn(CO)_4(PPh_3)Br$ with PPh_3 in KBr

8.2.2.1. Fine Power method

$Mn(CO)_4(PPh_3)Br$ (1% w/w) added to KBr powder (1 g sample). The solid mixture was thoroughly ground to give a fine homogenous powder (50-70 μm particle size. PPh_3 was also crushed and mixed with a fine powder of KBr to give a (20% w/w) PPh_3/KBr mixture (2 g). The ligand/KBr mixture was also ground thoroughly to obtain an evenly distributed fine solid mixture (40-60 μm particle size). The 20% (w/w) PPh_3/KBr mixture was mixed with an equal mass of finely ground KBr to yield a 10% (w/w) PPh_3/KBr mixture, which was used as background material for DRIFTS measurements. Equal amounts of the 1% (w/w) $Mn(CO)_4(PPh_3)Br$/KBr and 20% PPh_3/KBr were thoroughly mixed using a spatula to yield a 1:10 (w/w) of $Mn(CO)_4(PPh_3)Br/PPh_3$ mixture contained in a 10%(w/w) PPh_3/KBr mixture. The 10% (w/w) PPh_3/KBr mixture was then loaded in the reaction cell, and a background DRIFTS spectrum recorded. The powder was then replaced with the 1:10 (w/w) of $Mn(CO)_4(PPh_3)Br/PPh_3$ mixture in 10%(w/w) PPh_3/KBr. The reflectance spectrum of each sample was then measured at room temperature at 50°C, 60°C, 65°C and 70°C. Treatment of the obtained data yielded rate constants (*k*s), assuming first order kinetics.

8.2.2.2. Solvent method

$Mn(CO)_4(PPh_3)Br$ (1% w/w) in KBr powder was prepared (500 mg sample), ground into a fine powder (50-60 μm particle size) using a mortar and pestle and saved. Similarly, PPh_3 (20% w/w) in KBr was prepared (500 mg) and also ground to a fine powder (40-60 μm particle size). An equal mass of the two samples (400 g each) were placed in a 10 cm^3 reaction tube and dichloromethane (3 cm^3) introduced so that both the metal complex and the ligand completely dissolved. The solvent was removed by blowing nitrogen gas through the solution at room temperature. The removal of the solvent left a yellow residue made up of well dispersed $Mn(CO)_4(PPh_3)Br$ and PPh_3 in fine KBr. A 10% (w/w) PPh_3/KBr mixture was prepared as above and stored in the dessicator. Once the background spectrum was obtained using 10% (w/w) PPh_3/KBr, the reflectance spectra of the samples measured as a function of time at 50°C, 60°C, 65°C and 70°C. Treatment of the obtained data yielded rate constants (*k*s), assuming first order kinetics.

8.2.3. Effect of KBr particle size on the solventless reaction between $Mn(CO)_4(PPh_3)Br$ with PPh_3 at 60°C

$Mn(CO)_4(PPh_3)Br$ (1% w/w) in KBr was made by mixing the two solids in a sample vial so as to obtain a uniform solid mixture (1 g sample). A small portion of the sample (300 mg) was then ground in a mortar and pestle to obtain coarse grain sized particles (110-190 μm). Another portion (300 mg) was also ground to obtain an intermediate particle size (100-130 μm). The remaining sample was also ground to obtain a fine powder (50-70 μm) using a mortar and pestle, and placed in a labelled sample vial. PPh_3 was crushed and mixed with KBr so that a (20% w/w) PPh_3/KBr was formed (2 g). A small portion of the PPh_3/KBr mixture (500 mg) was ground to obtain a coarse particle size (130-180 μm) and stored. PPh_3/KBr mixture (500 mg) of intermediate grain size (110-130 μm) was made by grinding in a mortar and pestle. The remaining PPh_3/KBr mixture (500 mg) was also ground to obtain a fine powder (30-50 μm). The fine grain solid of the metal

complex in KBr was mixed with an equal mass of the fine grain ligand in the KBr mixture so that a 1:10 (w/w) $Mn(CO)_4(PPh_3)Br/PPh_3$ in fine KBr support was produced. Similarly, the intermediate and coarse grain mixtures of the metal complex and the ligand were mixed. The reflectance spectrum of each sample was measured using DRIFTS using 10% PPh_3 in KBr as background, at room temperature and periodically at 60°C using a computerised program at pre-set time intervals. Treatment of the obtained data yielded rate constants (*k*s), assuming first order kinetics.

8.2.4. The effect of supports on the solventless reaction between $Mn(CO)_4(PPh_3)Br$ with PPh_3 at 60°C

The solid support to be used (KBr, Al_2O_3, Na_2SO_4, $NaNO_2$, SiO_2, Na_2CO_3, $NaC_2H_3O_2$, $NaNO_3$, sucrose and TiO_2) was ground to a fine powder using a mortar and pestle and mixed with the metal complex to give $Mn(CO)_4(PPh_3)Br$/support (1% w/w) mixture. The solid mixture was thoroughly ground to generate a uniform mixture (1 g). PPh_3 was also crushed and mixed with a fine powder of support so that a (20% w/w) PPh_3/support was formed. The mixture was ground thoroughly to obtain an evenly distributed mixture (2 g of the sample was produced). The 20% (w/w) PPh_3/support mixture was mixed with an equal mass of finely ground support powder to yield a 10% (w/w) PPh_3/support mixture, which was used as background material for DRIFTS experimentation. Equal amounts of the 1% (w/w) $Mn(CO)_4(PPh_3)Br$/support and 20% PPh_3/support were thoroughly mixed using a spatula in a sample vial, to yield a 1:10 (w/w) of $Mn(CO)_4(PPh_3)Br/PPh_3$ mixture contained in a 10% (w/w) PPh_3/Support mixture. The 10% (w/w) PPh_3/support mixture was then loaded into the reaction cell, in the DRIFTS spectrometer, and a background spectrum run (taking 32 scans). The powder was then removed and replaced with the 1:10 (w/w) of $Mn(CO)_4(PPh_3)Br/PPh_3$ mixture in 10% (w/w) PPh_3/support. The reflectance of the solid mixture was then measured at room temperature to serve as a reference point. The sample was then heated to a preset temperature (60°C) and the preset computerized program recorded the reflectance of the sample at pre-determined time

intervals. The resulting data was analysed to determine the rate constant (*k*) of the reaction, assuming first order kinetics.

8.2.5. Variation of ligand: the solventless reaction of $Mn(CO)_4(L)Br$ with L to give $Mn(CO)_3(L)_2Br$ [L = P(*p*-MeO-$C_6H_4)_3$, P(*p*Me-$C_6H_4)_3$, P(*p*-F-$C_6H_4)_3$, and P(*p*-Cl-$C_6H_4)_3$)]

$Mn(CO)_4(L)Br$ (1% w/w) in KBr powder was prepared by mixing the metal complex with dry KBr powder. The solid mixture was thoroughly ground using a mortar and pestle to give a fine homogenous powder (40-70μm particle size). The solid ligand, L was crushed and mixed with a fine powder of KBr so that a (20% w/w) L/KBr mixture was formed. The ligand/KBr mixture was also ground thoroughly to obtain an evenly distributed fine solid solution (40-60μm particle size). The 20% (w/w) L/KBr mixture was mixed with an equal mass of finely ground KBr to yield a 10% (w/w) L/KBr mixture, which was used as background material for DRIFTS experimentation. Equal amounts of the 1% (w/w) $Mn(CO)_4(L)Br$/KBr and 20% L/KBr were thoroughly mixed using a spatula to yield a 0.5:10 (w/w) of $Mn(CO)_4(L)Br$/L mixture contained in a 10%(w/w) L/KBr mixture. The 10% (w/w) L/KBr mixture was then loaded in the reaction cell and a background spectrum run. The powder was then replaced with the 0.5:10 (w/w) of $Mn(CO)_4(L)Br$/L mixture in 10%(w/w) L/KBr. The reflectance of each sample was then measured at room temperature and periodically at 70°C, 80°C, and 90°C (as separate experiments) using a computer program at pre-set time intervals. Treatment of the obtained data yielded rate constants (*k*s), assuming first order kinetics.

8.3. RESULTS AND DISCUSSION

8.3.1. The effect of the amount of $Mn(CO)_4(PPh_3)Br$ on the reflectance spectra

The study was initiated by conducting a test run to check the deviation from linearity when the amount of $Mn(CO)_4(PPh_3)Br$ was plotted against reflectance at the three temperatures at which the experiment was to be conducted. **Figure 8.2** shows the plot of reflectance in Kubelka-Munk units versus the amount of $Mn(CO)_4(PPh_3)Br$ in KBr using DRIFTS.

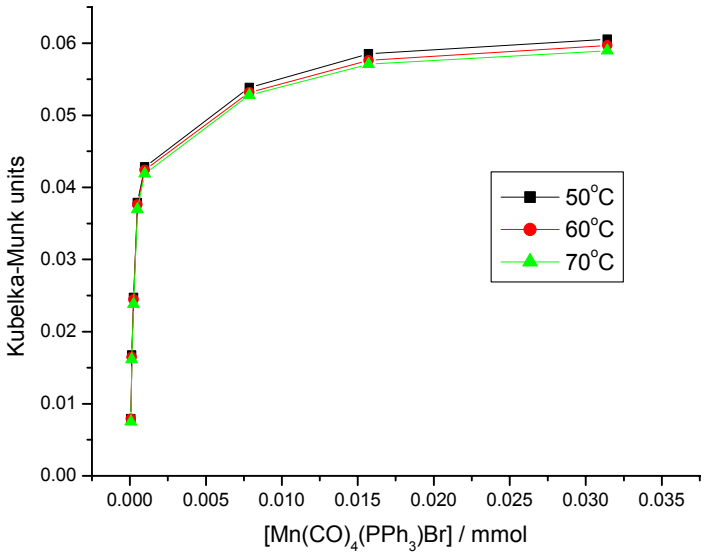

Figure 8.2. Plot of Kubelka-Munk units versus amount of $Mn(CO)_4(PPh_3)Br$ in KBr support using DRIFTS to check where deviation from linearity takes place due to the large amount of the metal complex used

The plot showed a linear dependence of reflectance on the amount of $Mn(CO)_4(PPh_3)Br$ when small amounts of the complex were used (<0.0098 mmol). Deviation occurred

when larger amounts of the complex were investigated. This study provides the limit on the amount of metal complex to be used in the DRIFTS study. The KBr acts as a solid diluent in a similar manner to the way in which a solvent is used. For meaningful experimentation, it was observed that the thermal experiments should be carried out using a maximum of 0.0098 mmol of $Mn(CO)_4(PPh_3)Br$ /100 mg KBr solid solution, corresponding to 0.50 mg of $Mn(CO)_4(PPh_3)Br$ in 100 mg of KBr solution. The useful data (adherence to linearity) could thus be obtained using 0.5% (w/w) or less of $Mn(CO)_4(PPh_3)Br$ in KBr.

8.3.2. The effect of the amount of ligand on the solventless reaction of $Mn(CO)_4(PPh_3)Br$ with PPh_3 in KBr matrix at 60°C

The next step was to check the conversion of $Mn(CO)_4(PPh_3)Br$ to $Mn(CO)_3(PPh_3)_2Br$ in the presence of PPh_3 in KBr matrix at 60^oC (**Figure 8.3**). The plot vividly showed the disappearance of the starting material peaks whilst the product peaks started to appear and grew with time. From the plot, the rate constant k was determined by following the disappearance of the starting material peak at 2094 cm^{-1} with time.

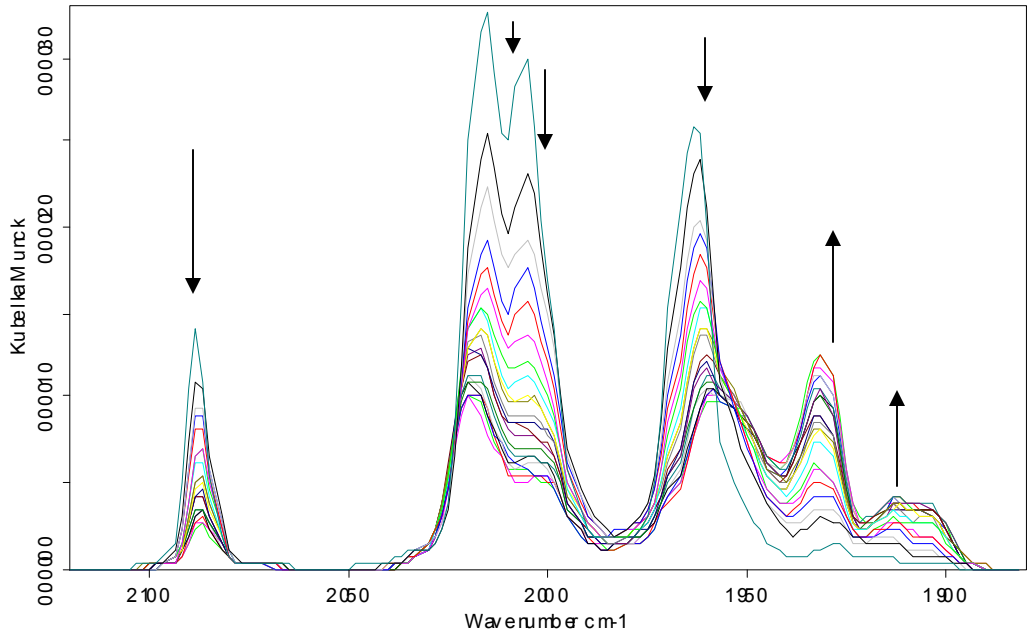

Figure 8.3. A plot of Kubelka-Munk units versus wavenumber for the solventless reaction between $Mn(CO)_4(PPh_3)Br$ and PPh_3 in KBr supported using DRIFTS

By varying the amount of the PPh_3 ligand while keeping the metal complex amount constant, the results shown in **Table 8.2** were obtained.

Table 8.2. Data showing the rate constants for the reaction of $Mn(CO)_4(PPh_3)Br$ with PPh_3 when varying the amount of the ligand (PPh_3) at 60°C

Mn/PPh_3 (mmol/mmol)	T/°C	k/s^{-1}
1:1	60	1.32E-4 ± 2.4E-5
1:2	60	1.38E-4 ± 1.8E-5
1:5	60	1.85E-4 ± 1.5E-5
1:10	60	2.14E-4 ± 2.0E-5
1:20	60	2.02E-4 ± 1.6E-5

The data showed a dependence of the rate of reaction on the ligand at a low $Mn(CO)_4(PPh_3)Br:PPh_3$ ratio. If the metal complex:ligand ratio is low (1:1) the chance of the two solids being in close proximity with the correct orientation to result in successful reaction is small, and thus the rate of reaction should be small. The cartoon in **Figure 8.4** depicts a possible microscopic representation of the reaction of the metal complex:ligand ratio of 1:1 in KBr medium.

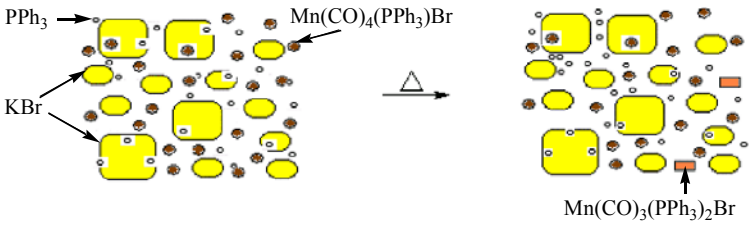

Figure 8.4. Cartoon depicting the solventless reaction of $Mn(CO)_4(PPh_3)Br:PPh_3$ (1:1 mole ratio) in a KBr matrix

At higher metal complex:ligand ratios ($\geq$ 1:5) there was little, if any, dependence of the rate of reaction on the ligand as shown by the rate constant values. The order of the reaction with respect to the concentration of PPh_3 is therefore zero beyond a 1:5 metal complex to ligand ratio. If the $Mn(CO)_4(PPh_3)Br:PPh_3$ mole ratio is 1:5 and beyond, it would mean that the ratio has reached a point whereby virtually every metal complex particle is in close contact with a ligand particle so that a chemical transformation could take place.

The results as interpreted pose a question as to the reaction mechanism. How can well-behaved kinetics be obtained from the interaction of two solids even for metal complex to ligand ratios of 1:1? This question will be discussed below.

8.3.3. The effect of metal complex amount on the solventless reaction of $Mn(CO)_4(PPh_3)Br$ with PPh_3 in KBr matrix using DRIFTS

By varying the amount of the metal complex while keeping the amount of the ligand constant, the data shown in **Table 8.3** were obtained for the transformation of $Mn(CO)_4(PPh_3)Br$ with PPh_3 at 50°C, 60°C and 70°C.

Table 8.3. Data showing the rate constants for the reaction of $Mn(CO)_4(PPh_3)Br$ with PPh_3 when varying the amount of the metal complex while keeping the amount of the ligand (PPh_3) constant at different temperatures

Mn/PPh_3 (μmol/μmol)	Mn/μmol	k @ 50°C $/s^{-1}$	k @ 60°C $/s^{-1}$	k @ 70°C $/s^{-1}$
1:1	314	7.49E-6	1.33E-4	4.57E-4
0.5:1	157	7.17E-6	1.17E-4	2.87E-4
0.5:1	78.6	5.96E-6	1.10E-4	9.13E-4
0.125:1	39.3	7.08E-6	9.14E-5	3.33E-4
0.0625:1	19.6	7.55E-6	8.67E-5	2.34E-4
0.0313:1	9.8	6.16E-6	7.18E-5	1.46E-4
0.0156:1	4.9	3.69E-6	4.50E-5	7.66E-5
0.0078:1	2.5	2.32E-6	2.31E-5	4.06E-5
0.0038:1	1.2	7.71E-7	1.43E-5	9.24E-6
0.0019:1	0.6	4.56E-7	5.83E-6	7.47E-6

The data tabulated above once again showed a dependence of the rate of reaction on the amount of the metal complex. As the amount of the metal complex was increased from 6.0×10^{-7}mol to 3.14×10^{-2}mol, the rate of the reaction increased at all temperatures.

The rate equation for the reaction is assumed to have the form

$$\text{rate} = k[Mn(CO)_4(PPh_3)Br]^{\mathbf{a}}[PPh_3]^{\mathbf{b}}$$

In **Section 8.32**, it was shown that by the use of excess L, then b= 0 in the above equation, i.e., the rate depended solely on the amount of metal complex raised to the power **a**. The natural logarithm of the rate of reaction then gives

$$\ln(\text{rate}) = \ln(k) + \mathbf{a}\ln([Mn(CO)_4(PPh_3)Br])$$

Thus a plot of ln(rate) versus ln[$Mn(CO)_4(PPh_3)Br$] should give a straight line with a slope that equals the order of the reaction (**a**) with respect to the metal complex. However **Figure 8.5** revealed that a plot of ln(k) versus ln([$Mn(CO)_4(PPh_3)Br$]) only gave a straight line at low Mn amounts. The deviation from linearity occurred when the amount of Mn ≥ 9.8 µmol in 100 mg KBr matrix was used. The 9.8 µmol of $Mn(CO)_4(PPh_3)Br$ in 100 mg KBr solid solution, corresponds to 0.50 mg of $Mn(CO)_4(PPh_3)Br$ in 100 mg of KBr, i.e., 0.5% (w/w) of $Mn(CO)_4(PPh_3)Br$ in KBr! This correlates with the limits determined in **Figure 8.2** and indicates that only when the amount of Mn ≤ 9.8 µmol in 100 mg KBr matrix can a kinetic analysis be performed.

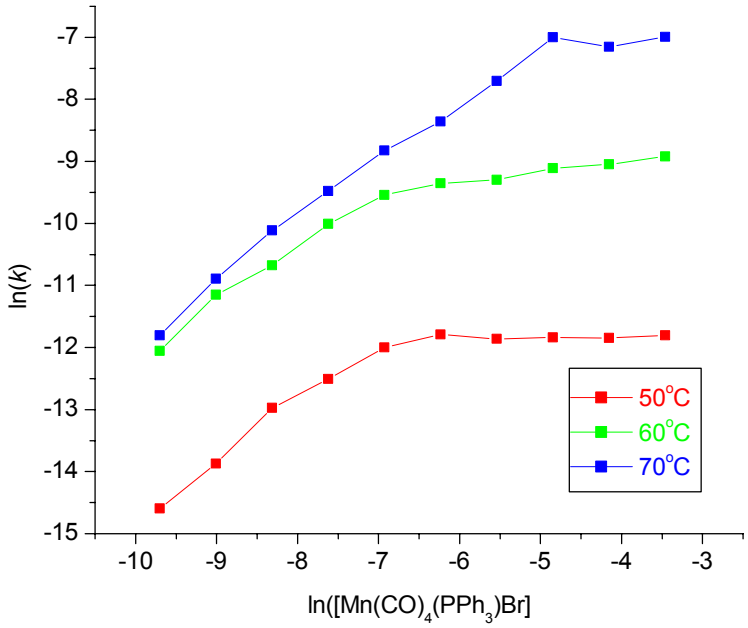

Figure 8.5. Plot of ln(k) versus ln([$Mn(CO)_4(PPh_3)Br$]) for the reaction of $Mn(CO)_4(PPh_3)Br$ with PPh_3 while varying the amount of the metal complex and keeping the amount of PPh_3 constant

Figure 8.6 shows the plot of ln(k) versus ln([$Mn(CO)_4(PPh_3)Br$]) for the reaction of $Mn(CO)_4(PPh_3)Br$ with PPh_3 when the amount in KBr is less than 9.8μmol/100mg of KBr.

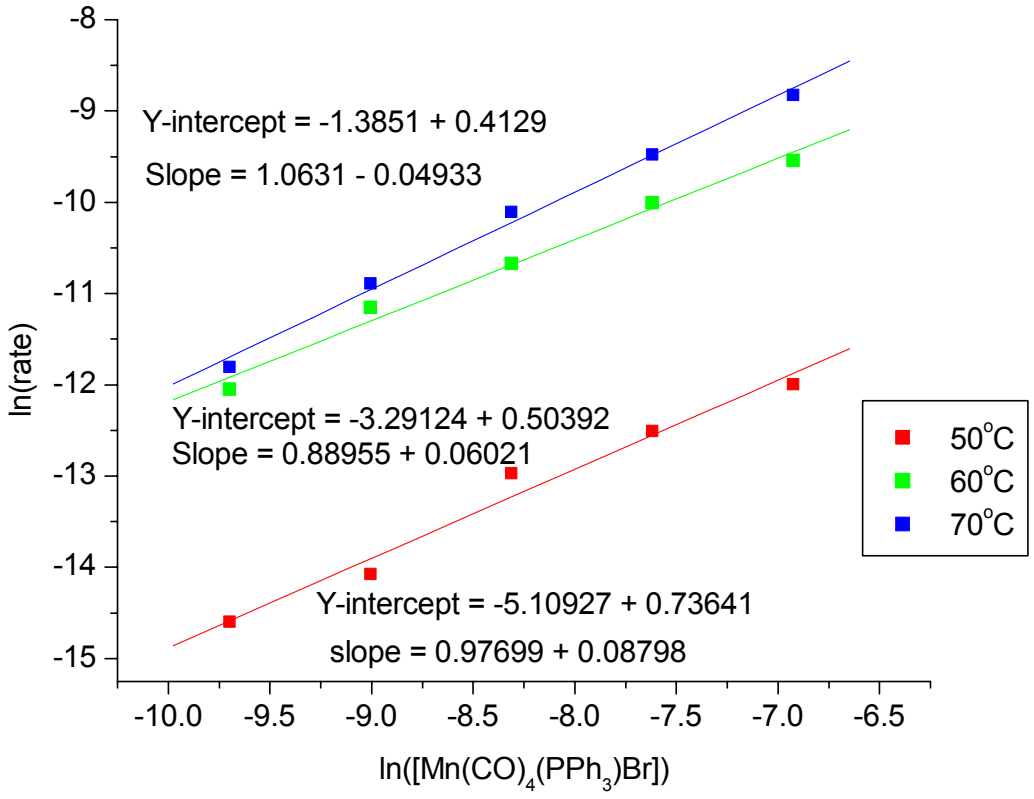

Figure 8.6. Plot of ln(k) versus ln([$Mn(CO)_4(PPh_3)Br$]) for the reaction of $Mn(CO)_4(PPh_3)Br$ with PPh_3 when varying the amounts of the metal complex and keeping the amount of PPh_3 constant

The slope obtained for the three plots of ln(k) versus ln([$Mn(CO)_4(PPh_3)Br$]) at each temperature was 1.00 ± 0.11. The results thus support earlier studies described (**Chapters 5** and **6**) that the reaction indeed followed pseudo first order kinetics and was solely dependent on the amount of the metal complex. The Y-intercept at each temperature yielded ln(k) such that the rate constant, k, at the specific temperature could be determined. The values are given in **Table 8.4**. The activation parameters of the reaction are also given in **Table 8.4**. Plotting ln(k) versus (1/T) (an Arrhenius plot), and ln(k/T)

versus (1/*T*) (an Eyring plot), the enthalpy change of activation ($\Delta H^{\ddagger}$), and the entropy change of activation ($\Delta S^{\ddagger}$) were determined.

Table 8.4. Kinetic parameters of the solventless reaction of $Mn(CO)_4(PPh_3)Br$ with PPh_3 obtained using DRIFTS

T/ C	T/K	1/T / K^{-1}	k	ln(k)	ln(k/T)	$\Delta H^{\ddagger}$/kJmol^{-1}	$\Delta S^{\ddagger}$/ Jmol^{-1}K^{-1}
50	323	0.00309	0.006	-5.11	-10.89	169 ± 28	204 ± 57
60	333	0.00300	0.037	-3.29	-9.10		
70	343	0.00291	0.250	-1.38	-7.22		

The enthalpy ($\Delta H^{\ddagger}$) and entropy ($\Delta S^{\ddagger}$) of activation of the reaction of $Mn(CO)_4(PPh_3)Br$ with PPh_3 in KBr matrix using DRIFTS were found to be 169 ± 16 kJmol^{-1} and 204 ± 23 Jmol^{-1}K^{-1} respectively.

8.3.4. The effects of sample preparation method on the solventless reaction of $Mn(CO)_4(PPh_3)Br$ with PPh_3 in KBr using DRIFTS

8.3.4.1. Fine Power Method

The method involved preparing the metal complex and the ligand in the KBr support separately as finely ground solid solutions. The two solid solutions were then mixed together prior to experimentation. In brief, $Mn(CO)_4(PPh_3)Br$ (1% w/w) in KBr (50-70 μm particle size) was mixed with 20% (w/w) PPh_3/KBr (40-60μm particle size) immediately before experimentation and the reaction carried out at 50°C, 60°C and 70°C. The enthalpy and entropy of activation of the reaction of $Mn(CO)_4(PPh_3)Br$ with PPh_3 in KBr matrix using the fine powder method were determined as in **Section 8.2.2.1** and found to be 164 ± 19 kJmol^{-1} and 275 ± 46 Jmol^{-1}K^{-1}.

Both the $\Delta H^{\ddagger}$ and $\Delta S^{\ddagger}$ values obtained were similar to the values obtained when the amount of the metal complex was varied while keeping the amount of the ligand constant. The $\Delta S^{\ddagger}$ did differ but the difference could be accounted for by the error bars (much larger when the fine powder method was employed). Hence the sample preparation method was shown not to be important.

8.3.4.2. Solvent Method

The method involved placing the metal complex and the ligand in finely ground KBr support (50-70μm particle size) followed by dissolution in dichloromethane. The solvent was quickly removed by blowing with inert gas to leave behind a solid solution ready for experimentation. The solid solution was made of $Mn(CO)_4(PPh_3)Br$ (1% w/w) in KBr and 20% (w/w) PPh_3/KBr (40-60μm particle size) immediately before experimentation. The procedure as outlined in **Section 8.2.2.2** was followed to obtain kinetic parameters.

The enthalpy of activation of the reaction was much higher when the solvent method was utilised (203 ± 21 $kJmol^{-1}$) signalling that more energy was required for the reaction to proceed. This was unexpected. Intuitively it would seem that the better the contact between the reagents the better the potential for reaction. However it appears that the role of the dispersant, KBr, must be important. The justification for the extra energy needed here can be explained by a microscopic representation shown in **Figure 8.7**. Using the solvent method, most of the reagents are assumed to interact more readily with the KBr support as depicted in **Figure 8.7** as opposed to the case whereby they were freely placed in between the KBr support when the fine KBr method was employed (**Figure 8.4**). Therefore, the probability of the reagent being in close proximity with the minimum energy and correct orientation to result in reaction to yield a new product was smaller when using the solvent method. The entropy of activation of the reaction was found to be 279 ± 39 $Jmol^{-1}K^{-1}$ when the solvent method was employed.

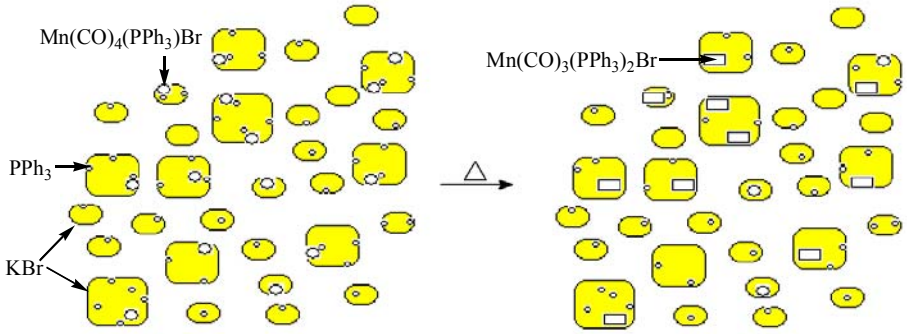

Figure 8.7. Cartoon depicting microscopic representation of the solventless reaction of $Mn(CO)_4(PPh_3)Br$ with PPh_3 (1:19 mol equiv) in KBr using the solvent method

8.3.5. Effects of particle size of the KBr support on the rate of the solventless reaction of $Mn(CO)_4(PPh_3)Br$ with PPh_3 at 60 C using DRIFTS

The aim here was to vary the particle size of the support (KBr) to determine whether the KBr particle size would affect the rate of reaction. A summary of the results obtained from the investigation is found in **Table 8.5** below.

Table 8.5. Activation energy for the solventless reaction between $Mn(CO)_4(PPh_3)Br$ and PPh_3 (1:19mol ratio) in KBr support at various temperatures using DRIFTS, (fine, intermediate and coarse grained powder mixture samples)

Mn/ mg (mmol)	PPh_3/ mg (mmol)	Mn/PPh_3/ w/w (mol/mol)	Support used	Particle size/ μm	k/s^{-1}	k/s^{-1}
2 (4)	20 (76)	1:10 (1:19)	Fine KBr	30-70	2.18E-4	2.37E-4
2 (4)	20 (76)	1:10 (1:19)	Intermediate KBr	100-130	4.47E-4	5.06E-4
2 (4)	20 (76)	1:10 (1:19)	Coarse KBr	110-190	6.57E-4	5.83E-4

As the KBr support particle size increased, the rate of reaction increased (when finely ground KBr support was used the rate of reaction was the slowest at 2.15×10^{-5} s^{-1}). The rationale for the results was that the finer support particles acted as a dispersant for the two reagents. The reacting particles were kept far apart and hence the probability of the two reacting particles being in close proximity was minimised (see **Figure 8.8**). This would result in a slower rate of reaction manifested by a smaller rate constant. This proposal is consistent with the data obtained in **Section 8.3.4.2**.

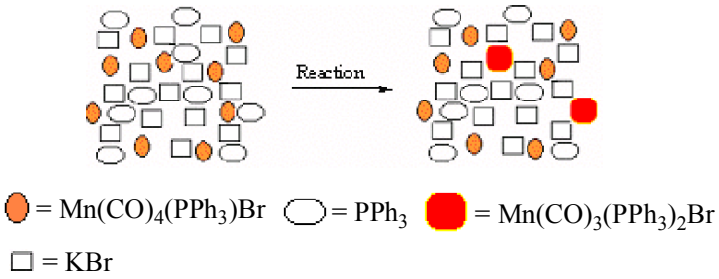

Figure 8.8. Cartoon showing the reaction of $Mn(CO)_4(PPh_3)Br$ with PPh_3 when fine KBr was used as a support

In contrast, when the support particle sizes were larger (compared to the reacting particles), they acted as spectators (rather than dispersants) such that the reacting particles were stationed between the support particles (**Figure 8.9**). Also there would have been less surface interaction between interacting particles (as shall be discussed in **Section 8.3.6**). Nonetheless there would have been particles that were in close proximity for a chemical reaction to take place if thermal energy was supplied.

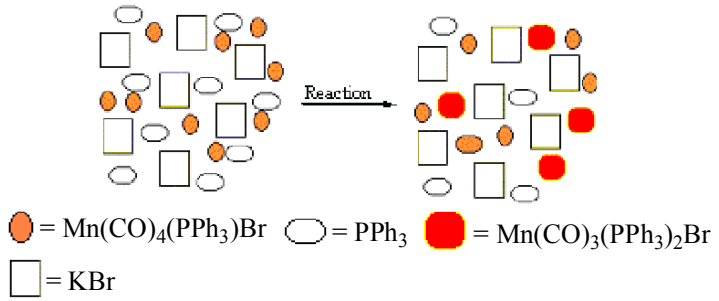

Figure 8.9. Cartoon showing the reaction of $Mn(CO)_4(PPh_3)Br$ with PPh_3 when coarse KBr was used as a support

8.3.6. The effect of support on the solventless reaction of $Mn(CO)_4(PPh_3)Br$ with PPh_3

The discussion on particle size (**Section 8.3.4**) suggested that the rate of the reaction should be influenced by the dispersant. A range of different dispersants (KBr, Al_2O_3, Na_2SO_4, $NaNO_2$, SiO_2, Na_2CO_3, $NaC_2H_3O_2$, $NaNO_3$, Sucrose and TiO_2), ground and filtered to provide the same particle size, was hence investigated in the solventless reaction. Data are shown in **Table 8.6**. For each support (dispersant) $Mn(CO)_4(PPh_3)Br$/support (1% w/w) and PPh_3/support (20% w/w) were made and the rates of reactions conducted at 60°C using DRIFTS. The determination of the rate constant followed the same methodology used in the earlier studies (an Arrhenius plot) and the results of the investigation are summarised in **Table 8.6**. Data are arranged with descending rate constants.

Table 8.6. The rate constants of the solventless reaction of $Mn(CO)_4(PPh_3)Br$ with PPh_3 (1:19mol ratio) in different support fine powders at 70°C using DRIFTS

Mn/ Mg (mmol)	PPh_3/ Mg (mmol)	Mn/PPh_3 / w/w (mol/mol)	Support used	Particle size/ μm	k/s^{-1}
2 (4)	20 (76)	1:10 (1:19)	SiO_2	40-60	2.08E-2
2 (4)	20 (76)	1:10 (1:19)	Sucrose	50-70	1.41E-2
2 (4)	20 (76)	1:10 (1:19)	Al_2O_3	30-50	8.65E-3
2 (4)	20 (76)	1:10 (1:19)	TiO_2	10-30	7.72E-3
2 (4)	20 (76)	1:10 (1:19)	$NaNO_3$	40-60	6.78E-3
2 (4)	20 (76)	1:10 (1:19)	Na_2CO_3	50-70	3.97E-3
2 (4)	20 (76)	1:10 (1:19)	$NaC_2H_3O_2$	50-70	3.40E-3
2 (4)	20 (76)	1:10 (1:19)	Na_2SO_4	50-70	3.12E-3
2 (4)	20 (76)	1:10 (1:19)	$NaNO_2$	40-60	2.24E-4
2 (4)	20 (76)	1:10 (1:19)	KBr	40-60	2.14E-4

The data obtained show a dependence of the rate of reaction on the type of support used. A range of values was observed with KBr giving the slowest rate (2.14×10^{-4} s^{-1}) and SiO_2 the fastest rate (2.08×10^{-2} s^{-1}). This is a wide range of values (100 × variation) suggesting that the dispersant plays a key role in the reaction. The choice of dispersant used does not allow for a rationalisation of the effect to be determined but in general it suggests that; (i) covalent and network solids give the highest rates and (ii) ionic solids give the slowest rates. Issues such as solubility, surface groups and particle size are also important. The important conclusion is that interactions do occur between the dispersant and the reactants.

8.3.7. The use of DRIFTS for the kinetic studies of the solventless reaction of $Mn(CO)_4(L)Br$ with ligand, L (where L. ≠ PPh_3)

The study detailed in **Chapter 7** indicated two issues that needed to be studied further, (i) when $Mn(CO)_4(L)Br$ reacted with L' the result was an exchange of L with L' and (ii) the reaction was independent of the entering ligand suggesting that the phenomenon was associated with the electronic effects related to the attached L on the Mn center. A way to look at these issues involved the study of the reaction of $Mn(CO)_4(L)Br$ with L (L = P(*p*-MeO-$C_6H_4)_3$, P(*p*Me-$C_6H_4)_3$, P(*p*-F-$C_6H_4)_3$, and P(*p*-Cl-$C_6H_4)_3$)) leading to the determination of the kinetic parameters for each reaction. The ligands were chosen such that steric effects were eliminated (all *para* substituted phosphines used had the same cone angle, θ = 145). However, their phenyl ring activation abilities varied. They are listed in decreasing order from OMe > Me > H > Cl> F. However, due to complications associated with phosphine substitution, rather than CO substitution, *viz*

$$Mn(CO)_4LBr + L' \rightarrow Mn(CO)_4L'Br + L$$

the incoming ligand and the ligand in the metal complex were left the same in the study. However, if the reaction is first order then the rate of reaction will be independent of the incoming ligand and the reaction rate will be determined by the electronic properties

associated with the attached ligand only. If the attached ligand, L, is electron donating then in principle a stronger M-CO bond should be formed and the reaction rate for M-CO bond cleavage should be decreased.

Consider **Figure 8.10.A**. An electron rich phenyl group should enrich the phosphorous group bonded to it, which in turn donates the electrons to the metal (Mn) centre. The metal centre will then in turn distribute the electrons to the carbonyl carbons, strengthening the M-CO σ bond. The result should be a smaller enthalpy of activation accompanying the reaction. Similarly, an electron withdrawing substituent on the phenyl group should result in a weaker M-CO bond (**Figure 8.10.B**) resulting in a larger enthalpy of activation.

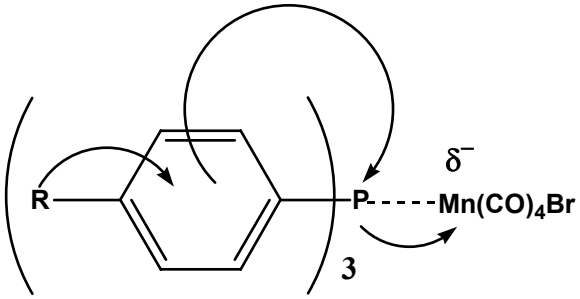

A. R = Electron donating substituent, eg, MeO-

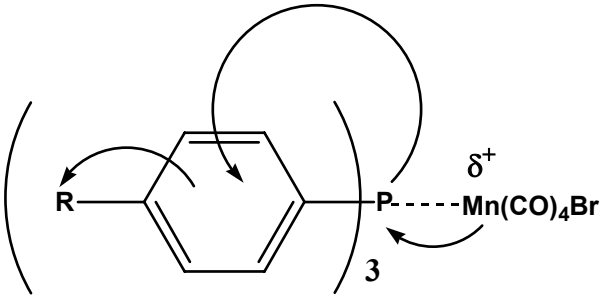

B. R = Electron withdrawing substituent, eg, Cl-

Figure 8.10. The effect of phenyl substituents on the M-CO bond strengths of $Mn(CO)_4(L)Br$ (where L = para substituted arylphosphine)

The data in **Table 8.7** shows the activation parameters for the reaction between $Mn(CO)_4(L)Br$ and L [L = P(*p*-MeO-$C_6H_4)_3$, P(*p*-Me-$C_6H_4)_3$, P(*p*-F-$C_6H_4)_3$, and P(*p*-Cl-$C_6H_4)_3$)] obtained using DRIFTS. The activation enthalpy change of formation of $Mn(CO)_3(P(p\text{-}MeO\text{-}C_6H_4)_3)_2Br$ (122 ± 11 $kJmol^{-1}$) is smaller than the one obtained when $Mn(CO)_4(PPh_3)Br$ reacted with PPh_3 under the same conditions (169 ± 28 $kJmol^{-1}$). The trend is expected because the ligand, (P(*p*-MeO-$C_6H_4)_3$, already attached to the metal complex, contains a strong phenyl ring activator (MeO-) resulting in the weakening of the CO ligands *trans* to it on the metal complex that then required less energy to be activated for the substitution reaction. The entropy change of activation was similarly small (38 ± 4 $Jmol^{-1}K^{-1}$). It is expected to have a positive entropy change for reactions that release a gas as a by-product (carbon monoxide gas).

Table 8.7. Activation parameters of the solventless reaction of manganese metal complexes with functionalised phosphines using DRIFTS

Metal Complex	Mp /°C	Ligand	Mp /°C	$\Delta H^{\ddagger}$ /$kJmol^{-1}$	$S^{\ddagger}$/$Jmol^{-1}K^{-1}$
$Mn(CO)_4(P(p\text{-}MeO\text{-}C_6H_4)_3)Br$	138	$P(p\text{-}MeO\text{-}C_6H_4)_3$	120	122 ± 10	38 ± 4
$Mn(CO)_4(P(p\text{-}Me\text{-}C_6H_4)_3)Br$	192	$P(pMe\text{-}C_6H_4)_3$	145	122 ± 11	27 ± 3
$Mn(CO)_4(P(p\text{-}F\text{-}C_6H_4)_3)Br$	112	$P(p\text{-}F\text{-}C_6H_4)_3$	80	115 ± 8	97 ± 12
$Mn(CO)_4(P(p\text{-}Cl\text{-}C_6H_4)_3)Br$	172	$P(p\text{-}Cl\text{-}C_6H_4)_3$	90	179 ± 32	203 ± 49
$Mn(CO)_4(PPh_3)Br$	131	PPh_3	78	169 ± 28	204 ± 57

Similarly, the activation enthalpy of formation of $Mn(CO)_4(P(p\text{-}Me\text{-}C_6H_4)_3)Br$, 122 ± 11 $kJmol^{-1}$ was also smaller that that of $Mn(CO)_4(PPh_3)Br/PPh_3$ reaction. The value is the same as the one obtained for the formation of $Mn(CO)_3(P(p\text{-}MeO\text{-}C_6H_4)_3)_2Br$ from the reaction of $Mn(CO)_4(P(p\text{-}MeO\text{-}C_6H_4)_3)Br$ with $P(p\text{-}MeO\text{-}C_6H_4)_3$ in fine KBr powder

obtained using DRIFTS (**Table 8.7**). The fact that the phenyl ring substituent, methyl group (Me-), is also a ring activator implies that the CO ligands *cis* to the phenyl group is weakly coordinated requiring less energy for the activation of the substitution reaction. The entropy change of activation was similarly small (27 ± 3 $Jmol^{-1}K^{-1}$). The enthalpy change of activation for $Mn(CO)_4(P(p\text{-}F\text{-}C_6H_4)_3)Br$ was smaller than expected (115 ± 8 $kJ.mol^{-1}$) (**Table 8.7**). The ligand attached to the metal complex had a phenyl ring deactivating substituent, fluoro (F-)), such that the reaction should have had a larger enthalpy of activation than the one obtained experimentally (at least higher in value than those for the formation of $Mn(CO)_3(P(p\text{-}MeO\text{-}C_6H_4)_3)_2Br$ and $Mn(CO)_3(P(p\text{-}Me\text{-}C_6H_4)_3)_2Br$). The corresponding entropy change of activation (97 ±12 $Jmol^{-1}K^{-1}$) was higher as expected of a reaction that results in the formation of a gas (carbon monoxide gas).

The enthalpy change of activation for $Mn(CO)_4(P(p\text{-}Cl\text{-}C_6H_4)_3)Br$ was high (179 ± 32 $kJmol^{-1}$) suggestive of a reaction that needed a large amount of energy to take place. The chloro substituent on the phenyl group of the substituted phenylphosphine ligand, was an electron-withdrawing substituent that withdrew electrons from the phenyl ring. Electron density on the metal was reduced with the result that the carbonyl ligands bonded *cis* to the phosphine ligand were strongly held by the metal centre. The manifestation of such strongly bound carbonyl ligands was a large enthalpy change of activation for the transformation as was the case for the reaction studied. The corresponding entropy of activation was similarly higher (203 ± 49 $J.mol^{-1}K^{-1}$). The production of carbon monoxide gas was the main contributor of the large entropy change.

How to rationalise the data! No correlation between the melting points of the metal complexes and the activation parameters was obvious (**Table 8.7)**. Similarly the melting points of the ligands did not correlate well with the activation parameters.

The electronic effects of the various ligands already attached on the metal complex were considered. The different substituents on the phenyl group of the various solid

phosphines used during the study listed in terms of their decreasing electronic contribution[28] are shown below.

$$R = MeO > Me > H > Cl > F$$

The first two substituents are electronic donating, i.e., increase the electron density of the phenyl ring. The last two are electron withdrawing, i.e., decrease the electronic density of the phenyl ring. R = H is the reference substituent. Apart from the metal complex containing P(*p*-F-C_6H_4)$_3$ ligand the others followed the trend as expected. So electronic effects of the ligand already attached on the metal complex governed the activation parameters of the reaction. A similar argument was reached when the pKa values of the ligands were considered. **Table 8.8** list the pKa[29] values of the ligands considered.

Table 8.8. pKa values of tertiary phosphines used during the study

Ligand	pKa
P(*p*-Cl-C_6H_4)$_3$	1.03
P(*p*-F-C_6H_4)$_3$	1.97
PPh_3	2.73
P(*p*-Me-C_6H_4)$_3$	3.84
P(*p*-MeO-C_6H_4)$_3$	4.59

The metal complex containing electronic-withdrawing ligand, $Mn(CO)_4$(P(*p*-Cl-C_6H_4)$_3$)Br, with the lowest pKa, had the highest energy of activation (179 ± 32 kJ.mol^{-1}) while complexes containing electronic-donating ligands with larger pKa values, $Mn(CO)_3$(P(*p*-MeO-C_6H_4)$_3$)$_2$Br and $Mn(CO)_3$(P(*p*-Me-C_6H_4)$_3$)$_2$Br) had smaller activation energies (both 122 ± 10 kJ.mol^{-1}). The odd one out was $Mn(CO)_4$(P(*p*-F-C_6H_4)$_3$)Br that had an activation energy (115 ± 8 kJ.mol^{-1}) that was lower than expected.

8.4. CONCLUSIONS

The solventless reaction of $Mn(CO)_4(PPh_3)Br$ with PPh_3 in a KBr matrix using DRIFTS was successfully conducted. The reaction also followed pseudo first-order kinetics under two conditions: (i) when the metal-to-ligand ratio was higher than 1:5 and (ii) when the metal complex amount used was ≤ 0.5 mg in 100 mg of KBr solid support. When those conditions were met, the activation enthalpy change of formation was found to be 169 ± 28 $kJmol^{-1}$ while the activation entropy change of formation was 204 ± 57 $Jmol^{-1}K^{-1}$, values larger than those recorded in solution (chloroform or TCE solutions) or without KBr. The KBr support clearly acted as a dispersant reducing the probability of two reacting particles interacting resulting in larger activation parameters.

Various experimental parameters were investigated to check their effect on the reaction kinetics. The first investigation involved a study of the sample preparation method. Use of a fine powder method gave activation parameters; $\Delta H^{\ddagger}$ = 163 $kJmol^{-1}$ and $\Delta S^{\ddagger}$ = 275 $Jmol^{-1}K^{-1}$ respectively. When the solvent method was employed the activation enthalpy and entropy changes were found to be 203 $kJmol^{-1}$ and 279 $Jmol^{-1}K^{-1}$ respectively. The sample preparation method thus influenced the reaction kinetics.

The second experimental parameter checked was the effect of KBr particle size on the rate of the reaction of $Mn(CO)_4(PPh_3)Br$ with PPh_3 in a KBr matrix as studied by DRIFTS. When fine powder support (30-70 μm) was used, a rate constant of 2.28×10^{-4} s^{-1} was obtained. When intermediate grain sized (100-130 μm) and coarse sized (110-190 μm) particles were used as support, the rates of the reaction were found to be 4.77×10^{-4} s^{-1} and 6.20×10^{-4} s^{-1} respectively. Thus the rate of the reaction progressively increased with particle size demonstrating that the particle support also influenced the rate of reaction.

The third parameter investigated was the nature of the solid support. Various solid supports were tested for the reaction and it was found that when the reaction was carried out in sucrose and SiO_2, the rate of the reaction was fastest (1.71×10^{-2} s^{-1} and 2.02×10^{-2} s^{-1} respectively). The reaction was the slowest when ionic solids, KBr, Na_2SO_4, $NaNO_2$, Na_2CO_3, $NaC_2H_3O_2$ and $NaNO_3$ were used. When alumina, Al_2O_3 and TiO_2 were used,

the reaction was slower (8.26×10^{-3} s^{-1} for Al_2O_3 and 6.81×10^{-3} s^{-1} for TiO_2). The findings demonstrate that the support matrix has an effect on the rate of the reaction.

The effect of varying the electronic parameter associated with the incoming ligand was also investigated by using a range of solid phosphines; P(*p*-C_6H_4-R)$_3$, (R = H, Ph, MeO, Cl, F). These ligands all have the same Tolman cone angles. To avoid the complications associated with phosphine substitution, rather than CO substitution, *viz*

$Mn(CO)_4LBr + L \rightarrow Mn(CO)_3LBr + CO$ [L= P(*p*-C_6H_4-R)$_3$, R = Ph, MeO, Cl, F]

the incoming ligand and the ligand in the metal complex were left the same in the study. The solventless reaction between $Mn(CO)_4$(P(*p*-MeO-C_6H_4)$_3$)Br and P(*p*-MeO-C_6H_4)$_3$ in fine KBr powder was studied using DRIFTS and gave an enthalpy change of formation and entropy change of formation of 122 ± 10 $kJmol^{-1}$ and 38 ± 4 $Jmol^{-1}K^{-1}$ respectively. The solventless reaction between $Mn(CO)_4$(P(*p*-Me-C_6H_4)$_3$)Br and P(*p*-Me-C_6H_4)$_3$ resulted in the activation enthalpy change of formation 124 ± 11 $kJmol^{-1}$ while its activation entropy change of formation was 27 ± 3 $Jmol^{-1}K^{-1}$. The activation parameters found for both complexes were unexpectedly lower than those obtained for the reaction of $Mn(CO)_4(PPh_3)Br$ with PPh_3 in fine KBr matrix under identical conditions. The results clearly show that solventless effects are important.

The solventless reaction of $Mn(CO)_4$(P(*p*-F-C_6H_4)$_3$)Br with P(*p*-F-C_6H_4)$_3$ in fine KBr powder using DRIFTS was conducted and its kinetic parameters deduced to be 115 ± 8 $kJmol^{-1}$ and 97 ± 12 $Jmol^{-1}K^{-1}$ respectively. The solventless reaction of $Mn(CO)_4$(P(*p*-Cl-C_6H_4)$_3$)Br with P(*p*-Cl-C_6H_4)$_3$ in fine KBr Powder using DRIFTS was also carried out and the activation enthalpy and entropy changes of formation were 179 ± 32$KJmol^{-1}$ and 203 ± 49 $Jmol^{-1}K^{-1}$ respectively.

8.5. REFERENCES

1. P. Kubelka and F. Munk, *Z. Tech. Phys.*, 1931, **12**, 593.
2. M. Fuller and P. Griffiths, *Anal. Chem*., 1978, **50**, 1906.
3. H. Gunzler and H. Gremlich, *IR Spectroscopy: An Introduction*, Wiley-VCH Verlag, Weinheim, 2002.
4. B. C. Smith, *Fourier Transform Infrared Spectroscopy*, CRC Press, New York, 2000.
5. P. J. Brimmer and P. R. Griffiths, *Appl. Spectrosc*., 1988, **42**, 242.
6. J. J. Benitez, M. A. Centeno, M. J. Capitan, J. A. Odriozolan, B. Viot, P. Verdier and Y. Laurent, *J. Mater. Chem.,* 1995, **5**, 1223.
7. O. Faix and J. H. Boettcher, *Holz als Roh-und Werkstoff*, 1992, **50**, 221.
8. Z. Krivacsy and J. Hlavay, *Spectrochim. Acta*, *Part A,* 1994, **50A**, 49.
9. M. L. E. TeVrucht and P. R. Griffiths, *Appl. Spectrosc*., 1989, **43**, 1492.
10. A. A. Christy, J. E. Tvedt, T. V. Karstand and R. A. Velapoldi, *Rev. Sci. Instrum.,* 1988, **59**, 423.
11. Y. K. Dijiba, A. Zhang and T. M. Niemczyk, *Int. J. Pharm.,* 2005, **289**, 39.
12. B. C. Smith, *Infrared Spectral Intepretation: A Systematic Approach*, CRC Press, Boca Raton, 1999.
13. J. Assmann, E. Loffler, A. Birkner and M. Muhler, *Catal. Today,* 2003, **85**, 235.
14. N. Shirahama, S. H. Moon, K. –H. Choi, T. Enjoji, S. Kawano, Y. Korai, M. Tanoura and I. Mochida, *Carbon,* 2002, **40**, 2605.
15. R. J. Gordon, N. J. Trivedi, B. P. Singh and E. C. Ellis, *Environ. Sci. Technol.,* 1988, **22**, 672.
16. A. Kumar and G. C. Pandey, *Polym. Sci.,* 1994, **2**, 911.
17. E. M. Suzuki and W. R. Gresham, *J. Forensic Sci.*, 1986, **31**, 931.
18. C. J. Lennard, W. D. Mazzella and P. A. Margot, *Analysis*, 1993, **21**, M34.
19. A. Tsuge, Y. Uwamino, T. Ishizuka and K. Suzuki, *Appl. Spectrosc.,* 1991, **45**,

1377.

20. G. C. Pandey, K. V. Rao and A. Kumar, *Polym. Test.*, 1995, **14**, 489.
21. S. S. Manzini and N. J. Coville, *Inorg. Chem. Commun*., 2004, **7**, 676.
22. B. D. Chandler and L. H. Pignolet, *Catal. Today,* 2001, **65**, 39.
23. M. D. Bala, A. Budhai and N. J. Coville, *Organomettalics*, 2004, **23**, 2048.
24. C. Bremard, *Coord. Chem. Rev.,* 1998, **178**, 1647.
25. I. Mohammed-Ziegler, *Spectrochim. Acta Part A,* 2003, **59A**, 3239.
26. H. Landmesser, H. Berndt, D. Kunath and B. Lucke, *J. Mol. Catal. A*, 2000, **162**, 257.
27. C. Bremard, G. Ginestet and M. Le Maire, *J. Am. Chem. Soc.,* 1996, **118**, 12724.
28. M. A. Fox and J. K. Whitesell, *Organic Chemistry 2nd ed*, Jones and Bartlett Publishers, Massachusetts, 1997, 559.
29. M. M. Rahman, H. Y. Liu, A. Prock and W. P. Glering, *Organometallics*, 1987, **6**, 650.

CHAPTER 9: OPTICAL MICROSCOPY EXPERIMENTS

9.1. INTRODUCTION

9.1.1. History and perspective

The development of light (optical) microscopy from its origin to modern times dates back to the 17th century when Willibrord Snell (1591-1626) and Rene Descartes (1596-1650) discovered the law of refraction[1]. This was followed by the establishment of geometrical optics by Isaac Newton (1672), Johannes Hevelius (1611-1687) and L. Euler (1747)[2]. Antoj van Leeuwenhoek (1632-1723) then improved the achromatic lens to get a microscope good enough to study protozoa, bacteria, yeast cells and nerve fibres[3]. Further refinements and inventions lead to the development of the light microscope into new models and eventually extensions to the use of electrons in the scanning electron microscope[4].

The application of optical microscopy interlaces many fields. In biology, examples of botanical[5,6], zoological[7] and anatomical[8,9] applications are numerous. Industrial research in mineral identification[10], pulp[11], paint[12], wear and lubrication[13] utilises the technique. Forensic science also uses the technique for the identification of narcotics[14], pigments[15], fibres[16], and pathogens[17].

In chemistry, optical microscopy has been used to study reaction mechanisms for decades[18]. For example the reaction mechanism of the double conversion between lead selenide and cadmium telluride was probed using the technique in 1976[19]. The mechanism of thermal dehydration of barium chlorate monohydrate [$(Ba(ClO_3)_2.H_2O$] was elucidated using the technique[20]. The thermal decomposition of $KMnO_4$[21], $RbMnO_4$[22] and $CsMnO_4$[23], $Ni(MnO_4)_2$[24] and $Cu(MnO_4)_2$[25], found to go through the melt,

were also probed using optical microscopy. Optical microscopy was also used in the kinetic study of dehydration of potassium tartrate hydrates[26].

Organic chemists have also found the technique useful in probing reaction mechanisms[27,28]. Solid-state organometallic isomerisation reactions of (CpR)M(XYZW) (R = H, alkyl; M = Re, W, Mo; X,Y,Z,W = CO, Br, I, RCN, PR, P(OR)) were studied using the same technique[29].

9.1.2. Aims

The aim of the study was to investigate the microscopic characteristics of the solventless reaction, $Mn(CO)_4(L)Br + L \rightarrow Mn(CO)_3(L)_2Br + CO$. The investigation involved an optical microscopy study observation of the reaction using reagents (powders or crystal). The investigation was performed to shed light on the mechanism of the reaction.

The experimental results of the reaction of $Mn(CO)_4(PPh_3)Br$ and PPh_3 to produce $Mn(CO)_3(PPh_3)_2Br$ in the absence of solvents as followed by DRIFTS and FTIRS left some questions unanswered. How was it possible to explain the excellent kinetic data for a solventless reaction at a molecular level? Why did mass transfer problems associated with condensed phase reactions have no impact on the reaction? How did two solid particles interact to lead to a successful chemical reaction in the absence of a medium that would allow diffusion of reactants to facilitate contact? How was the reaction sustained such that particles that were far away from each other eventually reacted?

9.2. EXPERIMENTAL PROCEDURES

9.2.1. The reaction Device

The optical microscopy study was conducted using a device designed by Bogadi *et al*[30]. The components of the device are given below.

9.2.1.1. Heating plate cell design

The homemade heating plate used for the study consisted of a transparent rectangular glass piece wound with a nichrome wire. A J-type thermocouple was also attached to the heating plate to measure temperature. The setup is shown **Figure 9.1**. The nichrome wire was coiled around the glass plate such that a small opening was left at the centre of the glass plate to place the material for study. This area was demarcated as the reaction site. Crystals or powdered materials were placed at the reaction site. The nichrome wire also served as a structural support to hold the glass piece in position inside the reaction chamber (see below) when experiments were undertaken. The thermocouple was attached as close as possible to the reaction site (without inhibiting light transparency from a microscope) to ensure that the reaction temperature was at the temperature registered by the thermocouple. The heating coil (nichrome wire) and the thermocouple were connected to a REX-P96 series (RKC Instrument Inc.) programmable temperature controller (PTC) that enabled control of the reaction temperature and time. A ±1°C controller fluctuation was observed, which averaged out to the set temperature over time and was thus considered negligible. Using a hand held thermocouple; a temperature fluctuation of ±1°C was observed when the reaction cell plate was heated in the temperature range 40-120°C



Figure 9.1. Heating plate design for the observation of solventless reactions

9.2.1.2. Reaction Chamber Design and Operation

A circular glass vessel made from a transparent glass material as shown below (**Figure 9.2**) was used as a reaction chamber. The chamber also contained inlet and outlet taps for the introduction of an inert gas. A groove big enough to allow the reaction plate to be inserted into the chamber was also made such that it had a tight fitting joint to seal off the chamber as desired. Once the heating plate was held in place inside the reaction chamber, a circular transparent glass top was then placed on the top of the chamber to seal it off. The glass top was smeared with high vacuum grease at the edges so that its placement at the top of the reaction chamber ensured tight sealing. The set up was then ready to follow a reaction once the system was flushed with an inert gas for a few min.

An independent thermocouple probe, linked to a fully calibrated Fluke Series II digital thermometer (Fluke Corporation), was used to calibrate the reaction cell. The probe was allowed to touch the reaction site at various sites, at different places where the reaction materials could be placed for reaction observation. A difference of not more than 2°C

between the digital thermometer reading and the temperature controller display was noted. Samples of benzil (95°C), acetanilide (115°C), phenacetin (135°C) and benzanilide (163°C) were placed at the reaction site one at a time, and heated to their respective melting points. Temperature measurement to within ±3°C of the various melting points was found possible[30]. The temperature uncertainty of the reaction cell was thus taken to be ±3°C.



Figure 9.2. The reaction chamber

The reaction chamber was then placed under a bifocal Olympus Polarising Microscope (equipped with a close circuit digital camera attachment) to allow for crystal observation (**Figure 9.3**). The gas inlet tap was attached to an ultra pure nitrogen gas source such a gentle stream of gas (a flow rate of about 0.50 dm^3/min) flowed through the system before the reaction was initiated. The flow rate was monitored using a gas bubbler, filled with paraffin oil, connected to the gas outlet ensuring that the reacting materials/crystals placed in the reaction cell are not disturbed. After about five min of degassing, the flow rate was reduced such that there was virtually no gas flow (a flow rate of less then 0.10 dm^3/min); but sufficient to ensure a positive pressure inside the chamber to minimise diffusion of atmospheric air into the chamber. The paraffin oil in the gas bubbler ensured

that atmospheric air did not diffuse into the reaction cell such that the system remained closed, under nitrogen, for the duration of the experiment.

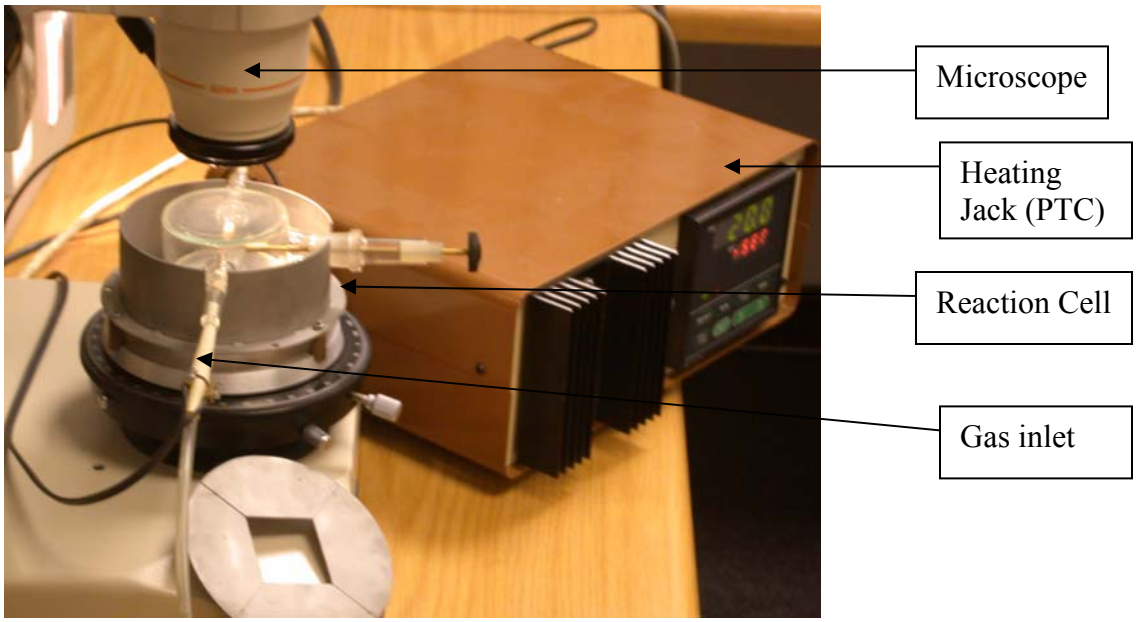

Figure 9.3. Depiction of the reaction chamber placed under an optical microscope for the study of $Mn(CO)_4(PPh_3)Br$ to $Mn(CO)_3(PPh_3)_2Br$ under nitrogen

Once the apparatus was placed under the microscope as shown above, observations were made.

9.2.2. Optical microscopy study if the solventless reaction of thoroughly mixed powders of $Mn(CO)_4(PPh_3)Br$ and PPh3 (1:1 mol equiv) at 60°C

An experiment was performed using equimolar amounts of $Mn(CO)_4(PPh_3)Br$ and PPh_3. The reagents were dissolved in DCM at room temperature and the resulting solution quickly evaporated to leave a thoroughly mixed mixture of the two reagents as a orange solid. The solid mixture was than placed in the reaction cell and the reaction monitored at 60°C.

An extension of the investigation involved linking the extent of the reaction to microscopic observation. In this case, equimolar amounts of reagents (as solid mixture) were allowed to react at 60°C for a time period. The reaction was terminated and the extent of the reaction determined by IR spectroscopy. The investigation was conducted over several time periods. Pictures were taken periodically to record the observations.

9.2.3. Optical microscopy study of the solventless reaction between $Mn(CO)_4(PPh_3)Br$ and PPh_3 using crystalline reagents at 42°C

A study was also undertaken using crystals of the two reagents, $Mn(CO)_4(PPh_3)Br$ and PPh_3. Three successive experiments were conducted. The first experiment was conducted by assembling the reagent crystals in isolation. The crystals were then observed under the microscope when heated at 60°C for an hour and cooled back to room temperature for two h. The second experiment started by rearranging the crystals in a way that some reagent crystals were touching. The reaction cell was then heated to 42°C and observation made for 3 h. The sample was then cooled back to room temperature for two more h. The last experiment involved placing more ligand crystals on the product-coated crystal that was formed from the second experiment. Once the crystals were touching the reaction cell was once more heated to 42°C and observations made for 30 min. The reaction was then allowed to cool overnight. Pictures were taken periodically to record the observations.

9.2.4. Thermally induced solventless reaction between $Mn(CO)_4(PPh_3)Br$ and $P(p\text{-}Me\text{-}C_6H_4)_3$ using crystalline reagents

Crystals of the two reagents were assembled in such a way that some were touching. The reaction cell was then heated to 70°C and observation made while taking pictures periodically.

9.3. RESULTS AND DISCUSSIONS

9.3.1. Optical microscopy study of the solventless reaction of thoroughly mixed powders of $Mn(CO)_4(PPh_3)Br$ and PPh_3 (1:1 mol equivalent) at 60°C

The microscopic interaction of the two reagents as a thoroughly mixed solid mixture (1:1 mol equiv) at 60°C was observed using optical microscopy as described in the experimental section (**Figure 9.4**).

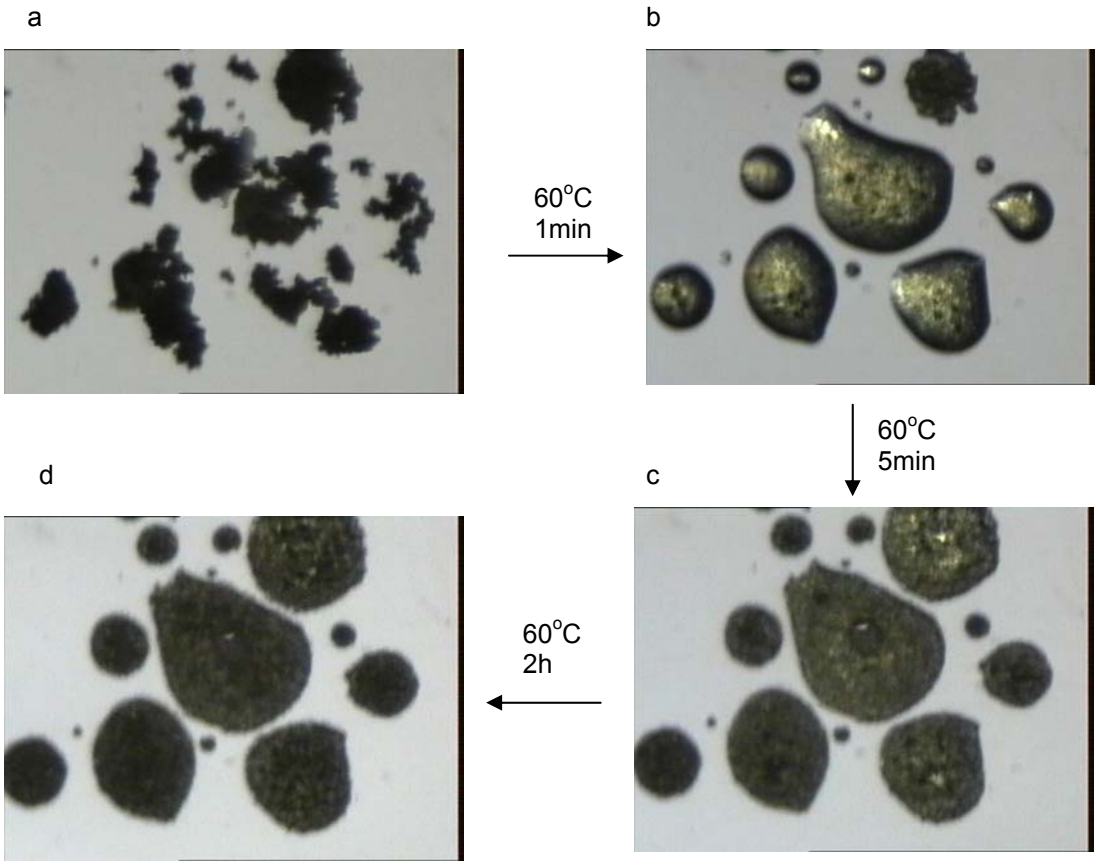

Figure 9.4. Pictures showing the solventless reaction of thoroughly mixed powders of $Mn(CO)_4(PPh_3)Br$ and PPh_3 (1:1 mol equivalent) at 60°C as seen through an optical camera (resolution, 80× magnification)

Figure 9.4a shows the thoroughly mixed powders of the two reagents before thermal activation. **Figure 9.4b** shows that the melting has occurred below the melting points of reactants. **Figure 9.4c** shows that the solidification of the reacted material has occurred. As more product formed (the yellow particles in the mixture) and less starting material was available for further reaction, the material solidified (**Figure 9.4c** after about 5 min). DRIFTS and FTIRS also monitored the experimental manifestation of the phenomenon.

As can be seen: what appeared to be a solid-state reaction is actually a **melt reaction**! The melt, (regardless of which reagent(s) melted) acted as a viscous medium that enabled the reagent(s) and product to diffuse and move about with greater freedom. The probability of the reagents finding each other in such media was facile.

The reaction could also be propelled by the energy released during the reaction (exothermic reaction). This manifested itself by the immediate melt formed engulfing all the reagents as seen in **Figure 9.4c**. As more products formed the reagents/product mixture solidified giving the impression of a solid-state reaction. The positioning of the solidified product was similar to the reactants enhancing the illusion of a solid-state reaction when viewed with the naked eye (compare **Figure 9.4a** and **Figure 9.4d**). The material remained as a solid mixture without much change when left to react for extended periods (**Figure 9.4d** after an hour of thermal experimentation).

In the next set of experiment an attempt was made to quantify the extent of the reactions of the observed microscopic reaction from optical microscopy using FTIRS studies.

Figure 9.5 displays the extent of the reaction as IR spectra were recorded on the material observed under the optical microscope. At the beginning of the reaction the FTIR spectrum that correlated with the starting complex, $Mn(CO)_4(PPh_3)Br$ is shown in **Figure 9.5a**.

a Starting materials, at room temperature before thermal experimentation



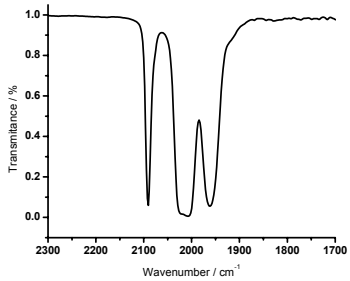

b Immediately when melting resumes under thermal experimentation at 60°C

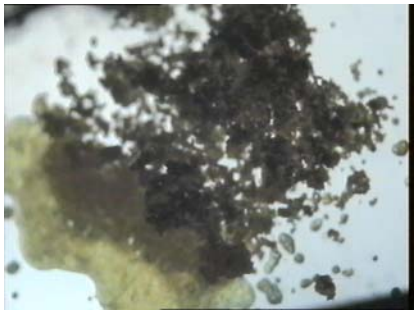

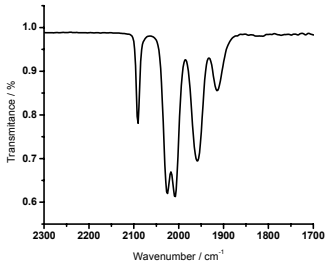

c After thermal experimentation for an hour at 60°C



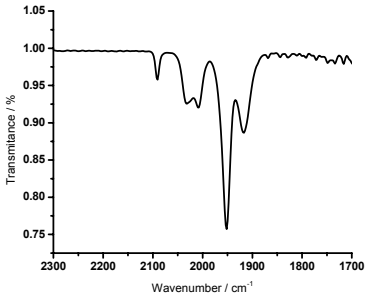

d After thermal experimentation for an 12 h at 60°C

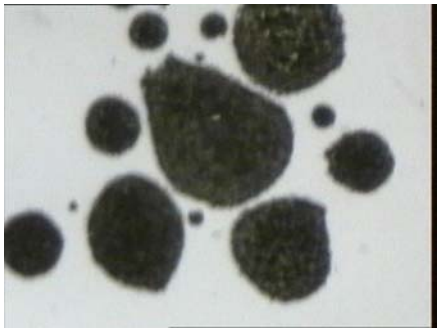

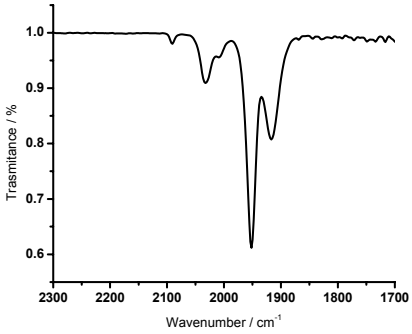

Figure 9.5. The relationship between microscopic visualisation and the extent of the solventless reaction of powdered $Mn(CO)_4(PPh_3)Br$ and PPh_3 (1:1 mol equivalent) at 60°C using optical microscopy and FTIRS

The sample taken immediately after the reaction mixture was allowed to reach the experimental temperature of 60°C (**Figure 9.5b**) showed a mixture that already contained the product. It showed that the reaction was fast and the reagents started to react at temperature lower than the experimentally set 60°C. The findings are not surprising because kinetic experiment was successfully conducted at 50°C using both FTIRS and DRIFTS.

Figure 9.5c depicted the reaction after an hour of reaction at 60°C and the corresponding FTIRS showed that the reaction was almost complete. The reaction was virtually complete after 12 h of experimentation at the reaction temperature (**Figure 9.5d**) as shown by the corresponding FTIRS spectrum. The reaction seemingly took longer to reach completion compared to the usual runs using FTIRS and DRIFTS. The reason for the delay was due to the fact that the reagents were spread out during the optical experimentation whereas they were mixed together during normal kinetic investigations. Nonetheless, we were able to link microscopic investigations to the extent of the reaction.

9.3.2. Optical microscopy study of the solventless reaction of $Mn(CO)_4(PPh_3)Br$ and PPh_3 using crystalline reagents at 42°C

The question of mechanism that remained unanswered: what brought about the melting? Which of the reagents melted first when they reacted? Crystals were arranged in a way that some crystals touched each other. Other crystals were arranged in isolation. **Figure 9.6** showed the arrangement of the assembled crystals before thermal experimentation at 42°C. The yellow crystals are the metal complex crystals, $Mn(CO)_4(PPh_3)Br$, while the grey crystals correspond to the ligand, PPh_3.

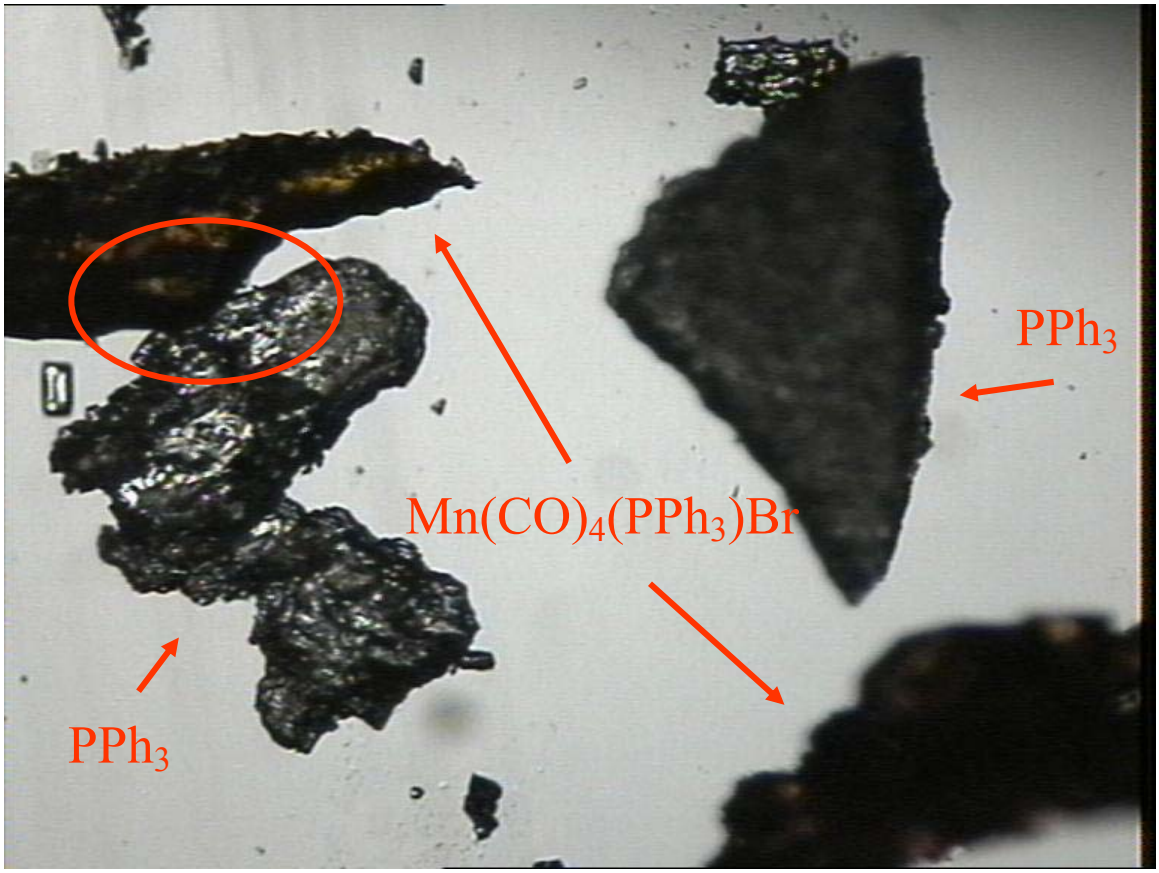

Figure 9.6. Picture showing the arrangement of $Mn(CO)_4(PPh_3)Br$ and PPh_3 crystals under a microscope before thermal experimentation

Figure 9.7 showed the sequence of events for the arranged reaction crystals under thermal experimentation at 42°C. **Figure 9.7a** represents isolated crystals of the two reagents that were allowed to stand at 60°C for an hour. The preliminary study was used to check as to whether the reaction was initiated by the sublimation of one of the reagents at the experimental temperature as some authors have alluded to. At the end of an hour at the set experimental temperature, there were no noticeable changes in the reagent crystals that would have signalled a reaction with the formation of new product(s). The physical properties (the positioning of the crystals, the colour and appearance) of the reactant crystals remained unchanged.

The crystals were then allowed to cool back to room temperature. The crystals were arranged such that some of the crystals touched as shown in **Figure 9.7b** (**Figure 9.6** shows the crystal arrangement as derpicted in **Figure 9.7b).** The temperature was raised to 42°C at which point the ligand, PPh_3 that was in contact with the metal complex started to melt (**Figure 9.7c**). Notice from the pictures that the isolated PPh_3 ligand and the metal complex did not melt.

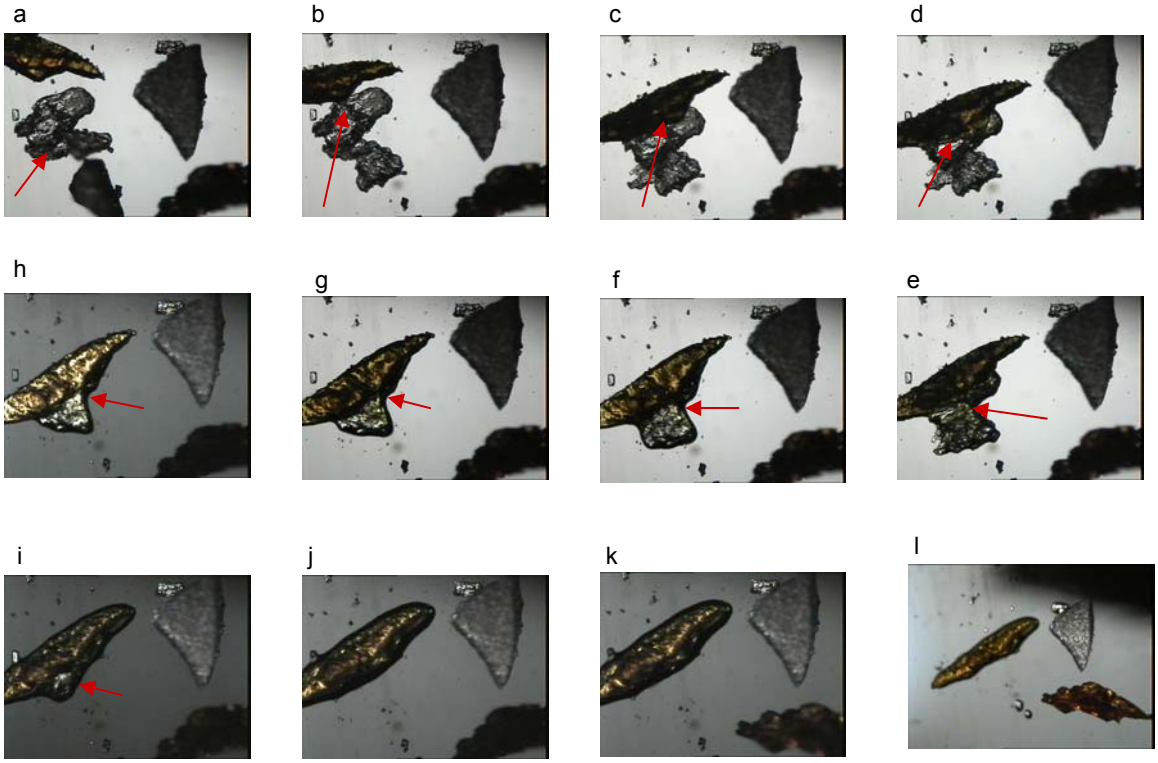

Figure 9.7. The reaction sequence of the thermal transformation of crystallised $Mn(CO)_4(PPh_3)Br$ with PPh_3 at 42°C observed using an optical microscope

a Isolated crystals heated at 60°C for an hour, b Reactant crystals in contact while others in islation prior to thermal experimentation, c Immediately when 42°C was reached, d After a minute at 42°C, e after two min, f After 3 min, g After 4 min, h After 5 min, i After 6 min, j After 10 min, k After 60 min and l After an hour, zoomed-out view.

Figure 9.7d-j shows the reaction progress as revealed by the consumption of PPh_3 as if the metal complex engulfed it. The colour of the reacting metal complex also changed

from yellowish brown to yellow signalling the formation of a new complex, ($Mn(CO)_3(PPh_3)_2Br$). During the reaction period, the isolated metal complex and the ligand neither reacted nor melted. **Figures 9.7j-k** showed the reaction after 10 min and an hour at 42°C respectively. The ligand that was in contact with the metal complex had been completely consumed. To determine if the sublimation initiation mechanism was responsible for the reaction, the sample was allowed to stand at the experimentally set temperature of 42°C for a further 6 h. **Figure 9.7k-l** showed the crystal arrangement at the end of the experiment. There was no visible change in the positioning of the isolated reactants. They neither change colour nor show different texture (the physical properties of the isolated reactants did not change as seen through the optical microscope). The presence of the product crystal did not assist the isolated reagents from reacting provided they remained isolated. Further, when the reagent crystals were subjected to higher temperatures while isolated from each other, they did not react.

What brought about the melting at 42°C? This effect presumably arises when the metal complex contaminates PPh_3. A DSC profile of the reacting crystals made by thoroughly mixing the two reagents failed to show an exotherm when 1°/min and 10°/min heating rates were used.

What is clear is that melting accompanies the reaction. Was melting the result of the reaction or the prerequisite for the reaction? The explanation came from knowledge of the reaction. **Scheme 9.1** shows a scheme for CO loss and formation of 5 coordinate intermediates.

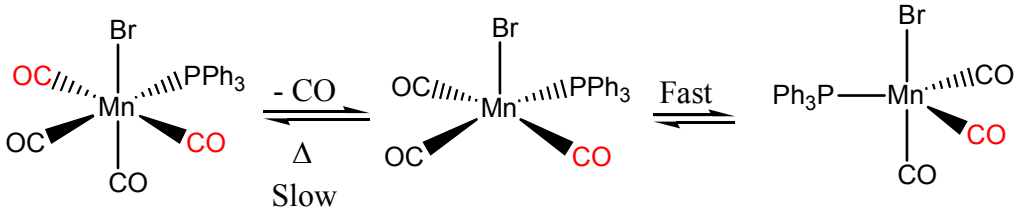

Scheme 9.1. The formation of the 5-coordianate intermediate by the partial carbon monoxide dissociation from the metal complex in the presence of heat

The proximity of an incoming ligand is critical here as it must be within 'reaction range' to interact with the 5-coordinate intermediate. If the proximity of the ligand particle is within the required range, CO ligand substitution by the PPh_3 should then take place. The substitution is favoured and driven by the entropy increase of the system during the transformation. Once the process has been initiated, the energy release would be enough to activate other metal complex particles, within its locality.

The combined energy release from many reaction sites at the contact point between the metal complex and the ligand should be enough to start continuous melting process. The pictures in **Figure 9.7** actually shows zonal melting of the ligand. The melting started at the contact points and gradually moved sideways as the reaction progressed; all the while the ligand was being consumed (**Figure 9.7c-g**). The explanation above tentatively argues in favour of the melting process taking place as a result of the energy given off during the reaction. It suffices to say that advanced methods of reaction analysis at the microscopic level like atomic force spectroscopy (AFM)[31] could further assist in generating an understanding of the solventless reaction studied.

Figure 9.8 shows the positioning of $Mn(CO)_4(PPh_3)Br$ and PPh_3 crystals before and after the reaction. The crystals hardly changed their positions at the end of the reaction. This was the reason why in initial studies the melting process was not detected when the reaction was followed by the infrared techniques. Only the PPh_3 crystals that were in contact with the metal complex were consumed.

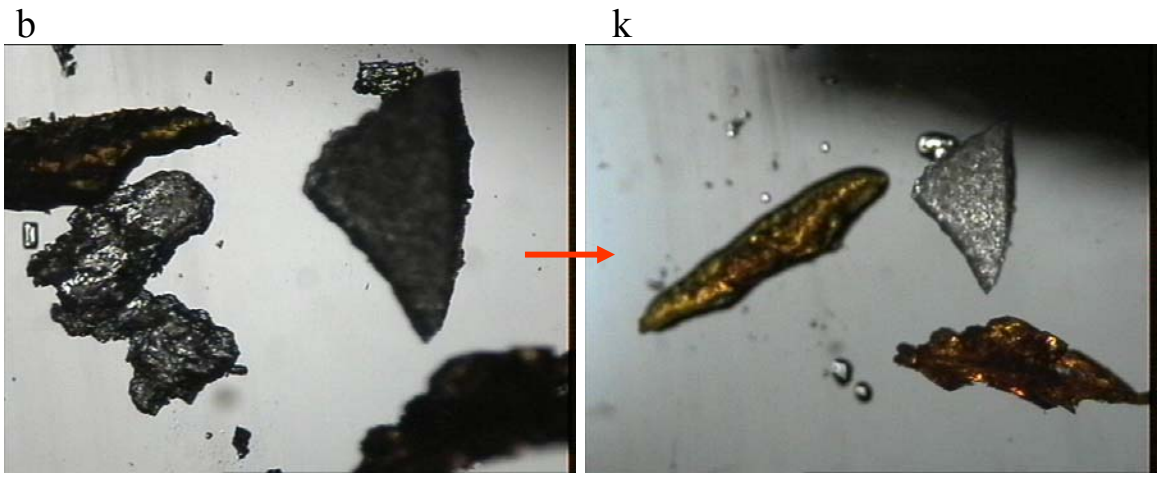

Figure 9.8. Pictures showing the positioning of crystals of $Mn(CO)_4(PPh_3)Br$ and PPh_3 before the reactions was initiated and at the end of thermal experimentation at 42°C as viewed under an optical microscope

The product formed was allowed to cool back to room temperature for two h before placing another PPh_3 crystal in contact with the product-coated starting metal complex (**Figure 9.9**). The reaction was then initiated by thermal heating to check whether there was further reaction to yield more products. **Figure 9.9a** shows the crystal arrangement after 6 h of additional reaction at 42°C and subsequent cooling back to room temperature for 2 h. **Figure 9.9b** shows a PPh_3 crystal already placed on the product-coated metal complex crystal at room temperature. The picture also displays the product-coated metal complex as shown by some golden yellow product flakes that were detached from the main crystal, which lay scattered in the vicinity of the crystal. As can be seen, the reaction was not initiated at room temperature (ten min) (**Figure 9.9b**).

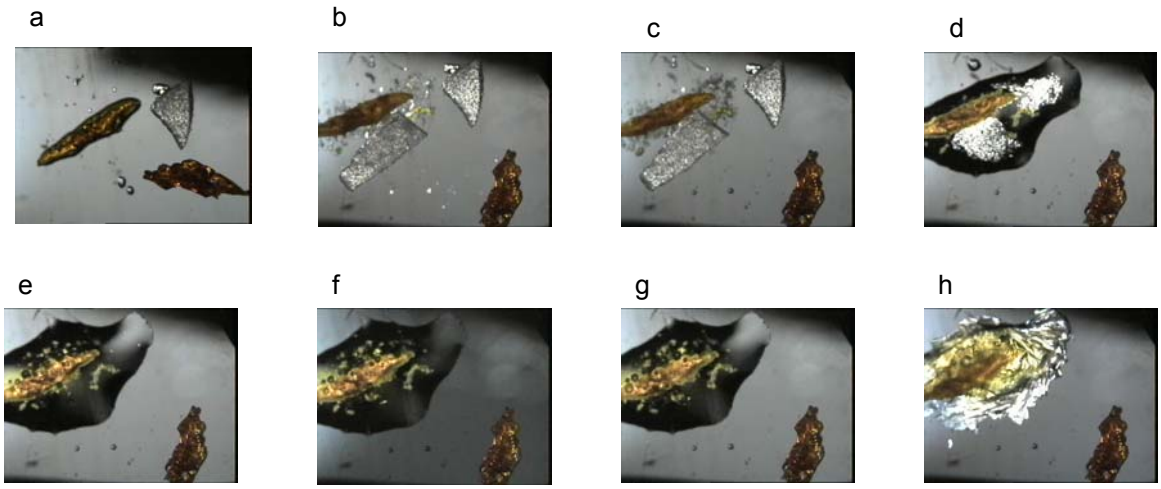

Figure 9.9. Pictures showing the reaction of $Mn(CO)_4(PPh_3)Br$ and PPh_3 at 42°C as viewed by an optical microscope after another ligand crytal was placed on the product-coated metal complex crystal

When the reaction mixture was heated to 42°C as shown by **Figure 9.9c**, the same phenomenon observed in earlier experiments was once more observed. The PPh_3 crystal that was in contact with the metal complex started to melt. The melting was instantaneous and the resulting melt engulfed the nearby PPh_3 crystal. This resulted in the formation of a large pool of ligand completely surrounding the metal complex (**Figure 9.9d**). The crystals were placed on a transparent glass slide and due to the fact that liquid PPh_3 has a smaller surface tension (25.5 mN/m at 95°C)[32], it would rather spread-out than coagulate in a small area. The observation revealed that a layer of product in the earlier experiment trapped the unreacted starting material. From previous experimental investigations it has been determined that the complex $Mn(CO)_3(PPh_3)_2Br$ did not react further with PPh_3 to give $Mn(CO)_2(PPh_3)_3Br$. This meant that if there was further reaction (as observed in **Figure 9.9d**), it would be the starting metal complex, $Mn(CO)_4(PPh_3)Br$ reacting with the now available molten ligand. The isolated $Mn(CO)_4(PPh_3)Br$ crystal did not melt during this process. What was more apparent than before was that the crystal started to disintegrate. Flakes of product material could be seen on the PPh_3 melt, which now acted as a solvent (**Figure 9.9e**).

Figure 9.9e also showed further disintegration of the crystal as the reaction progressed. Further disintegration of the crystal can be vividly seen in **Figure 9.9f-g**. The reaction mixture was cooled back to room temperature overnight (**Figure 9.9h**). The new material consisted of the product flakes and solid PPh_3 (excess ligand) at the edges. The isolated metal complex crystal was unaffected. The crystal that reacted changed its shape and it was no longer a continuous unit as it was before but made up of many microcrystals fused together. The conclusion from the observation is that crystal disintegration is necessary for further reaction. The mass transfer problems were overcome by having the ligand melt and the melt acted as the solvent medium to allow the metal complex crystal to reacted and form microcrystals of the product. Disintegration of the crystal was also necessary for the advancing ligand/product layer to reach the core of the crystal and formation of the product microcrystals.

The above experiment was conducted between a metal complex and a ligand that had a lower melting point than the ligand. Use of a ligand that melted above the melting point of the metal complex gave similar results. The reaction of [P(*p*-Me-$C_6H_4)_3$], that melted at 145°C, with $Mn(CO)_4(PPh_3)Br$ that melted at 131°C is shown in **Figure 9.10**.

In this experiment the metal complex that was in contact with the ligand melted first (**Figure 9.10a**). That the metal complex was the one that melted first was also demonstrated by the lack of melting of the distant ligand microcrystals. In the $Mn(CO)_4(PPh_3)Br/PPh_3$ experiment, the ligand completely melted but it was not the case here (**Figure 9.10b-g**).

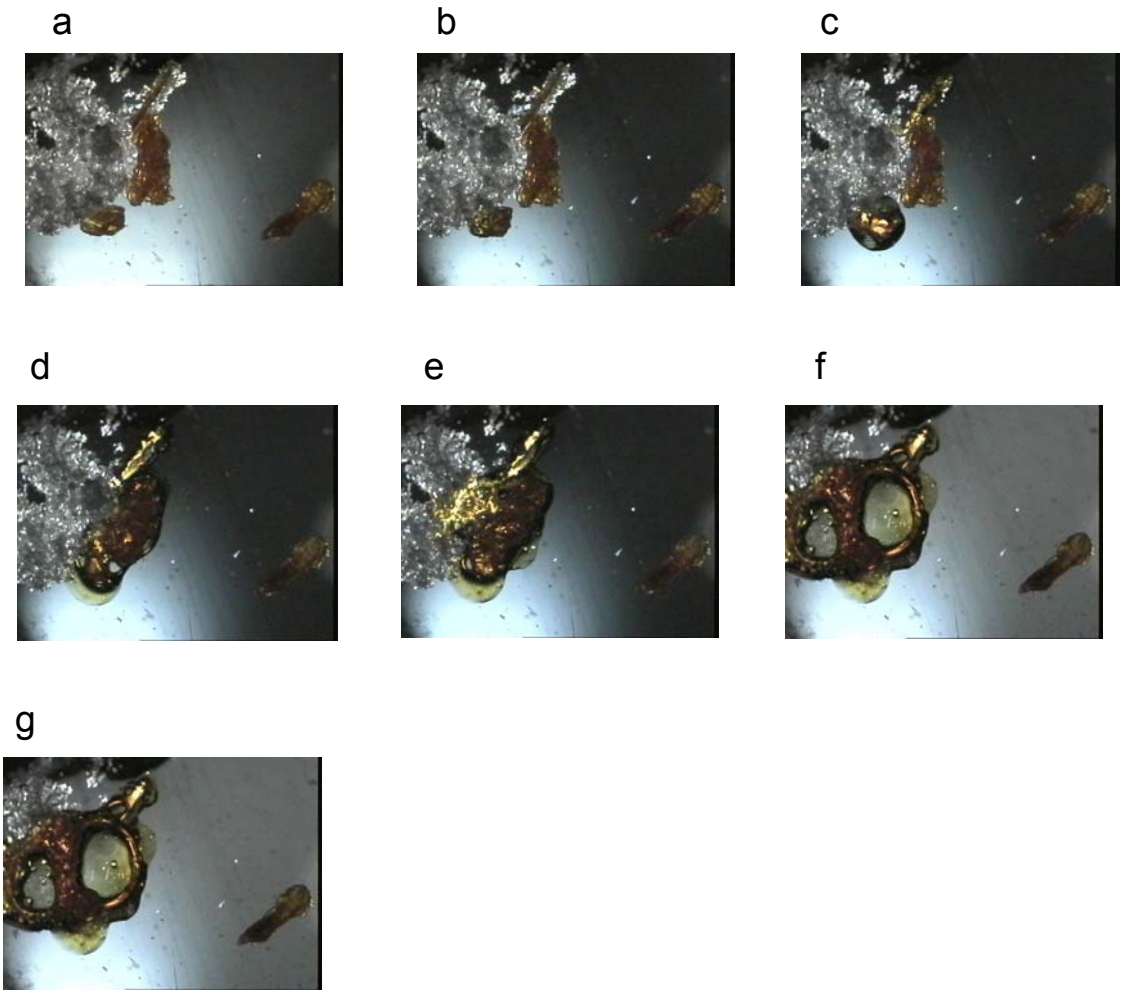

Figure 9.10. The reaction of $Mn(CO)_4(PPh_3)Br$ with P(*p*-Me-$C_6H_4)_3$ at 70°C under an optical microscope

In the melting process, the ligand crystal disintegrated during melting while the product microcystals that formed were visible as yellow matter suspended on the starting complex melt. There were huge air bubbles that formed during the reaction (notice the alien-eyed figures on the reaction slide in **Figure 9.10b-g**). These large gas bubbles were once again attributed to the CO gas evolved during the substitution reaction. At the end of the reaction, the isolated crystal of the metal complex remained unaffected; signalling that indeed the reaction also went through the melt and good contact between the reacting crystals is a requirement for the reaction.

9.4. CONCLUSIONS

An optical microscopy study of the solventless reaction between powders of $Mn(CO)_4(PPh_3)Br$ and PPh_3 was conducted successfully. The reaction was observed to proceed in the melt at temperatures lower than 60°C. The melting process was accompanied by a chemical reaction between the two reagents. As the product formed, it solidified such that the original positioning of the powder was maintained giving the impression of a solid-state reaction. The solid material that formed did not change in morphology nor did it react. This confirms that once the product, $Mn(CO)_3(PPh_3)_2Br$, was formed it did not react further to form $Mn(CO)_2(PPh_3)_3Br$. The correlation between the extent of the reaction and the microscopic observations was monitored. The reaction mixture was analysed by FTIRS as a function of time. Below 35°C the two solids remained as they were and were unable to melt and initiate the reaction.

The solventless reaction between crystals of $Mn(CO)_4(PPh_3)Br$ and PPh_3 was also followed by optical microscopy (42°C). The crystals were arranged such that when the reagent crystals were isolated from each other, no chemical reaction was observed at 60°C for 2 h. When the crystals were arranged so that the metal complex and ligand crystals touched, reaction was observed at $T \geq 42$°C. For this reaction it was noticed that the ligand crystal that was in contact with the metal complex crystal melted first and that the metal complex crystal gradually consumed the ligand as the reaction progressed. The molten PPh_3 ligand thus served as a medium that allowed for the diffusion of the reagents. The experiment also ruled out a mechanism entailing the sublimation of one of the reagents at the experimental temperature. The reaction thus occurred in the melt and was facilitated by the migration of reagents and products to give the well-behaved reaction kinetics that were observed using FTIRS and DRIFTS.

Optical microscopy was also used to observe the reaction between crystals of $Mn(CO)_4(PPh_3)Br$ and P(*p*-Me-$C_6H_4)_3$. In this reaction the ligand had a higher melting point than the metal complex. It was observed that the metal complex in contact with the ligand melted first while the isolated reagent crystals neither reacted nor melted. The

study further revealed that melting was a prerequisite for the reaction to take place, provided that the reactants were in contact. The reagent with the lower melting point was the one that melted to act as a fluid medium enabling diffusion of reactants and products to take place.

9.5. REFERENCES

1. W. F. Magie, *A Source Book in Physics*, McGraw Hill Book Co, New York, 1935.
2. G. Sarton, *A History of Science,* Vol 2, Harvard University Press, 1959.
3. G. L. Clark, *The Encyclopedia of Microscopy*, Reinhold Publishing Corporation, New York, 1961.
4. J. I. Goldstein, *Scanning Electron Microscopy and X-ray microanalysis*, Plenum Publishers, New York, 2003.
5. D. E. Bradley, *J. Roy. Micros. Soc*., 1956, **75**, 254.
6. K. Harris, *J. Gen. Microbiol.*, 1958, **19**, 55.
7. D. W. Fawcett and C. C. Selby, *J. Biophys. Biochem. Cytol*., 1958, **4**, 63.
8. F. S. Sjostrand, *Nature*, 1953, **171**, 30.
9. F. O. Schmitt, *Rev. Modern Phys.*, 1959, **31**, 455.
10. J. J. Comer and J. W. Turley, *J. Appl. Phys.,* 1955, **26**, 346.
11. K. Messner and E. Srebotnik, *FEMS Biol. Rev.,* 1994, **13**, 351.
12. N. D. P. Smith, *Trans. Inst. Met. Finish.*, 1955, **12**, 10.
13. E. Smith and J. Nutting, *Brit. J. Appl. Phys.,* 1956, **7**, 214.
14. G. Velarde, S. Ait-Aissa, C. Gillet, F. Rogerieux, C. Lambre, E. Vindimian and J. M. Porcher, *Toxicol. In Vitro*, 1999, **13**, 723.
15. R. A. Devilla, M. T. Brown, M. Donkin and J. W. Readman, *Aquatic Toxicol.*, 2005, **71**, 25.
16. K. de Clerck, P van Oostveldt, H. Rahier, B. van Mele, P Westbroek and P. Kiekens, *Polym.*, 2004, **45**, 4105.
17. V. A. Petrenko and I. B. Sorokulova, *J. Microbiol. Methods*, 2004, **58**, 147.
18. M. R. Montierth, R. S. Gordon and I. B. Cutler, *Mater. Sci. Res.,* 1969, **4**, 522.
19. V. Leute and R. Hornischer, *Berichte derBunsen-Gesellschaft,* 1976, **80**, 15.
20. G. G. T. Guarini, R. Spinicci and L. Virgili, *J. Therm. Anal.*, 1978, **13**, 263.
21. M.E. Brown, A.K. Galwey, M.A. Mohamed and H. Tanaka, *Thermochim. Acta,* 1994, **235**, 255.
22. A. K Galwey, S.A. Lyle and S.A.A. Mansour, *Thermochim. Acta*, 1994, **235**,239.

23. A.K. Galwey and S.A.A. Mansour**,** *Thermochim. Acta,* 1993, **228**, 379.
24. A.K. Galwey, S.A.A. Fakiha and K.M. Abd El-Salaam, *Thermochim. Acta,* 1992, **206**, 297.
25. A.K. Galwey, S.A.A. Fakiha and K.M. Abd El-Salaam, *Thermochim. Acta*, 1994, **239**, 225.
26. N.A. Baranov, V.B. Okhotnikov, L.I. Rynskaya, A.R. Semenov, A.K. Galwey and G.M. Laverty, *Solid State Ionics,* 1990, **43**, 37.
27. H. Tsuji and Y. Tezuka, *Biomacromolecules*, 2004, **5**, 1181.
28. G. V. Cave, C. L. Raston and J. L. Scott, *Chem. Commun.,* 2001, 2159.
29. L. Cheng and N. J. Coville, *J. Organomet. Chem.,* 1998, **571**, 149.
30. R. S. Bogadi, D. C. Levendis and N. J. Coville, *J. Am. Chem. Soc*., 2002, **124**, 1104
31. G. Kaupp, *Angew. Chem, Int. Ed.*, 1992, **31**, 592.
32. Canada's National Occupational Health and Safety Resources, www.cchos.ca.

CHAPTER 10: CRYSTALLOGRAPHIC STUDIES OF MANGANESE CARBONYL COMPOUNDS

10.1. INTRODUCTION

10.1.1. History and perspective

The word crystal has various meanings. Chemists define crystals as substances in which the atoms or molecules are closely packed together[1]. The molecules and atoms make up a highly ordered structure (crystal lattice) in which atoms are arranged in three dimensions. In crystallography, a crystal is defined as a solid that has a regularly repeating internal arrangement of atoms or molecules in three dimensions[2]. The internal regularity of a crystal is represented by a unit cell that is repeated continuously in three dimensions. Unit cells are considered building blocks of crystals.

All crystal structures may be described in terms of the unit cell and the atomic coordinates of the contents[3]. The structure of a crystal is determined by the size of its atoms or molecules and by the forces that hold them together. A molecule can be defined, in strictly geometrical terms, as a group of atoms in which the distance from any one atom to at least one other in the group is much smaller than any distance between atoms in different groups[4]. Interactions between molecules are assumed to be very weak and lacking in directionality. In this isotropic model, crystal structures are governed by close packing. The structure that makes the most economical use of space is the best one, and molecules crystallize so that the "bumps" in the surface of one fit into the "hollows" in the surface of the other.

The packing of molecules in crystals is a result of the compromise between different intermolecular interactions, the tendency towards close packing and symmetry

requirements[5]. All these factors influence each other to eventually determine the unique three-dimensional structure of a crystal.

Crystal structure analysis is typically based on the diffraction phenomenon caused by the interaction of matter with X-rays, electrons or neutrons[6]. X-rays are electromagnetic radiation with wavelengths is in the nanometre range. This radiation is useful because the wavelength is of the same order as that of distances between atoms, i.e., typically 1 - 3 Å. One of the prerequisites of the use of this method in elucidating crystal structure is the use of a suitable crystal[7].

Wilhelm Rontgen discovered X-rays in 1895[8]. Walther Friedrich, Paul Knipping and Max von Laue first demonstrated diffraction of X-rays by crystals in 1912[9]. X-ray diffraction by crystals represents the interference between X-rays scattered by the electrons in the atoms located in the unit cell. The reinforcement of the diffraction patterns made possible by the repeating unit cells in the crystal results in an observable effect. For example, Bragg in 1913 demonstrated that the measurement of the diffraction patterns gives information about electron density in the unit cell[10]. Some of the substances that were studied using this technique, in its infancy, include diamond[11], graphite[12], hexamethylbenzene[13] and anthracene[14]. As the techniques for structure determination by X-ray diffraction improved, molecules of greater complexity were studied. Examples include the study of vitamin B_{12}[15], myoglobin[16] and penicillin[17].

Most crystal structures can be characterised by four elements: (i) the size and shape of the unit cell, (ii) the space group of the atomic arrangement, (iii) the fractional coordinates of atoms and (iv) thermal ellipsoids of constant probability density. Parameters used to describe atomic arrangement are inter-atomic or bond distances, bond angles, coordination numbers, thermal ellipsoids, polyhedral volumes, polyhedral distortions and packing parameters.

10.1.2. Aims of the study

The aim of the study was to obtain X-ray crystal structure data of $Mn(CO)_4(PPh_3)Br$ [**3**] and $Mn(CO)_3(PPh_3)_2Br$ [**8**].

10.2. EXPERIMENTAL METHODS

A single crystal (0.40 × 0.40 × 0.31 mm^3) of **3** was placed at the end of a 0.3 mm Hilgenberg Mark capillary tube (Glass number 14, Lindemann-glass) and secured in position using a glass fibre. The glass fibre was then glued to the walls of the capillary and left to harden, undisturbed, for 2 h. The other crystal, **8** (0.38 × 0.22 × 0.12 mm^3), was mounted the same way. The mounted crystals were then secured, individually, to a brass-collar before moving them to a goniometer[18].

Intensity data were collected on a Bruker SMART 1K CCD area detector diffractometer with graphite monochromated Mo K_α radiation (50kV, 30mA). The collection method involved ω-scans of width 0.3°. Data reduction was carried out using the program *SAINT+* and face indexed absorption corrections were made using the program *XPREP*[19]. The crystal structure was solved by direct methods using *SHELXTL*[20]. Non-hydrogen atoms were first refined isotropically followed by anisotropic refinement by full matrix least-squares[21] calculations based on F^2 using *SHELXTL*. Hydrogen atoms were first located in the difference map then positioned geometrically and allowed to ride on their respective parent atoms. Diagrams and publication material were generated using SHELXTL and PLATON[22].

10.3. RESULTS AND DISCUSSION

Selected X-ray crystallographic data for $Mn(CO)_4(PPh_3)Br$ [**3**] and $Mn(CO)_3(PPh_3)_2Br$ [**8**] are shown in **Table 10.1**. The ORTEP diagrams of the two complexes are shown in **Figures 10.1** and **10.2** respectively. The crystal structures of both [**3**] and [**8**] were solved in the space group *P-1*.

As expected both structures revealed that the complexes had octahedral geometry. The first unit for [**3**] shows the bulky triphenylphosphine ligand occupying the axial axis *cis* to one of the carbonyl ligands (C4O4) (**Figures 10.1** and **10.2**). Due to π-back donation from the phosphine ligand, the Mn-C4 bond length [1.826(4) Å] is shorter than Mn-C1 [1.858(4) Å] and Mn-C3 [1.854(4) Å] bond lengths (**Table 10.1**). That the carbonyl ligand *trans* to Br ligand was tightly bound to the metal centre was highlighted by Mn-C2 bond length being shorter, 1.798(4) Å as expected. The value is similar to the literature value of 1.75 Å obtained for $Mn(CO)_4(PPh_3)Cl$ complex[23]. There was also significant π-back donation for the two CO ligands bonded *trans* to each other (Mn-C1 and Mn-C3) as evidenced by the longer M-C bonds compared to the rest. These bond length values are comparable to the value of 1.84 Å obtained for M-C bonds for *trans* carbonyl ligands in $Mn(CO)_4(PPh_3)Cl$ complex.

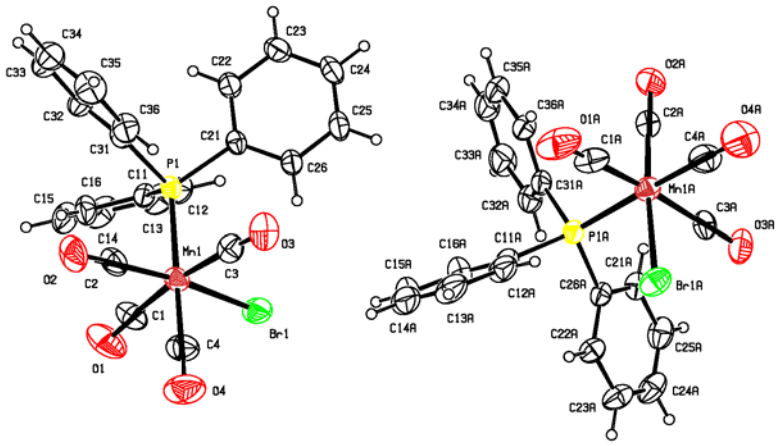

Figure 10.1. ORTEP diagram of $Mn(CO)_4(PPh_3)Br$ [**3**] depicting two units making up the unit cell with 30% probability thermal ellipsoid

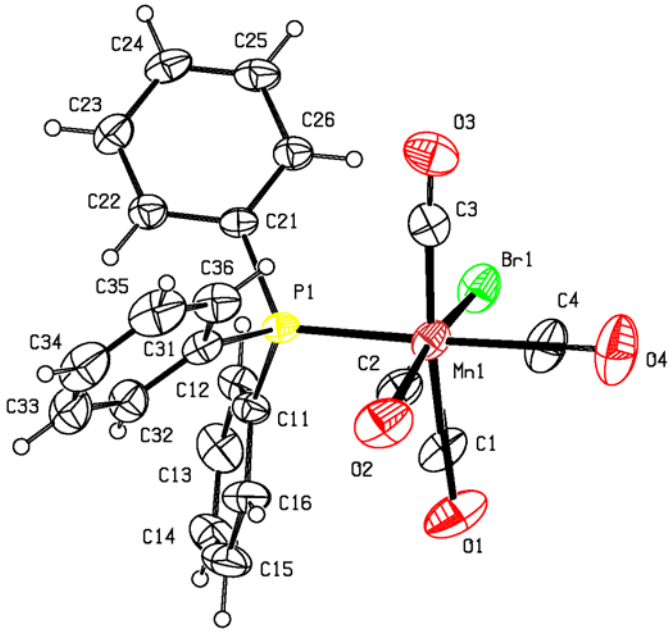

Figure 10.2. ORTEP diagram of $Mn(CO)_4(PPh_3)Br$ [**3**] depicting one of two units comprising the unit cell with 30% probability thermal ellipsoid

The second unit shows the phosphine ligand occupying the equatorial position (**Figures 10.1 and 10.3**). The placement of the two units ensures that minimum steric repulsion is attained and that maximum space is occupied.

Table 10.3 shows selected crystallographic structural data for **3** and **8**. That the complexes are related is demonstrated by similar unit cell parameters like Mn-Br bond length of 2.5252 Å for **3** and 2.5261 Å for **8**. The table also showed differences as well because of the presence of the additional bulky phosphine ligand in **8**. For instance, C1-Mn-C2 bond angles are different (92.14° for **3** and 86.11° for **8**).

Table 10.4 compares the crystallographic data for $C_{22}H_{15}BrMnO_4P$ [**3**] and $C_{22}H_{15}ClMnO_4P$. These two complexes crystallises in the same triclinic space group, *P-1*. The unit cell dimensions of $C_{22}H_{15}BrMnO_4P$ [**3**] are larger than those of $C_{22}H_{15}ClMnO_4P$. The softer and bulky bromo ligand also had a longer bond length [Mn-Br = 2.5252(6) Å] compared to Mn-Cl = 2.36 Å. In all the cases, the Mn-C bond lengths of $C_{22}H_{15}BrMnO_4P$ [**3**] were longer than those of $C_{22}H_{15}ClMnO_4P$. However, the Mn-P bond length of $C_{22}H_{15}BrMnO_4P$ (2.3670 Å) was shorter than that of $C_{22}H_{15}ClMnO_4P$ (2.40 Å).

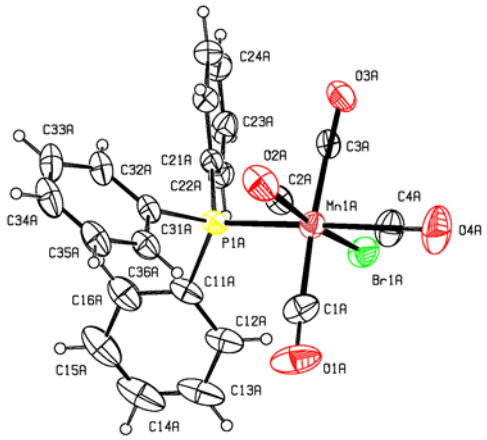

Figure 10.3. ORTEP diagram of $Mn(CO)_4(PPh_3)Br$ [**3**] depicting the other unit of the unit cell with 30% probability thermal ellipsoid

In terms of reactivity, one of Mn-C1 or Mn-C3 bonds is expected to be broken during the substitution reaction. The resulting substitution reaction led to the metal holding tightly onto the remaining carbonyl ligands demonstrated by the shortened Mn-C for all the carbonyls in **8** (See **Table 10.1**). The bulky triphenylphosphine ligand is accommodated in the octahedral sphere but distortion is evidenced by the bond angles not truly being those of a perfect octahedron [**8**] (see **Table 10.2** and **Figure 10.4**).

Table 10.5 compares the crystal data for $C_{39}H_{30}BrMnO_3P_2$ [**8**] and $C_{39}H_{24}BrCl_6MnO_3P_2.CHCl_3$[24]. The latter complex contain a *tri*(4-chlorophenyl)phoshine ligand rather than triphenylphosphine ligand [**8**]. In addition, the crystal structure incorporated a chloroform solvent per molecule. The complex, [**8**] crystallised in the triclinic space group *P-1* while $C_{39}H_{24}BrCl_6MnO_3P_2.CHCl_3$ crystallised in a monoclinic *P2/n* space group. The difference here is most likely influenced by the solvent.

The unit cell dimensions of $C_{39}H_{30}BrMnO_3P_2$ were much smaller than those of $C_{39}H_{24}BrCl_6MnO_3P_2.CHCl_3$ (see **Table 10.5**). Bond lengths and angles of the two complexes were comparable; Mn-P1 was 2.3333 Å for $C_{39}H_{30}BrMnO_3P_2$ and 2.3660 Å for $C_{39}H_{24}BrCl_6MnO_3P_2.CHCl_3$, P1-Mn-P2 angle was 176.61° for and 178.01° for $C_{39}H_{24}BrCl_6MnO_3P_2.CHCl_3$.

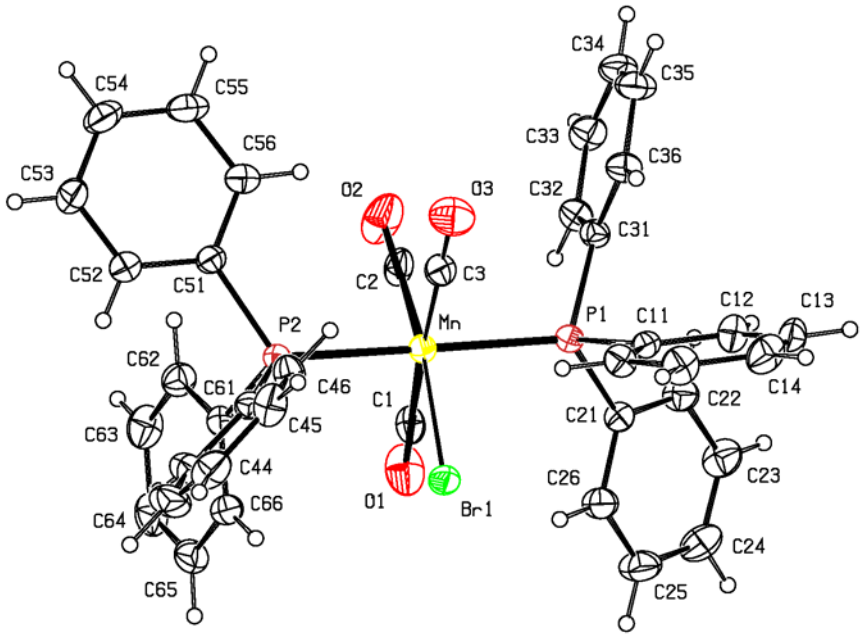

Figure 10.4. ORTEP diagram of $Mn(CO)_3(PPh_3)_2Br$ [**8**] with 30% probability thermal ellipsoid

10.4. CONCLUSIONS

The crystal structures of [**3**] and [**8**] were successfully determined by X-ray diffraction techniques. Both complexes crystallized in the *P-1* space group. The former complex contained four units per unit cell while the latter had two. Accommodation of the bulky triphenylphosphine ligand on the octahedral sphere caused distortion as evidenced by the bond angles being not truly those of a perfect octahedron. X-ray crystallographic data for $C_{22}H_{15}BrMnO_4P$ [**3**] was comparable to the data for $C_{22}H_{15}ClMnO_4P$.

10.5. APPENDIX

Table 10.1. Crystal data and structure refinement for **3**

Identification code	**3**	
Empirical formula	$C_{22}H_{15}BrMnO_4P$	
Formula weight	509.16	
Temperature	293(2) K	
Wavelength	0.71073 Å	
Crystal system	Triclinic	
Space group	P-1	
Unit cell dimensions	a = 10.5146(16) Å	α = 92.516(3)°.
	b = 14.165(2) Å	β = 99.213(3)°.
	c = 15.137(2) Å	γ = 99.818(3)°.
Volume	2186.9(5) $Å^3$	
Z	4	
Density (calculated)	1.546 Mg/m^3	
Absorption coefficient	2.528 mm^{-1}	
F(000)	1016	
Crystal size	0.40 x 0.40 x 0.31 mm^3	
Theta range for data collection	1.37 to 27.00°.	
Index ranges	-13<=h<=13, -18<=k<=18, -19<=l<=19	
Reflections collected	26186	
Independent reflections	9511 [R(int) = 0.0693]	
Completeness to theta = 27.00°	99.5 %	
Absorption correction	Integration	
Max. and min. transmission	0.5079 and 0.4312	
Refinement method	Full-matrix least-squares on F^2	
Data / restraints / parameters	9511 / 0 / 524	
Goodness-of-fit on F^2	1.024	

Final R indices [I>2sigma(I)]	R1 = 0.0385, wR2 = 0.0988
R indices (all data)	R1 = 0.0634, wR2 = 0.1111
Extinction coefficient	0.0142(6)
Largest diff. peak and hole	0.991 and -0.679 e.Å^{-3}

Table 10.2. Crystal data and structure refinement for **8**

Identification code	**8**	
Empirical formula	$C_{39}H_{30}BrMnO_3P_2$	
Formula weight	743.42	
Temperature	293(2) K	
Wavelength	0.71073 Å	
Crystal system	Triclinic	
Space group	P-1	
Unit cell dimensions	a = 10.2876(17) Å	α = 96.683(3)°.
	b = 12.373(2) Å	β = 104.350(3)°.
	c = 14.518(2) Å	γ = 105.715(3)°.
Volume	1689.7(5) Å^3	
Z	2	
Density (calculated)	1.461 Mg/m^3	
Absorption coefficient	1.705 mm^{-1}	
F(000)	756	
Crystal size	0.38 x 0.22 x 0.12 mm^3	
Theta range for data collection	1.48 to 27.00°.	
Index ranges	-13<=h<=13, -15<=k<=15, -18<=l<=18	
Reflections collected	20115	
Independent reflections	7345 [R(int) = 0.0434]	
Completeness to theta = 27.00°	99.5 %	
Absorption correction	Integration	
Max. and min. transmission	0.8216 and 0.5635	
Refinement method	Full-matrix least-squares on F^2	

Data / restraints / parameters	7345 / 13 / 443
Goodness-of-fit on F^2	1.025
Final R indices [I>2sigma(I)]	R1 = 0.0344, wR2 = 0.0777
R indices (all data)	R1 = 0.0589, wR2 = 0.0852
Largest diff. peak and hole	0.384 and -0.258 e.$Å^{-3}$

Table 10.3. Selected crystallographic structural data for **3** and **8**

Parameter	Complex **3**	Complex **8**
Bond Lengths (Å)		
Mn-Br		
Mn-Br(1B)	-	2.4716(15)
Mn-Br(1)	2.5252(6)	2.5261(10)
Mn-P		
Mn-P(1)	2.3670(9)	2.3331(7)
Mn-P(2)	-	2.3401(7)
Mn-CO		
Mn-C(1)	1.858(4)	1.822(3)
Mn-C(2)	1.798(4)	1.800(2)
Mn-C(3)	1.854(4)	1.838(5)
Mn-C(4)	1.826(4)	-
Mn-C(3B)	-	1.827(9)
C≡O		
C(1)-O(1)	1.116(5)	1.136(3)
C(2)-O(2)	1.139(4)	1.141(3)
C(3)-O(3)	1.138(4)	1.182(7)
C(3B)-O(3B)	-	1.174(11)
C(4)-O(4)	1.134(5)	-
Bond Angles (°)		
C(2)-Mn-C(1)	92.14(17)	86.11(12)
C(2)-Mn-C(3)	95.41(15)	93.0(2)
C(2)-Mn-C(4)	88.77(17)	-

C(1)-Mn-C(3)	171.92(16)	176.8(2)
C(1)-Mn-C(4)	89.6(2)	-
C(3)-Mn-C(4)	87.73(19)	-
C(1)-Mn-P(1)	92.69(13)	90.65(7)
C(2)-Mn-P(1)	90.95(12)	92.03(7)
C(3)-Mn-P(1)	90.06(11)	86.3(2)
C(4)-Mn-P(1)	177.74(15)	-
C(1)-Mn-P(2)	-	92.22(7)
C(2)-Mn-P(2)	-	89.97(7)
C(3)-Mn-P(2)	-	90.8(2)
C(1)-Mn-Br(1)	81.53(13)	85.11(8)
C(2)-Mn-Br(1)	173.59(12)	170.63(9)
C(3)-Mn-Br(1)	90.86(10)	95.9(2)
C(4)-Mn-Br(1)	90.13(12)	-
P(1)-Mn-Br(1)	90.41(2)	91.33(2)
P(2)-Mn-Br(1)	-	87.12(2)
P(1)-Mn-P(2)	-	176.61(2)

Table 10.4. Comparison of the crystal data for $C_{22}H_{15}BrMnO_4P$ and $C_{22}H_{15}ClMnO_4P$

Empirical formula	$C_{22}H_{15}BrMnO_4P$	$C_{22}H_{15}ClMnO_4P$
Formula weight	509.16	464.71
Temperature	293(2) K	293 K
Crystal system	Triclinic	Triclinic
Space group	P-1	P-1
a (Å)	10.5146(16)	9.970
b (Å)	14.165(2)	11.765
c (Å)	15.137(2)	9.636
α (°)	92.516(3)	92.04
β (°)	99.213(3)	96. 71
γ (°)	99.818(3)	73.22

Z	4	2
D_{calc} (Mg/m^3)	1.546	1.43
Bond Lengths (Å)		
Mn-X(1), X= Br or Cl	2.5252(6)	2.36
Mn-P(1)	2.3670(9)	2.40
Mn-C(1)	1.858(4)	1.84
Mn-C(2)	1.798(4)	1.75
Mn-C(3)	1.854(4)	1.84
Mn-C(4)	1.826(4)	1.75

Table 10.5. Comparison of the crystal data for $C_{39}H_{30}BrMnO_3P_2$ and $C_{39}H_{24}BrCl_6MnO_3P_2.CHCl_3$

Empirical formula	$C_{39}H_{30}BrMnO_3P_2$	$C_{39}H_{24}BrCl_6MnO_3P_2.CHCl_3$
Formula weight	743.42	1069.44
Temperature	293(2) K	293
Wavelength	0.71073 Å	
Crystal system	Triclinic	Monoclinic
Space group	P-1	P2/n
a (Å)	10.2876(17)	15.364(3)
b (Å)	12.373(2)	14.099(2)
c (Å)	14.518(2)	20.536(5)
α (°)	96.683(3)	90.0
β (°)	104.350(3)	103.947(10)
γ (°)	105.715(3)	90.0
Volume ($Å^3$)	1689.7(5)	4317.19(15)
Z	2	4
D_{calc} (Mg/m^3)	1.461	1.645
Absorption coefficient	1.705 mm^{-1}	1.901
Crystal size (mm)	0.38 × 0.22 × 0.12	0.3 × 0.2 × 0.2

R indices (all data) R_1, wR_2	0.0589, 0.0852	0.0742, 0.1513
Bond lengths (Å)		
Mn-Br(1)	2.5261(10)	2.5458(7)
Mn-P(1)	2.3331(7)	2.3260(11)
Mn-P(2)	2.3401(7)	2.3275(10)
Mn-C(1)	1.822(3)	1.7986(8)
Mn-C(2)	1.800(2)	1.7086(7)
Mn-C(3)	1.838(5)	1.804(4)
Bond angles (°)		
C(2)-Mn-C(1)	86.11(12)	85.58(17)
C(2)-Mn-C(3)	93.0(2)	85.66(17)
C(1)-Mn-C(3)	176.8(2)	171.03(8)
C(1)-Mn-P(1)	90.65(7)	89.82(12)
C(2)-Mn-P(1)	92.03(7)	91.27(13)
C(3)-Mn-P(1)	86.3(2)	88.41(12)
C(1)-Mn-Br(1)	85.11(8)	94.76(8)
C(2)-Mn-Br(1)	170.63(9)	178.87(12)
C(3)-Mn-Br(1)	95.9(2)	94.03(7)
P(1)-Mn-Br(1)	91.33(2)	89.82(3)
P(2)-Mn-Br(1)	91.33(2)	88.21(3)
P(1)-Mn-P(2)	176.61(2)	178.01(4)

10.6. REFERENCES

1. D. M. Blow, *Outline of Crystallography for Biologists*, Oxford University Press, New York, 2002.
2. J. P. Glusker, M. Lewis and M. Rossi, *Crystal Structure Analysis for Chemists and Biologists*, VCH Publishers, Inc, New York, 1994.
3. C. Hammond, *The Basic of Crystallography and Diffraction*, Oxford University Press, New York, 2001.
4. A. I. Kitaigorodskii, *Molecular Crystals and Molecules*, Academic Press, New York, 1973.
5. M. Kubicki, *J. Mol. Struct.,* 2005, **743**, 209.
6. R. Steadman, Crystallography, Van Nostrand Reinhold Press, New York, 1982.
7. R. Chang, *Physical Chemistry with Application to Biological Systems*, 2nd Ed, Collier Macmillan Publishers, London, 1981.
8. A. Stanton, *Science*, 1896, **3**, 227.
9. J. J. Stezowski, *Structural Crystallography in Chemistry and Biology*, Hutchinson and Ross, Stroudsburg, PA, 1981.
10. W. L. Bragg, *Proc. Roy. Soc (London).,* 1913, **A89**, 248.
11. W. H. Bragg and W. L. Bragg, *Nature,* 1913, **91**, 557.
12. J. D. Bernal, *Proc. Roy. Soc (London).,* 1924, **A106**, 749.
13. K. Lonsdale, *Nature*, 1928, **122**, 810.
14. W. H. Bragg, *Proc. Phys. Soc (London)*., 1922, **35**, 167.
15. D. C. Hodgkin, J. Pickworth, J. H. Robertson, K. N. Trueblood, R. J. Prosen and J. G. White, *Nature,* 1955, **176**, 325.
16. J. C. Kendrew, R. E. Dickerson, B. E. Strandberg, R. G. Hart and D. R. Davies, *Nature,* 1960, **185**, 422.
17. H. T. Clarke, J. R. Johnson and R. Robinson, *The Chemistry of Penicillin*, Princeton University Press, Princeton, 1949.
18. W. H. Wollaston, *Phil. Trans. Roy. Soc (London).,* 1809, **99**, 253.
19. Bruker *SAINT*+. Version 6.02 (includes XPREP and SADABS). Bruker

AXS Inc., Madison, Wisconsin, USA, 1999.

20. Bruker SHELXTL. Version 5.1. (includes XS, XL, XP, XSHELL) Bruker AXS Inc., Madison, Wisconsin, USA, 1999.
21. D. Sayre, *Computational Crystallography*, Clarendon Press, Oxford, 1982.
22. A. L. Spek, *J. Appl. Crystallogr.*, 2003, **36**, 7.
23. V. Heinrich, *Chem. Ber.*, 1971, **104**, 449.
24. M. A. Beckett, D. S. Brassington, S. J. Coles, T. Gelbrich, M. E. Light and M. B. Hursthouse, *J. Organomet. Chem.,* 2003, **688**, 174.

CHAPTER 11: SOLVENTLESS ZIRCONIUM CARBOXYLATE CHEMISTRY

11.1. INTRODUCTION

11.1.1. Historical perspective

Metal carboxylates are a group of compounds derived from an association of a metal-centre with a carboxylate group. The bonding occurs through one or two of the oxygen atoms to the metal centre (See below). These complexes differ from related compounds such as metal alkoxides and metal β-diketonates due to the different bonding modes generated by the presence of the carboxylate ligand ($RCOO^-$). The carboxylate ligand is a common ligand found in many transition metal complexes and it binds to a variety of metals displaying characteristic distinctive structural motifs (see below)[1].

Metal carboxylates have been known and applied in many areas of daily life from time immemorial. Alkali metal carboxylates were prepared by ancient German tribesmen around 100-44 BC[2] as soaps for daily washing. Lubricating properties of metallic soaps were also recognised much earlier (1400 BC) when lime soaps were used to lubricate chariot wheels in Egypt.

Today metal carboxylates find applications in various fields. Their applications depend largely on their physical state, stability, volatility, solubility and chemical reactivity. Metal carboxylates with moderate stability and high lability are used as homogeneous catalysts for commercial synthesis of numerous organic compounds. For example, a palladium(II) acetate trimer has been successfully used to synthesise vinyl acetates from ethylene and acetic acid[3]. Other metal carboxylates are used in soap, textile, paper, cement, petroleum, paint, varnish, pharmaceutical, and PVC industries[4]. Dirhodium tetracarboxylate complexes exhibit catalytic[5] and antitumor[6,7] activities.

Metal-Carboxylate bonding modes

The carboxylate ligand, $RCOO^-$, has properties influenced by the nature of the R group. Further the $RCOO^-$ ligand can bind through one or two oxygen atoms to a metal atom or ion[8]. This feature results in the formation of many coordination compounds due to the ability of the carboxylate ion to adopt various coordination modes[9]. The carboxylate anion can act as a counter anion or can bind covalently to the metal in monodentate, chelating (bidentate) and bridging modes. The wide variety of available groups (where R could be H, alkyl, aryl etc) also adds to the versatility of the ligand, thus producing different compounds.

The carboxylates of highly electropositive elements like sodium and potassium are reported to be ionic in nature. For example, the formate ion interacts with Na^+ as shown in **Figure 11.1**.

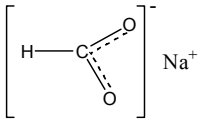

Figure 11.1. Ionic sodium formate displaying the uncoordinated carboxylate ligand

In metal carboxylates like the lithium acetate dihydrate complex, $Li(O_2CCH_3).2H_2O$, the carboxylate exhibits the monodentate bonding mode as shown in **Figure 11.2**.

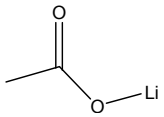

Figure 11.2. Structure of lithium acetate displaying the monodentate bonding mode of the carboxylate ligand

The carboxylate ligand can also covalently bind to metal centres and generate complexes with bidentate chelating bonding modes. **Figure 11.3** depicts the symmetrical and unsymmetrical chelating bonding modes of the $RCOO^-$ unit to Zn and Sn ions.

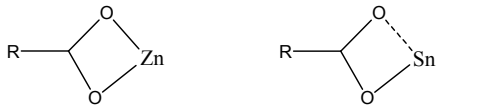

Figure 11.3. The two types of bidentate bridging modes exhibited by inorganic compounds containing the carboxylate ligand

The carboxylate ligand can also display bidentate bridging modes to two metal ions/atoms as shown in **Figure 11.4**. Both oxygen atoms of the carboxylate moiety are involved in forming carboxylate-metal interactions. The *syn-syn* geometry brings the metals close enough to form clusters with metal-metal bonds. The *anti-anti* and *anti-syn* geometries yield polymeric structures. All these bonding motifs result in the formation of different compounds with many industrial applications. Thus a study or organometallic reactions utilising the ligand is desirable.

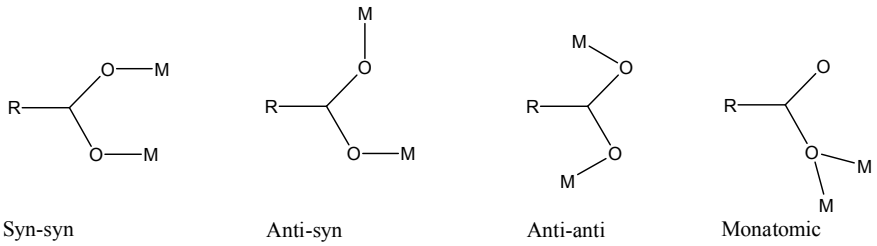

Figure 11.4. The four types of bidentate bridging modes exhibited by inorganic compounds containing the carboxylate ligand

Literature methods reported for the synthesis of metal carboxylates[10]

Metal carboxylates may be prepared by the reaction of aqueous or alcoholic solutions of various metal salts with stoichiometric amounts of sodium, potassium or ammonium carboxylates via an exchange reaction.

$$MX_n + nRCO_2M' \rightarrow M(O_2CR)_n + nM'X$$

(where M = metal of choice, eg Zr; M' = Na, K, NH_4; X = Cl, NO_3, SO_4 etc)

Another general methodology involves the reaction of the carboxylate in a non-aqueous medium like benzene, particularly for moisture sensitive metal complexes. Here, carboxylic acids are reacted with electropositive metals like sodium, potassium, caesium and rubidium to form the metallic salts of the acids.

$$2M + 2RCO_2H \rightarrow 2M(O_2CR) + H_2$$

(where M = Na, K, Rb, Cs)

In line with the theme of the thesis we wished to evaluate the possibility of synthesising metal complexes via the solventless reaction methodology described in earlier chapters. The example chosen was the reaction of the readily available zirconocene dichloride with solid aryl carboxylate ligands to yield zirconium carboxylate compounds. The objective was not to carry out a comprehensive study but to demonstrate the feasibility of a solventless transformation reaction for this class of reagents. The data were compared with equivalent reactions reported previously in the literature.

The chemistry, electronic structure and molecular geometries of bis(cyclopentadienyl) transition metal complexes, $(\eta^5\text{-}C_5H_5)_2ML_n$, are well documented in the literature[10,11]. Most of these are 4 four-coordinate, 16 electron complexes[12]. The structures of the less common five-coordinate complexes, $(\eta^5\text{-}C_5H_5)_2ML_3$, containing a bidentate (chelating) ligand have also been studied using XRD diffraction[13,14]. This study focused on expanding knowledge in the field by studying zirconium carboxylates in the solid-state.

11.1.2. Aims of the study

(i) Synthesise sodium aryl carboxylates using sodium metal and substituted benzoic acids

(ii) Synthesise zirconium carboxylates using zirconocenes dichloride with sodium aryl carboxylates in the absence of solvents

(iii) Follow the kinetics of the reaction using FTIRS and DRIFTS

(iv) Study the reaction microscopically using optical microscopy with the view of obtaining information on the mechanism of the reaction

11.2. EXPERIMENTAL

11.2.1. Synthesis of sodium benzoates[15]

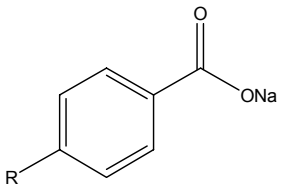

Figure 11.5. Structure of sodium benzoate [R = C_6H_5 (**a**), *p*-C_6H_4-NO_2 (**b**), *p*-C_6H_4-NH_2 (**c**)] used for the synthesis of zirconium carboxylate complexes

Lumps of sodium metal (1.0 g, 0.043 mol, 1.05 mol equiv) were allowed to react with absolute ethanol (50 cm^3) for an hour to generate sodium ethoxide at room temperature. The solution was then cooled to 0°C and benzoic acid (5.0 g, 0.041 mol), dissolved in absolute ethanol (30 cm^3), was then added dropwise to the sodium ethoxide for 30 min. The resulting suspension was allowed to react for 4 h at room temperature. The solvent was then removed *in vacuo* to leave behind a white powder. The powder was then dried overnight under suction at 70°C. The desired product (**Figure 11.5a**) was obtained as a white powder (5.87 g, 99% yield) and stored in a glove box. Similarly, 4-nitrobenzoic

acid (7.0 g, 0.0419 mol) was reacted with sodium (1.01 g, 0.044 mol, 1.05 mol equiv) in absolute ethanol (80cm^3) to obtain (7.92g, 99% yield) of the corresponding benzoate (**Figure 11.5b**) as white powder. The reaction of 4-aminobenzoicacid (6.0 g, 0.0437 mol), with sodium (1.06 g, 0.0459 mol, 1.05 mol equiv) in absolute ethanol (80 cm^3) yielded the corresponding benzoate (6.96 g, 99%yield), **Figure 11.5c**, also as a white powder. No characterisation of the sodium benzoates was made except to check for unreacted benzoic acid and solvent (ethanol) using ^{1}H NMR spectroscopy.

11.2.2. Synthesis of (η^5-C_5H_5)$_2$ZrCl(RCOO), [R = C_6H_5 (14), *p*-C_6H_4-NO_2 (15), *p*-C_6H_4-NH_2 (16)]

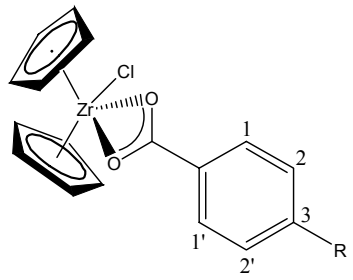

Figure 11.6. Structure of (η^5-C_5H_5)$_2$ZrCl(RCOO), R = C_6H_5, *p*-C_6H_4-NO_2, *p*-C_6H_4-NH_2

Zirconocene dichloride (100 mg, 0.342 mmol) was ground with sodium chloride (200 mg) to obtain a fine white powder in a glove box. Sodium benzoate (49.3 mg, 0.342 mmol, 1 mol equiv) was also ground with sodium chloride (200 mg) to obtain a homogeneous powder inside a glove box. The two powders were placed a 10 cm^3 test tube that was then sealed with a rubber septum. The test tube was placed in a larger reaction tube (about 40 cm in length), and the outer tube attached to a rotary evaporator. The mixture was then allowed to react under rotary motion (150 rpm) for 3 min at room temperature. The sample was then dissolved in dry deuterated chloroform and the reaction contents analysed using ^{1}H NMR spectroscopy. The presence of **14** was demonstrated, δ_H (400 MHz, $CDCl_3$) 6.30 (10H, s, 2 × Cp-), 7.47 (2H, m, Ar2-H, and

Ar2′-H), 7.56 (1H, m, Ar3-H) 8.05 (2H, dd, *J* 8.2 Hz and 0.8 Hz, Ar1-H, and Ar1′-H). The NMR spectrum is shown in **Figure11.7**. No optimisation studies were performed.

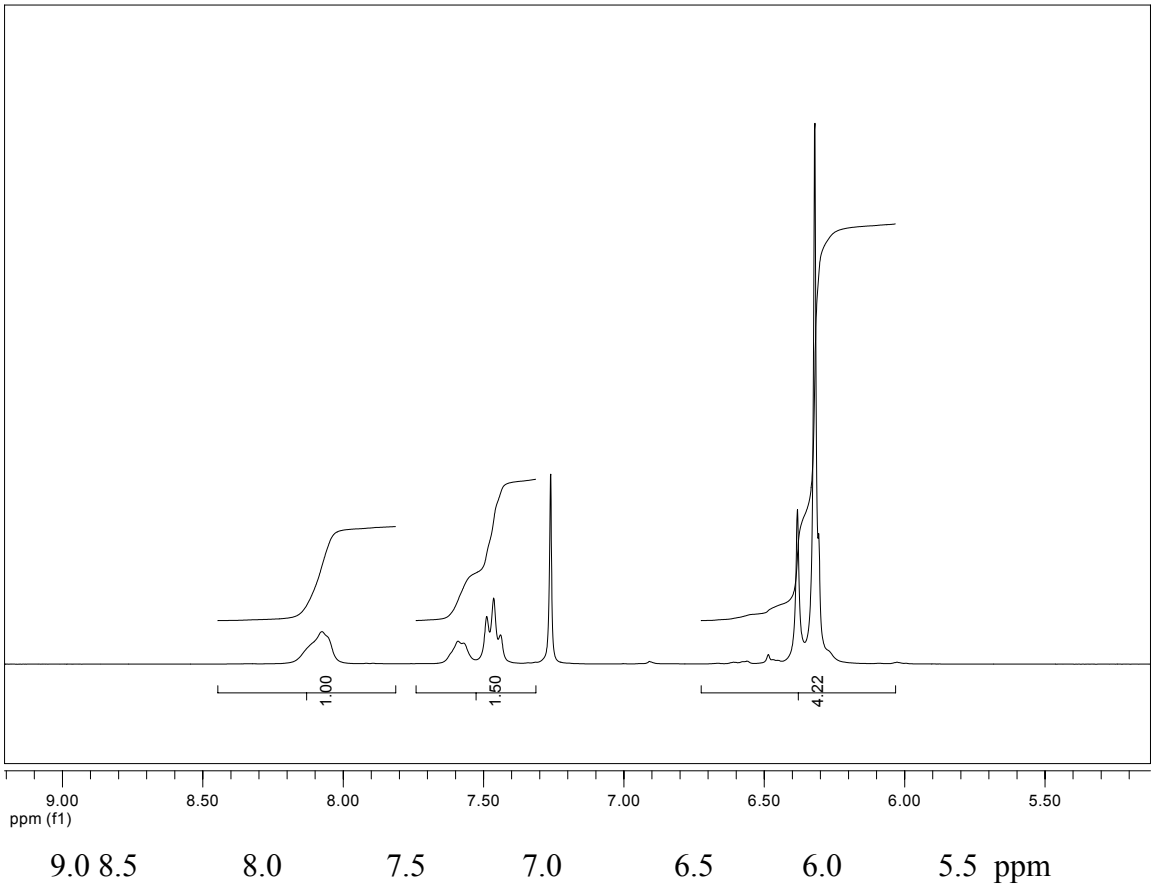

Figure 11.7. ^{1}H NMR spectrum of $(\eta^{5}\text{-}C_5H_5)_2ZrCl(C_6H_5\text{-}COO)$

The product consisted of a mixture of reactants and products. No purification or optimisation studies were performed. The reactant to product ratio was determined by ^{1}H NMR spectroscopy and was used to deduce the reaction extent. The same procedure was followed for the other substituted sodium carboxylates that were reacted with zirconocene dichloride. Amino carboxylate product, **15**; ^{1}H NMR data, δ_H (400 MHz, C_6D_6) 4.03 (2H, s, $-NH_2$), 6.35 (10H, s, 2 × -Cp), 6.68 (2H, d, *J* 8.1 Hz, Ar2-H, and Ar2′-H), 8.05 (2H, d, *J* 8.1 Hz, Ar1-H, and Ar1′-H). The nitro carboxylate product, **16**, was synthesised in a similar fashion; δ_H (400 MHz, C_6D_6), 6.39 (10H, s, 2 × -Cp), 7.49 (2H, d, *J* 8.1Hz, Ar2-H, and Ar2′-H), 8.08 (2H, d, *J* 8.1 Hz, Ar1-H, and Ar1′-H).

11.3. SINGLE CRYSTAL STUDIES

For crystal structure analysis, the reaction was conducted using 500 mg of zirconocene dichloride. At the end of the reaction, the reaction product was taken up in toluene (10 cm^3) and the solvent reduced to about 3 cm^3 before the addition of an equal volume of hexane and the solution placed in a freezer (-30°C) for 5 d. This yielded crystals good enough for single crystal studies. Single crystal XRD analysis was conducted as outlined in **Chapter 3**. In brief, intensity data were collected on a Bruker SMART 1K CCD area detector diffractometer with graphite monochromated Mo K_α radiation (50kV, 30mA). The collection method involved ω-scans of width 0.3°. Data reduction was carried out using the program *SAINT+*[16] and face indexed absorption corrections were made using the program *XPREP*. The crystal structure was solved by direct methods using *SHELXTL*[17]. Diagrams and publication material were generated using SHELXTL and PLATON[18].

11.4. RESULTS AND DISCUSION

11.4.1. Synthesis of sodium benzoates

The reaction of sodium metal with the substituted benzoic acids took place readily. The yields of the sodium benzoates synthesised were all near quantitative (99% based on the substituted benzoic acid used) (**Scheme 11.1**). ^{1}H NMR spectroscopy showed the absence of the starting material and complete removal of the solvent (ethanol) after prolonged drying at 70°C. The benzoates were insoluble in the solvent used. They were all white to pale yellow solids. They were all ground to fine powders (120-150 μm particle size) inside a glove box and stored for further experimentation.

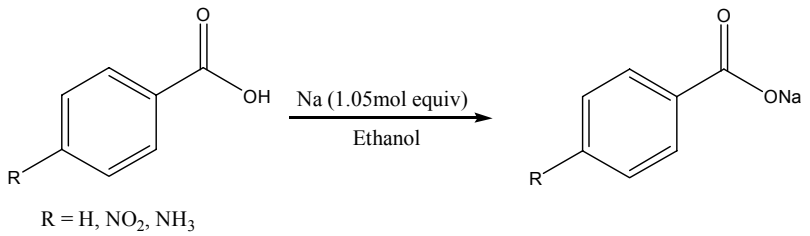

R = H, NO_2, NH_3

Scheme 11.1. Synthesis of sodium carboxylates by the reaction of substituted benzoic acids with sodium metal lumps in ethanol

11.4.2. Synthesis of zirconium carboxylates

The reaction between zirconocene dichloride and sodium benzoate in a NaCl matrix was found to be very facile. The formation of **14** (>80%) was observed for reactions that were conducted for 3 min under rotary motion (120 rpm) (**Scheme 11.2**). The reaction was so fast that even when the sodium carboxylate with a ring deactivating substituent (**Figure 11.5b**) was used, it was near complete after 3 min (>70% yield under rotary motion). The implication of the finding was that a simple kinetic study of the reaction system was not possible. When the reaction between zirconocene and sodium benzoate was conducted for 30 min, about 80% conversion was observed. Similarly for times exceeding two h the amount of product formed never changed much (~80%). Repeated investigation using the same reaction conditions showed that the reaction was independent of reaction time. One of two possible explanations accounted for the anomaly (i) either the solventless reaction took place as envisaged and was near complete after few min, or (ii) reaction took place in the NMR solvent. The latter was found to be the more logical explanation. This contrasted with literature results that showed slower reaction times (at least 10 h)[15,19]. While the preliminary results had indicated that the reaction appeared to occur in the absence of solvents a repeat of the reaction data revealed that the reaction was in fact a facile reaction in solution. This result is disappointing but is consistent with expectation of solventless reactions – no melt was observed or detected.

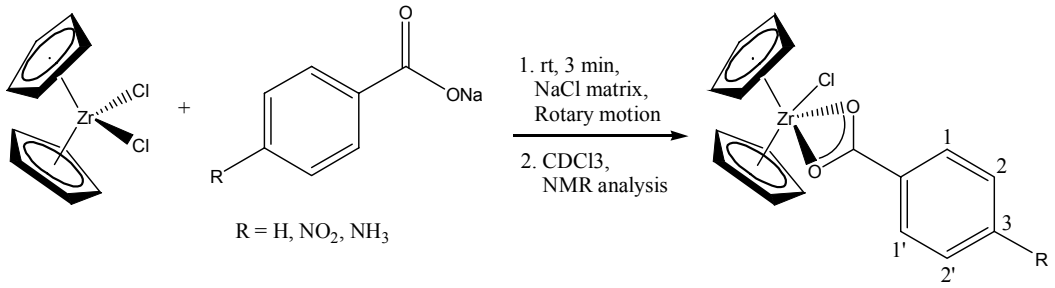

Scheme 11.2. Synthesis of carboxylatochlorobis(cyclopentadienyl)zirconium(IV) complexes

11.4.3. Single crystal analysis

Crystals of both **14** and **15** were obtained and analysed using the single crystal XRD technique. Selected structural parameters for **14** and **15** are shown in **Table 11.1.** The ORTEP diagrams of the two complexes are shown in **Figures 11.8 – 11.11**. From the diagrams it is clear that the molecules adopted a five-coordinate bent metallocene geometry such that the zirconium atom is attached to one chlorine atom, two symmetrically bound η^5-cyclopentadienyl ligands and a bidentate aryloxy ligand. The cyclopentadienyl rings were coordinated in a staggered conformation to minimize steric strain.

Table 11.1. Selected crystallographic structural data for **14** and **15**

Parameter		**14**	**15**
Bond Lengths (Å)			
Zr-Cl	Zr(1)-Cl(1)	2.5313(8)	2.5541(8)
Zr-C_{Cp}	Zr(1)-C(1)	2.517(2)	2.509(3)
	Zr(1)-C(2)	2.510(2)	2.528(3)
	Zr(1)-C(3)	2.523(2)	2.525(3)
	Zr(1)-C(4)	2.504(2)	2.519(3)
	Zr(1)-C(5)	2.525(2)	2.510(5)
Zr-O	Zr-O1	2.2546(19)	2.2947(18)

	Zr-O2	2.307(2)	2.2312(17)
C-O (carboxylato)	C-O1	1.265(3	1.276(3)
	C-O2	1.267(3)	1.275(3)
Bond Angles (°)			
Cl-Zr-O	Cl-Zr-O1		
	Cl-Zr-O2		
O1-Zr-O2	O1-Zr-O2	56.66(7)	57.50(6)
Cp-Zr-Cp	C1-Zr-C1a	158.24(13)	142.58(15)
	C1-Zr-C2a	134.00(9)	121.84(11)
	C1-Zr-C3a	126.84(8)	124.25(12)
	C1-Zr-C4a	140.78(9)	148.59(17)
	C1-Zr-C5a	169.77(10)	175.28(15)
O1-C-O2	O1-C-O2	117.6(2)	117.2(2)

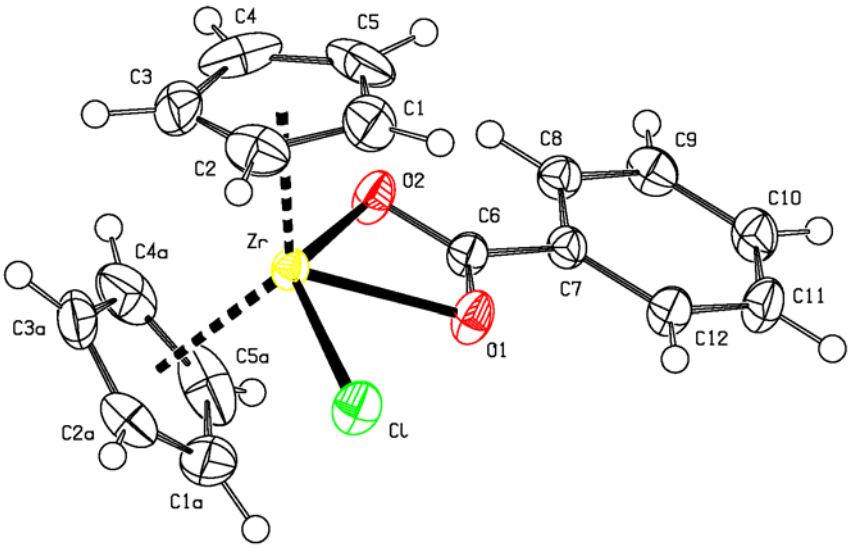

Figure 11.8. An ORTEP diagram of $(\eta^5\text{-}C_5H_5)_2ZrCl(C_6H_5\text{-}COO)$, **14**, showing one unit of 4 that makes up the unit cell

Complex **14** crystallised in an orthorhombic crystal system (space group Pnma) while **15** crystallised in monoclinic system (space group $P2_1/c$) (See **Tables 11.2** and **11.3**). The former had four units per unit cell while the latter had eight. Invariably, the unit cell dimensions of the latter were larger. The density, however, was found to be very similar, 1.635g/cm^3 and 1.634g/cm^3 for **14** and **15** respectively.

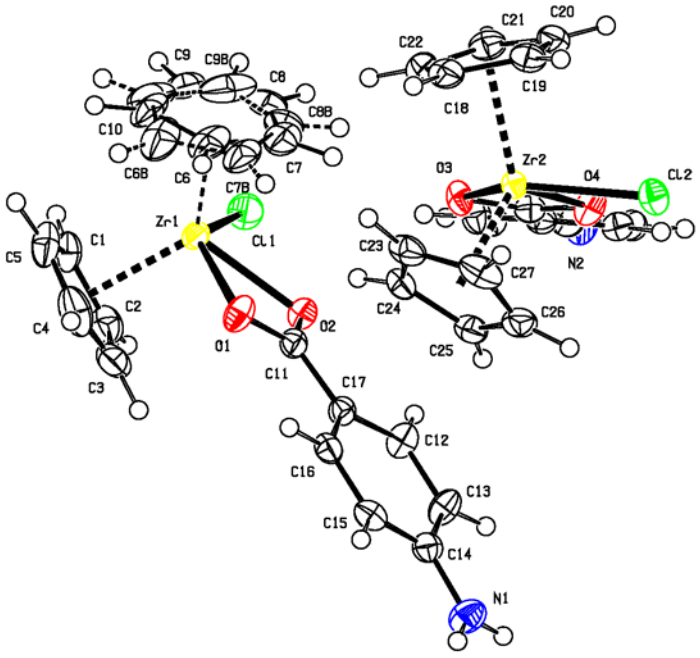

Figure 11.9. An ORTEP diagram of $(\eta^5\text{-}C_5H_5)_2ZrCl(RCOO)$, R = *p*-$C_6H_4$-$NO_2$, **15**, showing the positioning of two of 8 units that made up unit cell

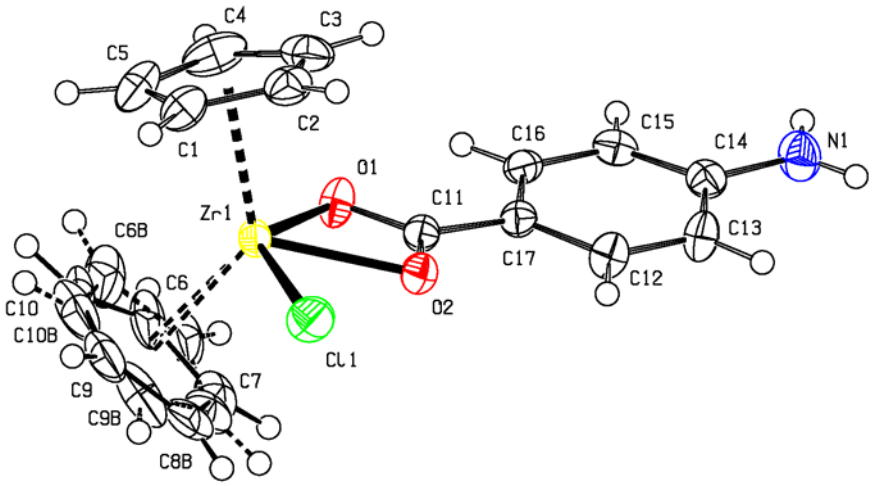

Figure 11.10. An ORTEP diagram of $(\eta^5\text{-}C_5H_5)_2ZrCl(RCOO)$, R = *p*-$C_6H_4$-$NO_2$, **15**, showing one of 8 units that made up unit cell

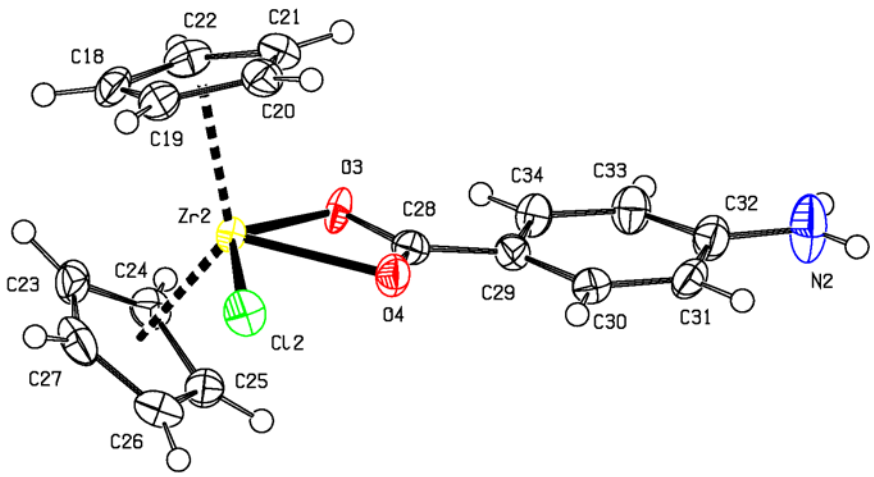

Figure 11.11. An ORTEP diagram of $(\eta^5\text{-}C_5H_5)_2ZrCl(RCOO)$, R = *p*-$C_6H_4$-$NO_2$, **15**, showing the other unit of 8 units that made up unit cell

Selected unit cell parameters of **14** and **15** are shown in **Table 11.1**. The bidentate aryloxy ligand bond distances [Zr-O, 2.307 (2) Å and 2.2546(19) Å] of **14** are longer than those of **15** [Zr-O, 2.2947(18) Å and 2.2312(17) Å]. This is due the electron withdrawing effect of the nitro substituent on the phenyl ring in **15**. These carboxylate bonding distances are similar to those obtained for (η^5-MeC_5H_4)ZrCl(α-$C_{10}H_7COO$) (**Figure 11.12**) complex reported to be 2.317(2) Å and 2.260(2) Å[20]. The literature values for bis(η^5-cyclopentadienyl)chloro(4-oxoferrocenebutanoyloxy)zirconium(IV) complex[21] (**Figure 11.13**) are 2.248(3) Å and2.287(3) Å. In all the cases above, the Zr-O bond distances per complex are not equal, indicating that the coordinating ability of the two oxygen atoms of the carboxylate is different. All these five coordinate Zr-O bond lengths are longer than Zr-O bond lengths of eight coordinate complexes $Zr(acac)_4$[22] that equals 2.198 Å, $Zr[SOCN(C_2H_5)_2]_4$[23] that is 2.190 Å and $[Zr(C_2O_4)_4]^{4-}$[24] (2.199 Å). The five coordinate Zr-O bond lengths mentioned above are also longer than Zr-O bond distances in 4-coordinate oxo-bridged dimeric complex, $[(\eta^5\text{-}C_5H_5)_2ZrCl]_2O$[25] reported to be 1.94 Å.

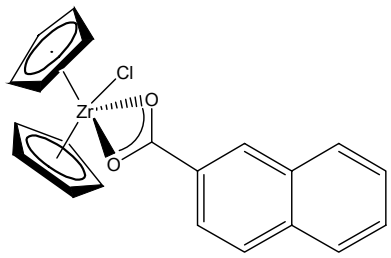

Figure 11.12. Structure of (η^5-MeC_5H_4)ZrCl(α-$C_{10}H_7COO$)

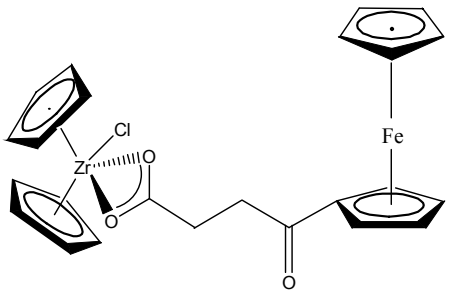

Figure 11.13. Structure of $(\eta^5\text{-}C_5H_5)_2ZrCl(FcCO(CH_2)_2COO)$

The carboxylate C-O bond distances of **14** and **15** [1.267(3) Å and 1.275(3) Å respectively] are longer than that of a normal C=O bond distance (1.22 Å) but shorter than those of normal C-O bond distance (1.43 Å). The Zr-Cl bond lengths of **14** and **15** were found to be 2.5313(8) Å and 2.5541(8) Å respectively. The latter bond length is slightly longer due to the electronic effect of NO_2 group attached to the phenyl ring. However, both Zr-Cl bond lengths are longer than the bond length in $(\eta^5\text{-}C_5H_5)_2ZrCl_2$, reported to be 2.44(1) Å as a result of steric crowding. The average distances between the zirconium and the carbon atoms of the two cyclopentadienyl rings for **14** and **15** were similar to those of $(\eta^5\text{-}MeC_5H_4)ZrCl(\alpha\text{-}C_{10}H_7COO)$, $[(\eta^5\text{-}C_5H_5)_2ZrCl(FcCO(CH_2)_2COO)$ and $(\eta^5\text{-}C_5H_5)_2ZrCl_2$.

The O1-Zr-O2 bond angle for **14**, **15**, $(\eta^5\text{-}MeC_5H_4)ZrCl(\alpha\text{-}C_{10}H_7COO)$ and $[(\eta^5\text{-}C_5H_5)_2ZrCl(FcCO(CH_2)_2COO)$ are 56.66(7)°, 57.50(6)°, 56.3(1)° and 57.0(1)° respectively. The O1-Zr-O2 bond angles for **14**, **15**, $(\eta^5\text{-}MeC_5H_4)ZrCl(\alpha\text{-}C_{10}H_7COO)$ and $[(\eta^5\text{-}C_5H_5)_2ZrCl(FcCO(CH_2)_2COO)$ are 117.6(2), 117.2(2), 117.3(1), 117.5(4) respectively. These bond angles are similar and are indicative of similar crystal structures.

Table 11.2. Crystal data and structure refinement for **14**

Identification code	**14**	
Empirical formula	$C_{17}H_{15}ClO_2Zr$	
Formula weight	377.96	
Temperature	173(2) K	
Wavelength	0.71073 Å	
Crystal system	Orthorhombic	
Space group	Pnma	
Unit cell dimensions	a = 13.077(3) Å	α = 90°.
	b = 10.621(2) Å	β = 90°.
	c = 11.056(2) Å	γ = 90°.
Volume	1535.5(5) $Å^3$	
Z	4	
Density (calculated)	1.635 Mg/m^3	
Absorption coefficient	0.890 mm^{-1}	
F(000)	760	
Crystal size	0.30 x 0.09 x 0.08 mm^3	
Theta range for data collection	2.41 to 28.31°.	
Index ranges	-17<=h<=17, -12<=k<=14, -11<=l<=14	
Reflections collected	10151	
Independent reflections	2008 [R(int) = 0.0442]	
Completeness to theta = 28.31°	99.9 %	
Absorption correction	Integration	
Max. and min. transmission	0.9322 and 0.7760	
Refinement method	Full-matrix least-squares on F^2	
Data / restraints / parameters	2008 / 0 / 112	
Goodness-of-fit on F^2	1.045	
Final R indices [I>2sigma(I)]	R1 = 0.0256, wR2 = 0.0575	
R indices (all data)	R1 = 0.0357, wR2 = 0.0608	
Largest diff. peak and hole	0.373 and -0.477 $e.Å^{-3}$	

Table 11.3. Crystal data and structure refinement for **15**

Identification code	**15**	
Empirical formula	$C_{17}H_{16}ClNO_2Zr$	
Formula weight	392.98	
Temperature	173(2) K	
Wavelength	0.71073 Å	
Crystal system	Monoclinic	
Space group	P2(1)/c	
Unit cell dimensions	a = 15.586(2) Å	α = 90°.
	b = 13.847(2) Å	β = 93.772(3)°.
	c = 14.832(2) Å	γ = 90°.
Volume	3194.1(8) $Å^3$	
Z	8	
Density (calculated)	1.634 Mg/m^3	
Absorption coefficient	0.861 mm^{-1}	
F(000)	1584	
Crystal size	0.44 x 0.30 x 0.20 mm^3	
Theta range for data collection	1.31 to 28.29°.	
Index ranges	-18<=h<=20, -18<=k<=12, -18<=l<=19	
Reflections collected	21082	
Independent reflections	7897 [R(int) = 0.0237]	
Completeness to theta = 28.29°	99.6 %	
Absorption correction	Semi-empirical from equivalents	
Max. and min. transmission	0.8466 and 0.7031	
Refinement method	Full-matrix least-squares on F^2	
Data / restraints / parameters	7897 / 70 / 425	
Goodness-of-fit on F^2	1.078	
Final R indices [I>2sigma(I)]	R1 = 0.0325, wR2 = 0.0797	
R indices (all data)	R1 = 0.0449, wR2 = 0.0848	
Largest diff. peak and hole	0.898 and -0.643 $e.Å^{-3}$	

11.5. CONCLUSIONS

Sodium benzoates (Na^+RCOO^-, R = C_6H_5, p-C_6H_4-NO_2, p-C_6H_4-NH_2, were successfully synthesized by the reaction of alcoholic solutions of stoichiometric amounts of sodium metal with aromatic carboxylic acids in 99% yield. The corresponding zirconium(IV) complexes, $(\eta^5\text{-}C_5H_5)_2ZrCl(RCOO)$, were synthesised successfully in over 70% yield by mixing powders of zirconocene dichloride with Na^+RCOO^-. Single crystal XRD study of **14** and **15** revealed that the carboxylato ligand was coordinated in a bidentate fashion (chelating) resulting in an 18 electron, five-coordinate zirconium complexes. The unit cell parameters of complexes **14** and **15** were similar to each other and comparable to literature values. Although the actual reaction was not solventless as envisaged the analysis of the compounds using single crystal XRD technique was done in the solid-state.

11.6. REFERENCES

1. R. L. Rardin, W. B. Tolman and S. J. Lippard, *New J. Chem.,* 1991, **15**, 417.
2. R. C. Mehrotra and R. Bohra, *Metal Carboxylates*, Academic Press INC, London, 1983.
3. P. M. Maitlis, *The Organic Chemistry of Palladium, Vol II,* Academic Press, New York, 1971.
4. S. B. Elliot, *The Alkaline Earth and Heavy Metal Soaps*, Reinhold, New York, 1946.
5. T. R. Felthouse, *Prog. Inorg. Chem*, 1982, **29**, 73.
6. R. A. Howard, E. Sherwood, A. Erck, A. P. Kimball and J. L. Bear, *J. Med. Chem*, 1977, **20**, 943.
7. A. Erck, E. Sherwood, J. L. Bear and A. P. Kimball, *Cancer Res*., 1976, **36**, 2204.
8. G. Wilkinson, R. D. Gillard and J. A. McCleverty, *Comprehensive Coordination Chemistry*, Volume 1-4, Pergamon Press, Oxford, 1987.
9. D. H. M. W. Thewissen, *J. Organomet. Chem*., 1980, **188**, 211.
10. C. A. Bertelo and J. Schwartz, *J. Am. Chem. Soc.,* 1975, **97**, 288.
11. J. C. Green, M. L. H. Green and C. K. Prout, *J. Chem. Soc*., *Chem. Commun*, 1972, 421.
12. J. L. Peterson and L. F. Dahl, *J. Am. Chem. Soc*., 1974, **96**, 2248.
13. M. E. Silver, O. Einstein and R. C. Fay, *Inorg. Chem*, 1983, **22**, 759.
14. T. D. Tilley, *Organometallics,* 1985, **4**, 1452.
15. Y. Zhou and H. Chen, *Polyhedron*, 1990, **9**, 2689.
16. Bruker (1999). *SAINT*+. Version 6.02 (includes XPREP and SADABS). Bruker AXS Inc., Madison, Wisconsin, USA.
17. Bruker (1999). SHELXTL. Version 5.1. (includes XS, XL, XP, XSHELL) Bruker AXS Inc., Madison, Wisconsin, USA.
18. A. L. Spek,. (2003). *J. Appl. Crystallogr.*, 2003, **36**, 7-13.
19. S. C. Dixit, R. Sharan and R. N. Kapoor, *Inorg. Chim Acta*, 1989, **158**, 109.
20. Z. Wang, S. Lu and H. Guo, *Polyhedron*, 1991, **10**, 2341.

21. M. A. Yongxiang, Z. Ying, W. Xin and M. A. Chunlin, *Polyhedron,* 1989, **8**, 929.

22. J. V. Silverton and J. L. Hoard, *Inorg. Chem*., 1963, **2**, 242.

23. W. L. Steffen and R. C. Fay, *Inorg. Chem.,* 1978, **17**, 2120.

24. G. L. Glen, J. V. Silverton and J. L. Hoard, *Inorg. Chem.,* 1963, **2**, 250.

25. J. F. Clarke and M. B. Drew, *Acta Crystallogr., Section B*, 1974, **30B**, 2267.

CHAPTER 12: ISOMERISATION OF OLEFINS: THE HYDROZIRCONATION REACTION

12.1. INTRODUCTION

12.1.1. Literature review

The driving force of all life forms is energy[1]. Animate carbonaceous matters are thermodynamically unstable systems requiring constant energy supply for survival. Even inanimate matter appears alive when supplied with energy[2]. The problem is that that the energy required for sustaining life must be in a usable form[3].

On earth, plants[4] and some bacteria[5] have the ability to trap solar energy using photosynthesis to produce carbohydrates and other organic matter from carbon dioxide and water readily found in our atmosphere, hydrosphere and stratosphere. All other life forms use the organics thus produced as their source of energy, directly by herbivores and indirectly by carnivores and scavenging creatures[6]. Some of the organic matter was fossilised millions of years ago as coal, natural gas and petroleum, and man has been able to tap into these reserves as an energy source for at least a millennium[7].

The advancement of the human race depends on their continual explorations of their habitat, mother earth, for new sources of energy for sustainability[8]. The sources however are limited and humans know it. In fact it is the source of conflict the world over[9], and those that have the resources jealously guard them like precious jewels. Those without restlessly seek means to have a share in one way or another resulting in occasional squabbling with those that held nature's honey-pot[10]. Nonetheless, if humans are to skirt a certain extinction caused by energy shortage as a collective, they must, at least, find renewable sources that can be habilitated to regenerate for later use and with greater access.

There are various alternative sources like space explorations to other planets in or closer to our solar system but such quests are presently foetal[11]. The one development that man has come-up was that has seriously boosted the production of ready-energy with restricted environmental waste is the use of catalysts in converting the limited natural hydrocarbons efficiently[12]. Catalysis is a special branch of chemistry important to both industry and society due to its application in the synthesis of more than 80% of all bulk and fine chemicals[13]. Catalysts have been used in the manufacture of foodstuffs, fuels, pharmaceuticals and other materials that have immensely improved the quality of lives of human beings.

The use of catalysts is one of the focus areas of green chemistry. This is because catalysts are mostly selective and are superior to stoichiometric reagents. The end result is the production of desired products with less side products as waste[13]. In addition a catalyst has the added advantage of being reusable- it can be used for several times to speed up a reaction and when its activity becomes low due to catalyst poisons it can be regenerated.

Catalysts that were employed in the early years of industrialisation were main-group element based[14]. Modern-day catalysts are largely transition metal based and their use, in industry, has been extensive in the last few decades[15]. When the catalyst and the reacting substances are present together in a single state of matter, usually as a gas or a liquid, it is customary to classify them as homogeneous catalysts. Many important modern examples of homogeneous catalysis are found in the petrochemical industry. The transition metal homogeneous catalysts that are in use have ligands bonded to the metal centre. It has been found that the ligands bonded to the metal centre can direct the course of a reaction[16]. A systematic modification of a ligand set can influence both the rate of a reaction and the final product(s) formed. Here, the electronic[17] and steric[18] effects (or a combination of both) are expected to influence catalyst behaviour. Large ligands will prevent substrates beyond a certain size from approaching a metal centre, resulting in changed selectivity. Larger ligands can also render the bond between the metal and the substrate weaker. Similarly the electron donating and accepting ability of a ligand can influence both reaction pathway and catalytic activity[19].

The conversion of crude petroleum to usable fuels results in the generation of small chain hydrocarbons as by-products that can be used in the chemical industry[20, 21,22]. Amongst these by-products are olefins. Some of the most useful industrial olefins are the mono α-olefins, which contain one terminal double bond. 1-Hexene for example, is an α-olefin monomer used in the production of both linear low-density polyethylene[23, 24] (LLDPE) and high-density polyethylene[25] (HDPE) polymers.

The α-olefins are also used in the production of alcohols that are in turn converted to plastics and detergents and for use as synthetic lubricants[26]. The small chain hydrocarbon, ethylene, is used to produce other long chain α-olefins by oligomerisation processes. The Chevron ethylene oligomerisation and Shell higher olefin processes (SHOP process) are two important oligomerisation pathways commonly used in industry.

There is another alternate reaction route that potentially could produce α-olefins. This is the conversion of internal olefins to terminal (α) olefins. The reaction is generally governed by thermodynamic considerations. Unfortunately, α-olefins are thermodynamically unfavoured relative to the internal olefins[27].

Attempts have been made to develop processes that would achieve the conversion of internal olefins to terminal olefins. For example, a patent has reported the use of boron compounds like diethyl borane to react with internal mono olefins to yield α-olefins but the reaction had low selectivity and required high temperatures[28].

The use of transition metal complexes for the isomerisation of an internal double bond to a terminal position has been investigated[29]. The conversion of an alkene into a transition metal alkyl involves two steps. Firstly, the coordination of the alkene to the transition metal atom and secondly, β-metal hydride addition to a coordinated unsaturated molecule **(Scheme 12.1)**.

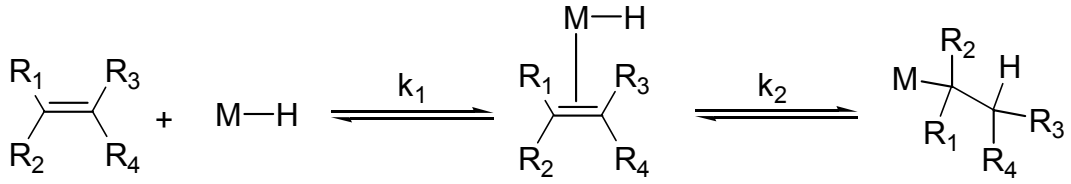

Scheme 12.1. The conversion of an alkene to a metal alkyl using a metal hydride

Note that R_1, R_2, R_3, R_4 are alkyl chains or hydrogen atoms. For many transition metal complexes, the magnitude of the equilibrium constant (k_1) depends on the number and size of alkyl substituents attached to the double bond[30]. As the size and number of alkyl groups increase, k_1 decreases. The β-hydride elimination/addition equilibrium constant (k_2) in transition metal complexes has been found to depend on the availability of electron density on the metal to stabilise the alkene complexes[31].

The above-mentioned process was exploited in an attempt to convert internal olefins to terminal olefins using zirconium chemistry[32]. In this instance, chlorobis(cyclopentadienyl) hydridozirconium(IV) was found to react under mild conditions with a variety of olefins to generate isolable alkylzirconium(IV) complexes[33]. The reaction that took place occurred with both internal and terminal olefins suggesting that the internal olefin was isomerised to an α-olefin in the process (See **Scheme 12.2**).

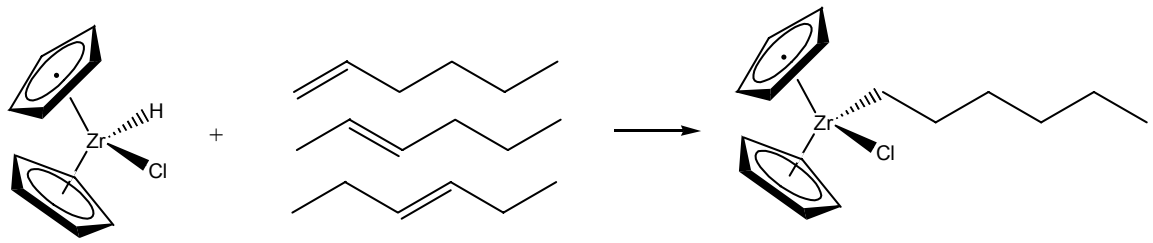

Scheme 12.2. Formation of terminal alkylzirconium complexes via hydrozirconation of hexene isomers

Here, hydrozirconation (as the reaction is termed) of olefins proceeded to place the zirconium moiety at the sterically least hindered position on the alkyl chain. The product

formation involved the regiospecific addition of Zr-H to the terminal double bond of 1-hexene. When there was an internal double bond, like *trans*-3-hexene, Zr-H addition was followed by rapid rearrangement via Zr-H elimination and re-addition to eventually place the metal complex at the least hindered terminal position of the alkyl chain (**Scheme 12.3**). The process is called hydrozirconation isomerisation and has been successfully used to synthesise terminal alcohols[34], alkyl halides[35,36], aldehydes, esters, carboxylic acids, acid halides and saturated alkanes via a Zr-C bond cleavage.

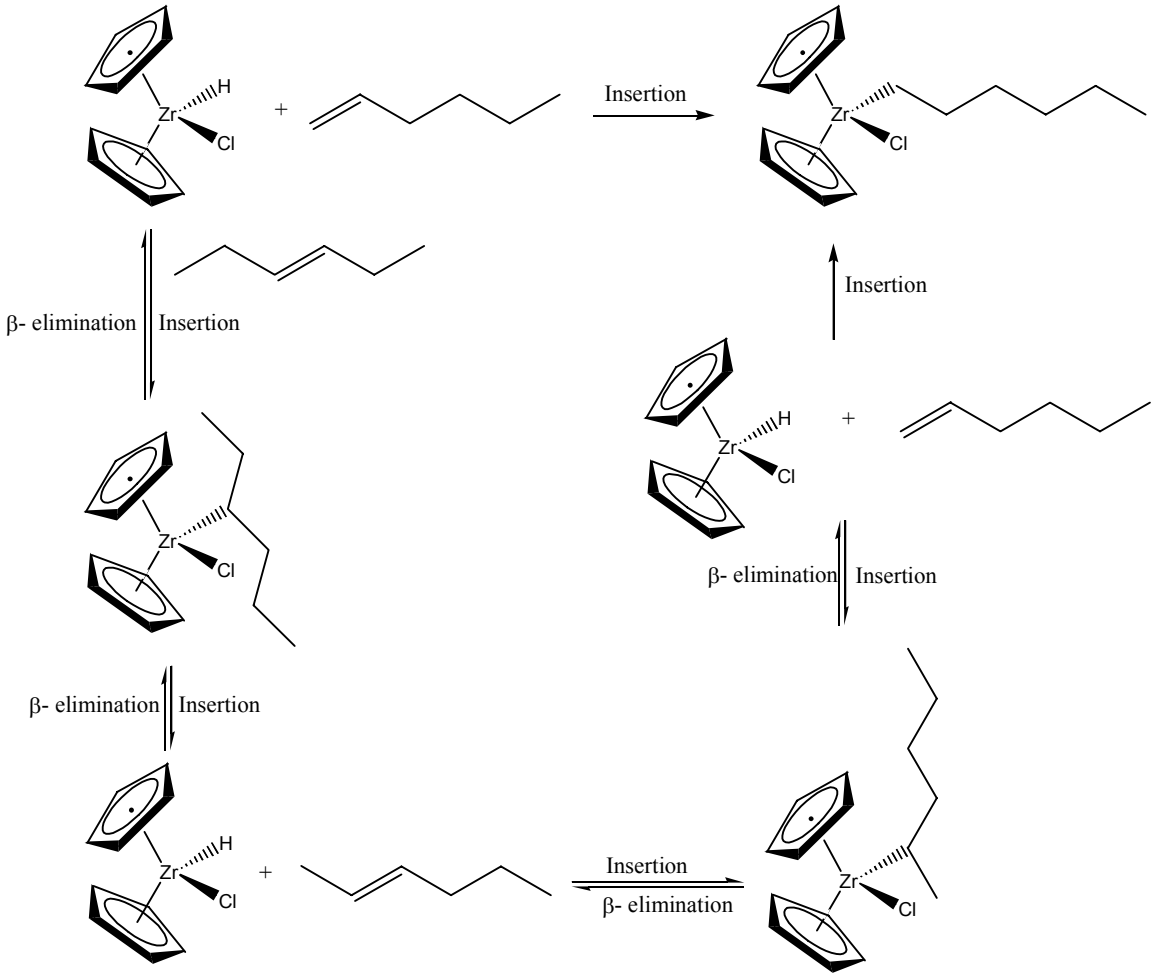

Scheme 12.3. Proposed hydrozirconation isomerisation of *trans*-3-hexene to *trans*-2-hexene and eventually forming terminal hexylzirconium complex via olefin insertion and β-elimination reactions

The recovery of α-olefins from these zirconium species has to date been controversial. Reported recovery of α-olefins from alkylzirconium complex is by use of a β-abstraction reagent like trityl chloride[37] as shown in **Scheme 12.4**. A problem associated with reaction procedure is the cost of the β-abstraction reagent and non-regeneration of the zirconium complex for further use.

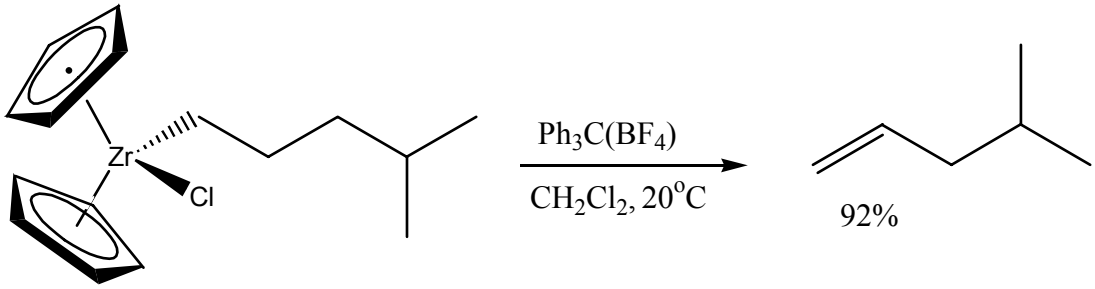

Scheme 12.4. The recovery of terminal olefins using β-abstraction reagent from alkylzirconium complexes

An alternative route to recovery of α-olefins is by cleavage of the alkyl group from Zr using olefins. Interestingly attempts to prepare terminal olefins by this route have generated conflicting results. On the one hand, a patent by Kidwell[38] *et al*., reported the displacement of the terminal olefin from alkylzirconium complex with a different olefin (**Scheme 12.5**).

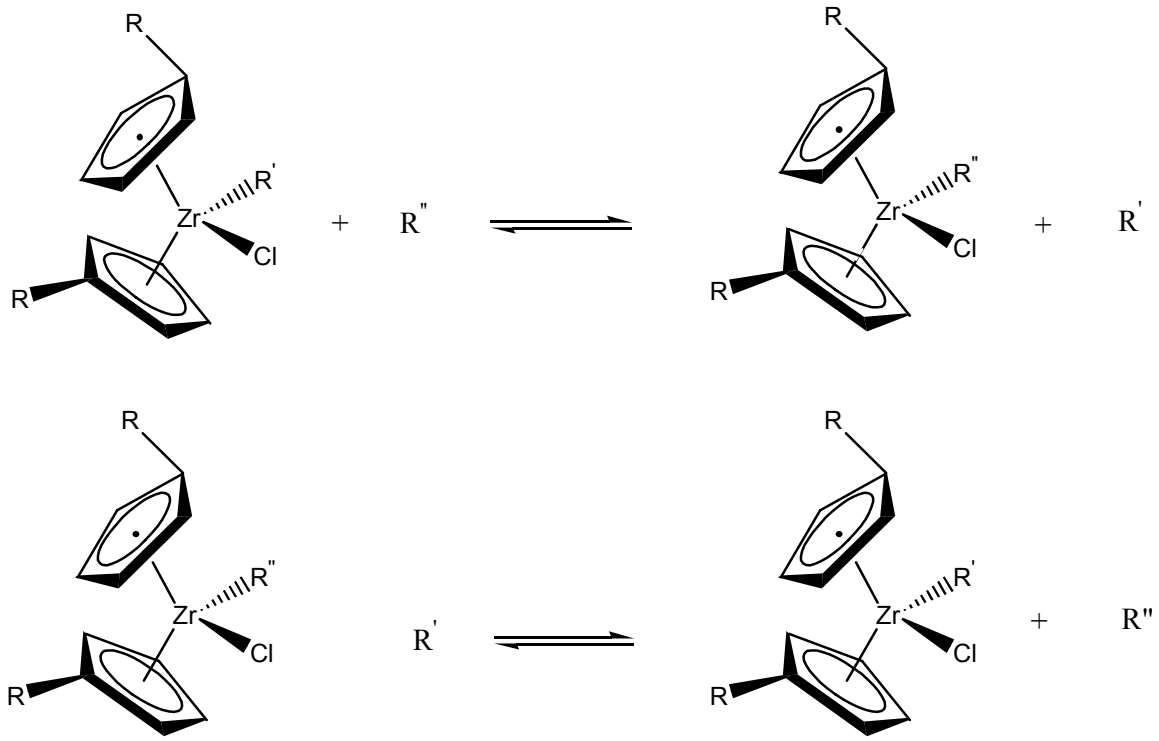

Scheme 12.5. Two pot displacement of α-olefins from the substituted alkylzirconium(IV) complexes using olefins of different chain lengths (R' and R")

On the other hand, a study by Chirik and co-workers[59] using carbon-13 labelled propylene revealed that the alkylzirconium moiety was not displaced by propylene under pressure (**Scheme 12.6**).

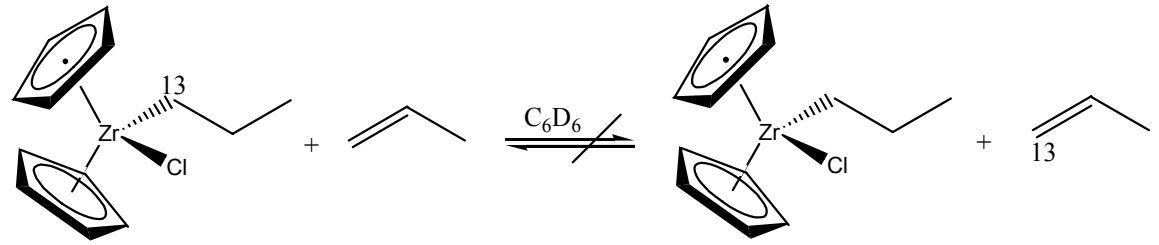

Scheme 12.6. The non-reactivity of propylene with the carbon-13 labelled chlorobis(cyclopentadienyl)propylzirconium(IV) complex in deuterated benzene

12.1.2. Aims of the study

Our research focused on four principal aims:

1. Synthesis of substituted cyclopentadienes
2. Synthesis of substituted bis(cyclopentadienyl)zirconium (IV) halides
3. Synthesis of substituted alkylzirconium(IV) halides
4. Isomerisation of internal hexene isomers to 1-hexene using substituted alkylzirconium(IV) halides as pre-catalysts

12.2. EXPERIMENTAL PROCEDURES

12.2.1. Synthesis of substituted cyclopentadienes

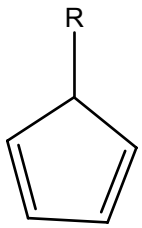

R = Me, Et, ^{i}Pr, ^{t}Bu, $SiMe_3$

The synthetic pathway used to synthesise the substituted cyclopentadienes required for the metallocene synthesis is outlined below. The procedure for the synthesis of each compound was similar. Only the protocol for the synthesis of ethylcyclopentadiene is given. The other compounds were synthesised by the same methodology.

Synthesis of ethylcyclopentadiene

NaH (49.3 g, 1.23 mol 1,02 mol equiv, 60% in mineral oil) was taken up in THF (600 cm^3) and cooled to 0°C in a 1 dm^3 Schlenk flask. Freshly cracked cyclopentadiene (80 g,

1.21 mol, 100 cm^3) was then added dropwise to the base-solvent mixture over an hour. The mixture was allowed to stir at the set temperature for an additional hour and then allowed to warm to room temperature overnight. The reaction mixture was cooled back to 0°C and stirred for 30 min. Ethyl bromide (111.2 g, 1.02 mol equiv, 76 cm^3) in THF (100 cm^3) was then added dropwise oven a period of an hour and the solution stirred at the set temperature for an additional 2 h after the addition of the electrophile. The reaction mixture was then allowed to warm back to room temperature over a period of 14 h. The resulting solution was then filtered through a column packed with celite to leave behind a white solid (NaBr) and some grey matter (most likely the mineral oil component that came with the base). The filtrate was washed with distilled water (3 × 50 cm^3) and the organic layer extracted with hexane (3 × 20 cm^3). The combined organic mixtures were dried with $MgSO_4$ and filtered through a glass frit to give a pale yellow solution. The homogeneous solution was fractionally distilled to remove solvent (hexane and toluene) and the remaining liquid collected by increasing the temperature to about 180°C to yield a cracked monomeric ethylcyclopentadiene mixture (55.8 g, 49%) as a colourless liquid that was stored at -60°C for later use.

^{1}H NMR ($CDCl_3$, ppm) δ: 1.14 (9H, t, -$CH_2C\mathit{H}_3$), 2.38 (6H, m, -$C\mathit{H}_2CH_3$), 2.90 (5H, m, -Cp), 6.23 (10H, m, -Cp)

All the other substituted monomeric cyclopentadienes produced were stored in a freezer at -60°C to minimise the dimerisation process.

12.2.2. Synthesis of substituted bis(cyclopentadienyl)zirconium (IV) halides

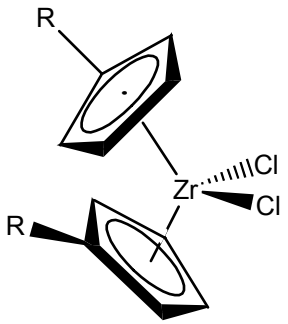

The retro Diels-Alder reaction of the substituted cyclopentadiene dimer was effected by heating the monomer at 160°C under reflux and collecting the colourless monomer that resulted. In a separate Schleck flask, *n*-BuLi (2 mol equiv) was taken up in hexane (200 cm^3) and cooled to 0°C. The monomeric substituted cyclopentadiene was diluted in an equal volume of hexane chilled to 0°C and added dropwise over a period of 20 min to the hexane-base mixture. A white solid deposited as the reaction progressed. The reaction was allowed to continue at the set temperature for an hour before the reaction vessel was warmed back to room temperature. The solvent was then removed under reduced pressure to leave behind a white solid that was then taken up in cold toluene (400 cm^3) and kept at 0°C (light yellow homogeneous solution). Zirconium(IV) chloride (1 mol equiv) was added to the solution in small portions over a period of 40 min under nitrogen counter flow at 0°C. The reaction was allowed to react at the mentioned temperature for two more h before warming to room temperature overnight. The solution was then filtered through a column packed with degassed celite to trap the salts produced. The solvent was then removed *in vacuo* to yield the desired metallocene as light yellow to colourless solids

12.2.3. Synthesis of chlorobis(η^5-cyclopentadienyl)hydrido-zirconium(IV) complex

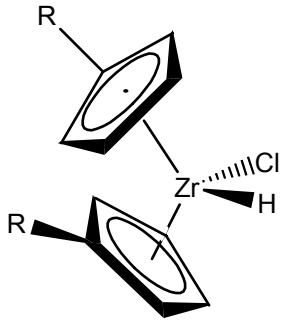

Cp_2ZrCl_2 (1.0 g, 3.42×10^{-3} mol) was dissolved in dry THF (20 cm^3) in a glove box to obtain a colourless solution. $LiAlH(t\text{-}OBu)_3$ (0.9 g, 3.42×10^{-3} mol, 1 mol equiv) was also dissolved in dry THF (10 cm^3), inside a glove box and the resulting homogeneous solution mixed with the metallocene solution by slow addition using a glass Pasteur

pipette under constant stirring. Immediate precipitation of a white powder occurred. The heterogeneous mixture was allowed to stir for an additional 50 min after which the solvent was filtered to leave behind white micro crystals. The crystals were allowed to dry overnight inside the glove box during which time they turned light pink in colour (0.73 g, 83% yield).

12.2.4. Synthesis of chlorobis(η^5-cyclopentadienyl)hexyl-zirconium(IV) Complex

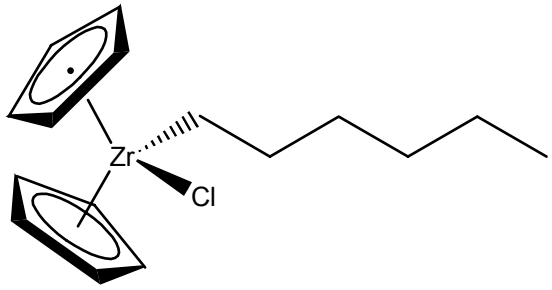

(η^5-$C_5H_5)_2ZrClH$ (0.5 g, 1.94×10^{-3} mol) was dissolved in toluene (10 cm^3). Hex-1-ene (0.16 g, 0.2 cm^3, 1mol equiv) was then added to the mixture, which was allowed to react for 4 h at room temperature under constant stirring. ^{1}H NMR analysis showed that the desired product was obtained due to peaks that were specific to the product. The solvent was removed *in vacuo* to leave behind a light yellow residue that was further dried overnight to yield a yellow amorphous compound (0.62 g, 94% yield). ^{1}H NMR, δ ppm 0.86 (3H, m, -$CH_2CH_2CH_2CH_2CH_2CH_3$), 1.05 (2H, m, -$CH_2CH_2CH_2CH_2CH_2CH_2CH_3$), 1.20 (6H, m, -$CH_2CH_2CH_2CH_2CH_2CH_3$), 1.54 (2H, m, -$CH_2CH_2CH_2CH_2CH_2CH_3$), 6.21 (10H, s, 2 × Cp).

12.2.5. Catalytic isomerisation of 1-hexene to internal hexene isomers

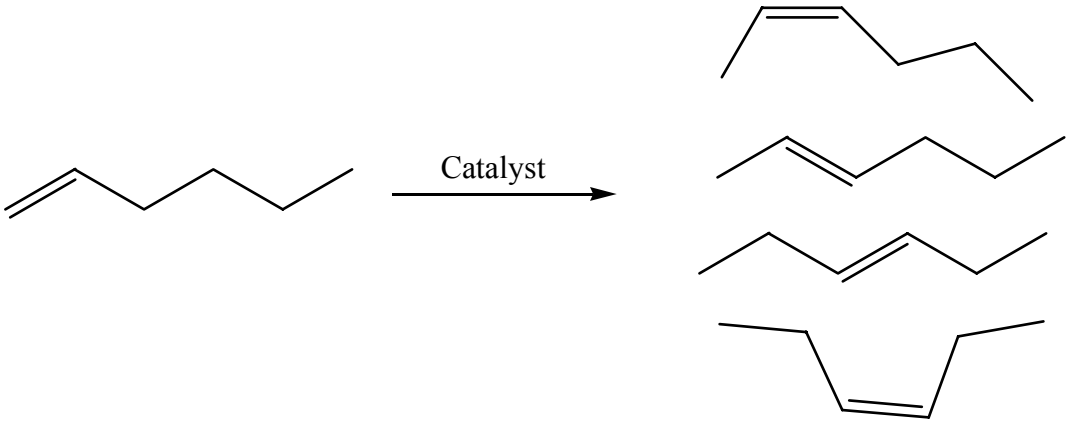

Various attempts to form isomers of 1-hexene are detailed below.

12.2.5.1. Isomerisation of 1-hexene using Na-Al_2O_3

Alumina (12.42 g) (Fluka, CP grade) was heated *in vacuo* at 150°C, in a 500 cm^{3} round bottom flask for 6 h and then cooled back to room temperature. Freshly cut sodium metal lumps (1.08 g, 0.047 mol, 10% mol equiv) were then added to the reaction vessel under a nitrogen counter flow. The solid mixture was then heated *in vacuo* at 150°C for an hour while being stirred vigorously using a stirrer bar. The action produced finely divided sodium metal granules adsorbed on alumina. The free flowing solid was then cooled back to room temperature and pre-dried 1-hexene (0.47 mol, 50 cm^{3}) was added to the solid. The heterogeneous mixture was stirred at room temperature for 16 h and the reaction mixture analysed using GC. Another investigation was conducted using the same reagents under reflux for two and 14 h respectively and the extent of isomerisation using a GC was also checked.

12.2.5.2. Isomerisation of 1-hexene using KO^{t}Bu in DMSO

The base, KO^{t}Bu, is extensively used in conjunction with DMSO as a solvent. We thus attempted the transformation by subjecting the olefin to the conditions above by taking freshly sublimed KO^{t}Bu (10% mol equiv) in 500 cm^3 round bottom flask. DMSO (200 cm^3) was then added to the base under nitrogen counter-flow at room temperature and the reaction mixture allowed to stand under constant stirring for an hour. 1-Hexene (1 mol) was added to the reaction mixture, which was stirred at room temperature for 22 h. The reaction mixture was analysed using a GC. The experiment was repeated using refluxing solution for 14 h and the reaction mixture analysed using a GC.

12.2.5.3. Isomerisation of 1-hexene using Rh(III) chloride trihydrate

$RhCl_3.3H_2O$ (13 mg) was taken in EtOH (1 cm^3) and 1-hexene (9 cm^3) in a round bottom flask containing boiling chips. The mixture was then allowed to stir at hexene reflux for 24 h. The mixture was cooled, and the alkene mixture distilled out of the mixture to yield 5 cm^3 of hexenes. The remaining mixture was distilled out to leave behind the metal catalyst for later use. Analysis of the alkene mixture using a GC was undertaken.

12.2.6. Evaluation of $(\eta^5\text{-Cp})_2ZrClC_6H_{13}$ as an isomerisation catalyst for 1-hexene

Chlorobis(η^5-cyclopentadienyl)hexylzirconium(IV) complex (12 mg, 0.0352 mmol) was taken in dry toluene (10 cm^3) in a Schlenk tube under inert gas. 1-Hexene (0.5 cm^3, 7.43 mmol, 211 mol equiv) was then added to the reaction mixture that was stirred for 48 h at room temperature. The reaction mixture was analysed using GC by withdrawing a minute amount of the mixture, which was then diluted with THF (2 cm^3) before analysis. The reaction mixture was then cannulated into a 20 cm^3 autoclave (See **Figure 12.1**), under nitrogen counter flow. The reaction chamber was then sealed shut and heated to 110°C and the reaction mixture reacted for 48 h at the set experimental temperature under

constant stirring. The reaction chamber was then cooled back to room temperature over a period of 2 h and the reaction content analysed by removing a small amount of the mixture, diluted with THF (2 cm^3) and analysed using a GC. The reaction vessel was once more sealed shut and heated to 150°C before being pressurised to 50 bars using argon gas. The mixture was then allowed to react at the experimental conditions for 24 h under constant stirring. The reaction vessel was then allowed to cool back to room temperature over a period of 2 h and the reaction mixture analysed by GC.

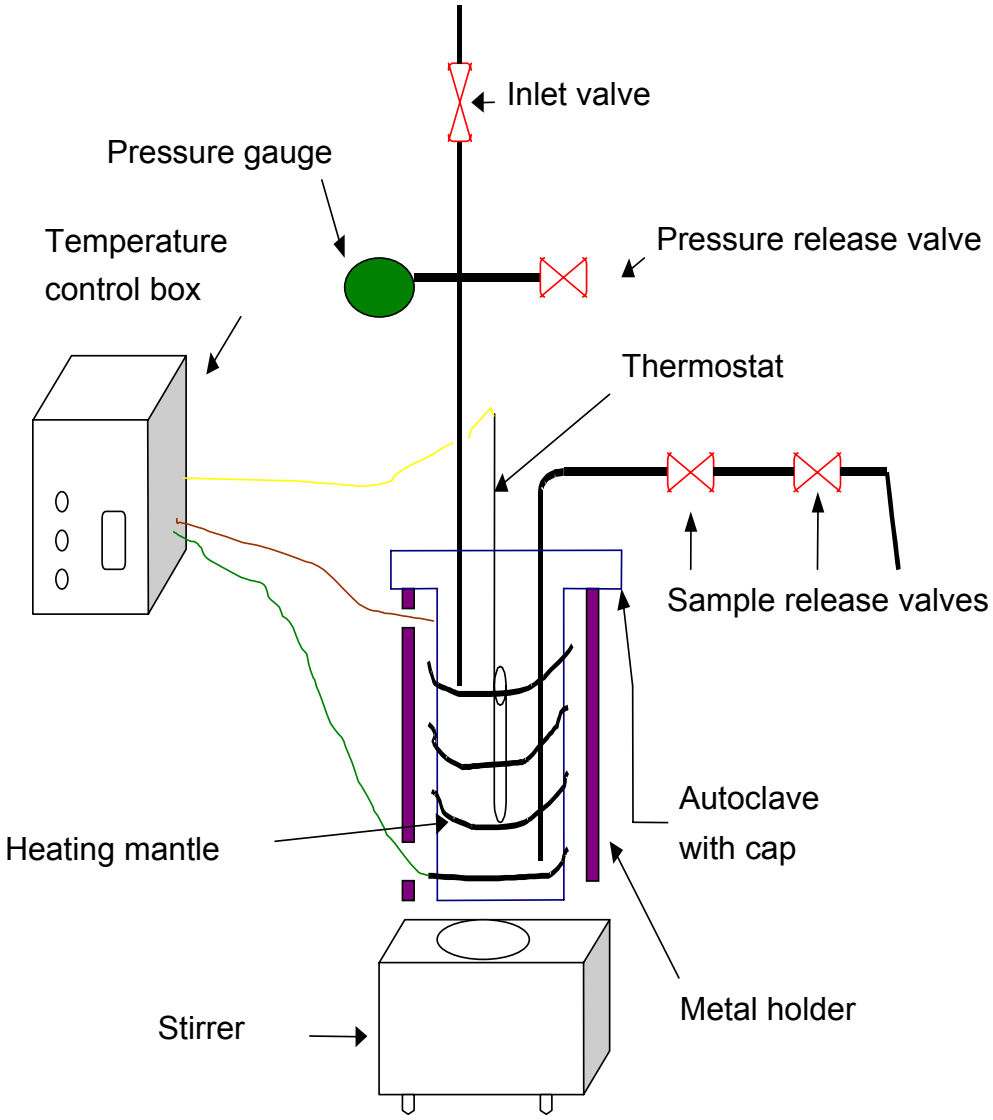

Figure 12.1. Schematic representation of an assembled autoclave used for the isomerisation of hexenes

12.2.7. Catalytic isomerisation of internal to terminal hexene double bond

12.2.7.1. Isomerisation of internal hexene isomers to 1-hexene using $(\eta^5\text{-Cp})_2Zr(Cl)C_6H_{13}$

Chlorobis(η^5-cyclopentadienyl)hexylzirconium(IV) (8 mg, 0.0235 mmol) was taken in dry toluene (10 cm^3) in a Schlenk tube under nitrogen gas. *Trans*-2-hexene (0.5 cm^3, 7.43 mmol, 316 mol equiv) was then added to the reaction mixture that was reacted at room temperature for 48 h. A small sample of the reaction mixture was withdrawn from the mother liquor and diluted with THF (2 cm^3) and the composition of the mixture determined using GC. The remaining reaction mixture was then transferred into a 20 cm^3 autoclave (See **Figure 1**), under nitrogen counter flow. The reaction chamber was then sealed shut and heated to 110°C and the reaction mixture reacted for 48 h. The reaction vessel was then cooled back to room temperature over a period of 2 h and the reaction content analysed by removing a small amount of the mixture, which was then diluted with THF (2 cm^3) and analysed using GC. The reaction vessel was once more sealed shut and heated to 150°C before being pressurised to 10 bar using argon gas. The mixture was then allowed to react at the experimental conditions for 24 h under constant stirring. The reaction mixture was analysed using GC after cooling back to room temperature. The experiment was repeated at 20 bar, 40 bar and 50 bar of pressure and temperature of 150°C for 24 h. Similar investigation was conducted using a hexene cocktail obtained by scrambling 1-hexene as detailed in **Section 12.2.5.3** in place of *trans*-2-hexene.

12.2.7.2. Isomerisation of internal hexene isomers to 1-hexene using substituted chlorobis(cyclopentadienyl)hexylzirconium(IV) complex

The appropriate pre-catalyst (0.05 mmol) was taken up in toluene (10 cm^3) and the internal hexene mixture (0.5 cm^3, 7.43 mmol, 158 mol equiv) in a 20 cm^3 Schlenk tube. A pre-dried autoclave evacuated using high vacuum pump for 10 min was then filled with argon gas while hot and allowed to cool back to room temperature before use. The reaction mixture was then cannulated from the Schlenk flask to the autoclave under a nitrogen counter flow. The valve was then closed and the reaction vessel heated to 150°C before being pressurised to 50 bars using argon gas under constant stirring. The reaction mixture was reacted at the set temperature for 24 h. At the end of the set time period, the reaction vessel was then cooled back to room temperature and the reaction sample analysed using GC.

12.2.7.3. Reaction of Cp_2ZrCl_2 / PEt_3 / *n*-BuLi with hexenes

$(\eta^5\text{-}C_5H_5)_2ZrCl_2$ (0.20 g, 6.84×10^{-4} mol) was taken in toluene (10 cm^3) and cooled to -78°C. 1.4 M *n*-BuLi (1.1 cm^3, 1.50×10^{-3} mol, 2.2 mol equiv) was then added drop wise to the colourless solution for 10 min, ensuring that the reaction temperature was maintained under nitrogen atmosphere. The reaction mixture was allowed to react at -78°C for an additional hour and the solution progressively turned light yellow during the reaction. PEt_3 (0.20 cm^3, 1.50×10^{-3} mol, 2.2 mol equiv) was then added to the mixture for 5 min and the mixture allowed to warm up to 0°C at which point the solution turned bright red. The reaction mixture was once more cooled back to -78°C and an internal hexene cocktail (2.0 cm^3, 29.7 mmol, 43 mol equiv) added to the mixture for 10 min after which it was allowed to react for an hour. A small reaction sample was withdrawn and diluted with toluene (2 cm^3) before being analysed using GC. The remaining solution was then allowed to warm back to 0°C for an hour, again withdrawing a small reaction sample for analysis. The solution colour changed from bright red to golden yellow once

0°C was reached. The reaction mixture was then warmed to room temperature for an hour, also taking a small sample for analysis. The solution colour changed from golden yellow to luminous yellow once the room temperature was reached. The remaining reaction mixture was then stirred at room temperature overnight under inert gas blanket and analysed using a GC.

12.2.7.4. Reaction of Cp_2ZrCl_2 / PPh_3 / *n*-BuLi with hexenes

$(\eta^5\text{-}C_5H_5)_2ZrCl_2$ (203 mg, 6.84×10^{-4} mol) was dissolved in toluene (10 cm^3) and cooled to -78°C using dry ice in acetone. 1.4 M *n*-BuLi (1.1 cm^3, 1.50×10^{-3} mol, 2.2 mol equiv) was then added drop wise to the colourless solution for over 10 min. The homogeneous mixture was reacted at -78°C for an additional hour. The solution progressively turned light yellow during the reaction signalling the formation of a new complex. PPh_3 (395 mg, 1.50×10^{-3} mol, 2.2 mol equiv) was then added to the mixture for 5 min and allowed to warm up to 0°C at which point the solution turned burgundy in colour. The contents were once more chilled to -78°C and an internal hexene cocktail (2.0 cm^3, 29.7 mmol, 43 mol equiv) added to the reaction mixture for 10 min under constant stirring. A small reaction sample was withdrawn hourly and diluted with toluene (2 cm^3) before GC analysis was undertaken.

12.2.7.5. Reaction of Cp_2ZrCl_2 / *n*-BuLi with hexenes

$(\eta^5\text{-}C_5H_5)_2ZrCl_2$ (72 mg, 2.46×10^{-4} mol) was dissolved in toluene (10 cm^3) and cooled to -78 C. 1.4 M *n*-BuLi (0.5 cm^3, 7×10^{-4} mol, 2.8 mol equiv) was then added drop wise to the colourless solution for 10 min. The resulting solution was reacted at -78 C for an additional hour. The solution progressively turned light yellow during the reaction signalling the formation of a new complex. An internal hexene cocktail (0.5 cm^3, 4.0 mmol, 16 mol equiv) was added to the reaction mixture for 10 min under constant stirring. A small reaction sample was withdrawn after 10 min and diluted with toluene (2 cm^3) before GC analysis was undertaken. The reaction mixture was then allowed to warm

back to room temperature for 14 h and the also analysed using GC. The reaction was repeated using varying amounts of $(\eta^5\text{-}C_5H_5)_2ZrCl_2$ (23.9 μmol, 78.9 μmol, 164 μmol, 246 μmol and 248 μmol) while keeping the amount of *n*-BuLi (0.7 mmol) and hexene mixture (4.0mmol) constant. The extent of isomerisation was determined after an hour and 14 h of reaction using a GC.

12.2.7.6. Reaction of *n*-BuLi with hexenes

n-BuLi (1.4 M, 0.5 cm^3) was taken in toluene (10 cm^3) at -78°C. The resulting solution was allowed to stir for 10 min to acclimatise at the set temperature before the introduction of the internal hexene isomer mixture (0.5 cm^3) under constant stirring for ten min. A sample was withdrawn for GC analysis. The reaction was allowed to continue for an hour and another reaction sample analysed by GC. The sequence was repeated for the other time periods.

12.2.7.7. Reaction of Cp_2ZrCl_2 / NaH with hexenes

$(\eta^5\text{-}C_5H_5)_2ZrCl_2$ (101 mg, 3.45×10^{-4} mol) was dissolved in toluene (10 cm^3) and cooled to -78 C. NaH (27.6 mg, 6.9×10^{-4} mol, 2.0 mol equiv), as a 60% mixture in mineral oil, was then added to the colourless solution as small portions for 10 min and allowed to stir for an additional hour. An internal hexene cocktail (1.0 cm^3, 8.0 mmol) was added to the reaction mixture for 10 min under constant stirring. The reaction mixture was then allowed to warm back to room temperature and reaction samples taken after 5, 45, 60 and 2880 h for GC analysis.

The dihydride complex $[(\eta^5\text{-}C_5H_5)_2ZrH_2]$ was then made by known synthetic manipulations and tested its activity for the reaction of interest. The next section details the investigation and the findings in this regard.

12.2.7.8. Reaction of Cp_2ZrH_2 with hexenes

The intermediate complex, μ-oxo-bis[chlorobis(η^5-cyclopentadienyl)zirconium(IV)] complex was synthesised using a literature method[39]. The dihydride pre-catalyst, bis(cyclopetadienyl)dihydridozirconium(IV) complex was synthesised as follows: $(Cp_2ZrCl)_2O$ (36mg) and $LiAlH_4$ (0.02 g, 1.4 mol equiv) were degassed three times in a 20 cm^3 Schleck tube and chilled to 0°C (**Scheme 10.10**). THF (10 cm^3), also at 0°C was then added to the solids and the heterogeneous mixture was allowed to warm-up to room temperature while stirring for 16 h. The assumed percentage yield is 66% (100 mg). The reaction mixture was then cooled back to -78°C and internal hexene isomers (0.5 cm^3) added over a period of 10 min. The mixture was allowed to react at the set temperature for an hour and a small amount of the sample withdrawn for GC analysis. The remaining mixture was warmed to 0 C and again a small sample withdrawn for analysis. The heterogeneous solution was finally warmed to room temperature and samples withdrawn after 3 and 21 h for GC analysis.

12.2.7.9. Reaction of $(R\text{-}C_5H_4)_2ZrBu_2$ with hexenes

Generally, the reaction was conducted as outlined below. $(Et\text{-}C_5H_4)_2ZrCl_2$ (g, 71.7 μmol) was dissolved in toluene (10 cm^3) and cooled to -78°C. 1.5 M *n*-BuLi (0.5 cm^3) was then added to the colourless solution for ten min and the reaction mixture stirred at the set temperature for an hour. The internal hexene isomer mixture (0.5 cm^3) was then added dropwise and allowed to react for ten min when a small reaction sample was with drawn for analysis. The remaining reaction mixture was reacted further for an hour and another minute sample withdrawn for analysis. The mother liquor was then warmed up to room temperature and reacted for 14 h and the reaction mixture analysed using GC. The methodology above was used for all the substituted zirconium metallocene reactions described below.

12.3. RESULTS AND DISCUSSION

12.3.1. Synthesis of substituted cyclopentadienes

Many *d*-block complexes contain a cyclopentadienyl ring[40]. More than 80% of all organometallic compounds known contain the cyclopentadienyl ligand[41]. Thus research in organometallic chemistry is almost incomplete without the use of this ligand type. Herein the synthesis of substituted cyclopentadienes and their use to make bent zirconium metallocenes are detailed. The use of zirconium(IV) metallocenes as olefin isomerisation catalysts is also included.

The substituted monomeric cyclopentadienes produced by the reaction of cracked cyclopentadiene with sodium hydride in tetrahydrofuran is shown in **Scheme 12.7**. The method involved the direct alkylation of the cyclopentadienyl anion (C_5H_5Na) with an appropriate alkyl halide. All five compounds (C_5H_4R, R = Me, Et, ^{i}Pr, ^{t}Bu, $SiMe_3$) were synthesised in satisfactory yields (42-68%) as monosubstituted alkylcyclopentadienes after thermal cracking. Literature methods using C_5H_5Na generated from sodium amalgam and monomeric cyclopentadiene resulted in comparable yields (for example, Cozak and co-workers[42] obtained cracked ethylcylopentadiene in 40% yield compared to 49% that we obtained using the above mentioned method). The trimethylsilylcyclopentadiene ($C_5H_4Si(CH_3)_3$) was the easiest to synthesise because of the acid nature of the trimethylsilyl chloride reagent[43]. Tertiary butylcyclopentadiene ($C_5H_4Bu^t$)[44] (42% yield) was the most difficult to synthesise because the reagent, Bu^tBr[45], a tertiary carbon containing electrophile, has less tendency to react. The yield although low was much higher than the literature value of 11.5%[46]. The improvement in yield was attributed to the efficient formation of the cyclopentadienyl anion (C_5H_5Na) coupled to milder reaction conditions using the electrophile (Bu^tBr). Characterisation of the compounds obtained was through ^{1}H NMR spectroscopy.

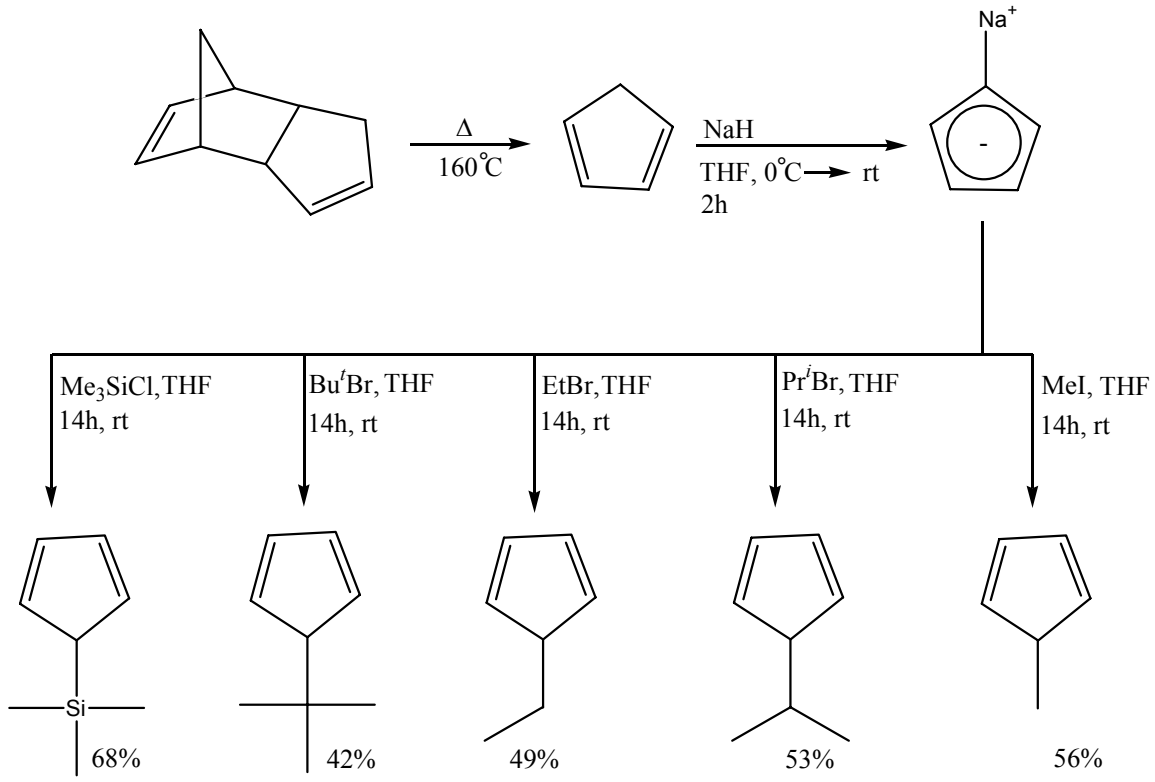

Scheme 12.7. Synthesis of substituted cyclopentadienes

12.3.2. Synthesis of substituted bis(cyclopentadienyl)zirconium (IV) halides

Substituted cyclopentadiene dimers were cracked to obtain the momeric forms. The monomers were then reacted with *n*-BuLi to generate nucleophiles, which were then reacted with zirconium(IV) chloride to generate the bent metallocenes. The details of the transformations are found in **Scheme 12.8** and the characterisation features of the metallocenes found in **Table 12.1**.

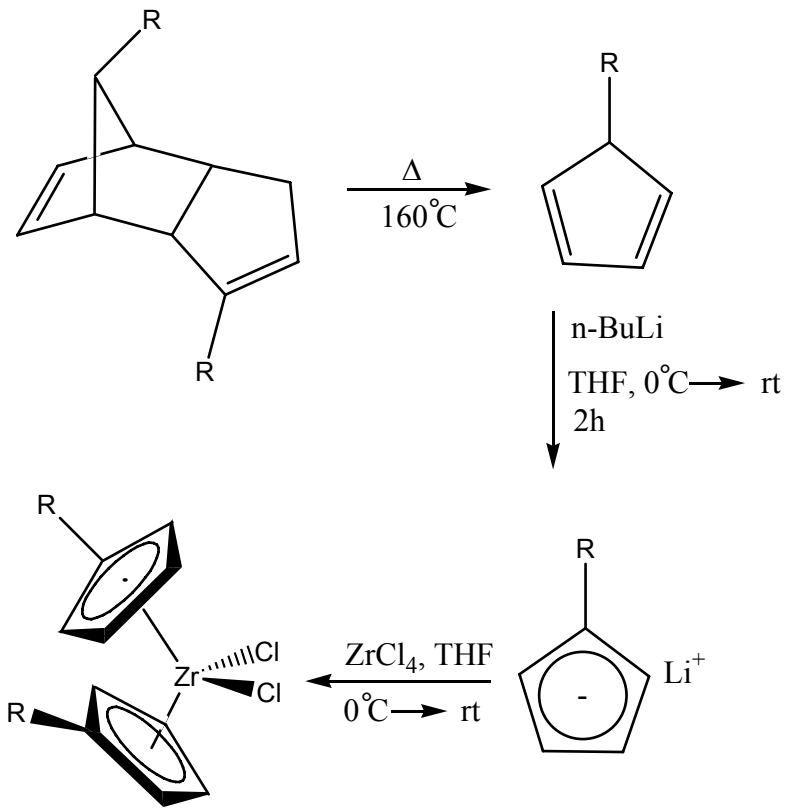

Scheme 12.8. Synthesis of dichlorobis(η^5-C_5H_4R)zirconium(IV) complexes using *n*-BuLi in THF

Table 12.1. The analysis of the dichlorobis(η^5-substitutedcyclopentadienyl)zirconium(IV) complexes obtained using *n*-BuLi in THF

Metallocene (R)	Yield[a] /%	Mp/°C	^{1}H NMR, C_5H_4R group /ppm	^{1}H NMR assignment, substituent/ppm
H	[b]	246-248	6.6 (5H, m)	-
Me	73 ()	179-181	6.31 (4H, m)	2.28 (3H, s, -CH_3)
Et	70 (50)	97-98	6.2 (4H, m)	2.6 (2H, q, *J* 7.2Hz,-CH_2CH$_3$), 1.0 (3, t, *J* 7.2Hz, -CH$_2$CH_3)
^{i}Pr	74 (65)	124-126	6.3 (4H, m)	4.1 (1H, m, -CH(CH$_3$)$_2$, 1.3 (6H, d, *J* 7.1Hz, -CH(CH_3)$_2$)
^{t}Bu	66 (63)	186-188	6.4 (4H, m)	1.2 (9H, s, -CCH_3)
Me_3Si	83 (84)	130-132	6.6 (4H, m)	0.4 (9H, s, -$SiCH_3$)

a Values in parenthesis are literature yields, as detailed in the journal by M. F. Lappert, C. J. Pickett, P. I. Riley and P. I. W. Yarrow, *J. Am. Chem. Soc., Dalton Trans.,* 1981, 805.

b An Aldrich product

The yields of zirconium(IV) dichlorides formed were comparable to the literature values. The chemical shifts (^{1}H NMR spectroscopy) in $CDCl_3$ were also similar to the recorded values signalling that the desired complexes were synthesised.

12.3.3. Synthesis of chlorobis(η^5-cyclopentadienyl)hydrido-zirconium(IV) complex

Treatment of zirconocene dichloride with LiAlH(*t*-OBu)$_3$[47] in THF at room temperature afforded the product (Schwartz' reagent)[48] in good yield (83% yield) after filtration as shown in **Scheme 12.9**. The yield was lower than the reported value (93%) presumably due to product loss through filtration.

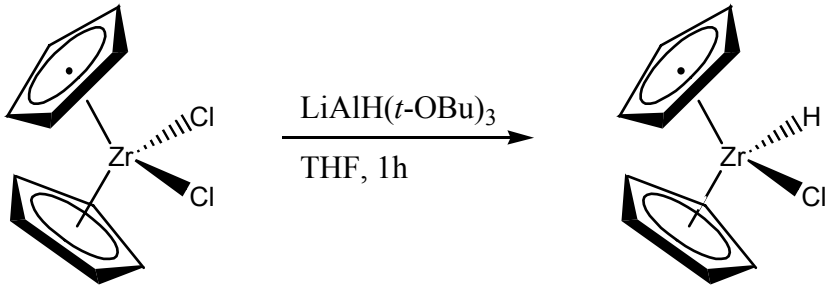

Scheme 12.9. Synthesis of chlorobis(η^5-cyclopentadienyl)hydridozirconium(IV) complex

12.3.4. Synthesis of chlorobis(η5-cyclopentadienyl)hexyl-zirconium(IV) Complex

The synthetic path chosen was hydrozirconation[49] using preformed Cp_2ZrClH[50]. The synthesised chlorobis(η^5-cyclopentadienyl)hydridozirconium(IV) complex was reacted with hex-1-ene, in toluene, at room temperature, for four h, to afford the desired product

(94%) as a semi-solid compound after filtration and drying. A diagrammatic representation of the transformation is shown in **Scheme 12.10**. ^{1}H NMR spectroscopy showed chemical shifts at 0.86, 1.05, 1.20 and1.54 ppm due to the hexyl group attached to the zirconium metal as proof that the desired complex was synthesised.

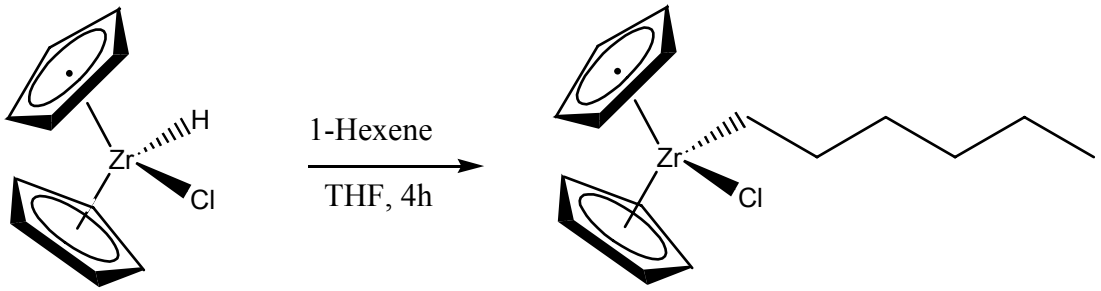

Scheme 12.10. Synthesis of chlorobis(η^5-cyclopentadienyl)hexylzirconium(IV) complex

12.3.5. Catalytic isomerisation of 1-hexene to internal hexene isomers

12.3.5.1. Isomerisation of 1-hexene using Na-Al_2O_3

Isomerisation of hex-1-ene to internal hexene isomers was attempted using sodium dispersed in alumina under hexene reflux[51]. The results of the investigation are found in **Table 12.2**. The results above showed that isomerisation using sodium metal dispersed in alumina was not successful at room temperature. The basic character of the metal was not strong enough to scramble the terminal hexene isomer to its more stable internal derivatives at the experimental conditions followed.

Table 12.2. Hexene isomers obtained when 1-hexene was stirred with Na-Al_2O_3 for 16 h at room temperature, as analysed using a GC

Hexene isomer	Isomer comp/% 16 h at rt	Isomer comp /% 2 hour reflux	Isomer comp /% 14 hour reflux
1-hexene	92.84	82.97	88.79
Trans-3-hexene	1.04	1.98	3.37
Trans-2-hexene and *cis*-3-hexene	2.89	13.02	1.68
Cis-2-hexene	3.22	1.98	1.59

The same reaction was conducted under refluxing hexene conditions for two h[52] (**Table 12.2**). This resulted in some isomerisation of the isomer to the more stable internal isomers. The double bond shift occurred by a chain mechanism involving allylic carbon anion (carbanion) intermediates[53] as shown in **Scheme 12.11**. There was bias towards the formation of *trans*-2-hexene (11.86%) compared to the other internal isomers. The selectivity could be explained in terms of isomerisation under basic conditions. The base would abstract the vinylic proton resulting in an anion being formed as an intermediate (**Scheme 12.11**). The intermediate would then isomerise the double bond to produce a more stable anion, with the negative charge now in the terminal position. The anion could then abstract a proton from the solvent, to regenerate the isomerised internal olefin (**Scheme 12.11**). Why specifically the trans-2-hexene? No conclusive answer could be given except to state that the *trans*-2-hexene is the kinetic product under the conditions employed.

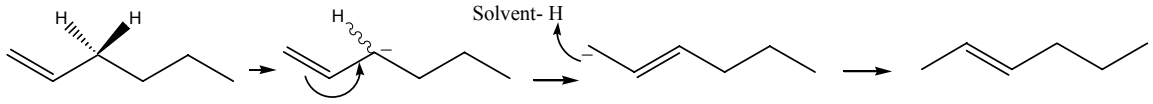

Scheme 12.11. Proposed pathway for the formation of trans-2-hexene from 1-hexene using Na-Al_2O_3 under reflux

The reaction of the terminal olefin with finely divided sodium powder in alumina under refluxing conditions for longer periods did not result in improved isomerisation to the

more stable internal isomers. Instead, the *cis*-2-hexene and *trans*-3-hexene isomers were produced in relatively large proportion relative to the other internal isomers. The results were in line with our expectations in that the thermodynamically stable isomers are favoured by longer reactions times[54].

12.3.5.2. Isomerisation of 1-hexene using K^{t}OBu in DMF

The relative success of the isomerisation under basic conditions using Na-Al_2O_3 led us to attempt the use of potassium tertiary butoxide (KO^{t}Bu)[55]. It is a more powerful and potent base known to isomerise double bonds[56].

Freshly sublimed KO^{t}Bu, dissolved in dimethyl sulfoxide (DMSO), was used as a base in an attempt to isomerise 1-hexene to the internal hexene isomers under hexene refluxing conditions[57]. At the end of the stipulated period the extent of isomerisation was determined using GC analysis. The details of the findings are found in **Table 12.3**.

Table 12.3. Hexene isomers obtained when 1-hexene was stirred with KO^{t}Bu in DMSO at various conditions

Hexene isomer	Isomer comp /% 22 h at rt	Isomer comp /% 14 hour reflux
1-hexene	95.64	95.14
Trans-3-hexene	0.47	0.82
Trans-2-hexene and *cis*-3-hexene	2.02	2.24
Cis-2-hexene	1.87	1.79

The isomerisation attempt using potassium tertiary butoxide in DMSO at room temperature did not yield the desired results (**Table 12.3**). Even when forcing conditions of hexene reflux were employed, isomerisation failed to take place (**Table 12.3**).

12.3.5.3. Isomerisation of 1-hexene using Rh(III) chloride trihydrate

The treatment of 1-hexene with catalytic amount of $RhCl_3.3H_2O$ (10% mol equiv) in ethanol, under reflux, afforded the isomerisation to the internal hexene isomers[58]. The composition of the isomers obtained is detailed in **Table 12.4**.

Table 12.4. Hexene isomers obtained when 1-hexene was stirred with Rh(III) chloride trihydrate as a catalyst for 24 under reflux, as seen using a GC

Hexene isomer	Isomer composition /%
1-hexene	1
Trans-2-hexene, *Trans*-3-hexene, *Cis*-3-hexene	76
Cis-2-hexene	23

The three isomers (t*rans*-2-hexene, *trans*-3-hexene and *cis*-3-hexene) were so close to each other that they were not fully resolved, thus their grouping into one product batch. What was interesting was that the isomer composition was close to the thermodynamic mixture as generated using ASPEN (**Table 12.5**).

Table 12.5. Thermodynamic isomer ratios of straight chain hexene isomers at 55° and 110°C as generated by ASPEN

Hexene Isomer	Amount /%
Hex-1-ene	1
Cis-hex-2-ene	33
Trans-hex-2-ene	41
Cis-hex-3-ene	4
Trans-hex-2-ene	20

We were now in a position to attempt the reverse isomerisation by converting internal hexene isomers to 1-hexene using the pre-catalysts that were synthesised.

12.3.6. Evaluation of $(\eta^5\text{-Cp})_2Zr(Cl)C_6H_{13}$ as an isomerisation catalyst for 1-hexene

Chlorobis(η^5-cyclopentadienyl)hexylzirconium(IV) complex was reacted with 1-hexene in toluene and the results of the study are summarised in **Table 12.6**. The purpose of the investigation was to check whether the pre-catalyst isomerised the terminal olefin to the internal alkenes. This was deemed important because if the catalyst catalysed the reaction in both directions, then the thermodynamic tendencies of the reaction under investigation would govern the reaction. If the catalyst is an isomerisation catalyst, then the olefin mixture at the end of the reaction will always be the thermodynamic favoured mixture (higher proportion of internal isomers).

Table 12.6. Isomerisation of 1-hexene to internal hexene isomers using chlorobis(η^5-cyclopentadienyl)hexylzirconium(IV) complex in toluene at various temperatures and pressures

P/Bar	*T*/°C	Time/h	1-Hexene	*Trans*-3-hexene *Cis*-3-hexene *Trans*-2-hexene	*Cis*-2-hexene
1	rt	48	100	0	0
1	110	48	100	0	0
50	150	24	100	0	0

It was apparent from the data tabulated above (**Table 12.8**) that the pre-catalyst did not act as an isomerisation catalyst as it failed to isomerise the terminal alkene to the thermodynamically stable internal alkenes even at elevated temperatures and pressure.

12.3.7. Catalytic isomerisation of internal to terminal Hexene double bond

12.3.7.1. Isomerisation of internal hexene isomers to 1-hexene using $(\eta^5\text{-Cp})_2Zr(Cl)C_6H_{13}$

Our initial investigation was to use one specific internal isomer and see whether it was isomerised using chlorohexylbis(cyclopentadienyl)zirconium(IV) complex. The investigation involved the isomerisation of *trans*-2-hexene. The choice of the isomer was rather arbitrary but we knew that it was the isomer that is preferentially produced when 1-hexene is isomerised using $RhCl_3.3H_2O$ catalyst in ethanol (**Section 12.3.5.3**). It was hoped that this would ensure that the isomerisation reaction under investigation would produce one product (1-hexene), making the study easier. The isomerisation reaction was carried out at 150°C and 50 bars in an autoclave for 24 h. The results of the investigation are found in **Table 12.7**.

Table 12.7. Isomerisation of *trans*-2-hexene to 1-hexene using chlorobis(cyclopentadienyl)hexylzirconium(IV) complex as analysed using GC

Isomer	Isomer composition /%
1-Hexene	6.10
Trans-3-hexene	3.62
Cis-3-hexene	8.22
Trans-2-hexene	78.76
Cis-2-hexene	3.30

The results obtained showed that the isomerisation of the internal hexene isomers took place slowly as only 6% of the terminal alkene was detected after 24 h of reaction at 150°C and 50 bars. Although the conditions employed were forcing, the isomerisation process was slow. The results supported the findings of Chirik *et al*[59] that an alkyl displacement using an olefin from the zirconium species is not facile. A general lack of β-

H elimination from primary alkyl complexes of the type $Cp_2Zr(CH_2CHR)(Cl)$ is the reason for the non-rearrangement and displacement[60].

The isomerisation reaction was also attempted using the thermodynamic internal isomer mixture generated using $RhCl_3.3H_2O$. The details of the results are summarised in **Table 12.8**. Both temperature and pressure were varied to check whether substantial isomerisation had taken place.

Isomerisation of the internal hexenes using the pre-catalyst did not take place. The percentage of hex-1-ene did not significantly improve even at high temperatures and pressures. The conclusion made from the study was that the attached hexyl group was firmly bound to the metal centre and not easily displaced by an olefin of the same chain length within the experimental conditions tested.

Table 12.8. Isomerisation of internal hexene isomers to 1-hexene using chlorohexylbis(cyclopentadienyl)zirconium(IV) complex

P/Bar	*T*/°C	Time/h	1-Hexene/%	*Trans*-3-hexene *Cis*-3-hexene *Trans*-2-hexene/%	*Cis*-2-hexene%
1	rt	48	1.1	76.4	22.5
1	110	48	1.2	76.6	22.2
10	150	24	1.2	77.00	21.8
20	150	24	1.4	84.3	14.3
40	150	24	3.9	87.1	9.0
50	150	24	3.2	77.6	19.2

12.3.7.2. Isomerisation of internal hexene isomers to 1-hexene using substituted chlorobis(cyclopentadienyl)hexylzirconium(IV) complex

The purpose of the investigation was to check whether the electronic and steric effects of the zirconium substituent could influence the isomeriation and detachment of an alkyl group from the zirconium species as a terminal olefin[61,62]. The Tolman cone angle of the cyclopentadienyl subtituents studied increased from H < Me < Et < ^{i}Pr < $SiMe_3$ < ^{t}Bu with relative similar electronic contribution[63]. We hoped that the difference in electronic and steric contribution of the subsituents would results in different catalytic activity.

The appropriate pre-catalyst was taken up in toluene and reacted with the internal hexene mixture in an autoclave at 150°C and 50 bars for 24 h. The hexene isomer mixture at the end of the reaction was analysed using a GC. **Table 12.9** summarises the results obtained from the investigation.

Table 12.9. Isomerisation of internal hexene isomers cocktail using substituted zirconium metallocenes in toluene at 150°C and 50 bar for 24 h

Metal complex, R = *n*-hexyl group	1-Hexene /%	*Trans*-3-hexene *Cis*-3-hexene *Trans*-2-hexene/%	*Cis*-2-hexene /%
$(\eta^5\text{-Me-}C_5H_4)_2ZrCl(R)$	3.1	78.6	18.3
$(\eta^5\text{-Et-}C_5H_4)_2ZrCl(R)$	5.4	77.4	17.2
$(\eta^5\text{-Bu}^t\text{-}C_5H_4)_2ZrCl(R)$	3.5	73.5	23.0
$(\eta^5\text{-Me}_3\text{Si-}C_5H_4)_2ZrCl(R)$	4.0	75.1	20.9

The results obtained using substituted zirconium metallocenes showed that the electronic and steric effects of the substituents on the cyclopentadienes had no influence on the isomerisation reaction studied. The amount of terminal olefin after 24 h of reaction was very small (less than 6%) for all the transformations indicative of no activity of the pre-catalysts.

12.3.7.3. Reaction of Cp_2ZrCl_2 / PEt_3 / *n*-BuLi with hexenes

The change of the spectator ligand, X, in Cp_2ZrX_2 to PEt_3 to form $Cp_2Zr(PEt_3)R$[64] was conducted to determine whether the isomerisation reaction followed by the alkyl detachment as a terminal olefin could be effected. $(\eta^5\text{-}C_5H_5)_2ZrCl_2$ was reacted with 1.4 M *n*-BuLi (2.2 mol equiv) at 78°C for an hour. PEt_3 (2.2 mol equiv) was slowly added to the mixture before warming to room temperature for 5 min and once more chilled back to 78°C. The reaction was carried out to generate $(\eta^5\text{-}C_5H_5)_2Zr(PEt_3)(C_4H_9)$ as a pre-catalyst. An internal hexene isomer mixture was then added to the basic mixture and the extent of isomerisation monitored periodically using an off-line GC as detailed in **Table 12.10**.

The reaction is thought to progress as outlined below (**Scheme 12.12**). For the fist time it was possible to detect higher percentages of the terminal olefin required (>20%). The highest percentage of 1-hexene detected (31%) was obtained when the reaction was allowed to react at -78°C for an hour. Reactions at higher temperatures for prolonged periods unfortunately resulted in lower percentages of the desired isomer.

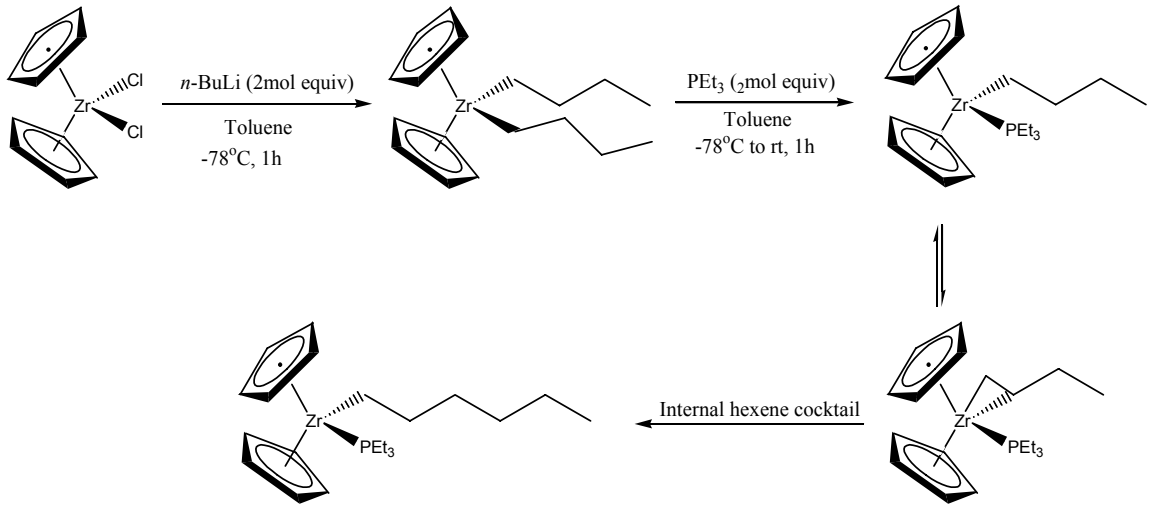

Scheme 12.12. The reaction of zirconocene with *n*-BuLi and PEt_3 to generate the pre-catalyst, $(\eta^5\text{-}C_5H_5)_2Zr(PEt_3)(C_4H_9)$ complex, required for olefin isomerisation

Table 12.10. Isomerisation of internal hexene cocktail to 1-hexene in toluene using (η^5-$C_5H_5)_2Zr(PEt_3)(C_4H_9)$ as a catalyst at various temperatures

Hexene isomer reacted	*T*/^{o}C	Time /h	1-hexene/%	*Trans*-2-hexene *Trans*-3-hexene *Cis*-3-hexene/%	*Cis*-2-hexene /%
Internal hexene cocktail	-78	1	31.6	59.6	87.8
Internal hexene cocktail	0	1	23.9	69.4	6.4
Internal hexene cocktail	rt	1	26.7	66.4	6.9
Internal hexene cocktail	rt	14	27.7	64.3	8.0

Further experimentation was carried out at -78°C, the temperature at which the highest degree of isomerisation was observed. The details of the findings are found in **Table 12.11**. The results failed to yield 1-hexene beyond a 34% conversion. The data showed that the amount of 1-hexene detected did not improve beyond 40% even when the reaction was carried out for 4 h at the experimental temperature.

Table 12.11. Isomerisation of internal hexene cocktail to 1-hexene in toluene using (η^5-$C_5H_5)_2Zr(PEt_3)(C_4H_9)$ as a catalyst at -78°C

Hexene isomer reacted	T/°C	Time /h	1-hexene/%	*Trans*-2-hexene *Trans*-3-hexene *Cis*-3-hexene/%	*Cis*-2-hexene /%
Internal hexene cocktail	-78	1	22.6	68.7	8.7
Internal hexene cocktail	-78	2	31.7	59.9	8.4
Internal hexene cocktail	-78	3	32.9	57.8	9.3
Internal hexene cocktail	-78	4	33.1	57.1	9.8

12.3.7.4. Reaction of Cp_2ZrCl_2 / PPh_3 / *n*-BuLi with hexenes

The success in obtaining about 30% 1-hexene from internal hexene isomers when using (η^5-$C_5H_5)_2Zr(PEt_3)(C_4H_9)$ as a pre-catalyst lead to the investigation of the same reaction using a bulkier phosphine, PPh_3, rather than PEt_3[65]. The reaction of (η^5-$C_5H_5)_2ZrCl_2$ with 1.4 M *n*-BuLi (2.2 mol equiv) and PPh_3 at 78°C generated the pre-catalyst (η^5-$C_5H_5)_2Zr(PPh_3)(C_4H_9)$ required for the isomerisation reaction. Once the hexene isomer mixture was added, the extent of the reaction was monitored hourly as detailed in **Table 12.12**. The sequence of reactions that generated the pre-catalyst is shown in **Scheme 12.13**. There was however no improvement of the percentage composition of the terminal olefin produced when a bulky phosphine was used (~30% of the product was obtained).

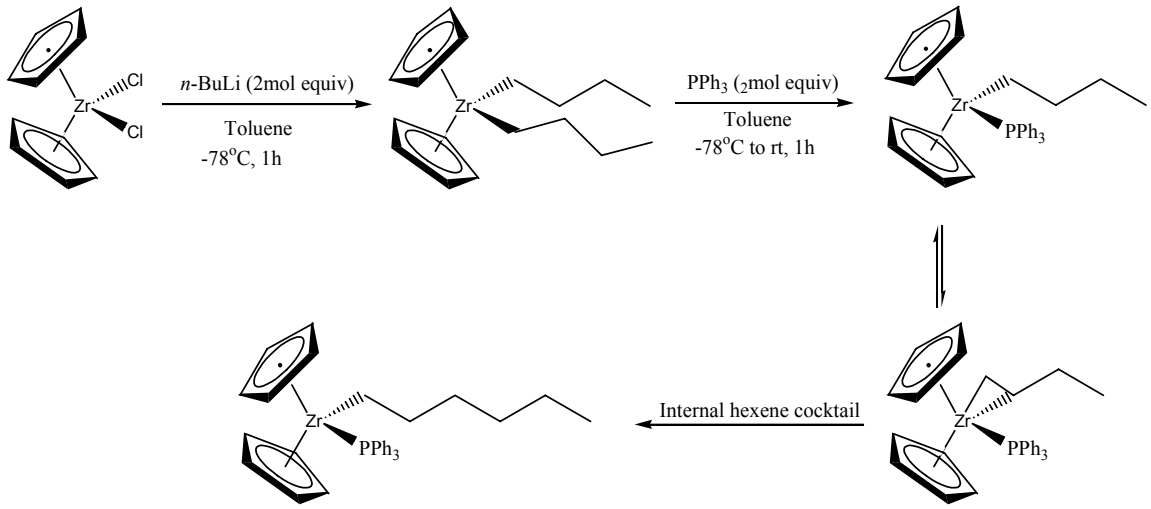

Scheme12.13. The reaction of zirconocene with *n*-BuLi and PPh_3 to generate the pre-catalyst, $(\eta^5\text{-}C_5H_5)_2Zr(PPh_3)(C_4H_9)$, required for olefin isomerisation

Table 12.12. Isomerisation of internal hexene cocktail to 1-hexene in toluene using $(\eta^5\text{-}C_5H_5)_2Zr(PPh_3)(C_4H_9)$ as a catalyst at 78°C

T/°C	Time /h	1-hexene/%	*Trans*-2-hexene *Trans*-3-hexene *Cis*-3-hexene/%	*Cis*-2-hexene /%
-78	1	30.7	59.5	9.8
-78	2	28.4	63.0	8.6
-78	3	23.7	70.9	5.4

12.3.7.5. Reaction of Cp_2ZrCl_2 / *n*-BuLi with hexenes

The next question that needed to be answered related to the role of the phoshine group in the isomerisation reaction. When the olefin was stirred in the presence of the phoshine alone, no isomerisation was observed. A reaction using *n*-BuLi together with Cp_2ZrCl_2 as reagents was then attempted.

Cp_2ZrCl_2 / 2(*n*-BuLi) reagents have found widespread use in organic synthesis and in catalysis[66]. Our quest was to check whether the system could work for the isomerisation reaction under investigation. The reaction of $(\eta^5\text{-}C_5H_5)_2ZrCl_2$ with 1.4 M *n*-BuLi (2.2 mol equiv) at 78°C generated the pre-catalyst $(\eta^5\text{-}C_5H_5)_2Zr(C_4H_9)_2$. Injecting internal hexene isomer mixture into the system followed by GC analysis using an off-line monitored the isomerisation reaction. **Table 12.13** shows the results obtained when the reaction was carried out using different amounts of the metal complex. **Scheme 12.14** shows how the pre-catalyst was formed.

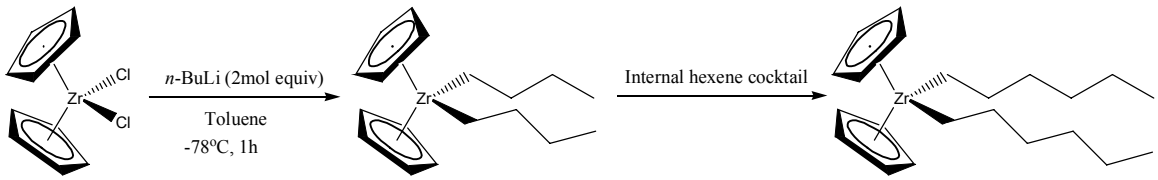

Scheme 12.14. The formation of bis(η^5-cyclopentadienyl)dibutylzirconium(IV) complex as a pre-catalyst for the isomerisation of internal hexene isomers to 1-hexene in toluene

Table 12.13. Isomerisation of internal hexene cocktail (4.0mmol, 0.5cm^3) using Cp_2ZrCl_2 and 1.4M *n*-BuLi in toluene

Cp_2ZrCl_2		nBuLi		*T*	Time	Isomerised hexene mixture			
Mass /mg	μmol	Vol /ml	Vol /mmol	/°C		1-Hexene /%	1-Hexene /μmol	The other 3-isomers /%	*Cis*-2-hexene /%
72	246	0.5	0.7	-78	10 min	16.5	666	62.6	20.9
72	246	0.5	0.7	rt	14 h	16.4	663	76.8	6.8
48	164	0.5	0.7	-78	10 min	14.0	566	66.8	19.2
48	164	0.5	0.7	rt	14 h	17.0	687	72.3	10.6
23	78.7	0.5	0.7	-78	10 min	25.9	1046	65.5	8.6
23	78.7	0.5	0.7	rt	14 h	19.6	792	67.4	13.0
7	23.9	0.5	0.7	-78	10 min	19.8	800	61.5	18.6
7	23.9	0.5	0.7	rt	14 h	28.4	1147	53.9	17.7
73	248	0.5	0.7	-78	10 min	16.5	666	62.6	20.9
73	248	0.5	0.7	rt	14 h	14.6	590	63.8	21.6
97	331	2.0	2.8	-78	30 min	37.5	1515	45.5	17.0
97	331	2.0	2.8	rt	5 h	40.2	1624	42.8	17.0
69	236	0.5	0.7	-78	10min	15.6	630	63.9	20.4
71	243	0.5	0.7	-78	10min	9.6	388	55.6	34.8
47	161	0.5	0.7	-78	10min	8.5	343	54.5	36.9
26	88.9	0.5	0.7	-78	10min	36.3	1466	52.3	11.4
5	17.1	0.5	0.7	-78	10min	13.2	533	55.4	31.4

The investigation revealed that isomerisation takes place when the system Cp_2ZrCl_2 / *n*-BuLi was used. It demonstrated that the phospine ligand was not necessary for the isomerisation reaction. Furthermore, the results also showed that there was no direct correlation between the amount of the zirconocene and the percentage of isomerised 1-hexene (17.1 μmol produced 13.2% while 243 μmol produced 9.6% are some of the examples that highlight the point). The general trend observed for the reaction carried out

at -78°C and those when warmed back to room temperature showed that the percentage of 1-hexene produced remained constant. The conclusion made based on the observation was that the reaction had gone to completion well before the ten min time interval was reached at -78°C and failed to continue thereafter. What was also observed was that when a higher amount of the base, *n*-BuLi was used, the amount of 1-hexene produced was significantly higher (2 cm^3 resulted in ~38-40% compared to 8-30% when 0.5 cm^3 was used).

The reaction was pursued further using a larger amount of the base and also increased amounts of the internal olefin mixture as detailed in **Table 12.14** below.

Table 12.14. Isomerisation of internal hexene cocktail (16.0mmol, 2.0cm^3) using Cp_2ZrCl_2 and 1.4 M *n*-BuLi in toluene

Cp_2ZrCl_2		nBuLi		*T*	Time	Isomerised hexene mixture			
Mass /mg	μmol	Vol /ml	Vol /mmol	/°C		1-Hexene /%	1-Hexene/ μmol	The other 3-isomers /%	*Cis*-2-hexene /%
239	818	2.5	3.5	-78	15min	19.42	3107	44.74	10.89
239	818	2.5	3.5	-78	1h	20.70	3312	47.18	5.75
239	818	2.5	3.5	0	1h	23.57	3771	38.08	9.09
239	818	2.5	3.5	rt	19h	21.68	3469	35.67	4.21

The percentage composition did not change when the reaction temperature was varied from -78 C to room temperature as was initially inferred (**Table 12.14**). It was deduced that the amount of the base influenced the percentage 1-hexene produced.

It was thought that the amount of cations (Li^+) present in solution may play a role in the reaction. The effect of increasing the amount of Li^+ cations present in solution was investigated. The investigation commenced with the introduction of sodium metal to the reaction mixture as detailed below (**Table 12.15**).

Table 12.15. Isomerisation of internal hexene isomers (0.5 cm^3) using Cp_2ZrCl_2 (102 mg) and 1.4 M *n*-BuLi in the presence of dispersed sodium in alumina (Na-Al_2O_3) for the generation of the active catalyst in toluene

Experimental conditions	*T* /°C	Time	1-Hexene /%	The other 3-isomers	*Cis*-2-hexene
Cp_2ZrCl_2 + Na-Al_2O_3	-78	15min	0.86	74.38	21.26
Cp_2ZrCl_2 + Na-Al_2O_3	rt	1h	-	79.14	19.85
+ nBuLi (0.7 mmol, 0.5 cm^3)	-78	30min	10.96	62.14	13.93
+ nBuLi (0.7 mmol, 0.5 cm^3)	rt	24h	9.54	56.92	15.45

When sodium dispersed in alumina was used in conjunction with zirconocene dichloride, no isomerisation took place. When *n*-BuLi was introduced to the reaction system, the amount of 1-hexene increased immediately. The conclusion made from the study was that Na-Al_2O_3 did not speed-up the reaction and that *n*-BuLi was necessary for the isomerisation reaction to take place.

The investigation was continued by the introduction of NaCl, rather than alumina as support. The results of the findings are detailed in **Table 12.16**.

Table 12.16. Isomerisation of internal hexene isomers (0.5 cm^3) using Cp_2ZrCl_2 (104 mg) and 1.4 M *n*-BuLi in the presence of dispersed sodium in sodium chloride (Na-NaCl) for the generation of the active catalyst in toluene

Experimental conditions	*T* /°C	Time	1-Hexene /%	The other 3-isomers	*cis*-2-hexene
Cp_2ZrCl_2 + Na-NaCl	-78 to rt	14 h	-	74.37	21.92
+ *n*-BuLi (0.98 mmol, 0.7 cm^3)	-78	15 min	11.34	56.29	13.37
+ *n*-BuLi (0.98 mmol, 0.7 cm^3)	-78	3 h	11.77	70.29	7.83
+ *n*-BuLi (0.7 cm^3)	rt	24 h	7.87	56.84	15.07

The reaction again failed to yield isomerised 1-hexene in the absence of *n*-BuLi. Once *n*-BuLi was introduced terminal olefin was detected but the amount of the isomerised terminal olefin remained constant once formed. As with Na-Al_2O_3, the dispersed sodium in sodium chloride did not speed-up the reaction and *n*-BuLi was necessary for the isomerisation reaction to take place.

The investigated was extended to include the use of sodium metal dispersed in lithium chloride as support (**Table 12.17**).

Table 12.17. Isomerisation of internal hexene isomers using Cp_2ZrCl_2 (105 mg, 359 μmol) and *n*-BuLi (0.7 mmol, 0.5 cm^3) in the presence of dispersed sodium in lithium chloride (Na-LiCl) at –78°C for the generation of the active catalyst in THF

Experimental conditions	*T*/°C	Time	1-Hexene /%	The other 3-isomers	*cis*-2-hexene
All reagents mixed	-78	10 min	8.74	47.89	12.64
All reagents mixed	rt	16h	17.70	40.15	11.92

Dispersed sodium in lithium chloride did not help speed-up the reaction but the amount of the isomerised olefin doubled as the reaction temperature was increased from -78°C to room temperature. The amount of isomerised terminal olefin produced was still much lower than desired.

12.2.7.6. Reaction of *n*-BuLi with hexenes

The reaction of olefins (terminal or internal) with *n*-BuLi as sole reagent was attempted. The details of the findings are summarised in **Table 12.18.**

Table 12.18. Isomerisation of internal hexene isomers using 1.4 M *n*-BuLi (0.5 cm^3) at -78°C in toluene (no zirconocene dichloride utilised)

Experimental conditions	*T*/°C	Time	1-Hexene /%	The other 3-isomers	*cis*-2-hexene
n-BuLi only	-78-rt	10 min	-	-	-
1-hexene (0.5 cm^3)	-78	30min	100	-	-
Hexene cocktail (0.5 cm^3)	-78	1h	-	78.2	21.8
Hexene cocktail (1.0 cm^3)	-78	1h	1.7	66.7	31.6
Hexene cocktail (1.0 cm^3)	rt	16	0.80	76.0	23.2

There was no isomerisation of internal or terminal hexenes that took place when *n*-BuLi was used alone (**Table 12.18**). The results thus showed that the isomerisation reaction only took place when zirconocene dichloride and *n*-BuLi contained in the reaction mixture.

What was apparent from all the reactions conducted was the formation of a stoichiometric amount of terminal olefin limited by the amount of the base, *n*-BuLi, used during the transformation (**Tables 12.13 –12.17**).

To check this proposal, the reaction with one specific internal hexene isomer, *cis*-2-hexene, was undertaken. **Table 12.19** below summarises the results obtained.

Table 12.19. Isomerisation of *cis*-2- hexene (4.0 mmol, 0.5 cm^3) using Cp_2ZrCl_2 and *n*-BuLi at –78°C for the generation of the active catalyst in toluene

		Cp_2ZrCl_2		*n*-BuLi		*T*	Time		
Mass /mg	μmol	Vol /cm^3	Vol /mmol	/°C		1-Hexene /%	The other 3-isomers /%	*cis*-2-Hexene /%
102	349	0.5	4.0	-78	10 min	22.4	-	24.0
102	349	0.5	4.0	-78	1h	23.4	-	23.1

There was no advantage in using one specific internal hexene isomer for the isomerisation reaction. Only the terminal hexene isomer was produced when the specified internal isomer was reacted enhancing our earlier finding that the metallocenes investigated were not isomerisation catalysts.

12.3.7.7. Reaction of Cp_2ZrCl_2 / NaH with hexenes

The use of a different base, sodium hydride (NaH) rather than *n*-BuLi was investigated next. $(\eta^5\text{-}C_5H_5)_2ZrCl_2$ and NaH (2.0 mol equiv) were reacted in toluene and hexene isomers introduced to check the extent of the isomerisation reaction. Samples were withdrawn at pre-set times and analysis conducted using an off-line GC. **Table 12.20** shows the results obtained while **Scheme 12.15** depicts the reaction pathway.

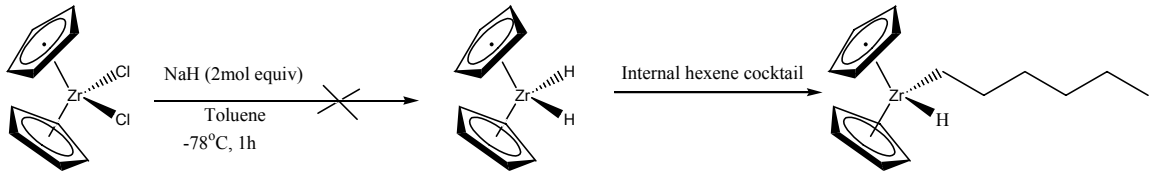

Scheme 12.15. The attempted transformation of $(\eta^5\text{-}C_5H_5)_2ZrCl_2$ with NaH in toluene to generate a pre-catalyst for the isomerisation of internal hexene isomers to 1-hexene

Table 12.20. Isomerisation of internal hexene isomers (1.0 cm^3) using Cp_2ZrCl_2 (101 mg) and NaH (27.6 mg, 2 mol equiv) in toluene at various temperatures

T/°C	Time/h	1-hexene/%	The other 3-isomers/%	2-*cis*-Hexene/ %
rt	5	1.6	82.0	16.4
rt	45	1.1	89.9	8.9
rt	60	0	87.9	12.1
rt	2880	1.1	88.2	10.7

The reaction failed to yield the desired 1-hexene even when the reaction was allowed to react for two d under the reaction conditions employed (**Table 12.20**). As shown in

Scheme 12.6, the base might not have been strong enough to yield the dihydride complex that could have potentially acted as a pre-catalyst for the isomerisation reaction of interest.

12.3.7.8. Reaction of Cp_2ZrH_2 with hexenes

Bis(cyclopetadienyl)dihydridozirconium(IV) complex was synthesised from the reaction of $(Cp_2ZrCl)_2O$ and $LiAlH_4$ in THF before the introduction of the hexene isomer mixture. The extent of isomerisation was checked using a GC at –78°C, 0°C and room temperature. One experiment was conducted under ultra-violet radiation. Results are shown in **Table 12.21** below while **Scheme 12.7** shows the reaction sequence.

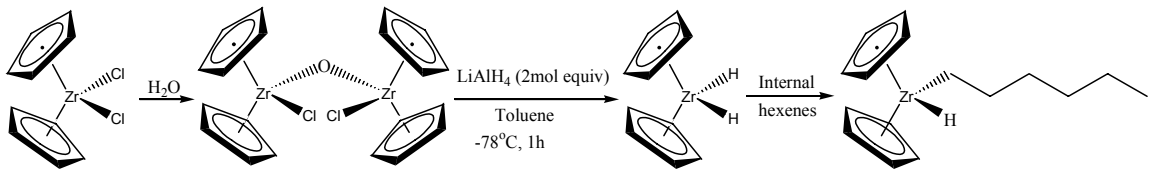

Scheme 12.16. The synthesis of bis(cyclopetadienyl)dihydridozirconium(IV) complex as a pre-catalyst for the isomerisation of internal hexene isomers to 1-hexene

Table 12.21. Isomerisation of internal hexene isomers (0.5 cm^3) using Cp_2ZrH_2 generated *in situ* from Cp_2ZrCl_2 and $LiAlH_4$ in toluene at various experimental conditions

Experimental conditions	*T* /°C	Time /h	1-Hexene /%	The other 3-isomers	*cis*-2-hexene
Internal hexenes(0.5 cm^3)	-78	1	0.9	69.7	29.4
Internal hexenes(0.5 cm^3)	0	1	1.3	74.8	23.9
Internal hexenes(0.5 cm^3)	rt	3	1.0	73.3	25.7
Internal hexenes(0.5 cm^3)	rt	21	0.7	75.5	23.8
Internal hexenes(0.5 cm^3), 294 nm irradiation at room temperature	rt	6	1.1	71.3	27.6

The isomerisation of the internal hexene isomers failed to take place under the reaction conditions employed. The results showed that even after irradiation of the solution with ultraviolet light for 6 h no isomerisation occurred.

The effect of high temperature and pressure on the reaction was also investigated. **Table 12.22** below shows the results obtained when the reactions was conducted under pressure and elevated temperatures.

Table 12.22. Isomerisation of internal olefins isomers using Cp_2ZrH_2 generated *in situ* from Cp_2ZrCl_2 and $LiAlH_4$ at elevated temperatures and pressures

Temp/°C	Pressure /bars	Time/h	1-Hexene	The other 3 Isomers	*Cis*-2-Hexene
64-66	1	22	0.54	87.01	8.61
50	50	47	0.68	90.58	6.03
50	50	65	1.05	74.16	23.81
150	50	25	1.47	80.05	15.96

Heating the reaction mixture at the refluxing internal hexene temperature did not result in isomerisation reaction leading to more 1-hexene being observed (**Table 12.22**). The isomerisation reaction failed to take place even at elevated pressures and temperatures (**Table 12.22**).

12.3.7.9. Reaction of $(R\text{--}C_5H_4)_2ZrBu_2$ with hexenes

The isomerisation reaction of internal hexenes took place when the system Cp_2ZrCl_2 / *n*-BuLi was employed. The investigation detailed here deals with the use of substituted zirconocene dichlorides as pre-catalysts in conjunction with *n*-BuLi. It was envisaged that the electronic and steric effects of the substituents would lead to better yields of the terminal olefin.

Scheme 12.17 outlines the general reaction pathway for the generation of the pre-catalysts used for the isomerisation of internal hexenes in toluene starting from (R-$C_5H_4)_2ZrCl_2$, R = Me, Et, ^{t}Bu, ^{i}Pr and Me_3Si). **Sections 12.3.7.9.1 - 12.3.7.9.5** deals with the chemistry of the generated species as outlined and how the isomerisation reaction was effected by the electronic and steric effects of the substituents on the cyclopentadienyl ring.

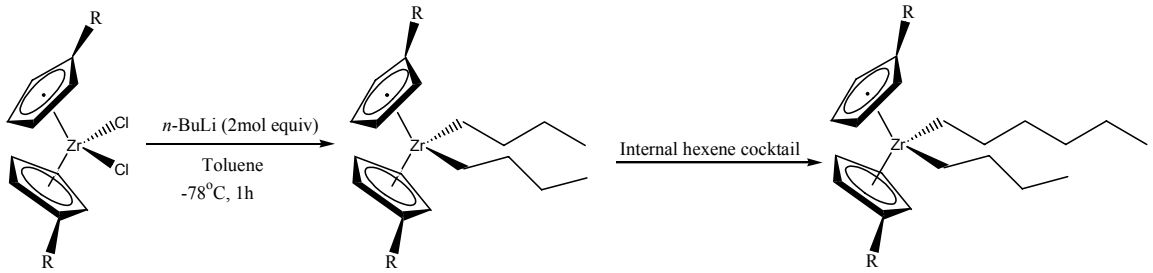

R = Me, Et, ^{t}Bu, ^{i}Pr, Me_3Si

Scheme 12.17. The synthesis of substituted dibutylzirconocene complexex and their use as catalyst for the isomerisation of internal hexene isomers to hex-1-ene

12.3.7.9.1. Reaction of (Me-$C_5H_4)_2ZrBu_2$ with hexenes

(Me-$C_5H_4)_2ZrBu_2$ was generated from the reaction of (Me-$C_5H_4)_2ZrCl_2$ with *n*-BuLi in toluene. The results of the isomerisation of intenal hexenes using (Me-$C_5H_4)_2ZrBu_2$ in toluene is shown in **Table 12.23**. The results showed that the isomerisation took place but the amount of the terminal olefin produced was similarly stoichiometric. Prolonged reaction at room temperature did not significantly increase the amount of the terminal alkene.

Table 12.23. The use of (Me-$C_5H_4)_2ZrBu_2$ generated *in situ* from *n*-BuLi and (Me-$C_5H_4)_2ZrCl_2$ for the isomerisation of internal hexenes in toluene

(Me-$C_5H_4)_2ZrBu_2$ /μmol	*T*/°C	Time	1-Hexene /%	The other 3 isomers /%	*cis*-2-hexene /%
83.2	-78	10 min	14.7	64.6	20.7
83.2	-78	1h	14.8	64.8	20.4
83.2	rt	14h	20.4	65.1	20.3

12.3.7.9.2. Reaction of (^{i}Pr-$C_5H_4)_2ZrBu_2$ with hexenes

(^{i}Pr-$C_5H_4)_2ZrBu_2$ was generated *in situ* from the reaction of *n*-BuLi and (^{i}Pr-$C_5H_4)_2ZrCl_2$ in toluene. The pre-catalyst was then used for the isomerisation of hexene isomers. The results of the investigation are summarised in **Table 12.24**. The amount of the terminal alkene produced from the reaction remained constant even when the reaction temperature was increased. The degree of isomerisation was comparable to that of (Me-$C_5H_4)_2ZrBu_2$.

Table 12.24. The use of (^{i}Pr-$C_5H_4)_2ZrBu_2$ generated *in situ* from *n*-BuLi and (^{i}Pr-$C_5H_4)_2ZrCl_2$ for the isomerisation of internal hexenes in toluene

(^{i}Pr-$C_5H_4)_2ZrCl_2$ /μmol	*T*/°C	Time	1-Hexene /%	The other 3 isomers /%	*cis*-2-Hexene /%
	-78	10 min	17.3	66.0	16.7
	-78	1h	24.4	54.7	20.9
	rt	17h	20.6	61.1	18.3

12.3.7.9.3. Reaction of (^{t}Bu-C_5H_4)$_2$ZrBu$_2$ with hexenes

The pre-catalyst was made from the reaction of (^{t}Bu-C_5H_4)$_2$ZrCl$_2$ and *n*-BuLi in toluene and reacted with hexene isomers to generate 1-hexene using an off-line GC. The results of the investigation are shown in **Table 12.25**. The percentage composition of the terminal olefin generated was much higher at -78°C after 10 min of experimentation. The amount seemingly decreased with time, and more so when the reaction mixture was warmed up to room temperature.

Table 12.25. The use of (^{t}Bu-C_5H_4)$_2$ZrBu$_2$ generated *in situ* from *n*-BuLi and (^{t}Bu-C_5H_4)$_2$ZrCl$_2$ for the isomerisation of internal hexenes in toluene

(^{t}Bu-C_5H_4)$_2$ZrBu$_2$ /μmol	*T*/°C	Time	1-Hexene /%	The other 3 isomers /%	*cis*-2-hexene /%
61.8	-78	10min	40.9	55.1	4.0
61.8	-78	1h	21.4	66.2	12.4
61.8	rt	14h	18.8	64.5	16.7

12.3.7.9.4. Reaction of (SiMe$_3$-C_5H_4)$_2$ZrBu$_2$ with hexenes

(SiMe$_3$-C_5H_4)$_2$ZrBu$_2$ was generated from the reaction of (SiMe$_3$-C_5H_4)$_2$ZrCl$_2$ and *n*-BuLi in toluene and reaction with internal hexene isomers was used to check the isomerisation reaction. Analysis was conducted using an off-line GC and the results obtained summarised in **Table 12.26**. The amount of the desired terminal olefin did not improve beyond 40% and it decreased when the reaction mixture was warmed up to room temperature.

Table 12.26. The use of $(SiMe_3\text{-}C_5H_4)_2ZrBu_2$ generated *in situ* from *n*-BuLi and $(SiMe_3\text{-}C_5H_4)_2ZrCl_2$ for the isomerisation of internal hexenes in toluene

catalyst /μmol	*T*/°C	Time	1-Hexene /%	1-Hexene/ μmol	The other 3 isomers /%	*cis*-2-Hexene /%
57.3	-78	10min	22.1	893	67.6	10.3
57.3	-78	1h	36.9	1491	55.4	7.7
57.3	rt	16h	17.0	689	63.0	20.0

12.3.7.9.5. Reaction of $(Et\text{-}C_5H_4)_2ZrBu_2$ with hexenes

$(Et\text{-}C_5H_4)_2ZrBu_2$ was synthesised from the reaction of $(Et\text{-}C_5H_4)_2ZrCl_2$ and *n*-BuLi in toluene and used as a pre-catalyst for the isomerisation of hexene isomers. The results of the investigation are summarised in **Table 12.27**. The amount of 1-hexene detected was significantly higher (42%) at -78°C after an hour than from previous investigations. As with other substituted metallocenes reaction investigated, the isomerised amount of hex-1-ene decreased upon increasing the reaction temperature to room temperature.

Table 12.27. The use of $(Et\text{-}C_5H_4)_2ZrBu_2$ generated *in situ* from *n*-BuLi and $(Et\text{-}C_5H_4)_2ZrCl_2$ for the isomerisation of internal hexenes in toluene

$(Et\text{-}C_5H_4)_2ZrCl_2$ /μmol	*T*/°C	Time	1-Hexene /%	The other 3 isomers /%	*cis*-2-Hexene /%
71.7	-78	10min	37.0	52.9	10.1
71.7	-78	1h	42.8	54.2	-
71.7	rt	16h	27.2	61.1	11.7

The investigating using $(Et\text{-}C_5H_4)_2ZrBu_2$ was scrutinised further at -78°C, the temperature at which there was greater 'catalyst' activity. The results obtained from the investigation are found in **Table 12.28**.

Table 12.28. Isomerisation of internal hexene isomers using (Et-C_5H_4)$_2$ZrBu_2 as a catalyst in toluene at -78°C

T /°C	Time	Internal hexane isomers/cm^3	1-Hexene /%	The other 3 isomers /%	*cis*-2-Hexene /%
-78	10min	0.5	40.0	47.5	12.5
-78	10min	1.0	18.6	72.8	8.6
-78	10min	2.0	4.7	65.2	30.1
-78	1h	0.5	23.8	54.8	21.4
-78	1h	1.0	8.9	64.2	26.9
-78	1h	2.0	5.2	66.2	28.6
-78	2h	0.5	22.6	54.7	22.7
-78	2h	1.0	9.0	83.8	7.2
-78	2h	2.0	5.1	87.2	7.7
-78	3h	0.5	23.0	54.9	22.1
-78	3h	1.0	9.0	66.4	24.6
-78	3h	2.0	4.5	64.5	31.0
0	1h	0.5	20.8	51.5	27.7
0	1h	1.0	9.3	64.2	26.5
0	1h	2.0	5.5	69.5	25.0

The results proved beyond doubt that the reaction was stoichiometric. As the amount of the internal olefin was doubled while keeping the amount of the catalyst constant, the amount of the isomerised olefin was almost halved.

12.4. CONCLUSIONS

Substituted cyclopentadienes (R-C_5H_4, R = Me, Et, ^{i}Pr, ^{t}Bu, $SiMe_3$) were synthesised in moderate yields (42 – 68%). They were successfully used to synthesise zirconium(IV) metallocene dichlorides (66 – 83% yield) that were screened as potential internal to terminal olefin isomerisation catalysts.

Due to the cost implication associated with internal hexenes, isomersaition reactions using, the readily available and cheap, 1-hexene to form internal hexene isomers were conducted. Methods using bases like Na adsorbed in silica and KO^{t}Bu in DMSO failed to isomerise 1-hexene. When catalytic amount of $RhCl_3.3H_2O$ in ethanol was used the thermodynamic mixture of linear hexenes were obtained.

When chlorobis(η^5-cyclopentadienyl)hexylzirconium(IV) was reacted with hex-1-ene under various experimental conditions, no internal hexene isomers were observed. The investigation ruled out the possibility of the complex acting as an isomerisation catalyst.

The reaction of chlorobis(η^5-cyclopentadienyl)hexylzirconium(IV) complex with internal hexene isomers failed to yield terminal olefins even under harsh experimental conditions. The findings were in line with the conclusion Chirik and co-workers made that revealed that the detachment of an alky moiety from a zirconium alkyl complex as a terminal olefin is not a facile process. Isomerisation reactions using substituted zirconium metallocenes also failed to produce the terminal olefin (hex-1-ene).

The reaction of Cp_2ZrCl_2 / PR_3 / *n*-BuLi , (R = Et, Ph) with hexenes yielded a stoichiometric amount of 1-hexene. The reaction was found to be catalytic in Cp_2ZrCl_2 but limited by the amount of *n*-BuLi. Further investigations revealed that the isomerisation reaction could take place when using the system Cp_2ZrCl_2 / *n*-BuLi, ruling out the need to use phosphines. Isomerisation experiments using phoshines or *n*-BuLi as sole reagents failed to take place proving the need to have the metal complex. The use of substituted zirconium metallocenes in conjunction with *n*-BuLi did not significantly improve the isomerisation reaction outcome. The reaction remained stoichiometric regardless of the manipulations attempted.

12.5. REFERENCES

1. H. W. Carhart, *J. Hazard. Mater.*, 1994, **36**, 133.
2. H Francis and Y. De Kouchkovsky, *Photosynth. Res.*, 1998, **57**, 231.
3. D. W. Urray, *J. Phys. Chem. Rev., Section B*, 1997, **101**, 11007.
4. M. L. Imhoff, L. R. Bounoua, L. C. Taylor, R. Harriss and W. T. Lawrence, *Nature*, 2004, **429**, 870.
5. N. Frigaard, D. A. Bryant, *Arch. Microbiol.*, 2004, **182**, 265.
6. V. Smetacek, *Ophelia Supplementum*, 1980**, 1**, 65.
7. A. Parker, *Kirk-Othmer Encyclopaedia of. Chemical. Technology*, 2nd Ed, Wiley, New York 1966, **10**, 179.
8. R. C. Darton, *Process Saf. Environ. Prot.*, 2003, **8**, 576.
9. P. R. Ehrlich and A. H. Ehrlich, *Amicus J.*, 1990, **12**, 22.
10. V. Hopp, *Eng. Life Sci.*, 2002, **2** 45.
11. F. J. Molster, L. B. F. M. Waters, *Lecture Notes Phys.*, 2002, **609**, 121.
12. W. Juszczyk, *Appl. Catal., A*, 2001, **206**, 67.
13 M. Beller, B. Zimmermann and H. Geissler., *Chem. Eur. J*, 1999, **5**, 1301-1305.
14. A. J. Hubert, and H. Reimlinger, *Synth.*, 1969, 97.
15. Y. M. A. Yamada, K. Takeda, H. Takahashi and S. Ikegami, *Tetrahedron Lett.,* 2003, **44**, 2379.
16. B. Cornils and W. A. Herrmann, *J. Catal.*, **216**, 23.
17. Z. M. Rodriguez, M. L. Clarke, D. F. Foster, D. J. Cole-Hamilton, A. M. Z. Slawin and J. D. Woollins, *J. Chem. Soc, Dalton Trans.,* 2001, **7**, 969.
18. C. Janiak, U. Versteeg, K. C. H. Lange, R. Weimann and E. Hahn, *J. Organometal. Chem.,* 1995, **501**, 219.
19. C. A. Tolman, *Chem. Rev.*, 1977, **77**, 313.
20. C. H. Angell, *US Patent*, 1939, US 2184069.
21. E. R. Kanhofer, *US Patent*, 1941, US 2237432.
22. C. Xie, J. Long, J. Zhang, Z. Li and X. Wang, *US Patent*, 2005, US 2005020867.
23. G. D. Galland, M. Seferin, R. S. Mauler and J. H. Z. Dos Santos, *Polym.*

Int., 1999, **48**, 660.

24. C. Andrei, G. Andrei, S. Pita, O. Pitpalac and I. Sonoc, *Revue Roumaine de Chimie*, 1990, **35**, 663.
25. P. T. Daniell, W. D. Heitz, T. E. Spriggs, T. J. Mcneil and K. J. Cann, 1994, *US Patent*, US 5371145.
26. R. Modler, E. Anderson and Y. Yoshida, CEH Marketing Research Report on Linear Alpha Olefins, March 1997.
27. H. C. Brown and M. V. Bhatt, *J. Am. Chem. Soc.,* 1966, **88**, 1440.
28. T. H. Johnson, *US Patent*, 1983, US 4423376.
29. E. L. Muetterties, *Transition Metal Hydrides,* Marcel Dekker, New York, 1971.
30 F. R. Hartley, *Chem. Rev*, 1973, **73**, 163.
31 J. W. Lauher and R. Hoffmann, *J. Am. Chem. Soc*, 1976, **98**, 1729.
32 D. W. Hart and J. Schwartz, *J. Am. Chem. Soc*, 1974, **96**, 8115.
33. D. W. Hart and J. Schwartz, *J. Am. Chem. Soc*, 1974, **96**, 8115.
34. T. F. Blackburn, J. A. Labinger and J. Schwartz, *Tetrahedron Lett*., 1975, 3041.
35. C. A. Bertelo and J. Schwartz, *J. Am. Chem. Soc*., 1976, **98**, 262.
36. D. W. Hart, T. F. Blackburn and J. Schwartz, *J. Am. Chem. Soc*., 1975, **97**, 679.
37. J. Schwartz and J. A. Labinger, *Angew. Chem. Int. Ed.*, 1976, **15**, 333.
38. R. G. Kidwell and G. J. Lynch, *Terminal Olefin Preparation*, US Patent 4125567, 1978.
39. P. C. Wailes, R. S. P. Coutts and H. Weigold, *Organometallic Chemistry of Titanium, Zirconium and Hafnium,* Academic Press, New York, 1974.
40. P. B. Hitchcock, J. F. Nixon and N. Sakarya, *J. Organomet. Chem.,* 2002, **662**, 193.
41. H. Schumann, *Pure Appl. Chem.,* 1991, **63**, 813.
42. D. Cozak, F. Gauvin and J. Demers, *J. Can. Chem.,* 1986, **64**, 71.
43. K. Sunkel and C. Stramm, *Inorganica Chim. Acta*, 2000, **298**, 33.
44. K. E. Du Plooy, C. F. Marais, L. Carlton, R. Hunter, J. C. A. Boeyens and N. J. Coville, *Inorg. Chem.,* 1989, **28**, 3855.
45. C. W. Jefford, R. McCreadie, P. Mueller, B. Siegfried, *J. Chem. Edu.,* 1971,

48, 708.

46. M. F. Lappert, C. J. Pickett, P. I. Riley and P. I. W. Yarrow, *J. Am. Chem. Soc., Dalton Trans.,* 1981, 805.
47. P. C. Wailes and H. Weigold, *J. Organomet. Chem.,* 1970, **24**, 405.
48. E Negishi, J. A. Miller and T. Yoshida, *Tetrahedron Lett.,* 1984, **25**, 3407.
49. D. W. Hart and J. Schwartz, *J. Am. Chem. Soc.,* 1974, **96**, 8115.
50. J. Schwartz, J. A. Labinger, *Angew. Chem. Int. Ed.,* 1976, **15**, 333.
51. W. O. Haag and H. Pines, *J. Am. Chem. Soc*., 1959, **82**, 387.
52. H. Pines and W. O. Haag, *J. Org. Chem*., 1959, **23**, 328.
53. H. Pines, J. A. Vesely and V. N. Ipatieff, *J. Am. Chem. Soc*., 1955, **77**, 347.
54. R. H. De Wolfe and W. G. Young, *Chem. Revs.,* 1958, **56**, 753.
55. J. I. Brauman and L. K. Blair, *J. Am. Chem. Soc.,* 1970, **92**, 5896.
56. A. Schreisheim, C. A. Rowe Jr and L. Naslund, *J. Am. Chem. Soc.,* 1963, **85**, 2111
57. S. Bank, *J. Org. Chem.,* 1972, **37**, 114.
58. D. L. Schmitt and H. B. Jonasen, *J. Organomet. Chem.,* 1973, **49**, 469.
59. P. J. Chirik, M. W. Day, J. A. Labinger and J. E. Bercaw, *J. Am. Chem. Soc.,* 1999, **121**, 10308.
60. K. L. Gell, B. Posin, J. Schwartz and G. M. Williams, *J. Am. Chem. Soc,* 1982, **104**, 1840.
61. A. Dormond, M. Fauconet, J. C. LeBlanc and C. Moise, *Polyhedron,* 1984, **3**, 897.
62. P. G. Gassman and C. H. Winter, *Organometallics*, 1991, **10**, 1592.
63. N. E. Grimmer, *The Ethane Polymerisation Behaviour of Zirconium Metallocenes: A Steric and Electronic Investigation Into The Influence of Substituent Effects,* Doctoral thesis, University of The Witwatersrand, 2000.
64. S. L. Buchwald, B. T. Watson and J. C. Huffman, *J. Am. Chem. Soc.,* 1987, **109**, 2544.
65. L. Gelmini and D. W. Stephan, *Organometallics*., 1988, **7**, 849.
66. E. Negishi and T. Takahashi, *Acc. Chem. Res*., 1994, **27**, 124.

CHAPTER 13: CONCLUSIONS AND FUTURE SUGGESTIONS

13.1. CONCLUSIONS

The thesis broadly focused on two objectives: (i) study of the solventless reactions of manganese carbonyl complexes and (ii) study of olefin catalysis using substituted *bis*(cyclopentadienyl)zirconium dichloride metallocenes.

Regarding the first objective, syntheses of manganese carbonyl complexes, $Mn(CO)_5Br$, $Mn(CO)_4LBr$ [L = PPh_3, P(*p*-MeO-$C_6H_4)_3$), P(*p*-Me-$C_6H_4)_3$), P(*p*-F-$C_6H_4)_3$ and P(*p*-Cl-$C_6H_4)_3$], $Mn_2(CO)_8Br_2$, $Mn(CO)_3LBr$ [L = PPh_3, P(*p*-MeO-$C_6H_4)_3$), P(*p*-Me-$C_6H_4)_3$), P(*p*-F-$C_6H_4)_3$ and P(*p*-Cl-$C_6H_4)_3$], was carried out successfully using modified synthetic protocols to give the materials in reasonable to good yields (19-91% yield). All the complexes formed were moisture stable in their crystal form.

An attempt to follow the kinetics of the reaction of $Mn(CO)_5Br$ with PPh_3 in the absence of solvents using FTIRS failed because the rate of formation of $Mn(CO)_4(PPh_3)Br$ was the same as the rate of its conversion to form $Mn(CO)_3(PPh_3)_2Br$. Attempts to conduct the experiments at lower temperatures (< 40°C) failed as the reaction did not take place. The route was then abandoned and alternative routes sought that would lead to the same product.

The solventless reaction of $Mn_2(CO)_8Br_2$ with PPh_3 as followed by DSC revealed a similar pathway to that of $Mn(CO)_5Br$ with PPh_3. The results signified a reaction that produced $Mn(CO)_4(PPh_3)Br$, which reacted further to yield $Mn(CO)_3(PPh_3)_2Br$. Without further experimentation, the route was also abandoned.

The solventless reaction of $Mn(CO)_4(PPh_3)Br$ with PPh_3 to form $Mn(CO)_3(PPh_3)_2Br$ as neat reagents using FTIRS was investigated. $Mn(CO)_3(PPh_3)_2Br$ was produced

selectively and a kinetic study was then undertaken. It was found that the reaction followed pseudo first order kinetics. The enthalpy change of formation of the reaction was found to be 143 ± 19 $kJmol^{-1}$ while the activation entropy change of formation was 104 ± 7 $Jmol^{-1}K^{-1}$.

The solventless reaction of $Mn(CO)_4(PPh_3)Br$ with PPh_3 to form $Mn(CO)_3(PPh_3)_2Br$ in chloroform and TCE solutions was conducted. The activation energy change was found to be 146 ± 8 $kJmol^{-1}$ and 137 ± 6 $kJmol^{-1}$ in TCE and chloroform respectively. The entropy change of activation was found to be 114 ± 6 $Jmol^{-1}K^{-1}$ and 97 ± 5 $Jmol^{-1}K^{-1}$ in TCE and chloroform respectively. The activation parameters were found to be similar for both solution and solventless transformations leading to the conclusion that the mechanism of the reaction was the same in both systems. The activation parameters supported a dissociative reaction mechanism.

The solventless reaction of $Mn(CO)_4(PPh_3)Br$ with PPh_3 in a KBr matrix using DRIFTS was investigated. The reaction also followed pseudo first order kinetics under two conditions: (i) when the metal to ligand ratio was higher than 1:5 and (ii) when the metal complex amount used was ≤ 0.5 mg in 100 mg of KBr solid support. The enthalpy change of formation was found to be 169 ± 28 $KJmol^{-1}$ while the activation entropy change of formation was 204 ± 57 $Jmol^{-1}K^{-1}$ under these conditions. These enthalpy values are also similar to those discussed above, while the enthalpy values were larger (but note the error bars).

The solventless reaction of $Mn(CO)_4(PPh_3)Br$ with PPh_3 in a solid matrix using DRIFTS was found to be dependent on the sample preparation method and the nature and size of the support particles.

The soventless reaction, $Mn(CO)_4LBr + L \rightarrow Mn(CO)_3L_2Br + CO$ [L= $P(p\text{-}C_6H_4\text{-}R)_3$, R = Ph, MeO, Cl, F] in KBr, using DRIFTS, was also studied. It was found that the electronic effects of the ligand already attached on the metal complex influenced the rate of the reaction. When R = MeO and Me, the enthalpy of activation was smaller than

when R= Cl and H). When R = F, the enthalpy of activation was unexpectedly found to be lower.

The solventless reaction between $Mn(CO)_4(PPh_3)Br$ and $P(p\text{-}MeO\text{-}C_6H_4)_3$ was monitored using ^{31}P NMR spectroscopy. The study revealed an additional reaction pathway that was not observed using FTIRS and DRIFTS. It showed that the phosphine ligand already attached to Mn also dissociated. The dissociation of phosphine ligand was faster than the dissociation of the CO ligand. The mixed ligand, $Mn(CO)_3(PPh_3)(P(p\text{-}MeO\text{-}C_6H_4)_3)Br$ was formed during the reaction.

The solventless reaction between $Mn(CO)_4(P(p\text{-}MeO\text{-}C_6H_4)_3)Br$ and PPh_3 was also monitored by ^{31}P NMR spectroscopy. Dissociation of $P(p\text{-}MeO\text{-}C_6H_4)_3$ from the metal complex was observed. Since $P(p\text{-}MeO\text{-}C_6H_4)_3$ ligand was able to substitute the PPh_3 ligand immediately we can conclude that it was a better Lewis base than PPh_3. $Mn(CO)_3(PPh_3)(P(p\text{-}MeO\text{-}C_6H_4)_3)Br$ was formed during the reaction.

Optical microscopy was used to probe the solventless reaction between powders of $Mn(CO)_4(PPh_3)Br$ with PPh_3. The reaction was observed to proceed in the melt at temperatures lower than 60°C. The melting process was accompanied by a chemical reaction between the two reagents.

The solventless reaction between crystals of $Mn(CO)_4(PPh_3)Br$ and PPh_3 was also followed by optical microscopy at 42°C. The crystals were arranged such that when the reagent crystals were isolated from each other, no chemical reaction was observed at 60°C for two hours. When the crystals were arranged so that the metal complex and ligand crystals touched, reaction was observed at $T \geq 42$°C. The reaction thus occurred in the melt and was facilitated by the migration of reagents and products to give the well-behaved reaction kinetics that were observed using FTIRS and DRIFTS. The results obtained demonstrated, on a small scale, that solventless transformation is a viable route in organometallic chemistry.

Single crystal XRD structures of $Mn(CO)_4(PPh_3)Br$ and $Mn(CO)_3(PPh_3)_2Br$ were determined. Both complexes crystallized in *P-1* space group. The data obtained were comparable with literature XRD data for similar structures.

The solventless reaction, $(\eta^5\text{-}C_5H_5)_2ZrCl_2 + Na^+RCOO^-$, R = C_6H_5, p-C_6H_4-NO_2, p-C_6H_4-NH_2 → $(\eta^5\text{-}C_5H_5)_2ZrCl(RCOO)$ + NaCl, was also investigated. Scrutiny of the reaction showed that it actually took place in the deuterated solvent during NMR analysis. Single crystal XRD study of $(\eta^5\text{-}C_5H_5)_2ZrCl(RCOO)$ R = C_6H_5, p-C_6H_4-NO_2 revealed that the carboxylato ligand was coordinated in a bidentate fashion (chelating) resulting in an 18 electron, five-coordinate zirconium complexes. The unit cell parameters of the two complexes mentioned above were similar to each other and comparable to literature values. Although the actual reaction was not solventless as envisaged the analysis of the compounds using single crystal XRD technique was done in the solid-state.

To extend the concept of green chemistry to catalytic synthesis, the conversion of intenal olefins to terminal olefins was undertaken. This investigation was the second objective of the thesis. Here, substituted cyclopentadienes (R = Me, Et, ^{i}Pr, ^{t}Bu, $SiMe_3$) were synthesised in good yields (42 – 68%). They were successfully used to synthesise zirconium(IV) metallocene dichlorides (66 – 83% yield) that were screened as potential internal to terminal olefin isomerisation catalysts.

The reaction of chlorobis(η^5-cyclopentadienyl)hexylzirconium(IV) with internal hexene isomers failed to yield terminal olefins even under harsh experimental conditions. The findings were in line with the conclusion Chirik and co-workers made that revealed that the detachment of an alky moiety from a zirconium alkyl complex as a terminal olefin is not a facile process. Isomerisation reactions using substituted zirconium metallocenes also failed to produce the terminal olefin.

The reaction of Cp_2ZrCl_2 + PR_3 + *n*-BuLi , (R = Et, Ph) with hexenes yielded a stoichiometric amount of 1-hexene. The reaction was found to be catalytic in Cp_2ZrCl_2 but limited by the amount of *n*-BuLi. Further investigations revealed that the

isomerisation reaction could take place when using the system Cp_2ZrCl_2 / *n*-BuLi, ruling out the need to use phosphines. The work thus provided a glimpse on how atom economy could be attained through the use of catalysts.

13.2. FUTURE SUGGESTIONS

The reaction between $Mn(CO)_4(PPh_3)Br$ and P(*p*-MeO-$C_6H_4)_3$ yielded $Mn(CO)_3(PPh_3)_2Br$, $Mn(CO)_3$(P(*p*-MeO-$C_6H_4)_3)_2Br$ and $Mn(CO)_3$(P(*p*-MeO-$C_6H_4)_3$)$(PPh_3)Br$ through the formation of an $Mn(CO)_4$(P(*p*-MeO-$C_6H_4)_3$)Br intermediate (**Scheme 7.2**). An extension of this investigation could be the reaction of tricarbonyl complex $Mn(CO)_4L_2$ with ligand L´ as shown in **Scheme 13.1** below.

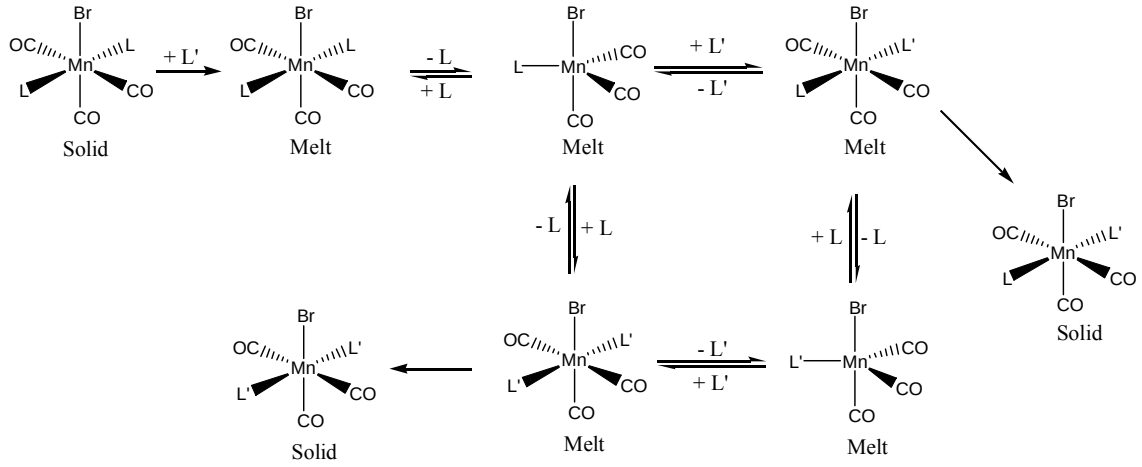

Scheme 13.1. Proposed solventless reaction sequence between $Mn(CO)_4L_2$ and L´

The scheme (**Scheme 13.1**) suggests that the tetracarbonyl complexes ($Mn(CO)_4LBr$ and ($Mn(CO)_4L´Br$, should not form if the reaction mechanism proposed in **Scheme 7.2** is correct because of the lack of additional CO ligand. The reaction could initially be conducted using Mn:L′ of 1:2 to compensate for the two complexes that will form.

The reaction shown below (**Scheme 13.2**) failed to take place in the absence of solvents due to steric bulk of the ligand [(L = tris(2,4-di-*t*-butylphenyl)phosphite]. However, if a relatively less bulky ligand, like PPh_3 is used instead, the reaction could, in theory, take

place as shown in **Scheme 13.3**. To test the hypothesis, the reaction could be attempted using a Mn:L´ ratio of 1:2. In this case only two tricarbonyl complexes can be produced, making the analysis easier than would be for the case shown in **Scheme 7.2**.

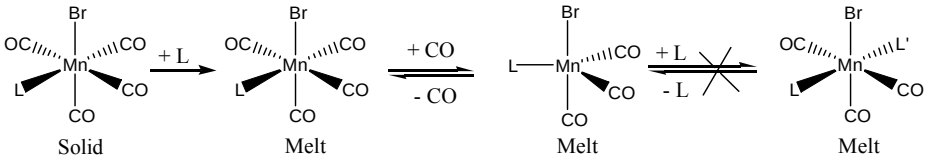

Scheme 13.2. Attempted synthesis of manganese tricarbonyl complex containing tris(2,4-di-*t*-butylphenyl)phosphite ligand.

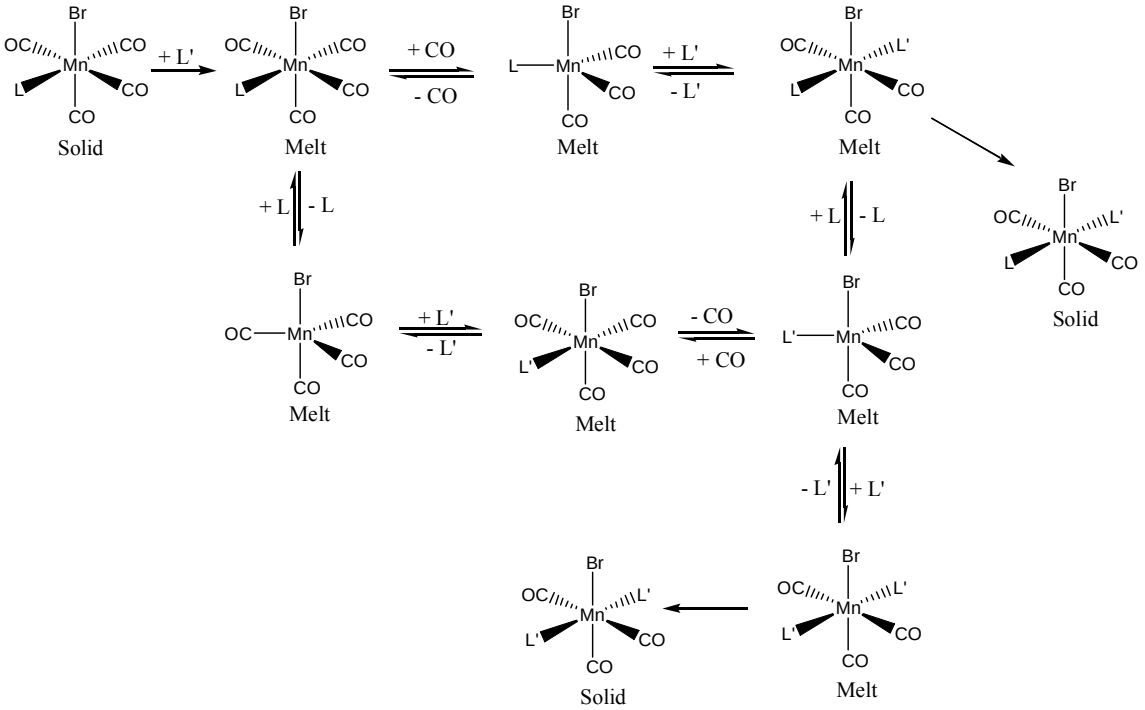

Scheme 13.3. Proposed reaction sequence of the reaction of bromotris(2,4-di-t-butylphenyl)phosphitetricarbonylmanganese(I) complex with PPh_3 in the absence of solvents

The reaction sequence shown in **Scheme 13.3** can be conducted in reverse. In this case, a tricarbonyl complex containing a bulky ligand, [(L = tris(2,4-di-*t*-butylphenyl)phosphite], is reacted with a less bulky phosphine, like PPh_3, such that only the mixed ligand

complex, Mn(CO)4LL´Br, is produced as shown in **Scheme 13.4**. The reaction sequences shown above also serve as a test for the proposed mechanism shown in **Scheme 7.2**.

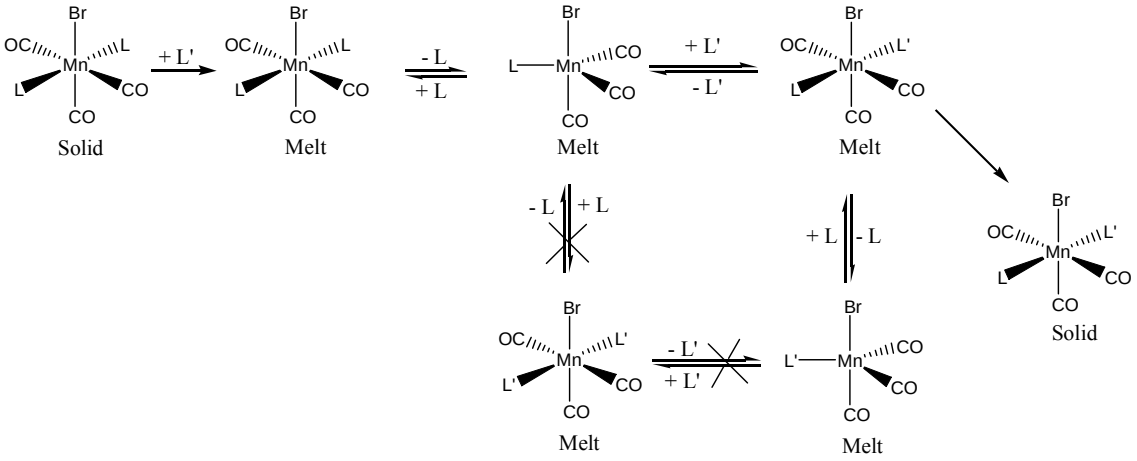

Scheme 13.4. Envisaged formation of a mixed manganese tricarbonyl complex containing tris(2,4-di-*t*-butylphenyl)phosphite as one of the ligands.

The methodology applied to manganese complexes could be extended to rhenium carbonyl complexes because of the similarities between the metals. The extension will generate kinetic data that will enrich the scientific research pool. The reaction is expected to be slower for rhenium complexes, but only a meticulous study could prove the assumption.

Solventless reactions of manganese complexes could also be extended to include the reaction of $MnMe(CO)_5$ with PPh_3, known to take place in solution. In solution, the reaction is thought to go through an intermediate, shown below, that has a solvent coordinated to the metal centre.

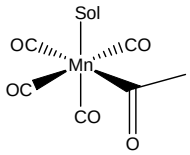

In the solventless reaction envisaged, there will be no solvent to occupy the vacant coordinated site. What course will the reaction take? Dimerisation will mostly likely take

place but that can only proven by a thorough study. How is the acyl group formed? Potentially, new compounds could also be formed in this study.

It is known that electron-withdrawing groups substituted into the methyl group of $MnMe(CO)_5$ dramatically slow-down the reaction. For example, the reaction of $[Mn(CH_2NO_2)(CO)_5]$ with PPh_3 is found to be less reactive. If the investigation is successful and the reaction of $MnMe(CO)_5$ is found to be fast, then complexes like $[Mn(CH_2NO_2)(CO)_5]$ could be used instead. Complexes like $Mn(CH_2Ph)(CO)_5$ and $Mn(CH_2SiMe_3)(CO)5$ that lack β-hydrogen atoms can be studied with ease.